

03092  
↓  
24



UNIVERSIDAD NACIONAL  
AVENIDA DE  
MEXICO

UNIVERSIDAD NACIONAL AUTONOMA DE MEXICO

Unidad Académica de los Ciclos Profesional y Posgrado  
del Colegio de Ciencias y Humanidades

Instituto de Geofísica  
Posgrado en Geofísica

MORFOLOGIA DE LA SUBDUCCION  
EN EL NORTE DE CHILE

TESIS  
PARA OPTAR AL GRADO DE DOCTOR EN GEOFISICA  
(SISMOLOGIA Y FISICA DEL INTERIOR DE LA TIERRA)

PRESENTA,

DIANA PATRICIA COMTE SELMAN

Ciudad Universitaria

Diciembre, 1993

TESIS CON  
FALLA DE ORIGEN

TESIS CON  
FALLA DE ORIGEN



## **UNAM – Dirección General de Bibliotecas Tesis Digitales Restricciones de uso**

### **DERECHOS RESERVADOS © PROHIBIDA SU REPRODUCCIÓN TOTAL O PARCIAL**

Todo el material contenido en esta tesis está protegido por la Ley Federal del Derecho de Autor (LFDA) de los Estados Unidos Mexicanos (México).

El uso de imágenes, fragmentos de videos, y demás material que sea objeto de protección de los derechos de autor, será exclusivamente para fines educativos e informativos y deberá citar la fuente donde la obtuvo mencionando el autor o autores. Cualquier uso distinto como el lucro, reproducción, edición o modificación, será perseguido y sancionado por el respectivo titular de los Derechos de Autor.

## RESUMEN

Se analiza la morfología de la subducción en la brecha sísmica del norte de Chile utilizando eventos registrados telesísmicamente y por redes locales. La brecha sísmica del norte de Chile ha sido definida en función del último terremoto que afectó la zona, ocurrido a fines del siglo pasado, el 10 de Mayo de 1877 ( $M_w \sim 8.7$ ). La sismicidad histórica es pobremente conocida en el norte de Chile debido a una tardía colonización española y a la escasez de poblados indígenas previos al siglo XIX. Sin embargo la ausencia de eventos mayores de subducción durante el presente siglo sugieren que la brecha sísmica del norte de Chile podría estar alcanzando su madurez. Debido a la similitud del ambiente tectónico entre el sur del Perú y norte de Chile, se analizan las variaciones espacio-temporales de la sismicidad en ambas brechas sísmicas, obteniéndose resultados contradictorios acerca de la madurez de ellas, lo que sugiere que la complejidad de las distribuciones observadas de sismicidad en brechas sísmicas no siempre pueden ser explicadas con modelos simples de acumulación y transferencia de esfuerzos a lo largo de la placa en subducción. Con el objeto de mejorar el conocimiento del marco tectónico de la brecha sísmica del norte de Chile, se realizaron dos experimentos locales de microsismicidad. La inversión simultánea de hipocentros y estructura de velocidades, utilizando dichos eventos locales, permitió definir una corteza oceánica en subducción que presenta un espesor aproximado de 10 km y se extiende hasta unos  $60 \pm 10$  km de profundidad. Esta profundidad está aparentemente asociada al cambio de fase de gabro a eclogita a lo largo de la litósfera oceánica en subducción, y también corresponde a la profundidad máxima del contacto sismogénico determinado tanto con datos locales como telesísmicos. Se sugiere, además, que este cambio de fase es uno de los mecanismos dominantes que controlan la profundidad máxima del contacto sismogénico. Se propone un método alternativo para la estimación de la extensión en profundidad de la zona acoplada interplaca, basado en el cambio del campo de esfuerzos en la parte superior de la placa en subducción, de compresional a tensional, lo que sería particularmente útil para casos donde no se cuenta con medidas geodésicas cosísmicas y donde hay una inadecuada cobertura azimutal de estaciones sismológicas para analizar los eventos típicos de subducción. Se observa que el cambio de esfuerzos compresionales a tensionales ocurre sistemáticamente en el norte y centro de Chile a unos  $60 \pm 10$  km de profundidad, no observándose variaciones en la dirección norte-sur. La sismicidad intraplaca de profundidad intermedia, registrada con los experimentos de microsismicidad, revela

que a una profundidad de ~100 km presenta una zona doble invertida ubicada bajo el arco volcánico, con eventos compresionales más profundos que los eventos tensionales. Esta zona doble es coherente con resultados numéricos que explican esta distribución del campo de esfuerzos a profundidades entre 90-150 km, en base a las diferentes comportamientos que presenta el estrato más superficial de la litósfera oceánica en subducción, producto de la transformación de gabro a eclogita y del estrato ubicado inmediatamente debajo de él formado por peridotita, con el aumento de presión y de temperatura que sufren durante el proceso de subducción. Finalmente, utilizando eventos registrados telesísmicamente se observa que la forma del contacto sismogénico no varía en el norte de Chile, manteniéndose su ángulo de subducción constante. Sin embargo, por debajo de la parte desacoplada de la placa en subducción, se observa una disminución gradual hacia el sur del ángulo de subducción, hecho que puede ser explicado como una respuesta regional al modo de subducción subhorizontal observado entre los 27°S y 33°S, considerando que hay continuidad lateral en la placa de Nazca.

V°B°

  
Dr. Gerardo Suárez  
Director de Tesis

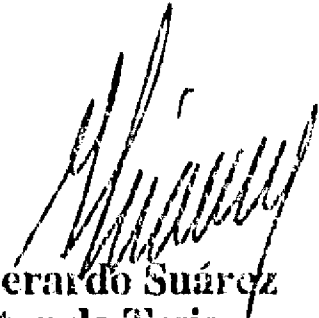


## ABSTRACT

The morphology of the subduction is analyzed in northern Chile seismic gap, using locally and teleseismically recorded earthquakes. The seismic gap in northern Chile has been defined by the last great earthquake that affected this region, on May 10, 1877 ( $M_w \sim 8.7$ ). There are no reliable historical documents previous to the XIX century, but the absence of any great thrust event observed during this century could suggest that northern Chile is a mature seismic gap. Due to the similar tectonic environment observed in the southern Peru and northern Chile seismic gaps, the spatio-temporal variations of seismicity are analyzed in both gaps in order to determine their maturity. However, contradictory results are obtained about the maturity of the northern Chile and southern Peru seismic gaps using alternative interpretations of simple accumulation and stress transfer models, suggesting that the complexity of the observed distribution of seismicity in seismic gaps can not always be explained with those relatively simple models. In order to better understand the tectonic framework of the northern Chile seismic gap, two locally microearthquake experiments were carried out there. The joint hypocentral and velocity structure inversion allow us to define an oceanic crust of  $\sim 10$  km-thick, subducting up to  $60 \pm 10$  km in depth. This depth is associated with the gabbro to eclogite phase transformation, and it also corresponds with the maximum depth of the seismogenic interplate contact determined with both, locally and teleseismically recorded events. An alternative way to determine the maximum depth of the interplate coupling zone is also proposed, based on the variations of the stress field observed in the upper-part of the slab, from compressional to tensional regime. This could be particularly useful for regions without coseismic geodetic measurements and where there is an inadequate azimuthal coverage of seismic stations for thrust events. This change occurs in northern and central Chile at about  $60 \pm 10$  km in depth, without variations along the strike of the trench. The intraplate seismicity, recorded by the microseismic experiments, exhibit an inverted double seismic zone at  $\sim 100$  in depth, located beneath the volcanic Andean belt, with compressional events deeper than tensional events. This double seismic zone agrees with numerical results that explain this stress distribution at depths between 90 to 150 km, based in the differential phase changes that occur in the layered structure of the subducting slab during its descent. Finally, using teleseismically recorded events, it can be observed that the shape of the seismogenic interplate contact does not exhibit

changes in the dip angle along the northern Chile region. However, downdip of the coupled region of the slab, a southward flattening of the slab can be observed. This flattening could be explained as a regional response of the subhorizontal mode of subduction observed between 27°S and 33°S, assuming that the Nazca plate is laterally continuous in northern Chile.

V°B°



Dr. Gerardo Suárez  
Director de Tesis

## RESUMEN

Se analiza la morfología de la subducción en la brecha sísmica del norte de Chile utilizando eventos registrados telesísmicamente y por redes locales. La brecha sísmica del norte de Chile ha sido definida en función del último terremoto que afectó la zona, ocurrido a fines del siglo pasado, el 10 de Mayo de 1877 ( $M_w \sim 8.7$ ). La sismicidad histórica es pobremente conocida en el norte de Chile debido a una tardía colonización española y a la escasez de poblados indígenas previos al siglo XIX. Sin embargo la ausencia de eventos mayores de subducción durante el presente siglo sugieren que la brecha sísmica del norte de Chile podría estar alcanzando su madurez. Debido a la similitud del ambiente tectónico entre el sur del Perú y norte de Chile, se analizan las variaciones espacio-temporales de la sismicidad en ambas brechas sísmicas, obteniéndose resultados contradictorios acerca de la madurez de ellas, lo que sugiere que la complejidad de las distribuciones observadas de sismicidad en brechas sísmicas no siempre pueden ser explicadas con modelos simples de acumulación y transferencia de esfuerzos a lo largo de la placa en subducción. Con el objeto de mejorar el conocimiento del marco tectónico de la brecha sísmica del norte de Chile, se realizaron dos experimentos locales de microsismicidad. La inversión simultánea de hipocentros y estructura de velocidades, utilizando dichos eventos locales, permitió definir una corteza oceánica en subducción que presenta un espesor aproximado de 10 km y se extiende hasta unos  $60 \pm 10$  km de profundidad. Esta profundidad está aparentemente asociada al cambio de fase de gabro a eclogita a lo largo de la litósfera oceánica en subducción, y también corresponde a la profundidad máxima del contacto sismogénico determinado tanto con datos locales como telesísmicos. Se sugiere, además, que este cambio de fase es uno de los mecanismos dominantes que controlan la profundidad máxima del contacto sismogénico. Se propone un método alternativo para la estimación de la extensión en profundidad de la zona acoplada interplaca, basado en el cambio del campo de esfuerzos en la parte superior de la placa en subducción, de compresional a tensional, lo que sería particularmente útil para casos donde no se cuenta con medidas geodésicas cosísmicas y donde hay una inadecuada cobertura azimutal de estaciones sismológicas para analizar los eventos típicos de subducción. Se observa que el cambio de esfuerzos compresionales a tensionales ocurre sistemáticamente en el norte y centro de Chile a unos  $60 \pm 10$  km de profundidad, no observándose variaciones en la dirección norte-sur. La sismicidad intraplaca de profundidad intermedia, registrada con los experimentos de microsismicidad, revela

## *Resumen*

que a una profundidad de ~100 km presenta una zona doble invertida ubicada bajo el arco volcánico, con eventos compresionales más profundos que los eventos tensionales. Esta zona doble es coherente con resultados numéricos que explican esta distribución del campo de esfuerzos a profundidades entre 90-150 km, en base a las diferentes comportamientos que presenta el estrato más superficial de la litósfera oceánica en subducción, producto de la transformación de gabro a eclogita y del estrato ubicado inmediatamente debajo de él formado por peridotita, con el aumento de presión y de temperatura que sufren durante el proceso de subducción. Finalmente, utilizando eventos registrados telesísmicamente se observa que la forma del contacto sismogénico no varía en el norte de Chile, manteniéndose su ángulo de subducción constante. Sin embargo, por debajo de la parte desacoplada de la placa en subducción, se observa una disminución gradual hacia el sur del ángulo de subducción, hecho que puede ser explicado como una respuesta regional al modo de subducción subhorizontal observado entre los 27°S y 33°S, considerando que hay continuidad lateral en la placa de Nazca.

## ABSTRACT

The morphology of the subduction is analyzed in northern Chile seismic gap, using locally and teleseismically recorded earthquakes. The seismic gap in northern Chile has been defined by the last great earthquake that affected this region, on May 10, 1877 ( $M_W \sim 8.7$ ). There are no reliable historical documents previous to the XIX century, but the absence of any great thrust event observed during this century could suggest that northern Chile is a mature seismic gap. Due to the similar tectonic environment observed in the southern Peru and northern Chile seismic gaps, the spatio-temporal variations of seismicity are analyzed in both gaps in order to determine their maturity. However, contradictory results are obtained about the maturity of the northern Chile and southern Peru seismic gaps using alternative interpretations of simple accumulation and stress transfer models, suggesting that the complexity of the observed distribution of seismicity in seismic gaps can not always be explained with those relatively simple models. In order to better understand the tectonic framework of the northern Chile seismic gap, two locally microearthquake experiments were carried out there. The joint hypocentral and velocity structure inversion allow us to define an oceanic crust of  $\sim 10$  km-thick, subducting up to  $60 \pm 10$  km in depth. This depth is associated with the gabbro to eclogite phase transformation, and it also corresponds with the maximum depth of the seismogenic interplate contact determined with both, locally and teleseismically recorded events. An alternative way to determine the maximum depth of the interplate coupling zone is also proposed, based on the variations of the stress field observed in the upper-part of the slab, from compressional to tensional regime. This could be particularly useful for regions without coseismic geodetic measurements and where there is an inadequate azimuthal coverage of seismic stations for thrust events. This change occurs in northern and central Chile at about  $60 \pm 10$  km in depth, without variations along the strike of the trench. The intraplate seismicity, recorded by the microseismic experiments, exhibit an inverted double seismic zone at  $\sim 100$  km in depth, located beneath the volcanic Andean belt, with compressional events deeper than tensional events. This double seismic zone agrees with numerical results that explain this stress distribution at depths between 90 to 150 km, based in the differential phase changes that occur in the layered structure of the subducting slab during its descent. Finally, using teleseismically recorded events, it can be observed that the shape of the seismogenic interplate contact does not exhibit

*Abstract*

changes in the dip angle along the northern Chile region. However, downdip of the coupled region of the slab, a southward flattening of the slab can be observed. This flattening could be explained as a regional response of the subhorizontal mode of subduction observed between 27°S and 33°S, assuming that the Nazca plate is laterally continuous in northern Chile.

## INTRODUCCION

El proceso de subducción en el norte de Chile está controlado por la interacción de las placas de Nazca y Sudamérica, con una velocidad relativa de convergencia de  $\sim 8.4$  cm/año y en una dirección  $N77^\circ E$  (DeMets et al., 1990). La edad promedio de la placa de Nazca en el norte de Chile es de  $\sim 60$  ma (Mayes et al., 1990). Este tipo de subducción, de una placa relativamente joven y rápida, se traduce en una zona interplaca fuertemente acoplada que puede generar grandes eventos inversos de bajo ángulo a lo largo del contacto sismogénico, una sismicidad intraplaca de profundidad intermedia preferencialmente tensional, con la presencia de una cadena de volcanes andesíticos distribuidos en una dirección paralela a la fosa.

### *Sismicidad Histórica y Variaciones Espacio-Temporales de la Sismicidad*

La sismicidad histórica indica que el último gran terremoto que afectó al norte de Chile ocurrió a fines del siglo pasado (10 de Mayo de 1877) con una magnitud  $M_w \sim 8.7$  y un largo de ruptura, estimado a partir de las distribuciones de las isosistas de intensidad VIII y de los tiempos de refracción del tsunami asociado, de aproximadamente 500 km (Lomnitz, 1971; Abe, 1979; Kausel, 1986; Comte y Pardo, 1991; Díaz, 1992). La documentación de grandes terremotos en la zona previos a 1800 es imprecisa y escasa. Por tanto, la estimación de un período de recurrencia para el norte de Chile es muy difícil. Sin embargo, la ausencia de grandes terremotos de subducción ( $M_S \geq 7$ ) durante el presente siglo sugiere que el norte de Chile es una brecha sísmica de importancia (Kelleher, 1972; McCann et al., 1979; Nishenko, 1985; Comte y Pardo, 1991).

Comte y Suárez (1993a) analizaron las variaciones espacio-temporales de las brechas sísmica del sur del Perú y del norte de Chile, utilizando los eventos reportados telesísmicamente por los catálogos del NEIC y PDE para el período 1965-1991, considerando que ambas brechas presentan similitudes. Por ejemplo, (i) ambas son zonas adyacentes, (ii) el último gran terremoto que afectó a cada una de estas regiones ocurrió hace  $\sim 120$  años, (iii) ninguna de ellas ha experimentado terremotos mayores de subducción durante el presente siglo, y (iv) la velocidad y la edad de la placa de Nazca es aproximadamente la misma. Aunque los tiempos de recurrencia y las longitudes de ruptura pueden variar entre ciclos sísmicos sucesivos (e.g., Comte et al., 1986;

## *Introducción*

Thatcher; 1990; Ruff, 1992), el hecho que los últimos terremotos que afectaron el sur del Perú (1868) y el norte de Chile (1877) tengan largos de ruptura del orden de 500 km, sugiere que éstos podrían representar los mayores eventos esperados para ambas regiones. De modo que, aunque el próximo gran terremoto de subducción que afecte cada una de estas regiones, no necesariamente será de la misma magnitud que el último observado, probablemente ocurrirá dentro de las áreas definidas por ellos..

Las distribuciones espacio temporales de ambas brechas presentan algunas similitudes: ni en el sur del Perú ni en el norte de Chile se observan los eventos compresionales en la zona cercana a la fosa que han sido considerados como una actividad precursora en algunas zonas de subducción. Ambas brechas presentan una actividad intraplaca de profundidad intermedia de carácter principalmente tensional, que es más intensa en el segmento del norte de Chile. Por otro lado, la variación del campo de esfuerzos de compresional a tensional en la parte superior de la placa en subducción ocurre en ambas regiones a ~200 de distancia desde la fosa, lo que está aparentemente relacionado con la profundidad máxima del contacto sismogénico.

Sin embargo, la distribución de sismicidad presenta algunas diferencias importantes: en el sur del Perú se observa un aumento de la actividad sísmica compresional cerca del contacto sismogénico desde 1987. Por el contrario, en el norte de Chile hay una ausencia de este tipo de actividad ( $m_b > 5.5$ ) desde la secuencia de 1967, lo cual podría aparentemente complementarse con un enjambre de eventos compresionales de menor magnitud que ocurrió durante 1987. La brecha del sur del Perú presenta un aumento de actividad tensional cercana a la fosa durante 1987, lo que no es observado en el norte de Chile.

A la luz del modelo de transferencia de esfuerzos, la continua actividad tensional de profundidad intermedia observada en el sur del Perú y en el norte de Chile, podría ser interpretada como que el contacto interplaca en ambas regiones estaría fuertemente acoplado. El hecho de que esta actividad sea más intensa en el norte de Chile, además de la ausencia de actividad compresional cerca del contacto interplaca, podría indicar que esta brecha estaría más madura que la del sur del Perú. Por otra parte, el aumento de actividad compresional cerca del contacto sismogénico y el aumento de actividad tensional en la zona cercana a la fosa observado en el sur del Perú desde 1987, podría interpretarse como un signo de un pre-deslizamiento sísmico cerca del contacto sismogénico. Entonces la ausencia de este tipo de actividad en el norte de Chile podría indicar que el sur del Perú es una brecha sísmica más madura que la del norte de Chile.



En resumen, se obtienen resultados contradictorios acerca de la madurez de las brechas sísmicas del sur del Perú y norte de Chile cuando se utilizan interpretaciones alternativas de modelos simples de distribución y transferencia de esfuerzos en la zona cercana al contacto sismogénico, sugiriendo que la complejidad de las distribuciones observadas de sismicidad en brechas sísmicas no siempre pueden ser explicadas con dichos modelos a lo largo de la placa en subducción.

*Modelo Bi-Dimensional de Velocidades de Ondas P Utilizando Datos Locales*

Para mejorar el conocimiento del marco tectónico de la brecha sísmica del norte de Chile, se realizaron dos experimentos locales de microsismicidad utilizando estaciones sismológicas portátiles, tanto analógicas como digitales. El primero de ellos se desarrolló en 1988 en la zona de Antofagasta, cerca del límite sur de ruptura del evento de 1877 (Comte et al., 1992, 1993a), y el segundo se realizó en torno a Iquique, que corresponde aproximadamente a la zona central del área estimada de ruptura del evento de 1877 (Comte et al., 1993b).

Los eventos registrados durante ambos experimentos se utilizaron para determinar simultáneamente sus hipocentros y la estructura bi-dimensional de velocidades de ondas *P* a lo largo de la placa en subducción de Nazca y la margen oeste de la placa continental Sud Americana (Comte et al., 1993c).

El método de inversión utilizado ha sido aplicado con éxito en una gran variedad de otros ambientes tectónicos. Sin embargo, es probablemente la primera vez que se aplica para un reducido número de eventos y estaciones (~200 eventos y ~20 estaciones, en cada experimento). Por lo tanto, no se justifica realizar una inversión tri-dimensional con muchos bloques independientes, y se determinó un modelo bi-dimensional con simetría a lo largo de la trinchera, que incluye las principales unidades tectónicas observadas en la región. Debido a que la mayoría de los eventos registrados están localizados en la placa en subducción, el megabloque asociado a ella fue el que presentó menores errores y mejor resolución. Además, aunque el número de eventos utilizados en cada experimento es aproximadamente igual, éstos están mejor distribuidos a lo largo de la placa en el caso de Antofagasta que en el de Iquique. Esto junto con el hecho que el experimento de Antofagasta contó con un mayor número de estaciones, se tradujo en una mejor resolución de la estructura de la litósfera oceánica bajo Antofagasta.

## Introducción

La velocidad determinada para el manto superior bajo el continente tiene una resolución menor que la obtenida para los otros bloques. Sin embargo, la inversión convirgió a valores  $\sim 8.4$  km/s en ambas regiones. Se observó una zona de bajas velocidades de onda  $P$  en la parte superior de la placa en subducción, la que fue interpretada como corteza oceánica de un espesor  $\sim 10$  km, cuya máxima profundidad estimada es de  $60 \pm 10$  km. Esta profundidad es asociada a la profundidad de transformación de fase de gabro a eclogita en la corteza oceánica, y también corresponde a la máxima profundidad del contacto sismogénico en la zona de subducción de Chile (Tichelaar y Ruff, 1991; Suárez y Comte, 1993).

De los varios mecanismos propuestos para controlar la profundidad máxima de acoplamiento (*e.g.*, Tichelaar y Ruff, 1991), Comte et al. (1993c) proponen que la correlación entre la profundidad de cambio de fase y la profundidad del contacto sismogénico interplaca, entre placas con diferentes edades, velocidades de convergencia, ángulos de subducción, espesores de la corteza continental e historia sedimentaria, sugiere que el efecto del cambio de fase podría ser dominante con respecto a la mayoría de los otros mecanismos mencionados.

### *Profundidad Máxima del Contacto Sismogénico*

Tichelaar and Ruff (1991) analizaron las zonas de subducción en Chile, como parte de un proyecto mundial para mapear la profundidad máxima y el ancho del contacto sismogénico, utilizando la profundidad focal de los eventos de subducción interplaca registrados telesísmicamente cuya magnitud es superior a 6.0. La principal conclusión de su trabajo es que hay un cambio en la profundidad máxima del acoplamiento interplaca en Chile aproximadamente en los  $28^\circ\text{S}$ . De acuerdo a sus resultados, al sur de esta latitud la zona sísmicamente acoplada en Chile se extiende hasta profundidades de 48 a 53 km, mientras que aparentemente sólo alcanzaría unos 36-41 km al norte de los  $28^\circ\text{S}$ .

Suárez y Comte (1993) discuten las dificultades asociadas en la determinación de la profundidad del contacto sismogénico, y los diferentes resultados que se pueden obtener cuando se utilizan datos telesísmicos y microsismicidad local. Idealmente, es deseable determinar la profundidad máxima de la zona acoplada utilizando medidas geodésicas de la ruptura cosísmica y réplicas en una región que haya sido afectada por un gran terremoto ( $M > 7.7$ ). Sin embargo, la escasez de eventos de gran magnitud y la

## *Introducción*

falta de datos geodésicos locales obligan al uso de medidas indirectas del tamaño del contacto sismogénico.

La zona propuesta por Tichelaar y Ruff (1991) con un acoplamiento sismogénico más superficial es observada solamente en la región de Taltal (entre 24° y 28°S), donde del total de 27 terremotos estudiados por ellos, sólo 5 se encuentran en esta región, cuyas magnitudes  $M_w$  varía entre 7.3 y 7.5. Con los datos históricos disponibles, no es claro definir si en el segmento de Taltal ha ocurrido un gran terremoto en los últimos 100 años, por lo tanto, se sugiere que el resultado obtenido por Tichelaar y Ruff (1991) que esta región tenga un contacto sismogénico anómalamente más superficial, puede ser resultado de haber considerado eventos de menor magnitud que aquellos observados en el resto de Chile.

Los datos provenientes de los experimentos de microsismicidad local en el norte de Chile (mencionados anteriormente), y en Chile central permiten a Suárez y Comte (1993) concluir que la profundidad máxima del contacto sismogénico en estas tres regiones de Chile se extiende consistentemente hasta unos 50 km, sin mostrar variaciones apreciables en una dirección norte-sur. Por tanto, dicha profundidad, al parecer, no está correlacionada con la edad y la geometría de la placa en subducción, ni con la presencia de volcanes en la placa superior o el espesor de sedimentos en la fosa.

Además, en las tres regiones de Chile analizadas por Suárez y Comte (1993) se observa un cambio del campo de esfuerzos en la parte superior de la placa en subducción, de compresional a tensional, a aproximadamente 70 km de profundidad. Este cambio podría estar relacionado con el inicio de la parte desacoplada de la placa subducente, de modo que el régimen compresivo causaría no sólo eventos a lo largo del contacto interplaca, sino que también eventos intraplaca de fallamiento inverso de mayor ángulo. A cierta profundidad, cuando la placa comienza a estar completamente desacoplada de la placa superior, se observarían los eventos tensionales asociados a su buyancia negativa. Por tanto, la transición del comportamiento compresional a tensional, podría reflejar las condiciones mecánicas del contacto interplaca y podrían ayudar a mapear indirectamente la profundidad del acoplamiento.

*Una Zona Doble Invertida en el Norte de Chile*

La sismicidad intraplaca de profundidad intermedia, registrada con los dos experimentos de microsismicidad realizados en el norte de Chile revela que a una profundidad de ~100 km se observan eventos tensionales consistentemente más superficiales que eventos compresionales. Esto sugiere la posibilidad de una zona doble, ubicada bajo el arco volcánico activo, con una polaridad invertida con respecto a las zonas sísmicas dobles tradicionales observadas en el mundo (Comte y Suárez, 1993b).

Los eventos de profundidad intermedia han sido generalmente interpretados como evidencia de una litósfera fría penetrando en el manto. La mayoría de las placas en subducción exhiben fallamientos intraplaca de carácter tensional, lo que ha sido asociado al efecto gravitacional que sufre la placa en subducción, una vez que ha superado la profundidad de acoplamiento interplaca. Sin embargo, también se ha observado en algunas zonas de subducción la presencia de zonas sísmicas dobles, donde una capa de eventos compresionales se ubica sobre una de eventos tensionales. Ambas capas sísmicas están separadas por ~40 km a una profundidad de ~60 km, uniéndose a una profundidad de 200 km. En general, las zonas sísmicas dobles han sido asociadas con el desdoblamiento que experimenta la placa en subducción al sufrir un cambio brusco en su radio de curvatura bajo el contacto sismogénico, y se han propuesto una variedad de mecanismos para explicarlas, como por ejemplo: esfuerzos asociados a cambios de fase, combamiento de la placa debido a su propio peso, esfuerzos termo-elásticos.

Aunque la sismicidad de profundidad intermedia es caracterizada por eventos tensionales en el norte de Chile, hay un evento de carácter compresional ( $M_S=6.1$ ) ubicado a una profundidad de ~130 km, bajo el arco volcánico. Este evento registrado telesísmicamente, refuerza la proposición de la zona sísmica doble invertida más general que la únicamente observada con eventos registrados por redes locales.

Recientemente, Kirby y Hacker (1993) modelaron la distribución de esfuerzos inducidos por los cambios de presión y temperatura en la litósfera oceánica en subducción a profundidades entre 90 y 150 km. Sus resultados numéricos sugieren que la corteza basáltica se densifica en eclogita debido al aumento de presión inducido durante el descenso de la placa y a la deshidratación de la corteza oceánica, que es la fuente del arco volcánico. Sin embargo, la peridotita que compone la parte del manto

*Una Zona Doble Invertida en el Norte de Chile*

La sismicidad intraplaca de profundidad intermedia, registrada con los dos experimentos de microsismicidad realizados en el norte de Chile revela que a una profundidad de ~100 km se observan eventos tensionales consistentemente más superficiales que eventos compresionales. Esto sugiere la posibilidad de una zona doble, ubicada bajo el arco volcánico activo, con una polaridad invertida con respecto a las zonas sísmicas dobles tradicionales observadas en el mundo (Comte y Suárez, 1993b).

Los eventos de profundidad intermedia han sido generalmente interpretados como evidencia de una litósfera fría penetrando en el manto. La mayoría de las placas en subducción exhiben fallamientos intraplaca de carácter tensional, lo que ha sido asociado al efecto gravitacional que sufre la placa en subducción, una vez que ha superado la profundidad de acoplamiento interplaca. Sin embargo, también se ha observado en algunas zonas de subducción la presencia de zonas sísmicas dobles, donde una capa de eventos compresionales se ubica sobre una de eventos tensionales. Ambas capas sísmicas están separadas por ~40 km a una profundidad de ~60 km, uniéndose a una profundidad de 200 km. En general, las zonas sísmicas dobles han sido asociadas con el desdoblamiento que experimenta la placa en subducción al sufrir un cambio brusco en su radio de curvatura bajo el contacto sismogénico, y se han propuesto una variedad de mecanismos para explicarlas, como por ejemplo: esfuerzos asociados a cambios de fase, combamiento de la placa debido a su propio peso, esfuerzos termo-elásticos.

Aunque la sismicidad de profundidad intermedia es caracterizada por eventos tensionales en el norte de Chile, hay un evento de carácter compresional ( $M_S=6.1$ ) ubicado a una profundidad de ~130 km, bajo el arco volcánico. Este evento registrado telesísmicamente, refuerza la proposición de la zona sísmica doble invertida más general que la únicamente observada con eventos registrados por redes locales.

Recientemente, Kirby y Hacker (1993) modelaron la distribución de esfuerzos inducidos por los cambios de presión y temperatura en la litósfera oceánica en subducción a profundidades entre 90 y 150 km. Sus resultados numéricos sugieren que la corteza basáltica se densifica en eclogita debido al aumento de presión inducido durante el descenso de la placa y a la deshidratación de la corteza oceánica, que es la fuente del arco volcánico. Sin embargo, la peridotita que compone la parte del manto

## *Introducción*

superior de la placa en subducción, no experimenta cambios de fase debido a que es estable a grandes presiones. Este cambio diferencial de volumen produce una deformación tensional en la capa transformada de la corteza oceánica, e induce una deformación compresional cerca del límite superior del manto de la placa en subducción.

La distribución de esfuerzos generado por dichos cambios de fase podría explicar la zona sísmica doble invertida observada en el norte de Chile, y también el hecho que es observada principalmente con eventos de menor magnitud.

### *Distribución de Esfuerzos y Geometría de la Placa de Nazca*

La distribución de esfuerzos a lo largo de la placa de Nazca en subducción en el norte de Chile es analizada por Comte y Suárez (1993c), utilizando los mecanismos focales obtenidos con la inversión de ondas de período largo *P*, *SV*, y *SH* de 15 eventos registrados telesísmicamente ( $m_b \geq 5.5$ ) y de 107 eventos con mecanismos focales reportados por otros autores, que ocurrieron durante 1962 y 1987.

Una determinación hipocentral conjunta se realizó para los 107 eventos mencionados y 154 eventos adicionales ( $m_b \geq 5.0$ ) que no tienen mecanismos de foco reportados. El control de profundidad está dado por la profundidad de los 15 eventos modelados y el control epicentral se obtuvo utilizando eventos de calibración registrados por redes locales.

La geometría de la subducción en el norte de Chile se obtiene combinando los eventos registrados telesísmicamente y la microsismicidad local, donde el límite superior de la placa en subducción, en la zona del contacto sismogénico, se definió utilizando los eventos inversos de bajo ángulo, y en la parte más profunda se utilizó principalmente la distribución de los eventos con la profundidad.

Comte y Suárez (1993c) proponen que el ángulo de subducción, en la zona del contacto sismogénico, es constante en el norte de Chile ( $19^\circ$  a  $27^\circ$ S). Sin embargo, a partir de la zona desacoplada se observa una disminución del ángulo de subducción a partir de  $\sim 22^\circ$ S. Esta disminución podría estar correlacionado con la interacción de la estructura batimétrica del Perdida Ridge con la subducción y con las variaciones de edad reportadas (el extremo norte es más antiguo que el extremo sur) en el norte de Chile. Sin embargo, considerando que existe continuidad lateral en la placa de Nazca, la variación del ángulo de subducción observada podría ser debida a una deformación

### Introducción

regional asociada al modo de subducción subhorizontal observado entre los 28° y 33°S, de modo que el inicio del cambio de una subducción normal a una subhorizontal podría comenzar en ~22°S y ocurrir de una forma gradual.

Comte et al. (1993b) y Suárez y Comte (1993b) sugieren que el cambio del campo de esfuerzos de compresional a tensional, observado en la parte superior de la placa en subducción con eventos locales, podría ser un medio alternativo para estimar la profundidad máxima del contacto sismogénico, principalmente en las regiones que no tienen medidas geodésicas co-sísmicas y una inadecuada cobertura azimutal para eventos típicos de subducción. La profundidad máxima de dicho cambio estimada con microsismicidad local ( $60 \pm 10$  km) concuerda con la observada con eventos registrados telesísmicamente, aunque en este caso la definición del cambio es más imprecisa debido a que no siempre hay suficientes eventos para su determinación.

Se observa también una distribución compleja de eventos tensionales ubicados bajo el contacto sismogénico. Dichos eventos podría ser una complicación adicional en la determinación del cambio del campo de esfuerzos de compresional a tensional, sin embargo, los eventos tensionales son preferencialmente más profundos que los compresionales y en general, son más escasos. La presencia de los eventos tensionales bajo el contacto sismogénico podría sugerir que el efecto gravitacional que domina la placa en subducción a partir de la parte desacoplada, puede actuar ocasionalmente en las partes más profundas de la placa en subducción, bajo la zona acoplada.

Es interesante mencionar que la diferencia en las profundidades máximas observadas entre los eventos típicos de subducción ( $40 \pm 10$  km) y el cambio de compresional a tensional ( $60 \pm 10$  km) observado en la parte superior de dicha placa puede significar que probablemente a profundidades entre 40 y 60 km no se nucleará un gran evento inverso de bajo ángulo. Sin embargo, grandes eventos de subducción pueden extender su ruptura hasta los 60 km de profundidad.

### REFERENCIAS

- Abe, K., Size of the great earthquakes of 1837-1974 inferred from tsunami data, *J. Geophys. Res.*, **84**, 1561-1568, 1979.
- Comte, D. y M. Pardo, Reappraisal of great historical earthquakes in the northern Chile and southern Peru seismic gaps, *Natural Hazards*, **4**, 23-44, 1991.

### Introducción

- Comte, D. y G. Suárez, Spatio-temporal variations of seismicity in the southern Perú and northern Chile seismic gaps, *in press Pure and Applied Geophys.*, 1993 a.
- Comte, D., y G. Suárez, An inverted double seismic zone in Chile: Evidence of phase transformation in the subducted slab, *in press Science*, 1993b.
- Comte, D. y G. Suárez, Stress distribution and geometry of the subducting Nazca plate in northern Chile using teleseismically recorded earthquakes, en preparación 1993 c.
- Comte, D., A. Eisenberg, E. Lorca, M. Pardo, L. Ponce, R. Saragoni, S. K. Singh, y G. Suárez, The 1985 central Chile earthquake: A repeat of previous great earthquakes in the region?, *Science*, **233**, 449-453, 1986.
- Comte, D., M. Pardo, L. Dorbath, C. Dorbath, H. Haessler, L. Rivera, A. Cisternas, y L. Ponce, Crustal seismicity and subduction morphology around Antofagasta, Chile: preliminary results from a microearthquake survey, *Tectonophys.*, **205**, 13-22, 1992.
- Comte, D., M. Pardo, L. Dorbath, C. Dorbath, H. Haessler, L. Rivera, A. Cisternas, y L. Ponce, Seismogenic interplate contact zone and crustal seismicity around Antofagasta, northern Chile using local data, *in press Geophys. J. Int.*, 1993a.
- Comte, D., G. Suárez, T. Monfret, M. Pardo, L. Ponce y J. Domínguez, Preliminary results of a seismic experiment in northern Chile during July and August, 1991, *in press Geofísica*, 1993 b.
- Comte, D., S. W. Roecker, y G. Suárez, velocity structure in northern Chile: Evidence of subducted oceanic crust in the Nazca plate, *in press Geophys. J. Int.*, 1993c.
- DeMets, C., R. G. Argus, and S. Stein, Current plate motions, *Geophys. J. Int.*, **101**, 425-478, 1990.
- Díaz, J., Estudio de fuentes de tsunamis y terremotos: aplicación en el norte de Chile y sur del Perú. Tesis para obtener el grado de Oceanógrafo, Universidad Católica de Valparaíso, 1992.
- Kausel, E., Los terremotos de Agosto de 1868 y Mayo de 1877 que afectaron el sur del Perú y norte de Chile, *Boletín de la Academia Chilena de Ciencias*, **3**, 8-12, 1986.
- Kelleher, J., Rupture zones of large South American earthquakes and some predictions, *J. Geophys. Res.*, **77**, 2089-2103, 1972.
- Kirby, S., y B. Hacker, Earthquakes at the deep roots of arc volcanos, *EOS*, **76**, 70, 1993.
- Lomnitz, C., Grandes terremotos y tsunamis en Chile durante el período 1535-1955, *Geofis. Panam.*, **2**, 151-178, 1971.



*Introducción*

- Mayes, C. L., L. A. Lawver, y D. T. Sandwell, Tectonic history and new isochron chart of the South Pacific, *J. Geophys. Res.*, **95**, 8543-8547, 1990.
- McCann, W. R., S. P. Nishenko, L. R. Sykes, y J. Krause, Seismic gaps and plate tectonics: Seismic potential for major boundaries, *Pure Appl. Geophys.*, **117**, 1082-1147, 1979.
- Nishenko, S., Seismic potential for large and great interplate earthquakes along the Chilean and southern Peruvian margins of South America: A quantitative reappraisal, *J. Geophys. Res.*, **90**, 3589-3615, 1985.
- Ruff, L., Asperity distributions and large earthquake occurrence in subduction zones, *Tectonophys.*, **211**, 61-83, 1992.
- Suárez, G., y D. Comte, Comment on "Seismic coupling along the Chilean subduction zone" by B. W. Tichelaar and L. R. Ruff, *J. Geophys. Res.*, **98**, 15,825-15,828, 1993.
- Thatcher, W., Order and diversity in the modes of Circum-Pacific earthquake recurrence, *J. Geophys. Res.*, **95**, 2609-2623, 1990.
- Tichelaar, B. W., y L. R. and Ruff, Seismic coupling along the Chilean subduction zones, *J. Geophys. Res.*, **96**, 11,997-12,022, 1991.

SPATIO-TEMPORAL VARIATIONS OF SEISMICITY  
IN THE SOUTHERN PERU AND NORTHERN CHILE SEISMIC GAPS

Diana Comte<sup>1,2</sup> and Gerardo Suárez<sup>1</sup>

<sup>1</sup>UACPyP, Instituto de Geofísica, UNAM, México D.F. 04510, México

<sup>2</sup>also at Depto de Geología y Geofísica, U. de Chile Casilla 2777, Santiago, Chile.

*Pure and Applied Geophysics, 140, N°2, 317-330*

*Abstract.*- The spatio-temporal variation of seismicity in the southern Peru and northern Chile seismic gaps are analyzed with teleseismic data ( $m_b \geq 5.5$ ) between 1965 and 1991, to investigate whether these gaps present the precursory combination of compressional outer-rise and tensional down-dip events observed in some other subduction zones. In the outer-rise and the inner-trench (0 to 100 km distance from the trench) regions, lower magnitude ( $5.0 \leq m_b < 5.5$ ) events were also studied. The results obtained show that the gaps in southern Peru and northern Chile do not present compressional outer-rise events. However, both gaps show a continuous, tensional down-dip seismicity. For both regions, the change from compressional to tensional regime along the slab occurs at a distance of about 160 km from the trench, apparently associated with the coupled-uncoupled transition of the interplate contact zone. In southern Peru, an increase of compressional seismicity near the interplate zone and of tensional events ( $5.0 \leq m_b \leq 6.3$ ) in the outer-rise and inner-trench regions is observed between 1987 and 1991. A similar distribution of seismicity in the outer-rise and inner-trench regions is observed with earthquakes ( $m_b < 5.5$ ). In northern Chile there is a relative absence of compressional activity ( $m_b \geq 5.5$ ) near the interplate contact since the sequence of December 21, 1967. After that, only a cluster of low-magnitude compressional events have been located in the area 50 to 100 km from the trench. The compressional activity occurring near the interplate zone in both seismic gaps represents that a seismic preslip is occurring in and near the plate contact. Therefore, if this seismic preslip is associated with the maturity of the gap, the fact that it is larger in southern Peru than in northern Chile may reflect that the former gap is more mature than the latter. However, the more intense downdip tensional activity and the absence of compressional seismicity near the contact zone observed in northern Chile, may also be interpreted as evidence that northern Chile is seismically more mature than southern Peru. Therefore, the observed differences in the distribution of stresses and seismicity analyzed under simple models of stress accumulation and transfer in coupled subduction zones are not sufficient to assess the degree of maturity of a seismic gap.

### *Introduction*

Southern Peru and northern Chile are two adjacent seismic gaps in the circum-Pacific region (Kelleher, 1972; McCann et al., 1979; Nishenko, 1985; Lay et al., 1989; Comte and Pardo, 1991). The last two earthquakes with destructive tsunamis occurred there in 1868 ( $M_w=8.8$ , southern Peru) and 1877 ( $M_w=8.8$ , northern Chile) (Dorbath et al., 1990; Comte and Pardo, 1991), and no large thrust events ( $M_S>8.0$ ) have affected these regions during this century. Thus, both gaps are interesting regions to analyze their seismicity during the last 27 years of reliable hypocenters and focal mechanism catalogs.

Studies of temporal variations of down-dip intraplate and outer-rise earthquakes in coupled subduction zones have been reported by several authors (e.g. Malgrange and Madariaga, 1983; Christensen and Ruff, 1983; 1988; Dmowska et al., 1986; Astiz and Kanamori, 1986; Dmowska et al., 1988; Dmowska and Lovison, 1988; Lay et al., 1989). These studies show that in some gaps, a precursory combination of shallow compressional outer-rise and tensional down-dip events is observed before the occurrence of a great earthquake.

Dmowska et al. (1988) presented a simple one-dimensional model of stress accumulation and transfer in coupled subduction zones during the earthquake cycle, concluding that the combination of both high compressional stress in the outer-rise and tensional intraplate stress in the descending slab imply that the locked thrust zone is subjected to high shear loading, and consequently are signals of maturity of the corresponding seismic cycle. Dmowska et al. (1988) also suggested that in some cases, the lower portions of the interplate thrust contact undergo periods of active seismicity mainly in the last part of the cycle.

These periods of activity are preceded by a temporary quiescence of extensional seismicity downdip in the slab, suggesting that thrust events in the lower, and hence hotter, regions of the contact zone may be a sign of an aseismic preslip taking place there prior to a great earthquake. However, if a preslip episode is included in their model, the behavior in the downdip and the outer-rise zones is appreciably modified; if the slip is large enough, it can reverse the predicted shallow compressional outer-rise and tensional downdip events prior to the expected great earthquake. Thus a combination of tensional outer-rise earthquakes and compressional downdip events could be also a precursory signal of terminal maturity in a subduction zone, resulting in an ambiguous signal of the stress transfer model.

Lay et al. (1989) presented a systematic analysis of circum-Pacific subduction zones where large interplate thrust events occur. They conclude that outer-rise compressional events have occurred prior to several large thrust events, whereas outer-rise tensional events generally occur after interplate ruptures. In the intermediate depth range, large down-dip tensional events generally precede interplate thrust faulting, and are often concentrated near the down-dip edge of the coupled zone. Lay et al. (1989) also proposed an schematic dynamic stress model that summarizes their observations.

Taking into account that the southern Peru and northern Chile seismic gaps are considered mature seismic gaps (e.g. Lay et al., 1989; Comte and Pardo, 1991), the aim of this work is to analyze the space-time variations of the seismicity in both gaps, in order to see whether they present the predicted precursory combination observed in some other seismic gaps.

#### *Teleseismic Data Used in the Analysis*

The presumed rupture areas of the 1868 and 1877 great earthquakes are presented on Figure 1. Unfortunately, no permanent local seismic networks exist in southern Peru and northern Chile. Thus only a spatio-temporal analysis of the seismicity observed with global networks can be carried out. In this analysis, the USGS-NEIC (1965-1988) and PDE (1989-1991) catalogs are used and a cut-off magnitude of  $m_b=5.0$  was determined for the whole region based on the  $\text{Log}(N)$  versus  $m_b$  relation (Figure 1). However, this analysis is done only for events of magnitudes greater than 5.5 because they present a better epicentral control and the majority of them have well constrained focal mechanism solutions.

For southern Peru and northern Chile regions, a plot of distances normal to the trench versus time was drawn in order to observe globally the spatio-temporal behavior of the seismicity including the outer-rise and the down-dip regions (Figures 2a, 2b and 3a). Table 1 presents the events with reported focal mechanisms used in following discussion.

For the region located between distances of -100 to 100 km from the trench, an analysis of lower magnitude events ( $5.0 \leq m_b < 5.5$ ) is also carried out in order to observe in more detail the variations of seismicity in this specific region (Figures 2c and 3b). This is because the outer-rise region exhibits the least ambiguous behavior, where compressional activity is observed apparently only prior to major thrust earthquakes (Christensen and Ruff, 1988, Lay et al., 1989).

*Spatio Temporal Variation of Seismicity in Southern Peru*

In southern Peru, the sequence of great historical earthquakes is well documented, with at least three great events reported in 1604, 1784 and 1868 with estimated magnitudes greater than 8.5, determined from macroseismic information (Dorbath et al., 1990; Comte and Pardo, 1991). Between the 1604 and the 1784 earthquakes, two other large events occurred in 1687 and 1715, with estimated magnitudes of between 7.5 and 8.0; together, both events apparently filled the estimated rupture zone of the great events that occur in the region. Based on this sequence of great earthquakes, it is reasonable to expect that this region is mature and nearing the next great event (Comte and Pardo, 1991).

If this were the case, the expected behavior of the seismicity, as was observed in some other subduction zones, would consist of shallow compressional earthquakes near the outer-rise and tensional down-dip events at depth. This stress distribution has been interpreted as a result of a locked interplate boundary where the oceanic plate in the outer-rise is under increased compression, and the downgoing slab stretches under tension from the interplate coupled zone.

Four compressional events ( $m_b \geq 6.0$ ) can be observed in southern Peru (Figure 2a): on November 29, 1989 in the northern edge of the presumed 1868 rupture area, on August 13, 1987 in the southern edge of the 1868 rupture area, and the two subsequent events located around the middle of that area, on February 16, 1979 and April 12, 1988. The presence of frequent tensional intraplate activity can also be observed in southern Peru (Figure 2a), and a change from compressional to tensional regime can be noted at about 160 km from the trench; this change is probably associated with the coupled-uncoupled transition of the interplate contact zone. That is, from distances of about 160 to 350 km from the trench the seismic activity is mainly tensional, and from 100 to 160 km from the trench the seismicity is mainly compressional.

It is interesting to note that the two events: the normal-faulting event of July 30, 1965 (72 km depth) and the thrust event of August 13, 1987 (36 km depth) occurred at approximately the same epicenter but with a difference in depth of about 36 km. This is similar to the sequence of the normal-faulting event of March 3, 1965 (72 km depth) and the thrust-faulting event of July 9, 1971 (52 km depth) that occurred near La Ligua (central Chile) (Malgrange and Madariaga, 1983). In this case, with a longer time interval between them (about 22 years) than in La Ligua.

Offshore, an absence of seismicity between -100 to 100 km from the trench can be

observed between 1965 and 1987, followed by two tensional events that occurred on March 10, 1987 ( $m_b=5.5, 5.7$ ) at about 50 km from the trench, preceding a larger normal faulting outer-rise event on March 9, 1988 ( $m_b=6.0$ ) (Figure 2a). The reverse and normal faulting events that occurred after 1987 between -100 to 350 km from the trench (Figure 2b), may be explained by a mechanical pull and push interaction along the slab.

The compressional events near the contact zone that have occurred since 1987 in southern Peru, could be interpreted as a sign of a seismic preslip near the seismogenic contact zone. This apparent preslip and the burst of tensional intraplate activity may reflect the maturity of the southern Peru seismic gap. However, it does not present the expected precursory compressional outer-rise events in the case of earthquakes with magnitudes  $m_b \geq 5.5$ .

The behavior observed in the outer-rise and the inner-trench regions for low magnitude events ( $5.0 \leq m_b < 5.5$ ) is very similar to that observed for earthquakes of greater magnitude ( $m_b \geq 5.5$ ); tensional events are observed near the trench and compressional events downdip from it (Figure 2c). There are four low magnitude ( $5.0 \leq m_b < 5.5$ ) compressional events in southern Peru on January 22, 1978 ( $m_b=5.4$ ), April 15, 1978 ( $m_b=5.3$ ), March 7, 1980 ( $m_b=5.4$ ) and July 11, 1982 ( $m_b=5.3$ ) which are located close to the compressional event of February 16, 1979 ( $m_b=6.2$ ) and its main aftershock ( $m_b=5.5$ ). This compressional sequence between 1978 and 1982 preceded by about nine years the one that occurred between 1987 and 1989. The two outer-rise events and the two events located very close to the trench are too small ( $m_b \sim 5.0$ ) to determine a CMT solution or a first motion focal mechanism.

### *Spatio-Temporal Variation of Seismicity in Northern Chile*

The distribution of seismicity in northern Chile is more complicated than that of southern Peru because the sequence of historical earthquakes is not well established. The last great earthquake occurred in 1877. Unfortunately, the preceding great events are not well documented due to the absence of population before the XIX century. This region is in a similar tectonic environment as that of southern Peru, so the periods of recurrence in both regions are probably of the same order. Thus northern Chile has been considered, as the southern Peru region, as a seismic gap of substantial maturity (Lay et al., 1989; Comte and Pardo, 1991).

Only two compressional events ( $m_b \geq 6.0$ ) have occurred in northern Chile (Figure 3a)

since 1965: the December 21, 1967 thrust event ( $m_b=6.3$ ) located near the southern edge of the presumed rupture area of the 1877 great earthquake, and the November 28, 1970, compressional event ( $m_b=6.0$ ) located at about 100 km to the north of the 1967 earthquake. Large downdip tensional events ( $m_b \geq 6.0$ ) in the subducted slab exhibit a quasi-random distribution in time and space. The larger tensional earthquakes are those of August 20, 1965 ( $m_b=6.2$ ), May 11, 1967 ( $m_b=6.1$ ), December 27, 1967 ( $m_b=6.4$ ), June 19, 1970 ( $m_b=6.2$ ), November 30, 1976 ( $m_b=6.5$ ), May 26, 1980 ( $m_b=6.1$ ), December 12, 1980 ( $m_b=6.1$ ), and August 8, 1987 ( $m_b=6.4$ ).

Malgrange and Madariaga (1983) studied a sequence of earthquakes near Tocopilla ( $21.5^\circ\text{S}$ ) that started with a thrust event on December 21, 1967 ( $m_b=6.4$ ). This interplate event was followed by a sequence of deeper, intraplate earthquakes in the downgoing slab showing a combination of tensional (December 25, 1967;  $m_b=5.8$ , and June 19, 1970;  $m_b=6.2$ ), and compressional (November 28, 1970;  $m_b=6.0$ ) events. This suite of events occurred in close epicentral proximity. Without direct evidence of a double seismic zone in northern Chile, Malgrange and Madariaga (1983) interpreted the tensional events as a possible effect of the slab pull felt below the seismogenic zone associated with the December 21, 1967 thrust event.

In order to complete the sequence of the 1967-1971 earthquakes, the focal mechanisms of the August 21, 1971 ( $m_b=5.5$ ) event and the November 28, 1970 ( $m_b=5.9$ ) aftershock were determined using the polarity of first motions reported by the ISC bulletin (Figure 4a and 4b). Although the nodal planes of the fault plane solutions are not constrained, it is clear from the first motion data that they are reverse faulting events. As in southern Peru, the change from compressional to tensional regimes along the slab in northern Chile occurs at a distance of about 160 km from the trench (Figure 3a). The presence of frequent tensional activity in the subducted slab observed in the northern Chile gap may be interpreted as the result of the strongly coupled seismogenic thrust zone associated with the 1877 earthquake.

Northern Chile does not show the presence of outer-rise seismic activity ( $m_b \geq 6.0$ ). In fact, there is only one outer-rise event which occurred on February 23, 1975 ( $m_b=5.6$ ) (Figure 3a). The focal mechanism of this event was determined based on the first motion reported by the ISC and it shows normal faulting. Unfortunately, the data is not sufficient to constrain the fault planes (Figure 4c). As was shown for southern Peru, the northern Chile gap also does not present compressional outer-rise events of  $m_b \geq 5.5$ . However, four lower magnitude, outer-rise events ( $5.0 \leq m_b < 5.5$ ) can be observed in

northern Chile (Figure 3b); no reliable focal mechanisms are available for these events. The behavior of the compressional seismicity (Figure 3b) for this lower magnitude interval, is different to that observed for higher magnitudes ( $m_b \geq 5.5$ ). The absence of seismicity observed at distances of 0 to about 100 km from the trench for events  $m_b \geq 5.5$  is filled with smaller events  $5.0 \leq m_b < 5.5$ . A cluster of compressional events can be observed between 50 to 100 km from the trench, from May to August, 1987. This distribution of seismicity may be interpreted as seismic preslip occurring near the coupled zone, in a manner similar to that observed in southern Peru, but with lower magnitude events.

### *Summary and Conclusions*

The purpose of this work was to analyze two clearly recognized seismic gaps, in southern Peru and northern Chile, making use of current models of space-time variations in seismicity in order to elucidate their degree of maturity. Both gaps present some similarities: (1) the last great earthquake in each region occurred about 120 years ago, and no large thrust events have taken place within the gaps during the present century; (2) In both cases, the rate of convergence and the age of the oceanic sea-floor near the trench is almost identical. Therefore, it is expected that they would exhibit very similar patterns of seismicity. Although some similarities exist, the distribution of seismicity in the two gaps presents some important differences, mainly near the interplate contact zone. At this point, it is interesting to mention that, although observations in other subduction zones of the world show that the earthquake recurrence times and rupture length can vary between successive earthquake cycles (e.g. Comte et al., 1986; Thatcher, 1990; Ruff, 1992), the fact that the last great earthquakes that affected southern Peru (1868) and northern Chile (1877) have rupture lengths of about 450 km, suggests that they could represent the largest events of these regions. Therefore, the next great earthquakes may not necessarily be of the same magnitude as the latest events, but probably they will occur within the seismic gap areas analyzed by this work.

Neither southern Peru nor the northern Chile gaps clearly exhibit the precursory compressional outer-rise events during the time period studied. Furthermore, both gaps present down-dip intraplate tensional seismicity in the subducted slab, which is more intense in the northern Chile segment. For both regions, the change from compressional



to tensional regime within the subducted slab occurs at about 160 km from the trench, which is apparently associated with the coupled-uncoupled transition of the interplate contact zone.

There are, however, some differences in the space-time distribution of stresses and of seismicity in both gaps. In southern Peru, an increase of compressional seismicity near the contact zone is observed since 1987. In contrast, the northern Chile gap exhibits an absence of compressional activity ( $m_b \geq 5.5$ ) near the interplate contact since the December 21, 1967 sequence. This absence, however, is apparently filled with a cluster of lower magnitude compressional events that occurred during 1987. Also, the southern Peru gap shows a burst of tensional activity near the inner- and outer-rise zone during 1987, which is not observed in northern Chile.

Under an interpretation of stress transfer in the subduction zones, the continuous downdip tensional activity observed in southern Peru and northern Chile may be interpreted as evidence that these regions are strongly coupled. However, the fact that both the downdip tensional activity is more frequent in northern Chile than in southern Peru and that there is an absence of compressional activity ( $m_b \geq 5.5$ ) near the contact zone in northern Chile, may be considered as evidence that this gap is more mature than southern Peru.

On the other hand, the burst of both compressional seismicity near the contact zone, and the tensional activity near the inner- and outer-rise regions observed in southern Peru since 1987, may be interpreted in turn as a sign that a seismic preslip is taking place near the interplate contact. If the apparent seismic preslip is associated with the maturity of the gap, the fact that it is observed in northern Chile with lower magnitude earthquakes than those observed in southern Peru, may be then interpreted as representing that southern Peru is a more mature seismic gap than northern Chile.

In summary, contradictory results are obtained about the maturity of the northern Chile and southern Peru gaps using alternative interpretations of simple stress distribution and transfer models in and near the coupled interface in a subduction zone. Although similarities are observed in both gaps, there are sharp differences in the spatial distribution of seismicity and in the stress patterns in both segments of this subduction zone.

These results suggest that the complexity of the observed distribution of seismicity in seismic gaps can not always be explained with simple models of accumulation and transfer of stresses along the slab. Furthermore, the available database (~30 years) of reliably located seismicity for which focal mechanisms exist may not be sufficiently long

to draw firm conclusions about the long term distribution of stresses near the coupled zone.

### Acknowledgements

This work was greatly improved by the comments of R. Dmowska and one anonymous reviewer. We thank S. K. Singh and D. Byrne for their suggestions. The research was partially funded by Fundación Andes, Chile grant C-52040.

### References

- Araujo, M. and Suárez, G. (1993), Detailed geometry and state of stress of the subducted Nazca plate beneath central Chile and Argentina: Evidence from teleseismic focal depth determinations. *Geophys. J. Int.* in press.
- Astiz, L. and Kanamori, H. (1986), Interplate coupling and temporal variation of mechanisms of intermediate-depth earthquakes in Chile. *Bull. Seismol. Am.* 76, 1614-1622.
- Astiz, L., Lay, T., and Kanamori, H. (1988), Large intermediate-depth earthquakes and the subduction process. *Phys. Earth Planet. Inter.* 53, 80-166.
- Christensen, D., and Ruff, L. (1983), Outer-rise earthquakes and seismic coupling. *Geophys. Res. Lett.* 10, 697-700.
- Christensen, D., and Ruff, L. (1988), Seismic coupling and outer-rise earthquakes. *J. Geophys. Res.* 93, 13421-13444.
- Comte, D., Eisenberg, A., Lorca, E., Pardo, M., Ponce, L., Saragoni, R., Singh, S. K., and Suarez, G. (1986), The 1985 central Chile earthquake: A repeat of previous great earthquakes in the region?. *Science*, 233, 449-453.
- Comte, D., and Pardo, M. (1991), Reappraisal of great historical earthquakes in the Northern Chile and Southern Peru seismic gaps. *Natural Hazards* 4, 23-44.
- Dmowska, R., Lovison, L., and Rice, J. (1986), Stress accumulation and transfer between a subduction slab and the thrust contact zone during the whole earthquake cycle (abstract). *Eos Trans. AGU* 67, 307.
- Dmowska, R., Rice, J., Lovison, L., and Jossell, D. (1988), Stress transfer and seismic phenomena in coupled subduction zones during the earthquake cycle. *J. Geophys. Res.* 93, 7869-7884.
- Dmowska, R., and Lovison, L. (1988), Intermediate term seismic precursors for some

- coupled subduction zones. *Pure Appl. Geophys.* 126, 643-664.
- Dorbath, L., Cisternas, A., and Dorbath, C. (1990), Quantitative assesment of great earthquakes in Peru. *Bull. Seism. Soc. Amer.* 80, 551-576.
- Isacks, B., and Molnar, P. (1971), Distribution of stresses in the descending lithosphere from a global survey of focal-mechanism solutions of mantle earthquakes. *Rev. Geophys. Space Phys.* 9, 103-174.
- Kelleher, J. A. (1972), Rupture zones of large South American earthquakes and some predictions. *J. Geophys. Res.* 77, 2087-2103.
- Lay, T., Astiz, L., Kanamori, H., and Christensen, D. (1989), Temporal variation of large intraplate earthquakes in coupled subduction zones. *Phys. Earth Planet. Inter.* 54, 258-312.
- Malgrange, M., Deschamps, A., and Madariaga, R. (1981), Thrust and extensional faulting under the Chilean coast: 1965, 1971 Aconcagua earthquakes. *Geophys. J. R. Astron. Soc.* 66, 313-331.
- Malgrange, M., and Madariaga, R. (1983), Complex distribution of large thrust and normal-fault earthquakes in the Chilean subduction zone. *Geophys. J. R. Astron. Soc.* 73, 489-505.
- Nishenko, S. (1985), Seismic potential for large and great interplate earthquakes along the Chilean and southern Peruvian margins of South America: A quantitative reappraisal. *J. Geophys. Res.*, 90, 3589-3615.
- Stauder, W. (1973), Mechanism and spatial distribution of Chilean earthquakes with relation to subduction of the oceanic plate. *J. Geophys. Res.* 78, 5033-5061.
- Stauder, W. (1975), Subduction of the Nazca plate under Peru as evidenced by focal mechanisms and by seismicity. *J. Geophys. Res.* 80, 1053-1064.
- Ruff, L. (1992), Asperity distributions and large earthquake occurrence in subduction zones. *Tectonophys.*, 211, 61-83
- Thatcher, W. (1990), Order and diversity in the modes of circum-Pacific earthquake recurrence. *J. Geophys. Res.* 95, 2609-2623.

Table 1

Yr	M	D	h:m	Lat (S)	Lon (W)	Depth	$m_b$	T	Ref
1965	06	12	18:50	-20.500	-69.300	102	5.8	N	ST73
1965	07	30	05:45	-18.100	-70.800	72	6.0	N	ST73
1965	08	20	09:42	-18.900	-69.000	128	6.2	N	ST73
1965	12	30	06:16	-16.600	-71.100	112	5.7	N	IM71
1966	03	08	20:46	-20.000	-68.900	112	5.7	N	ST73
1966	08	24	07:17	-19.900	-69.100	100	5.5	N	ST73
1967	05	11	15:05	-20.258	-68.691	79	6.1	N	ST73
1967	12	21	02:25	-21.800	-70.000	33	6.3	C	ST73
1967	12	25	10:41	-21.500	-70.400	53	5.8	N	ST73
1967	12	27	09:17	-21.200	-68.300	135	6.4	N	ST73
1968	10	31	09:15	-16.289	-73.298	67	5.7	C	ST75
1969	07	19	04:54	-17.254	-72.519	54	5.9	C	ST75
1970	06	17	04:44	-15.753	-71.835	91	5.9	N	ST75
1970	06	19	10:56	-22.193	-70.515	52	6.2	N	ST73
1970	11	28	11:08	-20.921	-69.830	33	6.0	C	ST73
(*)	1970	11	28 14:45	-20.924	-69.872	34	5.9	C	CS
1971	08	14	15:00	-21.775	-67.230	189	5.7	N	AR92
1971	08	21	12:47	-21.774	-70.211	17	5.8	C	CS
1975	02	23	03:53	-21.727	-71.356	33	5.6	N	CS
1976	11	30	00:40	-20.520	-68.919	82	6.5	N	AL88
1977	12	31	07:53	-15.300	-71.680	158	5.9	N	CMT
1978	01	22	21:19	-16.131	-73.656	49	5.4	C	CMT
1978	04	15	13:49	-16.470	-73.514	50	5.3	C	CMT
1979	02	16	10:08	-16.390	-72.658	53	6.2	C	CMT
(*)	1979	02	16 22:18	-16.500	-72.656	52	5.5	C	CMT
1979	05	04	17:21	-21.560	-68.284	81	5.6	N	CMT
1979	05	21	22:22	-15.250	-70.089	208	6.0	C	CMT
1979	09	15	10:02	-15.634	-69.559	214	5.6	C	CMT
1980	03	07	08:25	-16.689	-72.952	43	5.4	C	CMT
1980	05	26	18:41	-19.364	-69.238	114	6.1	N	CMT
1980	06	16	05:45	-22.029	-68.459	87	5.5	N	CMT
1980	12	11	18:15	-21.272	-68.153	80	6.1	N	CMT
1981	03	26	18:04	-19.370	-68.957	138	5.8	N	CMT
1981	04	16	22:05	-20.162	-70.699	33	5.1	C	CMT
1981	06	21	10:30	-20.256	-70.446	36	5.2	C	CMT
1982	07	11	02:13	-16.649	-73.214	38	5.3	C	CMT
1982	09	15	20:22	-14.493	-70.785	128	6.0	N	CMT
1982	12	31	03:47	-20.993	-68.464	118	5.7	N	CMT
1983	01	10	09:17	-22.006	-68.470	121	5.6	N	CMT
1983	05	23	00:54	-19.065	-69.139	110	5.5	N	CMT
1983	09	01	20:01	-17.330	-69.932	105	6.0	N	CMT
1984	02	26	08:18	-17.316	-70.526	113	5.8	N	CMT
1984	06	18	11:20	-15.705	-72.491	116	5.8	N	CMT
1985	05	18	16:59	-19.000	-69.053	109	5.5	N	CMT
1986	02	20	09:16	-21.122	-70.116	33	5.7	N	CMT
1986	03	15	11:29	-18.909	-67.391	243	5.6	N	CMT

Table 1 (continued)

Yr	M	D	h:m	Lat (S)	Lon (W)	Depth	$m_b$	T	Ref
1987	03	10	00:22	-18.448	-72.035	41	5.7	N	CMT
(*)	1987	03	10 02:18	-18.341	-71.976	36	5.5	N	CMT
	1987	03	12 06:07	-18.467	-72.192	35	5.1	N	CMT
	1987	05	12 16:12	-21.694	-68.222	77	5.5	N	CMT
	1987	05	23 05:01	-20.151	-70.688	36	5.3	C	CMT
	1987	06	11 05:08	-20.559	-70.855	33	5.1	C	CMT
	1987	06	19 19:00	-21.213	-68.362	86	5.6	N	CMT
	1987	08	08 15:48	-19.022	-69.991	69	6.4	N	CMT
	1987	08	13 15:23	-17.897	-70.931	36	6.1	C	CMT
	1987	08	24 06:09	-20.096	-70.632	33	5.2	C	CMT
	1987	12	03 11:04	-21.380	-68.215	117	5.5	N	CMT
	1988	02	22 19:13	-20.833	-69.785	70	5.9	N	CMT
	1988	03	09 21:33	-17.327	-74.154	32	6.0	N	CMT
	1988	04	12 23:19	-17.192	-72.305	33	6.1	C	CMT
	1988	04	12 23:55	-17.478	-72.503	33	5.4	C	CMT
	1988	04	13 00:39	-17.256	-72.518	16	5.9	C	CMT
	1988	04	13 06:22	-17.489	-72.505	36	5.2	C	CMT
	1988	04	17 02:50	-17.420	-72.387	33	5.4	C	CMT
	1988	07	04 13:54	-17.636	-71.718	19	5.8	C	CMT
	1989	02	17 15:12	-17.509	-72.609	48	5.3	C	CMT
	1989	03	29 04:06	-18.353	-72.380	42	5.4	N	CMT
	1989	04	05 23:47	-20.816	-69.427	115	5.6	N	CMT
	1989	11	01 06:40	-21.252	-68.099	143	5.8	N	CMT
	1989	11	29 01:00	-15.781	-73.254	74	6.1	C	CMT
	1990	01	05 13:03	-19.258	-69.529	109	5.0	N	CMT
	1990	04	04 05:47	-16.179	-72.974	93	5.5	N	CMT
	1990	04	20 18 23	-14.859	-71.374	144	5.1	N	CMT
	1990	06	08 13:49	-17.573	-71.824	27	5.6	C	CMT
	1990	06	18 19:02	-21.825	-68.438	117	5.3	N	CMT
	1990	06	21 11:48	-19.648	-69.128	103	5.3	N	CMT
	1990	08	15 13:23	-18.834	-69.096	120	5.2	N	CMT
	1990	08	28 08:58	-19.645	-69.876	64	5.2	N	CMT
	1990	10	10 01:00	-19.503	-66.618	266	5.8	N	CMT
	1990	11	04 18:13	-15.721	-72.619	121	5.4	C	CMT
	1991	05	24 20:50	-16.506	-70.701	128	6.3	N	CMT
	1991	07	09 05:54	-20.599	-68.803	101	5.3	N	CMT
	1991	07	23 19:44	-15.679	-71.574	5	5.0	N	CMT
	1991	08	27 04:16	-20.855	-68.775	123	5.0	N	CMT
	1991	08	27 11:46	-16.278	-73.278	74	5.3	N	CMT
	1991	08	27 11:58	-21.657	-68.506	116	5.1	N	CMT
	1991	08	27 11:46	-16.278	-73.278	74	5.3	N	CMT
	1991	12	02 17:27	-15.867	-69.288	241	5.1	N	CMT
	1991	12	15 18:56	-17.521	-70.422	104	5.6	N	CMT

Table 1.- Catalog of events with focal mechanism solutions used in this study. Yr M D: Date (year, month, day); h:m: Origin time (hour : minute); T: N (tensional) and C (compresional).  
References: ST73: Stauder (1973); IM71 Isacks and Molnar (1971); ST75: Stauder (1975); AL88: Astiz et al. (1988); AR92: Araujo and Suarez (1993); CMT: Centroid Moment Tensor (Harvard); CS: this work.

## FIGURE CAPTIONS

**Figure 1.-** Southern Peru and northern Chile regions, where the dashed lines indicate the 1868 and 1877 estimated rupture zones (Comte and Pardo, 1991). Earthquake frequency-magnitude relation for southern Peru and northern Chile regions using the NEIC (1965-1988) and PDE (1989-1991) catalogs is also shown in the lower-left corner. N is the accumulated number of events of magnitude  $m_b$  or greater.

**Figure 2a.-** To the left, the distance from the trench (D, km) versus time (yr) plot of events ( $m_b \geq 5.5$ ) in southern Peru is shown. The dashed line indicates the location of the trench. To the right, the epicentral distribution of events is presented. Solid circles denote compressional events, open circles denote normal faulting, and open rectangles correspond to unknown focal mechanism solutions (Table 1). The size of the symbols is related to the magnitude of the events, as it is indicated on the Figure. Each event with known focal mechanism solution is identified with the year, month and day of occurrence; an asterisk is used for the second event, when two earthquakes occurred on the same day.

**Figure 2b.-** Enlargement of the data shown in Figure 2a for the 1987-1991 time interval. Symbols as in Figure 2a.

**Figure 2c.-** Distance from the trench versus time plot (to the left) and epicentral distribution (to the right) of events  $5.0 \leq m_b < 5.5$ , in the inner- and outer-rise southern Peru region.

**Figure 3a.-** Distance from the trench versus time plot (to the left) and epicentral distribution (to the right) of events  $m_b \geq 5.5$  in northern Chile. Symbols as in Figure 2a.

**Figure 3b.-** Distance from the trench versus time plot (to the left) and epicentral distribution (to the right) of events  $5.0 \leq m_b < 5.5$ , in the inner- and outer-rise northern Chile region. Symbols as in Figure 2a.

**Figure 4.-** Lower hemispheric projections of the first motion polarities reported by the ISC bulletin for three northern Chile events. Closed and open circles represent compressional and dilational first motion. The data are not sufficient to constrain the fault planes, but it can be observed that the August 21, 1971 ( $m_b=5.5$ ) and the November 28, 1970 ( $m_b=5.9$ ) earthquakes are compressional; and the February 23, 1975 ( $m_b=5.6$ ) outer rise event is tensional.

Figure 1

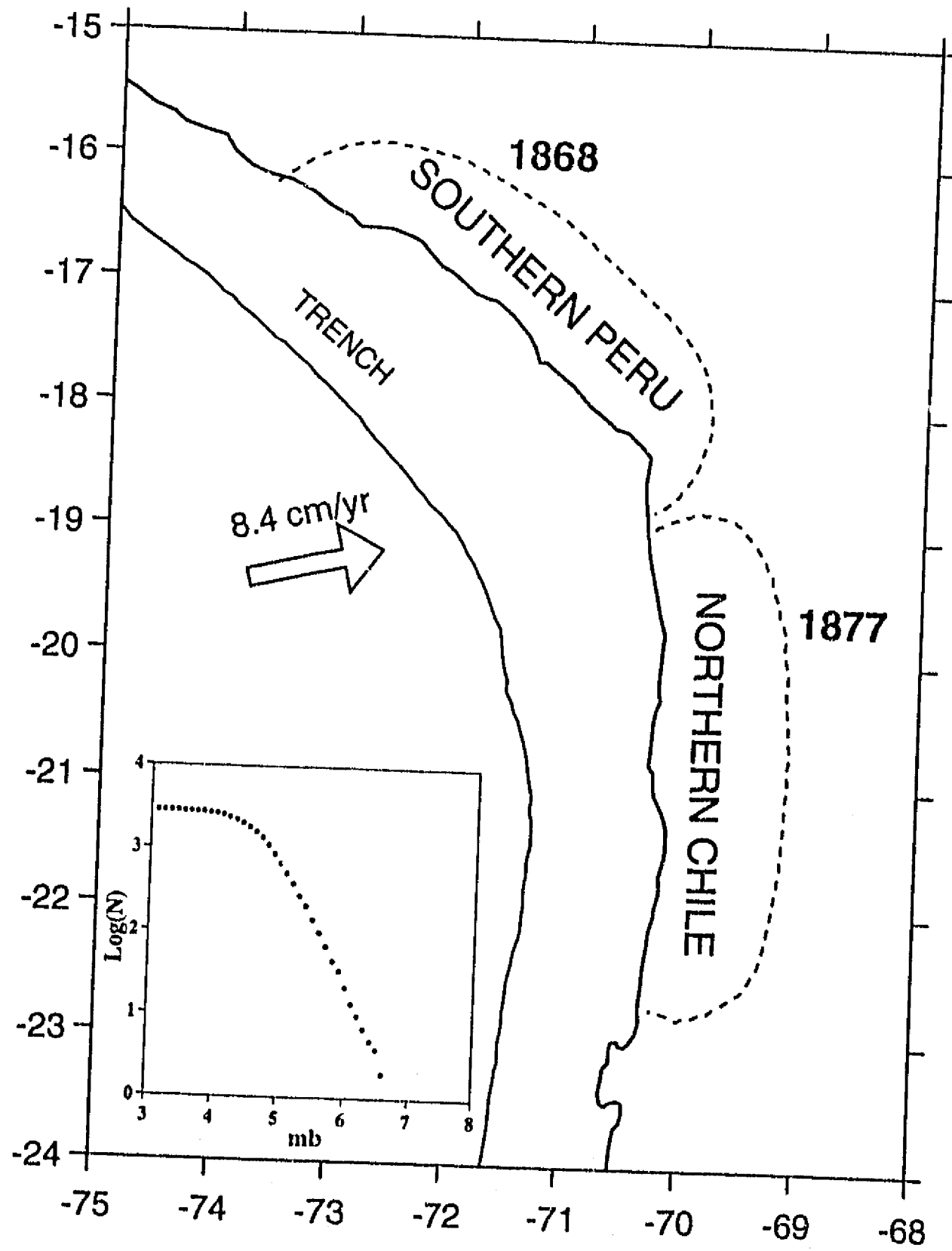
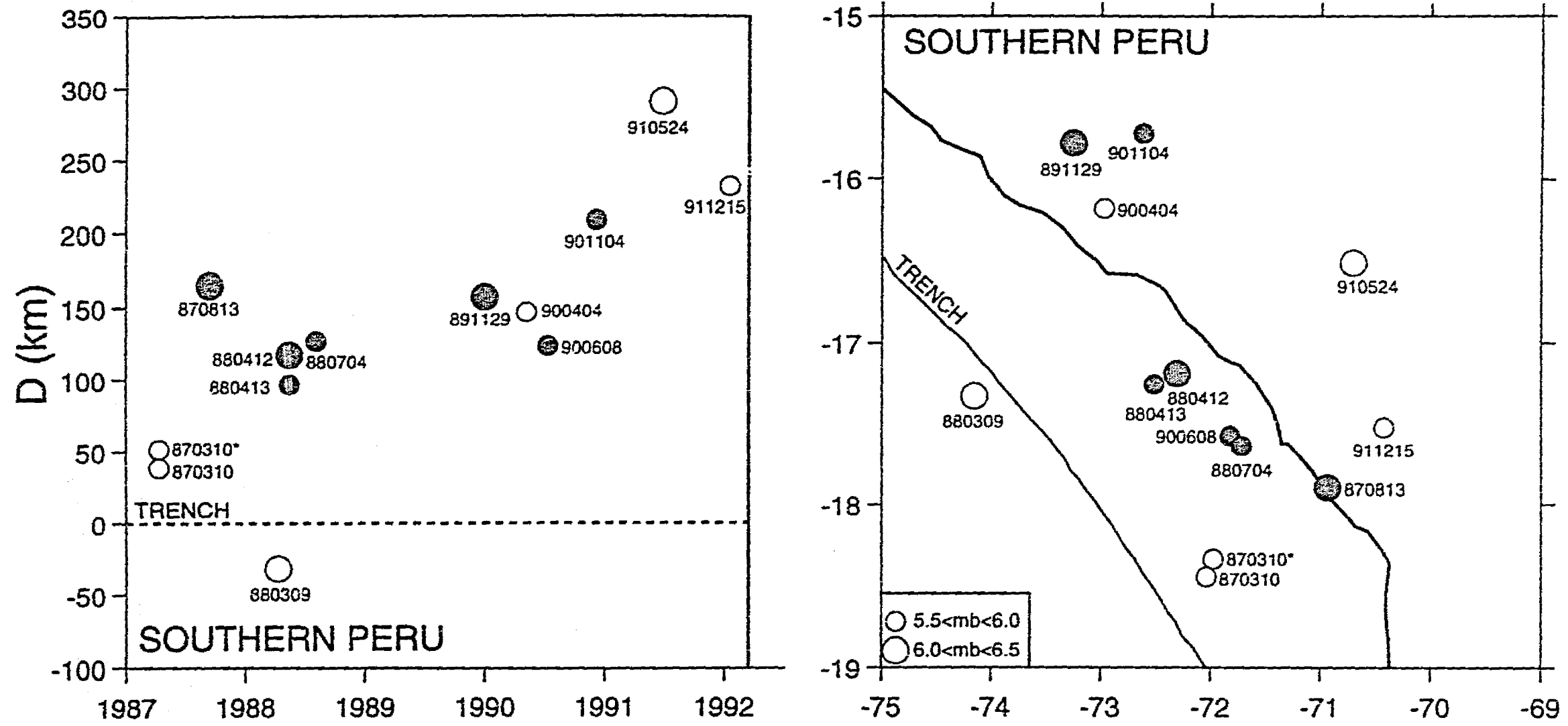






Figure 2b



Comte and Suarez: Spatio-Temporal Variations of Seismicity

30

Figure 2c

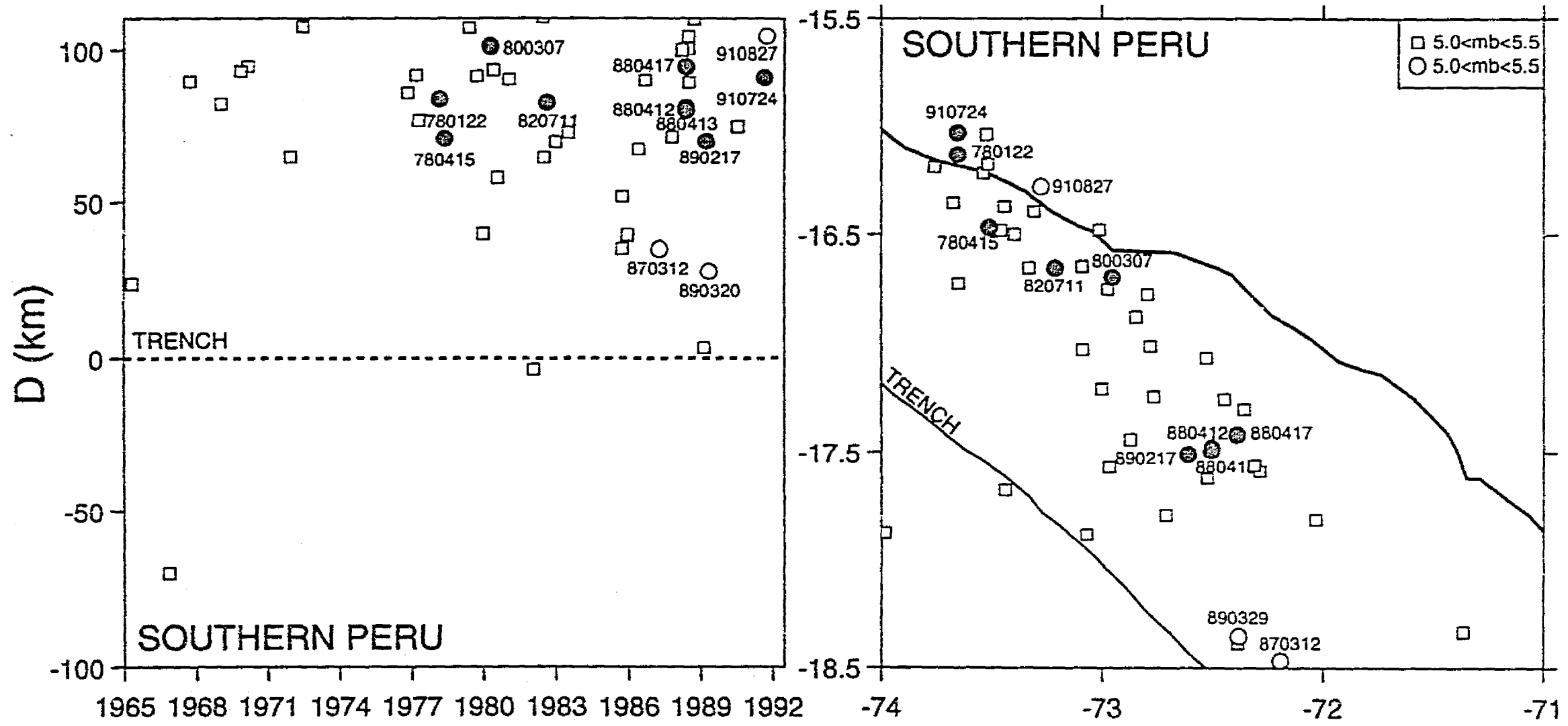


Figure 3a

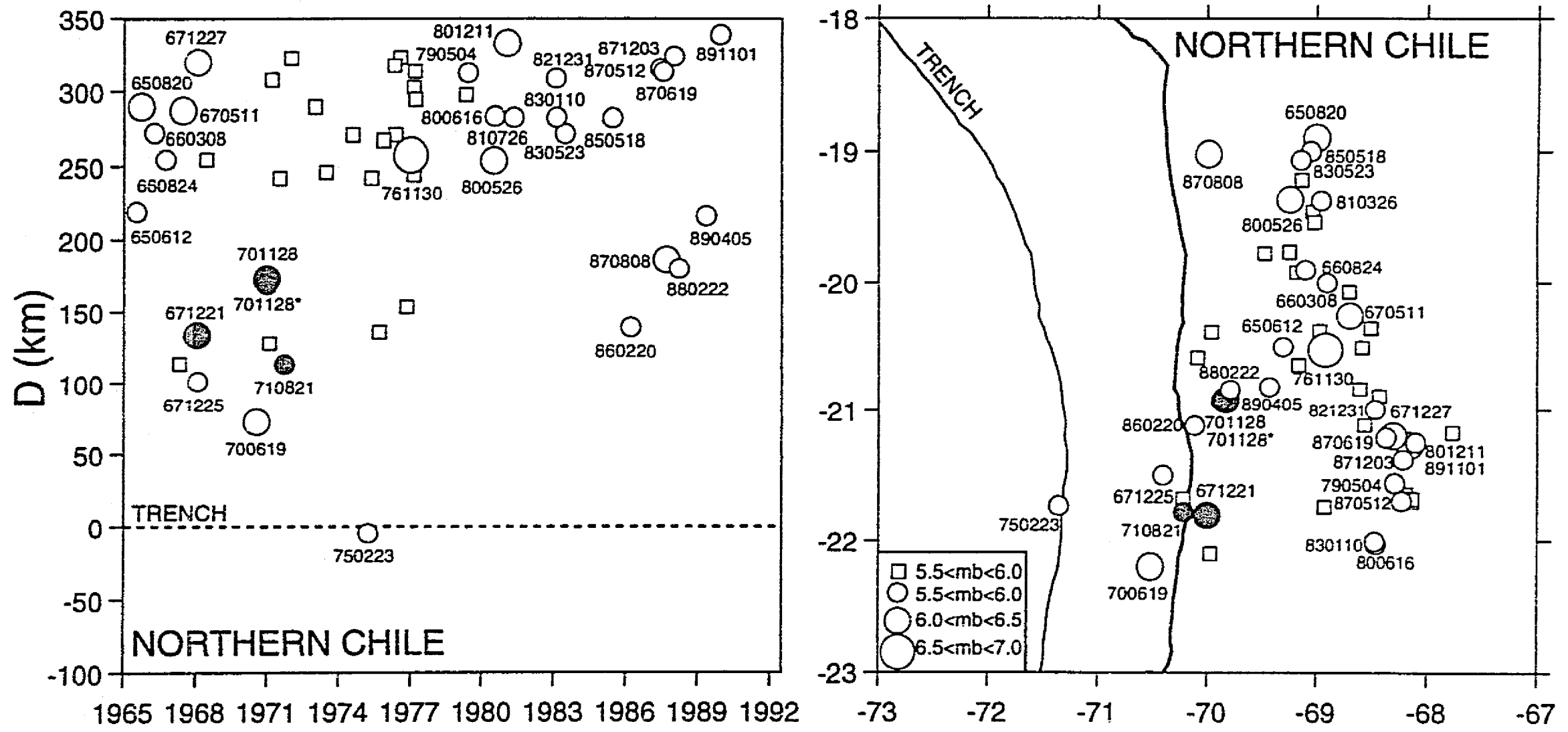


Figure 3b

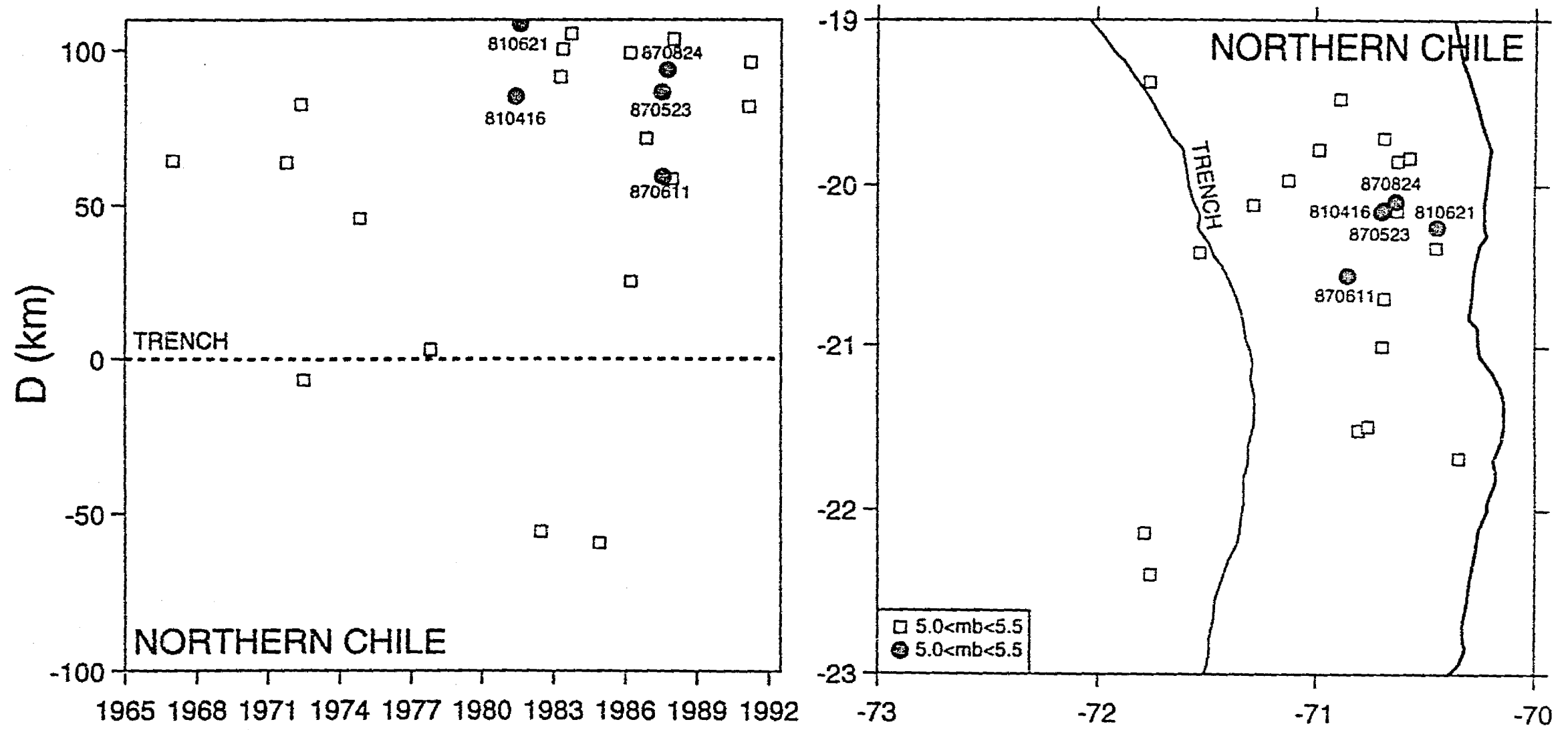
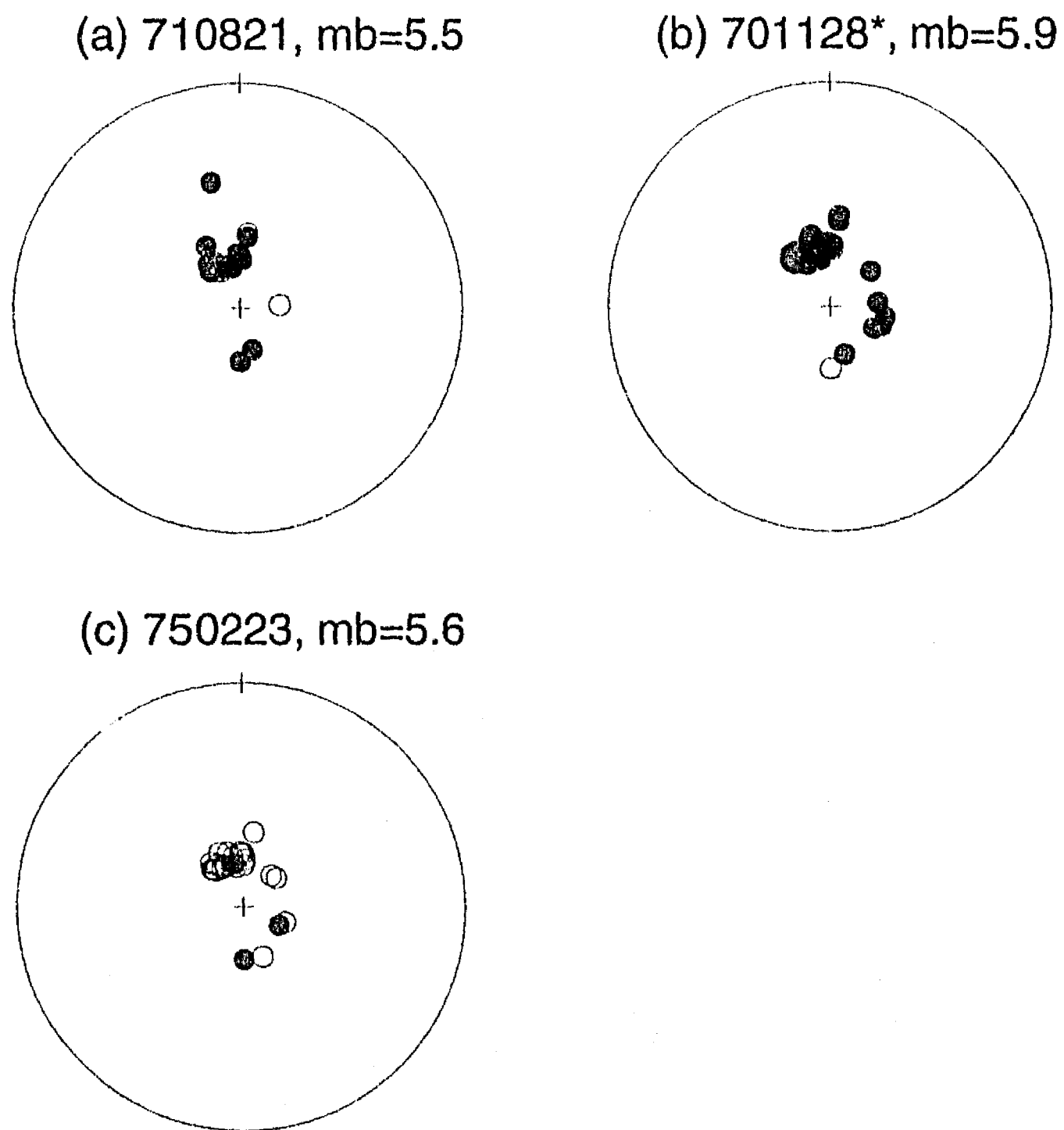


Figure 4



SEISMOGENIC INTERPLATE CONTACT ZONE AND CRUSTAL  
SEISMICITY AROUND ANTOFAGASTA, NORTHERN CHILE  
USING LOCAL DATA

D. Comte<sup>1,3</sup>, M. Pardo<sup>1,3</sup>, L. Dorbath<sup>2,4</sup>, C. Dorbath<sup>2,4</sup>,  
H. Haessler<sup>2</sup>, L. Rivera<sup>2</sup>, A. Cisternas<sup>2</sup>, and L. Ponce<sup>3</sup>

<sup>1</sup>Depto de Geología y Geofísica, U. de Chile, Casilla 2777, Santiago - Chile

<sup>2</sup>Institut de Physique du Globe de Strasbourg, 5 Rue Rene Descartes, 67084 Strasbourg Cedex, France

<sup>3</sup>UACPyP, Instituto de Geofísica, UNAM, México D.F. 04510, México

<sup>4</sup>ORSTOM, 213 Rue La Fayette 75480 Paris, Cedex 10, France

*Geophysical Journal International, en prensa*

SUMMARY

During september and october of 1988, a microseismic field experiment was carried out around the city of Antofagasta, northern Chile, with 29 portable analog and digital stations. A total of 197 reliable microearthquake locations and 19 focal mechanisms were determined. We propose the possibility to estimate the maximum depth of the coupled-uncoupled transition of the subducting lithosphere using local data, defined by the depth of the expected change of the stress field from compressional to tensional along the slab. This change is observed at about 70 km in depth in the Antofagasta field work. Two estimations of the width of the seismogenic interplate contact are discussed: (1) The maximum depth of the coupled zone defined by the observed maximum depth of the shallow-dipping thrust events recorded during the experiment of 47 km, corresponding to a width of the seismogenic contact zone of about 90 km. (2) The maximum depth of the coupled zone defined by the depth of the observed change from compressional to tensional stress field which is 70 km and corresponds to a width of the seismogenic contact zone of about 130 km. With both values, the maximum magnitude  $M_S$  estimated for the region varies between 8.6 to 8.7. No shallow event associated with the Atacama fault system was observed during the experiment.

**Key words:** microseismicity, morphology of the subduction, seismogenic interplate contact, northern Chile, Atacama fault .

## INTRODUCTION

Northern Chile has been recognized as an important seismic gap where a major earthquake may be expected in the near future. (Kelleher 1972; McCann et al. 1979; Nishenko 1985; Comte & Pardo 1991). However, the Wadati-Benioff zone is poorly established because almost all the seismic studies related to northern Chile (e.g., Barazangi & Isacks 1976; Araujo 1985; Chowdhury & Whiteman 1987; Isacks 1988) have used teleseismic data, due to the lack of regional and local networks.

The region studied here is close to the southern edge of the region which ruptured during the last great ( $M_w=8.8$ ) 1877 earthquake (Dorbath et al. 1990; Comte & Pardo 1991). No major thrust event ( $M_S>7.5$ ) has affected this region during this century. Moreover, no historical great earthquake is known to have occurred in the coastal zone south of Antofagasta ( $24^\circ$  to  $25^\circ$ S).

During september and october, 1988 a joint experiment involving the University of Chile, the Institut de Physique du Globe de Strasbourg and the Institut Français de Recherche Scientifique pour le Développement en Coopération (ORSTOM) was conducted over an area of about 150 km in width around Antofagasta (northern Chile) to study the morphology of the subducted slab and the extent of the coupled zone between the Nazca and the South American plates.

The extent of seismically coupled zones have been studied in subduction regions mainly using globally recorded data. Recently, Tichelaar & Ruff (1991) studied the seismic coupling along the Chilean subduction zone using  $M>6$  events. However due to the lack of significant thrust events in northern Chile since the great 1877 earthquake, reliable estimation of the maximum depth of coupling in this region using teleseismic data is uncertain.

In this study, we analyze the subduction morphology around Antofagasta using reliable local data. We also propose a possibility to map the coupled-uncoupled transition along the subducting slab to estimate the maximum depth of the seismogenic contact zone.

Another objective of the 1988 campaign was to investigate the crustal seismicity in relation with the main tectonic features. In northern Chile two mega-fault systems are present: the Atacama fault and the Coastal Scarp. The nature and the kinematics of both structures have been controversial: Arabaz (1971) stated that the Atacama fault acts mainly as a normal fault, while Armijo & Thiele (1990) observed mostly left lateral

movement along the central part of the fault. Naranjo (1987) suggests that the Atacama fault is presently inactive as a strike-slip fault, and Yañez (1992) indicates that the Atacama fault was very active during the Mesozoic, but may have remained inactive since the Tertiary because of the migration of the volcanic front 200 km landward.

## DATA ACQUISITION AND PROCESSING

### *Seismological network*

A seismological network of 29 portable stations was installed around the city of Antofagasta with a 150 km radius during September-October 1988 (Figure 1). The location of each station was determined using topographic maps (1:50.000) and the satellite positioning system TRANSIT. The error in the locations is estimated to be less than 150 m (Table 1).

Three types of seismic stations were used: (1) Thirteen MEQ-800 smoked-paper recording stations with vertical L-4C (1 Hz) seismometers. The gains were set up at 84 dB with open filters, and the paper speed was 60 mm/min. The drifts of the internal clocks were measured by comparing the internal time with the reference time pulses transmitted by the WWN (Colorado, U.S.A.) or LOL (Argentina) stations. (2) Eight digital GEOSTRAS variable gain stations with three-component L-22 (2 Hz) seismometers. The digital signals were multiplexed and registered on magnetic tapes. The time signals were obtained from the worldwide OMEGA system. (3) A telemetric digital network of 7 stations with vertical L-4C (1 Hz) seismometers whose signals were radio-transmitted and recorded at a central station which was also equipped with a three component L-22 (2 Hz) seismometer. The signals and the OMEGA time were multiplexed and recorded on magnetic tapes.

### *Location of the events*

For the analog records the accuracy of the P and of the S readings are estimated to be about 0.1 s and 0.5 s respectively, while for the digital stations the accuracy of these readings is about 0.01 s and 0.2 s, respectively. The highest precision S wave arrival times were obtained using the horizontal components of the digital instruments. For some periods the OMEGA clock was not synchronized with the radio signal at some GEOSTRAS stations. In these cases absolute time was not available and only the polarity and the S-P time were used.



The events were located using the HYPO71PC program (Lee & Valdes 1978). The velocity model used (Table 2) was inferred from the seismic refraction studies conducted by Wigger (1988) near Antofagasta. The readings with high residuals were verified and reread.

The following parameters were varied to check the reliability of the solutions: (i) the initial depth, from 0 to 250 km in variable (10-25 km) intervals, (ii) the velocity model was changed to a simple one consisting of a layer over a half-space, and (iii) the  $V_p/V_s$  ratio was varied from 1.6 to 1.8 at 0.4 increments. An event location was considered reliable if it fulfilled the following criteria: (1) It had a minimum of 10 phase readings, including at least 3 S phases, and the distance between the epicenter and the nearest station with an S reading was smaller than the calculated depth. (2) The epicentral and the depth variations were smaller than  $\pm 2.5$  km, when the initial depth and the velocity model were varied as mentioned before. (3) The epicentral and the depth variations were lesser than  $\pm 5$  km, when the  $V_p/V_s$  ratio was varied as is indicated in (iii).

With these criteria, 197 reliable locations were determined with magnitudes  $2 \leq M_d \leq 5$  and  $RMS \leq 0.3$  s. These events were then used as master events to relocate all the microearthquakes that do not fit the distance-depth criterion, but have at least 20 phase readings. Forty eight events were thus relocated. The epicentral distribution of the reliable and relocated events is shown in Figure 1. The magnitude  $M_d$  was estimated with the coda duration  $T$  and the epicentral distance  $D$  according to the relation given by Lee et al. (1972),  $M_d = 0.87 + 2 \log(T) + 0.0035D$ , where  $T$  is in seconds and  $D$  in kilometers.

No event was located from the trench to 80 km eastward with the criteria described above, probably due to the lack of off-coast coverage. The seismic activity is not evenly distributed but clusters in elongated bands nearly parallel to the coast and intense swarms, particularly to the east. An important part of the seismicity took place eastward, outside of the network.

Considering that the definition of the auxiliary nodal plane of the focal mechanisms is not always well constrained, a joint focal mechanism and stress tensor inversion were carried out from the first motion polarities using the Rivera and Cisternas (1990) algorithm. The 15 individual and the four composite focal mechanisms obtained are presented in Figures 2 and 3 (Table 3). The composite mechanisms (2, 5, 6, and 16, Table 3) combine events with epicentral and depth differences of less than 10 km.

Six cross-sections from 0 to 600 km distance from trench in the direction of the convergence of the Nazca plate with a width of  $0.4^\circ$  were drawn using both reliable and

relocated events (Figures 1 and 4). Because the relocated events are mostly on the edges or outside of the network, these events were included in the cross-sections mainly to obtain a more complete coverage of the coastal and the down-dip parts of the slab. Lateral lower hemispheric projection of the focal mechanisms obtained are shown in Figure 5.

## RESULTS

### *Wadati-Benioff zone*

We find that at shallow depths (20-70 km) the dip angle of the subducting plate is about  $18^\circ$  and at greater depths (70-250 km) the dip angle steepens to about  $30^\circ$  (Figure 5). These values agree with those determined using global data (Jarrard, 1986).

The cross-sections C2, C3 and C4 show a weak activity within the area of the network coverage, at distances of between 150 and 220 km from the trench (Figure 4). This decrease in seismic activity is not observed in C1 and C5. The C6 cross-section corresponds to the southern edge of the network, and it will not be included in the following discussion because it has only few events, and most of them are relocated microearthquakes. A quite similar pattern of seismic activity is also observed in other parts of the subduction zones along South America, for example in southern Peru (Grange et al. 1984).

Another absence of seismicity is observed from about 130 to 200 km in depth along the slab. This absence is well correlated with the presence of the active volcanoes in the Andean range and it probably correspond to partial melting of the upper-part of the subducted slab..

In C3, C4, C5 and C6 cross-sections, a cluster of seismicity is also observed at depths between 200 to 260 km.

### *Reverse faulting events*

Three shallow-dipping thrust faulting focal mechanism solutions were determined: two for individual earthquakes (3 and 4) and the third is a composite solution of two events (5) (Figure 3a, Table 3). Within the uncertainties of the poorly constrained nodal plane of the focal mechanism solutions of these thrust events (indicated in Figure 2), we can conclude that the average slip direction of these events are not in contradiction with that estimated in the region from global plate tectonic models ( $N77^\circ E$ , NUVEL-1, DeMets et al. 1990).

The depth of the thrust events varies from 32 to 47 km at distances between 90 and 140 km from the trench (Figure 5). The seismogenic interplate contact thus reaches at least 47 km in depth. This depth is about twice the maximum depth observed for Guerrero, México (20-25 km) and it is in accordance with the scale relation 2:1 pointed out by Suárez et al. (1990) for the subduction zones of Mexico and Chile.

Four reverse faulting mechanisms with a high dip angle were also determined (1, 2, 6, and 7; Figure 3a). These events occurred from 120 to 200 km from the trench at depths varying from 40 to 78 km and should be interpreted as resulting of faulting within the subducted slab (Figure 5).

#### *Shallow normal faulting events*

Two normal faulting focal mechanisms were determined (12 and 13, Figure 3b, Table 3). The events occurred at a distance of 130 km from the trench at depths of 38 and 52 km respectively, in the same distance range from the trench where thrust faulting is also observed (Figure 5). The tensional field associated with these events contrasts with the compressional field found at the same distances from the trench and at about the same depths. These epicenters are close to the site where the main branch of the Atacama fault changes its azimuth from N45°E to a more NS direction (Figure 3b). Considering the depth of both events it is difficult to associate them with the Atacama fault system, and in Figure 5 it can be observed that they are clearly inside the Wadati-Benioff plane. More data are needed to establish if there is a relation between the two phenomena.

#### *Intermediate-depth normal faulting events*

Ten normal faulting events were determined (8, 9, 10, 11, 14, 15, 16, 17, 18, and 19, Figure 3b, Table 3). These intraplate events occurred at distances of some 200 to 290 km from the trench and their depths varied from 68 to 85 km (Figure 5). Therefore, a change from compressional to tensional stress field can be observed approximately at 200 km from the trench, corresponding to a depth of about 70 km.

#### *Crustal seismicity*

Twelve microearthquakes were located with depths shallower than 30 km (Figure 6). However, most of them have epicenters in the ocean and are probably associated to the slab. One event close to the main branch of the Atacama fault system had a depth of 28 km, its focal mechanism is not reliable, and it is probably associated with the subduction

of the Nazca plate and does not reflect crustal deformation of the overlying plate (Figure 5).

A cluster of three events (shown by crosses in Figure 6) with depths lower than 5 km corresponds to blasts in the Mantos Blancos mine. Thus, we conclude that no shallow microearthquake associated with the Atacama fault system occurred during the period of the experiment.

## DISCUSSION

### *Seismogenic plate contact*

The seismogenic coupled zone corresponds to the interplate contact that can generate large underthrusting events. The maximum depth of the coupled-uncoupled transition has been determined using the observed maximum depth of the shallow dipping thrusting fault event using teleseismic data (e.g., Tichelaar & Ruff 1991; Pacheco et al. 1992).

Local microseismic experiments offer a possibility to estimate the maximum depth of the coupled interplate region. The expected behavior of the stress acting along the slab is a compressional field in the contact zone and a tensional field from the coupled to uncoupled transition. This possibility is particularly useful for subduction regions that have local networks with inadequate azimuthal coverage for thrust events which occur mainly off-shore, and their locations and focal mechanisms are, in general, not reliable. Specially for these regions, this transition occurs inland and within the coverage of the local networks. Therefore, the depth of the change between the compressional to tensional stress field along the slab could be an advantageous alternative to estimate the maximum depth of the coupled zone.

In the Antofagasta field experiment we observe that the maximum depth of the shallow dipping thrust faulting events is about 47 km, the high angle reverse faulting events occur in the range of 40 to 78 km depth, and the deeper normal faulting events occur between 68 to 85 km in depth (Figure 5). Therefore, a change from a compressional to a tensional stress field along the slab occurs at about 70 km in depth and at distances of around 200 km from the trench; this corresponds approximately to the Pre-Cordillera. The depth of the stress change along the slab correlates with the crustal thickness of about 70 km under the Pre-Cordillera determined by refraction and gravity studies (Wigger, 1988). We can not distinguish if the high dipping reverse faulting events are on the interplate contact or below it, but we can follow the change of compressional to tensional stress field along

the slab.

The minimum depth of the seismogenic zone could be considered to be about 10-15 km, because for shallower depths the poorly consolidated sediments that form the accretionary prism can deform aseismically (Byrne et al. 1988; Marone & Scholz, 1988).

Therefore, there are two possibilities: (1) the coupled zone extends from 10-15 km to 47 km in depth, with a width of the seismogenic contact zone of about 90 km, and (2) the coupled zone extends to about 70 km in depth, where the transition from the compressional to tensional stress field is observed. In this case the width of the seismogenic coupled zone could reach about 130 km.

If we assume the rupture length of 420 km determined by Comte & Pardo (1992) for the last great 1877 earthquake occurred in the region, and considering the two seismogenic contact widths determined before, the maximum magnitude  $M_S$  (Kanamori & Anderson 1975) estimated for the zone varies between 8.6 to 8.7.

### *Crustal seismicity*

In a preliminary report Comte et al. (1991) associated some shallow events with the Atacama fault system. However, when the digital data were included in the analysis, these events were relocated within the subducted slab, therefore, during this seismic experiment no shallow event could be associated with the Atacama fault system.

Armijo & Thiele (1990) proposed a ramp model to explain the left lateral displacements observed in the central part of the Atacama fault system, instead of the right lateral ones which should be expected from the orientation of the fault and the direction of the Nazca plate convergence. This model assume that the Coastal Scarp and the Atacama fault may interact with the subduction interface at depth, with two changes in the dip angle of the descending slab: one located at approximately 25 km in depth, and at a distance of about 80 km from the trench associated with the Coastal Scarp; the second change located at approximately 50 km in depth, at a distance of 150 km from the trench. Armijo & Thiele (1990) argue that this change in dip controls the geometry of the Atacama fault system. The first change that occurs under the ocean cannot be verified with the data collected during this experiment because the coverage of the network was mainly inland; the second one does occur within the network coverage and it is not observed on the different cross-sections, where the slab appears as a rather smooth surface.

Based on seismic experiments of short duration it is not always possible to define if a

continental fault system is active. It has been observed that the most active segments of a fault, from a microseismic point of view, are not necessarily the same segments that can generate major earthquakes (Wesnousky 1990). Thus, the lack of shallow seismic activity associated with the Atacama fault system during the September and October, 1988 field experiment does not constitute a strong argument in favor of the hypothesis proposed by Yañez (1992) who considers that this fault is no longer active.

### CONCLUSIONS

We suggest an alternative way to estimate the depth of the coupled-uncoupled transition in the subduction lithosphere using reliable local data, defined by the depth where a change from compressional to tensional stress field along the slab is observed.

In the case of Antofagasta, northern Chile, two estimates of the maximum depth of the seismogenic coupled zone are obtained. One defined by the maximum depth of the shallow-dipping thrust events, and the other defined by the depth where the change from compressional to tensional stress field is observed. In the first case we obtain a maximum depth of 47 km with a width of the seismogenic contact zone of about 90 km. In the second case we obtain a maximum depth of 70 km, with a corresponding width of the seismogenic contact zone of about 130 km. With both width estimations of the seismogenic zone, the maximum magnitude  $M_S$  expected for the studied region could reach about 8.6 to 8.7.

No shallow event associated with the Atacama fault system was observed during the experiment. The ramp and the lateral decoupling along the subduction plate boundary model proposed by Armijo & Thiele (1990) for the central part of this fault system, is not confirmed by the geometry of the Wadati-Benioff zone determined in this study.

### ACKNOWLEDGEMENTS

We sincerely thank G. Suárez, S. K. Singh, and D. Byrne for their helpful comments. This work was greatly benefited from critical reviews by P. Bernard and H. Lyon-Caen. This research was partially supported by ORSTOM and the Fundación Andes-Chile, grant C-52040. We also thank to the Chilean and French staff for their participation during the field work.

## REFERENCES

- Arabasz, W. J., 1971. Geological and geophysical studies of the Atacama fault zone in northern Chile, Ph. D. thesis, Calif. Inst. Technol., Pasadena, Calif.
- Araujo, M., 1985. Estudio de sismos en el noreste argentino  $m_b \geq 5.6$  mediante mecanismos de foco y modelado de ondas de cuerpo, Ms. C. thesis, Facultad de Ciencias-UNAM, Mexico.
- Armijo, R. & Thiele, R., 1990. Active faulting in northern Chile: ramp stacking and lateral decoupling along a subduction plate boundary?, *Earth Planet. Sci. Lett.*, **98**, 40-61.
- Barazangi, M. & Isacks, B., 1976. Spatial distribution of earthquakes and subduction of the Nazca plate beneath South America, *Geology*, **4**, 686-692.
- Byrne, D., Davis, D. & Sykes, L., 1988. Loci and maximum size of thrust earthquakes and the mechanics of the shallow region of subduction zones, *Tectonics*, **7**, 833-857.
- Comte, D. & Pardo, M., 1991. Reappraisal of great historical earthquakes in the Northern Chile and Southern Peru seismic gaps, *Natural Hazards* **4**, 23-44.
- Chowdhury, D. K. & Whiteman, S. K., 1987. Structure of the Benioff zone under southern Peru to central Chile, *Tectonophysics*, **134**, 215-226.
- DeMets, C., Gordon, R. G., Argus, D. F. & Stein, S., 1990. Current plate motions, *Geophys. J. Int.*, **101**, 425-478.
- Dorbath, L., Cisternas, A. & Dorbath, C., 1990. Quantitative assesment of great earthquakes in Peru, *Bull. Seism. Soc. Amer.* **80**, 551-576.
- Isacks, B., 1988. Uplift of the central Andean plateau and bending of the Bolivian orocline, *J. Geophys. Res.*, **93**, 3211-3231.
- Jarrad, R., 1986. Relations among subduction parameters, *Rev. Geophys.* **24**, 217-284.
- Kanamori, H. & Anderson, D., 1975. Theoretical basis of some empirical relations in Seismology, *Bull. Seism. Soc. Amer.*, **65**, 1073-1095.
- Kelleher, J., 1972. Rupture zones of large South American earthquakes and some predictions, *J. Geophys. Res.*, **77**, 2087-2103.
- Lee, W., Bennett, R. & Meagher, K., 1972. A method of estimating magnitude of local earthquakes from signal duration. U. S. Geological Survey, OPEN-FILE REPORT.

- Lee, W. & Valdes, C. M., 1978. HYPO71PC: A personal computer version of the HYPO71 earthquake location program. U. S. Geological Survey, OPEN-FILE REPORT.
- Marone, C. & Scholz, C., 1988. The depth of seismic faulting and the upper transition from stable to unstable slip regimes, *Geophys. Res. Lett.*, **15**, 621-624.
- McCann, W., Nishenko, S. P., Sykes, L. R. & Krause, J., 1979. Seismic gaps and plate tectonics: seismic potential for major boundaries, *Pure Appl. Geophys.*, **117**, 1082-1147.
- Naranjo, J. A., 1987. Interpretación de la actividad cenozoica superior a lo largo de la zona de la falla de Atacama, Norte de Chile, *Revista Geológica de Chile*, **31**, 43-55.
- Nishenko, S., 1985. Seismic potential for large and great interplate earthquakes along the Chilean and southern Peruvian margins of South America: A quantitative reappraisal, *J. Geophys. Res.*, **90**, 3589-3615.
- Pacheco, J. F., Sykes, L. R. & Scholz, C., 1992. Nature of seismic coupling along simple plate boundaries of the subduction type. Submitted to *J. Geophys. Res.*
- Rivera, L. and Cisternas, A., 1990. Stress tensor and fault plan solutions for a population of earthquakes. *Bull. Seismol. Soc. Am.*, **80**, 600-614
- Suárez, G., Monfret, T., Wittlinger, G. & David, C., 1990. Geometry of subduction and depth of the seismogenic zone in the Guerrero gap, Mexico, *Nature*, **345**, 336-338.
- Tichelaar, B. & Ruff, L., 1991. Seismic coupling along the Chilean subduction zone, *J. Geophys. Res.*, **96**, 11997-12022.
- Wesnousky, S. G., 1990. Seismicity as function of cumulative geologic offset: some observations from southern California, *Bull. Seism. Soc. Am.*, **80**, 1374-1381.
- Wigger, P. J., 1988. Seismicity and crustal structure of the central Andes. In: Lecture notes in Earth Sciences. The southern central Andes. Contributions to structure and evolution of an active continental margin. Springer-Verlag, 209-227.
- Yañez, G., 1992, On the mechanics of strike-slip faulting of forearc slivers, in preparation.



TABLE 1  
ANALOG MEQ-800 STATION

STA	LAT °(S)	LON °(W)	ELEV	LOCATION
CAL	22 28.81	69 01.52	2030	Calama
HOS	22 57.47	70 16.69	270	Hornitos
DVM	23 15.05	70 20.61	360	Desv. Mejillones
CLB	23 20.37	69 46.09	1320	Culebron
MIR	23 21.44	70 10.60	1225	Miranda
CHO	23 03.33	69 35.59	1570	Chacabuco
FAR	23 29.87	70 17.92	950	Farol
CUE	23 37.68	69 56.31	960	Cuevitas
COL	23 46.60	70 26.33	150	Coloso
TOS	23 54.86	70 15.51	720	Tosca
YUG	24 01.23	69 51.77	1250	Yugoslavia
YNG	24 05.36	70 05.14	1070	Yungay
ROS	24 27.43	69 53.50	1470	Rosario

DIGITAL GEOSTRAS STATION

SRA	22 51.98	69 20.84	1800	Sierra Gorda
TAM	22 38.71	70 14.58	270	Tamira
ESM	22 56.04	69 51.99	1510	Esmeralda
MBL	23 27.27	70 01.62	840	Mantos Blancos
MOR	23 30.58	70 33.02	220	Moreno
MAG	24 05.72	69 35.80	1400	Magnesia
SGR	24 13.06	69 49.50	1130	San Gregorio
LVI	24 28.99	70 18.89	1930	Los Vientos

DIGITAL TELEMETRIC STATION

LVI	24 28.99	70 18.89	1930	Los Vientos
MIC	22 49.55	70 13.96	1527	Michilla
ANG	23 06.04	70 30.70	710	Angamos
VAL	23 09.94	69 59.79	1400	Valenzuela
MAR	23 15.68	69 31.12	1720	Morrito
SCR	23 26.77	69 35.24	1820	San Cristobal
LMO	23 33.94	70 16.57	1000	Los Morros
AVI	24 06.73	69 15.38	2250	Augusta Victoria
CRI	24 10.03	70 22.27	1620	Cerro Sta. Rita

TABLE 1.- Analog MEQ-800, digital Geostras, and digital telemetric stations locations. Latitude and longitude are given in degrees and minutes. Elevations is in meters relative to the mean sea level. STA is the name of the station.

TABLE 2  
VELOCITY STRUCTURE

Vp(km/s)	h(km)
5.5	00
6.2	06
6.8	10
7.2	29
8.0	55

TABLE 2.- Velocity structure model used to locate hypocenters of the recorded events (modified from Wigger,1988).

TABLE 3

N <sup>o</sup>	FAULT PLANE			DEPTH	MAGNITUD
	$\phi^{\circ}$	$\delta^{\circ}$	$\lambda^{\circ}$	H	M <sub>d</sub>
1	321.8	48.1	111.0	52	3.2
2*	344.0	62.6	144.3	40-48	3.2-3.4
3	11.9	12.5	107.2	34	2.8
4	359.2	18.9	104.2	32	2.4
5*	359.7	13.5	103.7	41-47	2.7-2.7
6*	24.3	64.5	62.7	56-63	2.9-2.9
7	28.9	34.1	93.9	69	2.8
8	108.4	45.1	-119.5	80	4.2
9	260.5	20.0	-67.0	99	3.5
10	200.4	45.7	-74.7	85	3.4
11	283.7	41.8	-106.9	78	2.9
12	270.2	60.2	-79.7	52	3.1
13	0.8	79.6	-95.7	38	2.2
14	22.4	53.0	-71.6	68	3.1
15	243.4	60.6	-44.2	81	3.8
16*	353.3	55.7	-99.5	81-74	3.6-3.7
17	158.3	35.3	-107.8	104	3.6
18	180.8	24.7	-91.3	106	3.5
19	177.1	28.2	-94.0	117	3.6

TABLE 3.- Focal mechanism solutions obtained from the first motion polarities using the Rivera and Cisternas (1990) algorithm N<sup>o</sup>: identification number of the event, same used in Figures 2, 3, and 5.  $\phi^{\circ}$ ,  $\delta^{\circ}$ ,  $\lambda^{\circ}$ : strike, dip and rake of the focal mechanism. H: depth in km. M<sub>d</sub>: Coda-duration magnitude according to the relation given by Lee et al. (1972)

## FIGURE CAPTIONS

**Figure 1.-** Distribution of the Antofagasta-1988 temporary seismic network (white symbols inland). Epicentral distribution of the seismicity recorded in this experiment. Filled circles correspond to reliable solutions, and open circles denote the relocated events. The rectangle indicates the coverage of the seismic network. Six profiles in the direction of convergence are also shown. Solid triangles indicate the active volcanoes in the Andean range.

**Figure 2a.-** Joint focal mechanism and stress tensor inversion solutions from the first motion polarities using the Rivera and Cisternas (1990) algorithm for the reverse faulting events. Open squares denotes dilation and dark squares denotes compression. An estimation of the uncertainty of the fault plane pole is shown for each mechanism. In the lower part of the Figure, the orientation and the associated uncertainty of the compressional ( $\sigma_1$ ), tensional ( $\sigma_3$ ), and intermediate ( $\sigma_2$ ) axis of the obtained stress tensor are also shown.

**Figure 2b.-** Joint focal mechanism and stress tensor inversion solutions from the first motion polarities using the Rivera and Cisternas (1990) algorithm for the normal faulting events. Symbols as in Figure 2a. When there is no uncertainty region for the fault plane pole, it means that the fault planes are not well constrained.

**Figure 3a.-** Focal mechanism solutions in lower hemispheric projection of shallow-dipping and high-angle reverse faulting events. The epicentral distribution of the reliable seismicity recorded during the experiment is also presented. The number in the upper part of each mechanism correspond to its identification number (Figure 5, Table 3). Symbols as in Figure 1.

**Figure 3b.-** Focal mechanism solutions in lower hemispheric projection of normal faulting events are presented. Symbols as in Figure 3a.

**Figure 4.-** Depth distribution in the direction of the Nazca plate convergence of the reliable and relocated events (dashed and open circles, respectively) of the profile indicated in Figure 1. The projection of the trench, the coastline, and the volcano (triangles) are also shown. Crosses in C3 profile correspond to blast of the Mantos Blancos mine.

**Figure 5.-** Composite depth distribution from C1 to C6 cross-section from Figure 4. The lateral lower hemispheric focal mechanism solutions obtained is also shown. Each mechanism is identified by its number and keyed to Table 3.

**Figure 6.-** Shallow seismicity near the Atacama fault system. Crosses indicate the three explosions of the Mantos Blancos mine occurred during the period of this experiment.

Figure 1

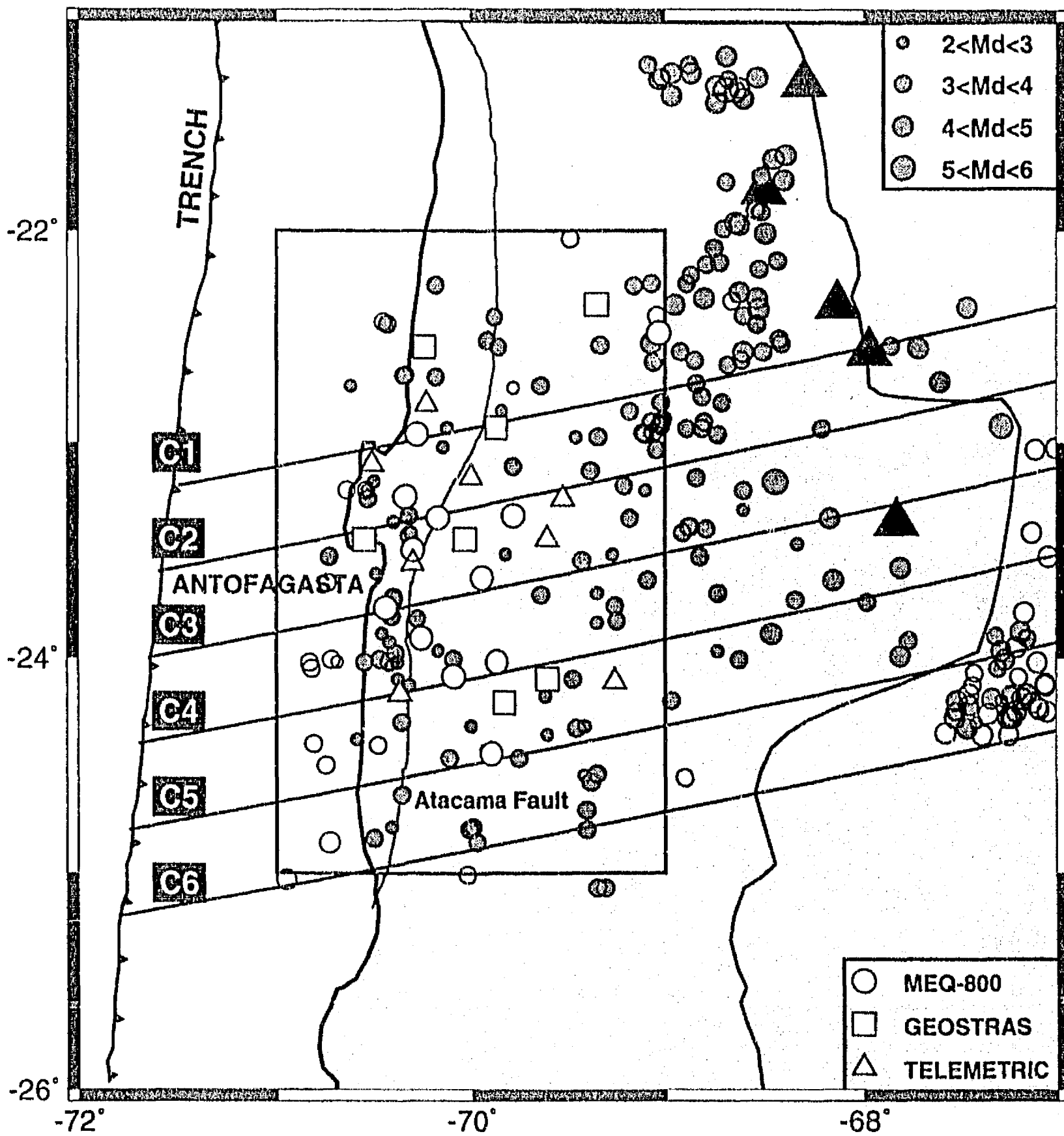


Figure 2a

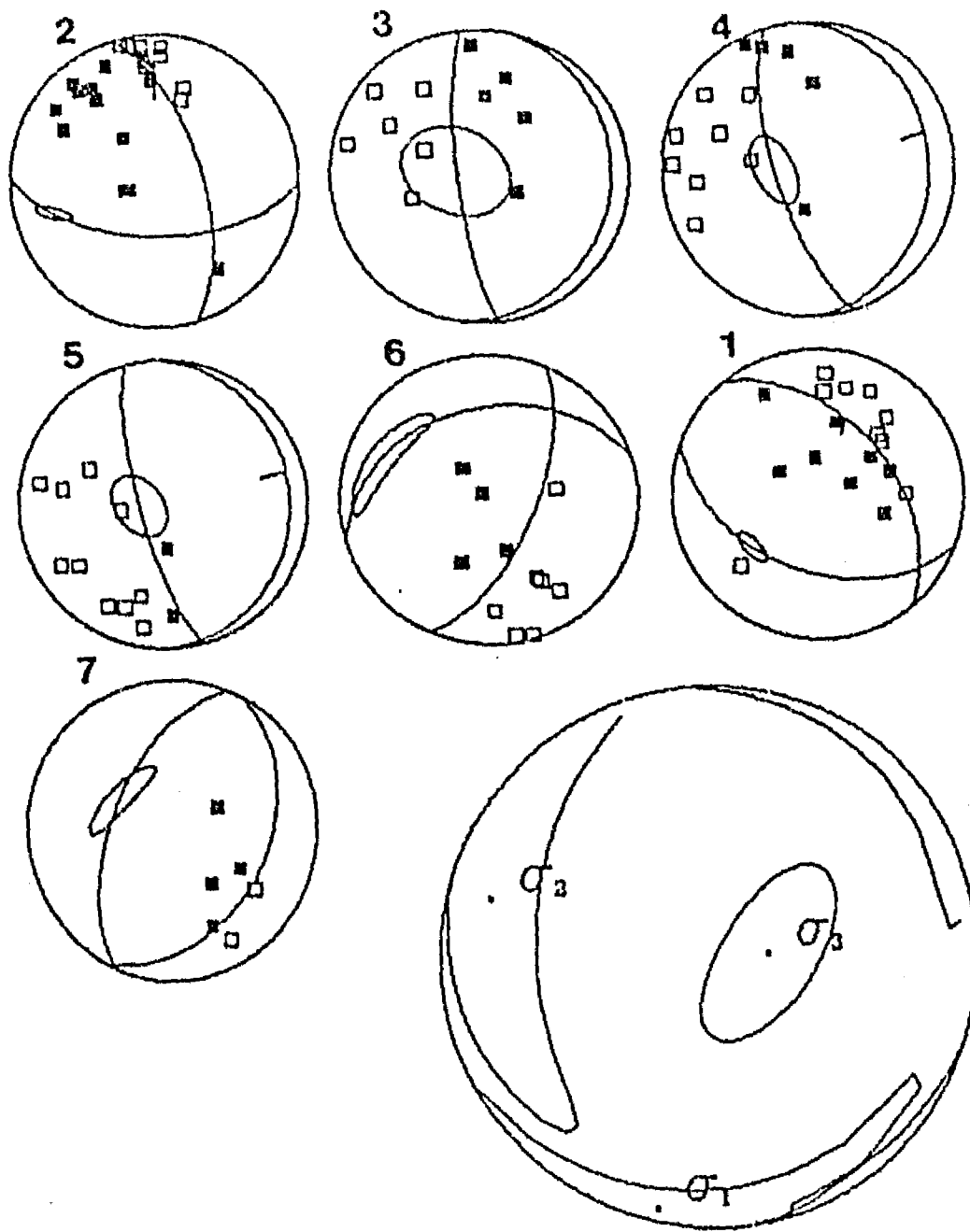


Figure 2b

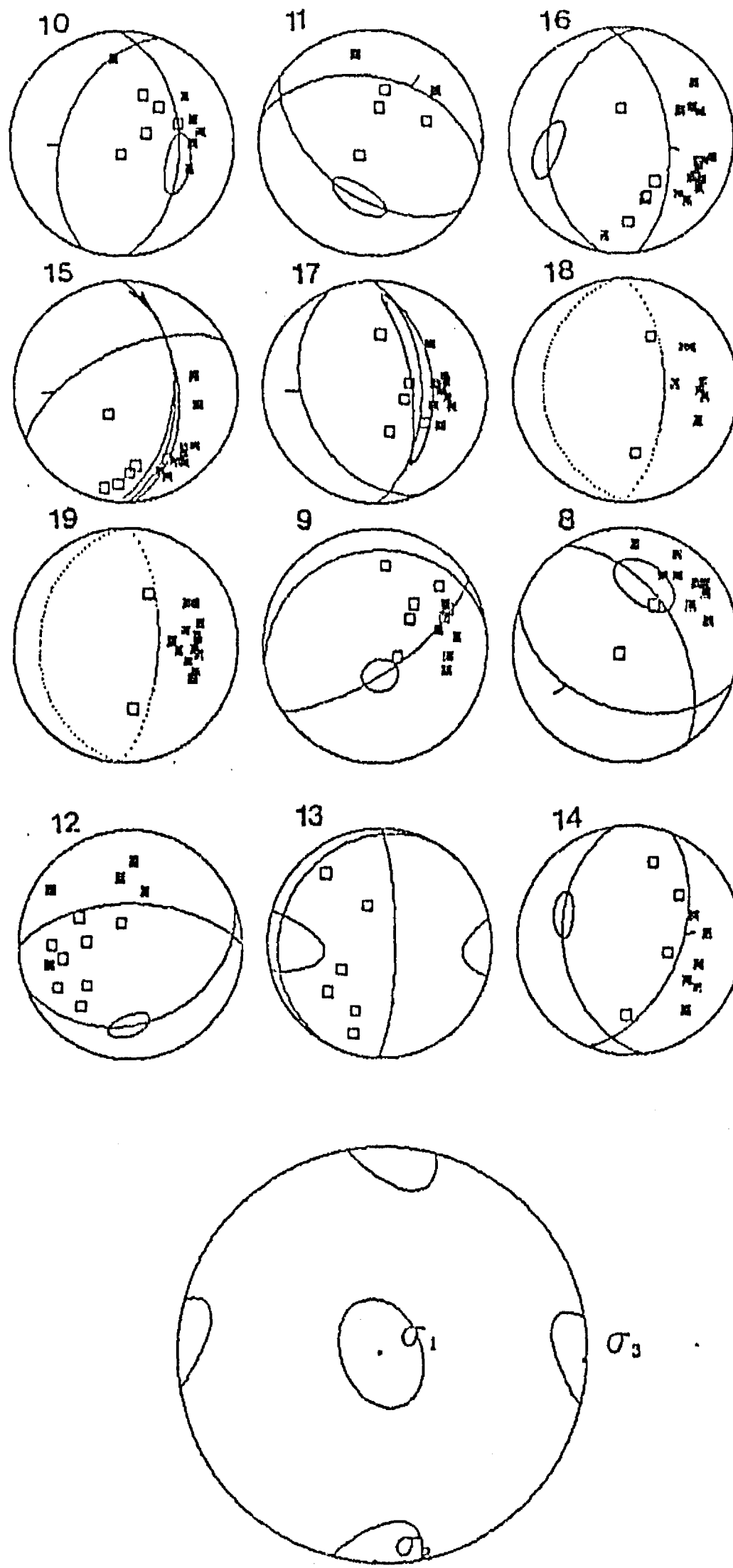


Figure 3a

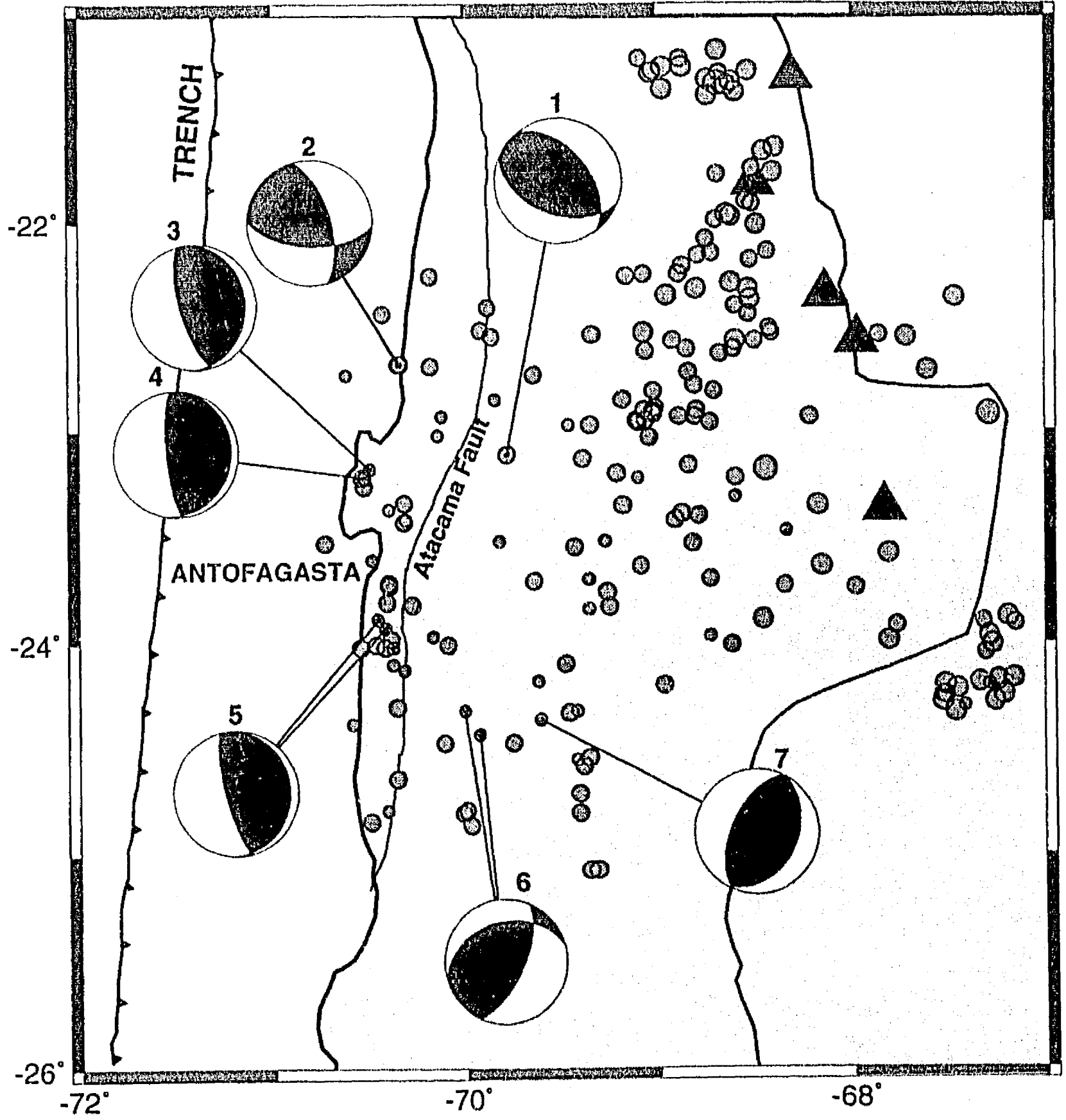


Figure 3b

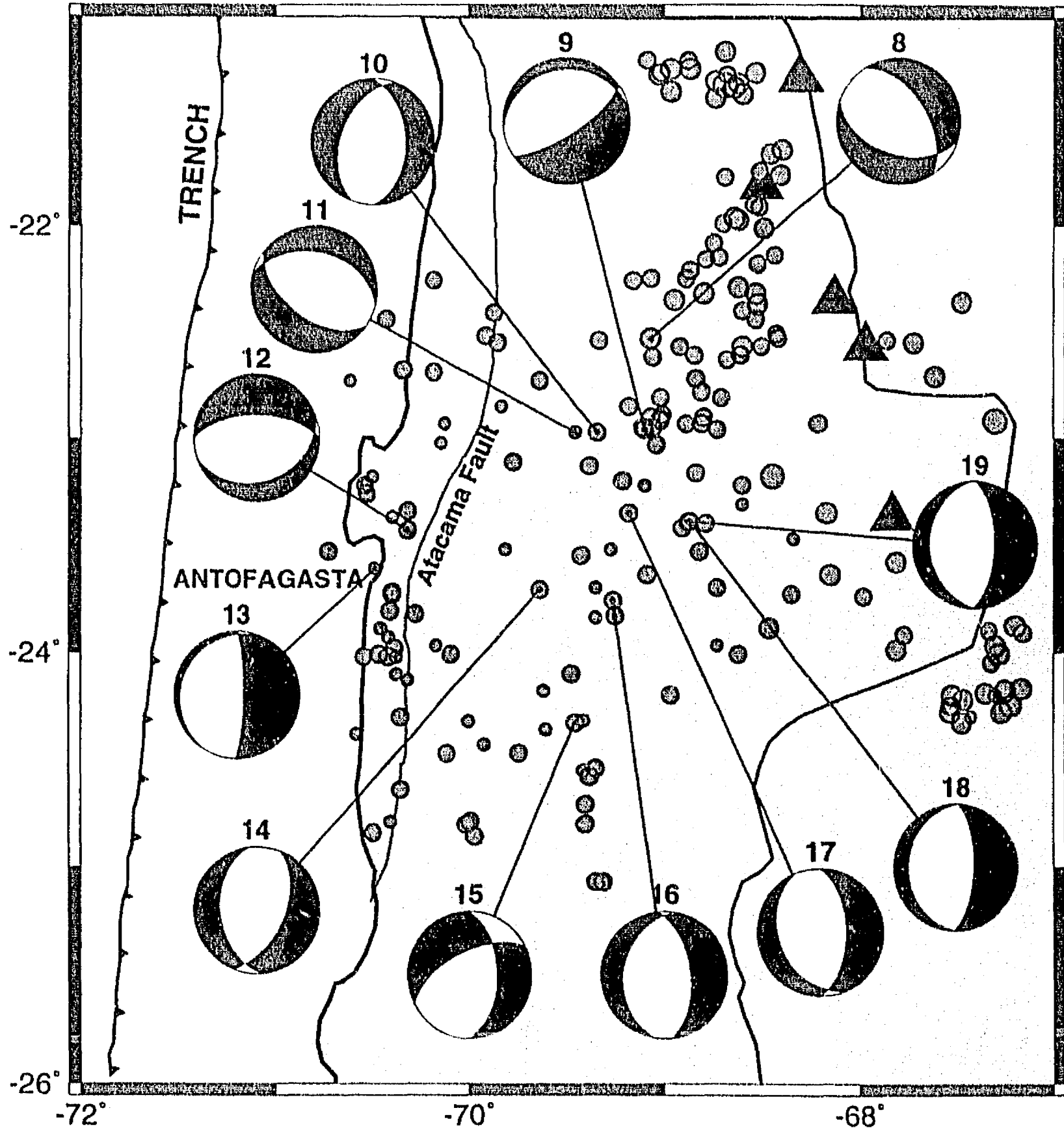




Figure 4

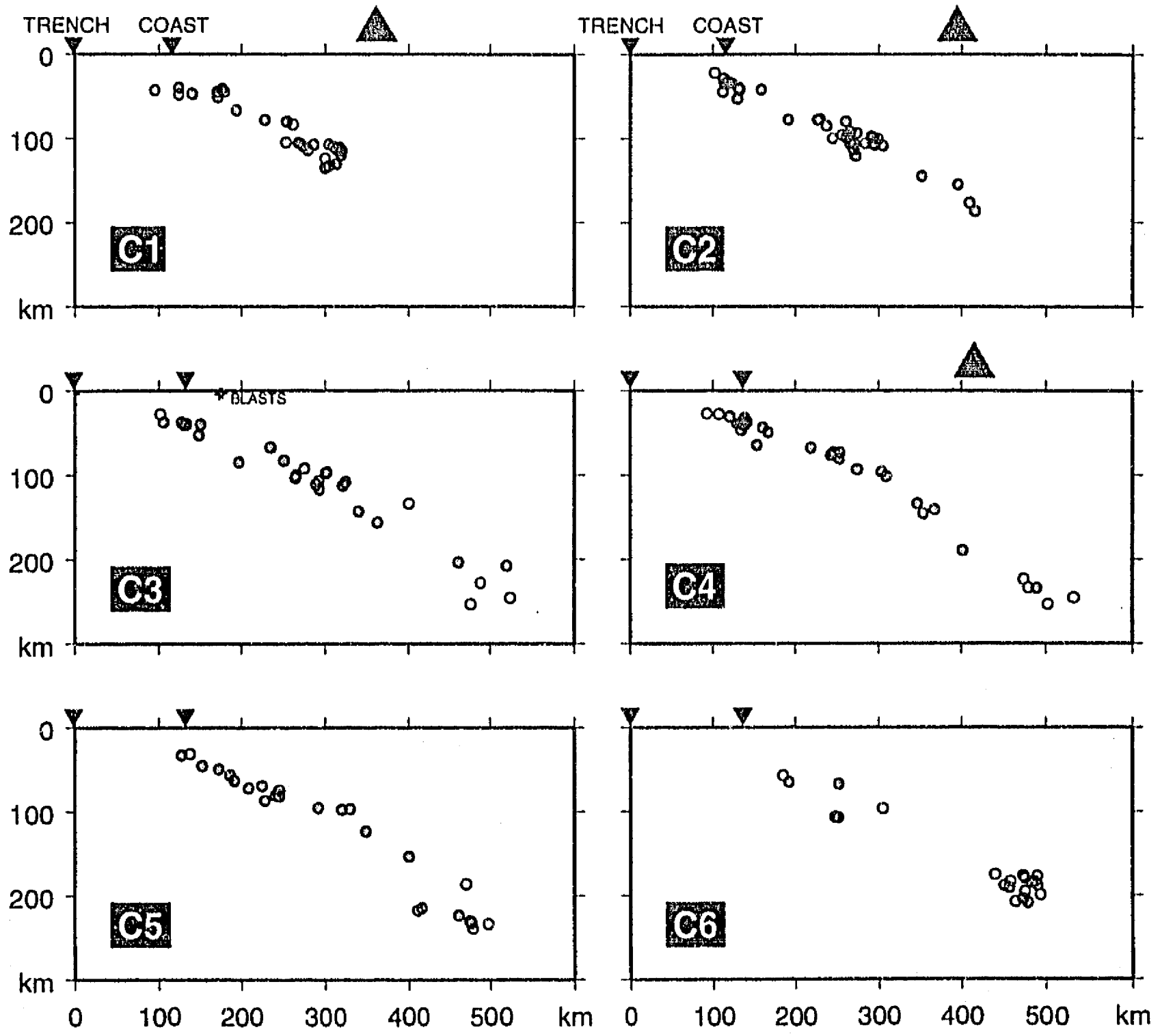


Figure 5

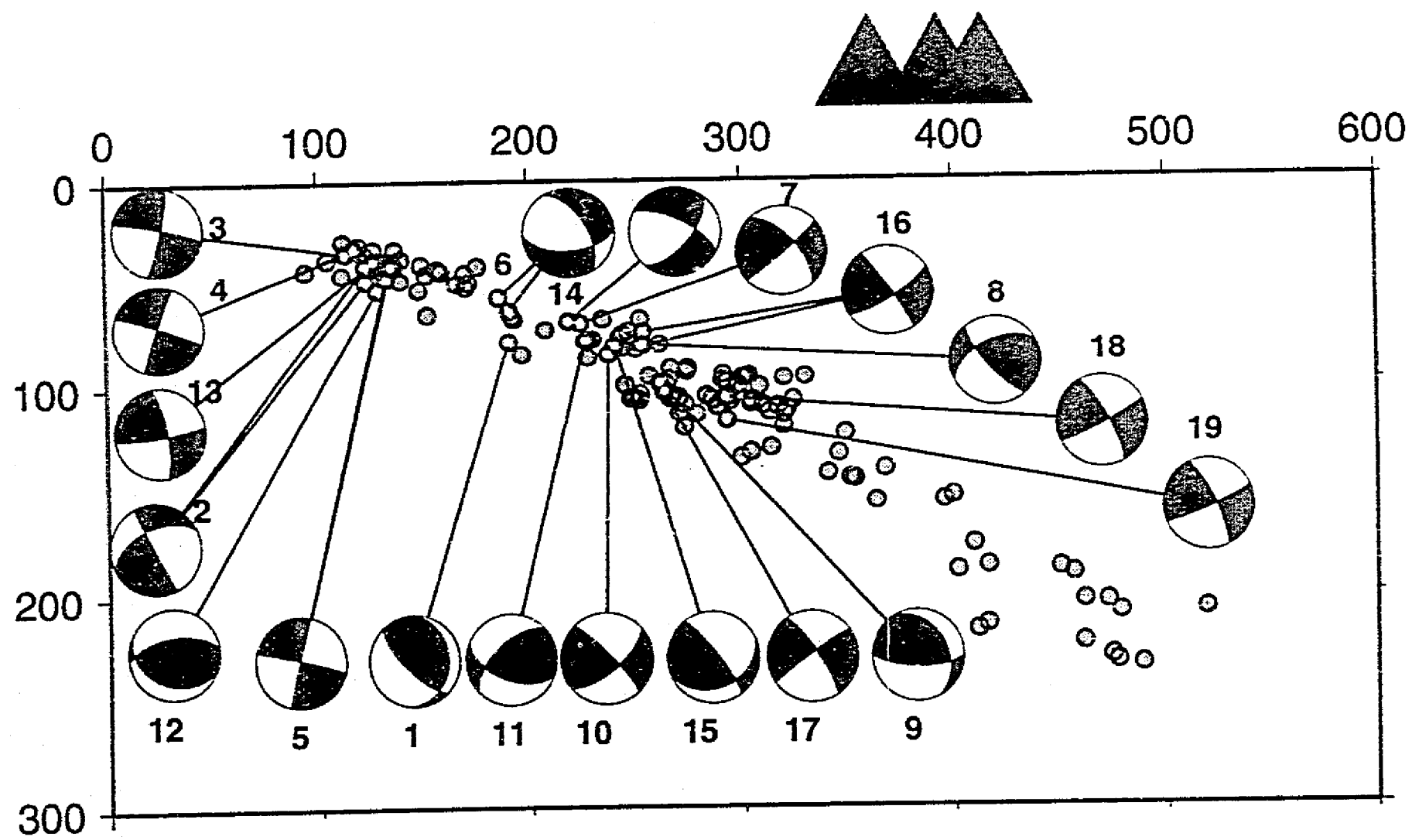
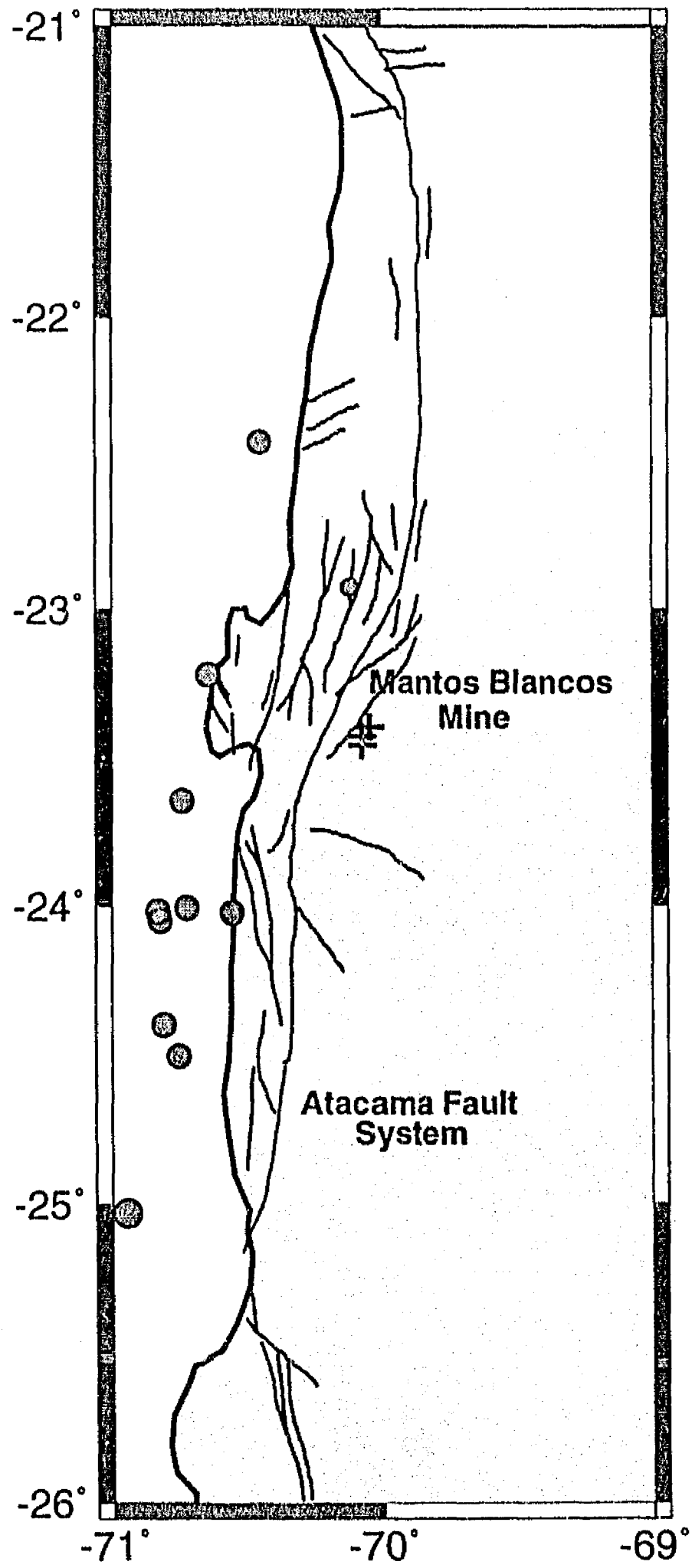


Figure 6



COMMENT ON "SEISMIC COUPLING ALONG THE CHILEAN SUBDUCTION  
ZONE" BY B. W. TICHELAAR AND L. R. RUFF

Gerardo Suárez and Diana Comte<sup>1</sup>

Instituto de Geofísica, Universidad Nacional Autónoma de México, 04510 México D. F.;

<sup>1</sup> Also at: Depto. de Geología y Geofísica, U. de Chile, Casilla 2777, Santiago, Chile

*J. Geophys. Res.*, Vol. 98, B9, 15,825-15,828

In a recent paper, Tichelaar and Ruff [1991a] (hereafter referred as TR91) studied the Chilean subduction zone as part of a worldwide project to map the depth extent and the width of the seismogenic interplate contact in subduction regimes [Tichelaar and Ruff, 1991b]. In their paper, the maximum depth of seismic coupling is defined by the focal depth of the interplate thrust events with magnitudes greater than 6.0 [TR91]. The focal depths of these earthquakes were determined by the omnilinear inversion of long period P waves. Depth uncertainties of the earthquakes studied were then estimated using a bootstrapping technique.

The main conclusion of their paper is that there is a change in the maximum depth of seismogenic coupling in the Chilean subduction zone at 28° S. According to their results, to the south of this latitude the seismically coupled zone in Chile extends to depths of 48 to 53 km, whereas it appears to be only 36 to 41 km deep to the north of 28° S. This statement is made despite the fact that TR91 report an interplate thrusting earthquake on December 21, 1967 ( $M_w=7.1$ ) in northern Chile (at approximately 22° S) with a focal depth of about 47 km, indicating a depth of coupling not very different to that observed to the south of 28°S.

The purpose of this comment is, first, to discuss locally-recorded data using permanent and temporary networks in Chile, which suggest that the depth of the coupled zone does not vary along the Chilean subduction zone as suggested by TR91. Secondly, and perhaps more important in our view, we would like to bring to discussion the difficulties involved in measuring the depth of the seismogenic plate contact, and the different values that are determined when alternative data are utilized; in particular, we note different results from earthquakes with magnitudes greater than 6.0 versus data from microseismicity studies.

As a definition we will take that of TR91: "the seismically coupled zone is the depth

range of the plate interface that is capable of producing an underthrusting event". Ideally, we would like to determine the maximum depth of this coupled zone by measuring the actual coseismic rupture using geodetic and aftershock data recorded in a region where a large earthquake ( $M > 7.7$ ) presumably broke the whole seismic interface. The infrequent occurrence of large magnitude events and the dearth of local geodetic data forces us to use indirect means of measuring the zone of coupling. TR91 used earthquakes with magnitudes larger than 6.0 for two reasons: 1) this is the minimum magnitude for which the high quality seismograms necessary in the inversion scheme can be recorded at teleseismic distances; and 2) they argue that the determination of the depth transition from unstable to stable sliding should be based on the study of earthquakes with major moment release.

The first argument stems from practical reasons. The second one, however, may not have a physical meaning as it depends strongly on the scale of the asperities or heterogeneities in the fault plane. Interplate thrust earthquakes of smaller magnitude can also reflect the depth at which brittle behavior occurs and, as we will discuss below, the microseismicity can also be used to map the coupled contact in subduction zones. Furthermore, using only large events to map the depth of coupling presents an unavoidable drawback because of their non-uniform distribution along the strike of subduction.

In reality, the presumed zone of shallow seismogenic coupling is observed by TR91 only in the region of Taltal, between  $24^{\circ}$  and  $28^{\circ}$  S; out of a total of 27 earthquakes studied by TR91, only five lie in this region (Figure 1). The region of Taltal lies between the rupture zones of the great earthquakes of 1877 ( $M_w=8.8$ ) [Comte and Pardo, 1991] and 1922 ( $M_S=8.4$ ) [Kelleher, 1972]. Three events occurred in this area in 1966, 1983, and 1987. The magnitudes ( $M_w$ ) of these events range from 7.3 to 7.5 [TR91]. With the historical data available, it remains unclear whether the Taltal segment has been broken by a great earthquake in the last 100 yrs. Therefore, the question of whether this region has an abnormally shallow zone of seismogenic coupling which may result in smaller thrust earthquakes than those observed in the rest of the Chilean coast has important implications in seismic hazard evaluation.

A temporary seismological network of twenty nine portable, digital and analog stations with a radius of about 150 km was installed in 1988 around the city of Antofagasta (Figure 1), [Comte et al., 1992]. The temporary network spanned part of the rupture area of the 1987 earthquake ( $M_w=7.3$ ). A total of about 250 hypocenters were well determined

during the eight-week duration of the experiment. Only three focal mechanisms show thrust faulting along the interface (Figure 1). The deepest thrust earthquake has a depth of 47 km and it lies within the northern limit of the Taltal region; the other two earthquakes are at depths of between 32 and 34 km (cross-section BB' in Figure 2). The microearthquakes listed were located with a minimum of ten phase readings, including at least three S-wave phases. In all cases, the epicentral distance to the nearest recording station was smaller than the focal depth. The robustness of the hypocentral depths was tested varying the initial depth, the velocity structure, and the  $V_p/V_s$  ratio used in the location algorithm; in these tests the observed variations in focal depth were always smaller than  $\pm 5$  km.

In 1991, a second temporary network was installed around the city of Iquique, inside the presumed rupture zone of the great 1877 earthquake (Figure 1). As in the case of the Antofagasta experiment described before, the occurrence of thrust events on the interface is rare compared with the presence of the high-angle, reverse faulting events and down-dip, tensional earthquakes. The fault plane solution of the only interplate event recorded shows a similar mechanism to those observed in Antofagasta (Figure 1), and it has a focal depth of 41 km (cross-section AA' in Figure 2). Errors in the hypocentral depths are similar to those discussed above for Antofagasta. It is important to point out that about 200 km to the south of Iquique, almost halfway between the two cross-sections discussed above, the December 21, 1967 earthquake is reported by TR91 at a depth of 47 km.

Another example is central Chile near Valparaíso, where the earthquake of March 3, 1985 occurred. Aftershocks of this event were recorded from March 6 to 17, by a combination of permanent stations from the local network and temporary instruments [Comte et al., 1986]. The average dip angle of the thrust faulting aftershocks is  $20^\circ$ , and the deepest event lies at a depth of 53 km (cross-section CC' in Figure 2). Moreover, the background seismicity recorded by the permanent central Chile network from 1986 to 1987, and data recorded during a local microseismic experiment in 1986 show interplate thrusting events [Fuenzalida, 1988] extending to depths of up to 48 km with an average dip angle of  $19^\circ$  (cross-section CC' in Figure 2). Therefore, the depth of the seismogenic coupling in Chile extends to approximately 50 km along the whole subduction zone without showing appreciable variations in maximum depth extent or dip angle ( $\sim 20^\circ$ ). The landward extent of the coupled zone along the Chilean subduction zone has a width of approximately 40 to 60 km.

On the four cross-sections on Figure 2, the depth at which there is a change from high-

angle reverse faulting to down-dip tensional events is also shown. In cases where few interplate thrust earthquakes occur, this transition may be an alternative method to determine changes in the maximum depth of seismogenic coupling. The simple mechanical idea behind this is that near and below the interplate surface, where unstable sliding occurs, the subducted slab is under compression. The compressive regime causes not only thrusting along the plate interface, but also intraplate, reverse faulting earthquakes within the slab. At a certain depth the slab becomes completely decoupled from the upper plate and begins to sink due to its negative buoyancy. The sheet of tensional events in the slab reflects the resulting tensional stress due to slab pull [e.g., Spence, 1989]. Thus this transition from compressive to tensional behavior would reflect the mechanical conditions in the shallow part of the subducted slab and may help to map indirectly whether the depth of seismogenic coupling changes along strike. In the three regions where good local data exists to control this change, Antofagasta, Iquique, and Valparaíso, this transitional depth lies consistently at a depth of about 70 km (Figure 2).

In conclusion, the maximum depth of the seismogenic coupling along the Chilean subduction zone extends consistently to about 50 km, and does not show appreciable variations along the strike of the trench. Therefore, the depth of seismic coupling, at least in the Chilean subduction zone, is apparently uncorrelated to the age of the subducting plate and its relative rate of motion [Van den Beukel and Wortel, 1987; 1988], the geometry of the slab downdip of the seismogenic plate contact, the presence of volcanoes in the upper plate, or the thickness of sediments in the trench.

#### ACKNOWLEDGEMENTS

The Iquique experiment was funded by a grant from the International Development Research Center (IDRC) of Canada to the Pan American Institute of Geography and History, and by the Institut Français de Recherche Scientifique pour le Développement en Coopération (ORSTOM). The Antofagasta-1988 and the central Chile-1986 experiments were also partially funded by ORSTOM. D. Comte acknowledges the support of the Andes Foundation grant C-52040. This work was finished while one of us (GS) was visiting the U. S. Geological Survey in Golden, Colorado; the use of their facilities is greatly appreciated. We thank D. Byrne, W. P. Chen, C. Mendoza and W. Spence for their critical review of the manuscript.

#### REFERENCES

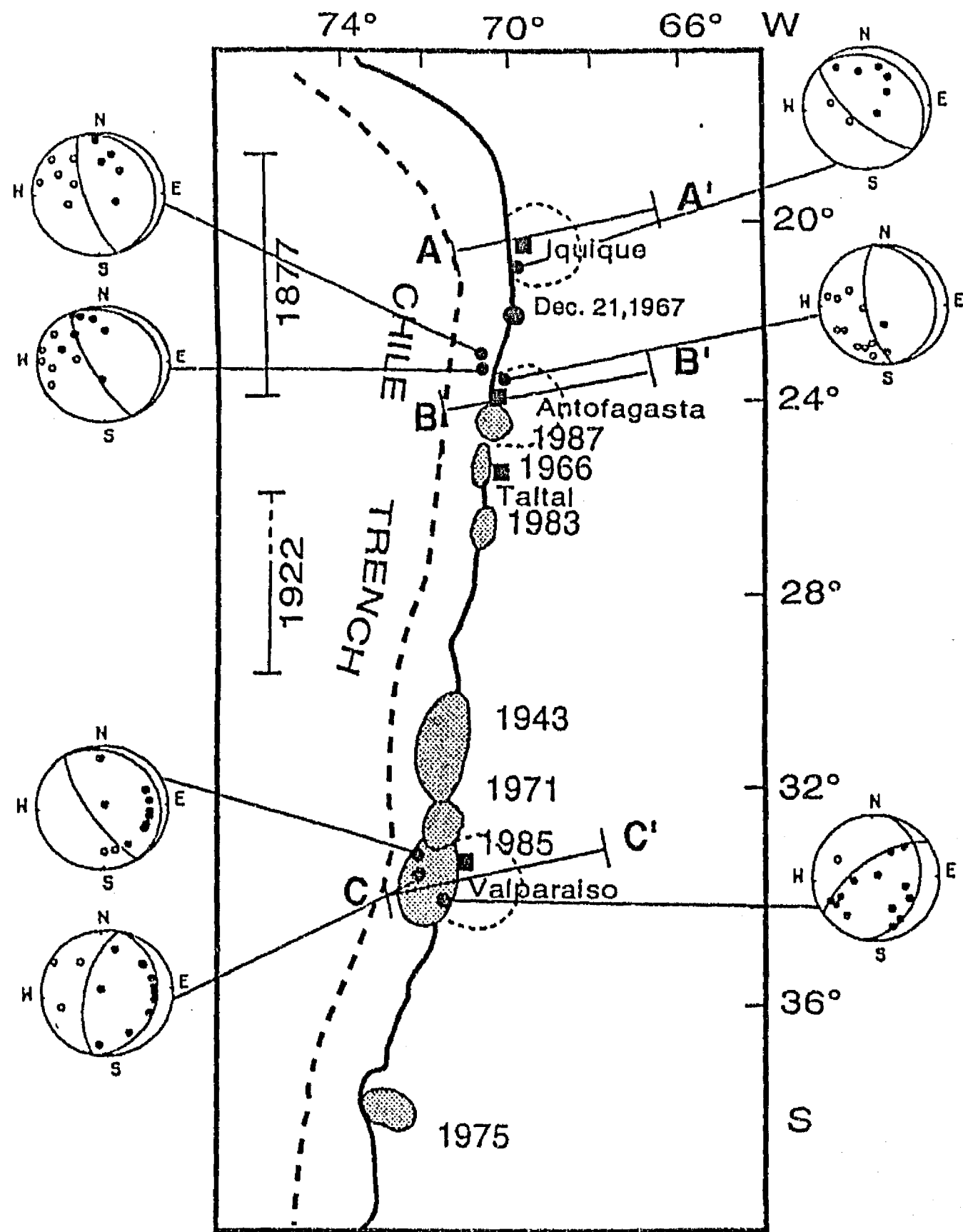
- Comte, D., A. Eisenberg, E. Lorca, M. Pardo, L. Ponce, R. Saragoni, S. K. Singh, and G. Suárez, The 1985 central Chile earthquake: A repeat of previous great earthquakes in the region?, *Science*, **233**, 449-453, 1986.
- Comte, D. and M. Pardo, Reappraisal of great historical earthquakes in the northern Chile and southern Peru seismic gaps, *Natural Hazards*, **4**, 23-44, 1991.
- Comte, D., M. Pardo, L. Dorbath, C. Dorbath, H. Haessler, L. Rivera, A. Cisternas, and L. Ponce, Seismogenic interplate contact zone and crustal seismicity around Antofagasta, northern Chile using local data, submitted to *Geophys. J. Int.*, 1992.
- Fuenzalida, A., Estudio detallado de la subducción litosférica de Chile central, Ms. C. Thesis, 136 pp., Univ. of Chile, Chile, 1988.
- Kelleher, J. A., Rupture zones of large South American earthquakes and some predictions, *J. Geophys. Res.*, **77**, 2087-2103, 1972.
- Spence, W., Slab pull and the seismotectonics of the subducting lithosphere, *Rev. Geophys. Space Phys.*, **25**, 55-69, 1987.
- Tichelaar, B. W., and L. R. Ruff, Seismic coupling along the Chilean subduction zone, *J. Geophys. Res.*, **96**, 11,997-12,022, 1991a.
- Tichelaar, B. W., and L. J. Ruff, Mechanism of seismic coupling along subduction zones (abstract), *Trans. Am. Geophys. Union, EOS*, **72**, 347, 1991b.
- Van den Beukel, J., and R. Wortel, Temperatures and shear stresses in the upper part of a subduction zone, *Geophys. Res. Lett.*, **14**, 1057-1060, 1987.
- Van den Beukel, J., and R. Wortel, Thermo-mechanical modeling of arc-trench regions, *Tectonophys.*, **154**, 177-193, 1988.

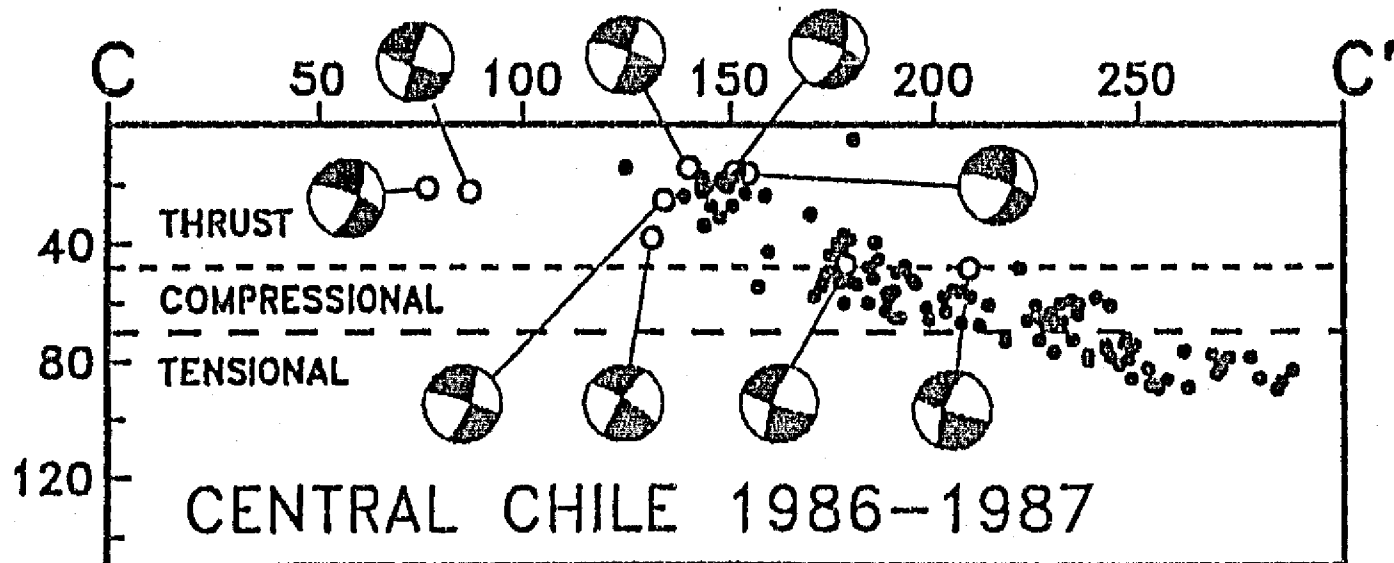
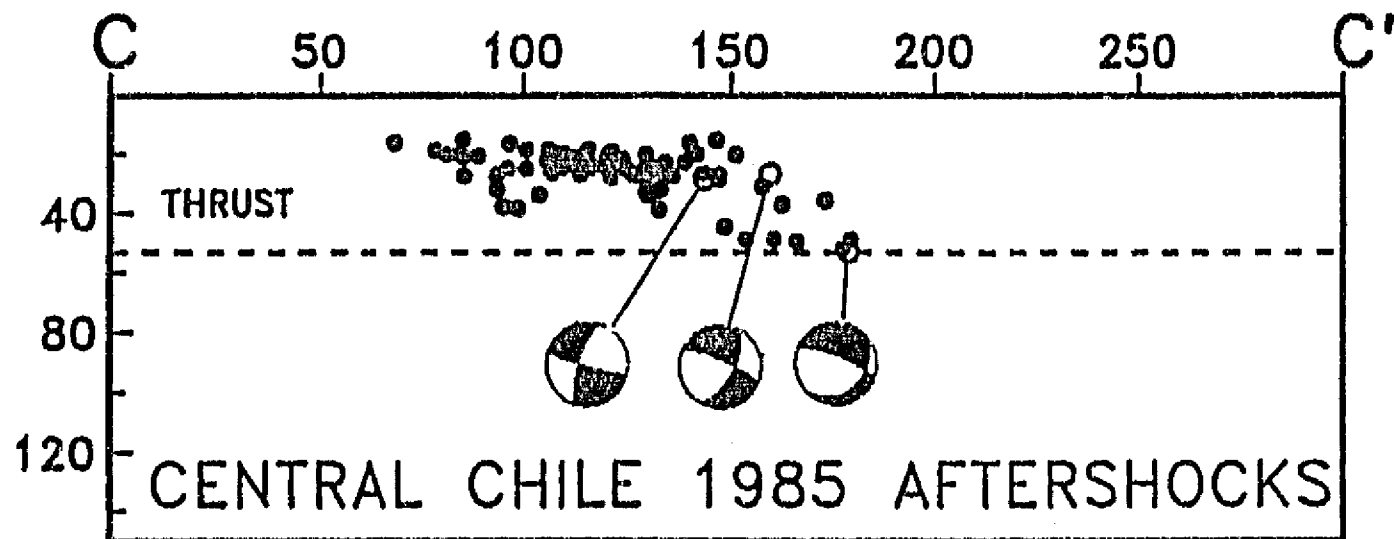
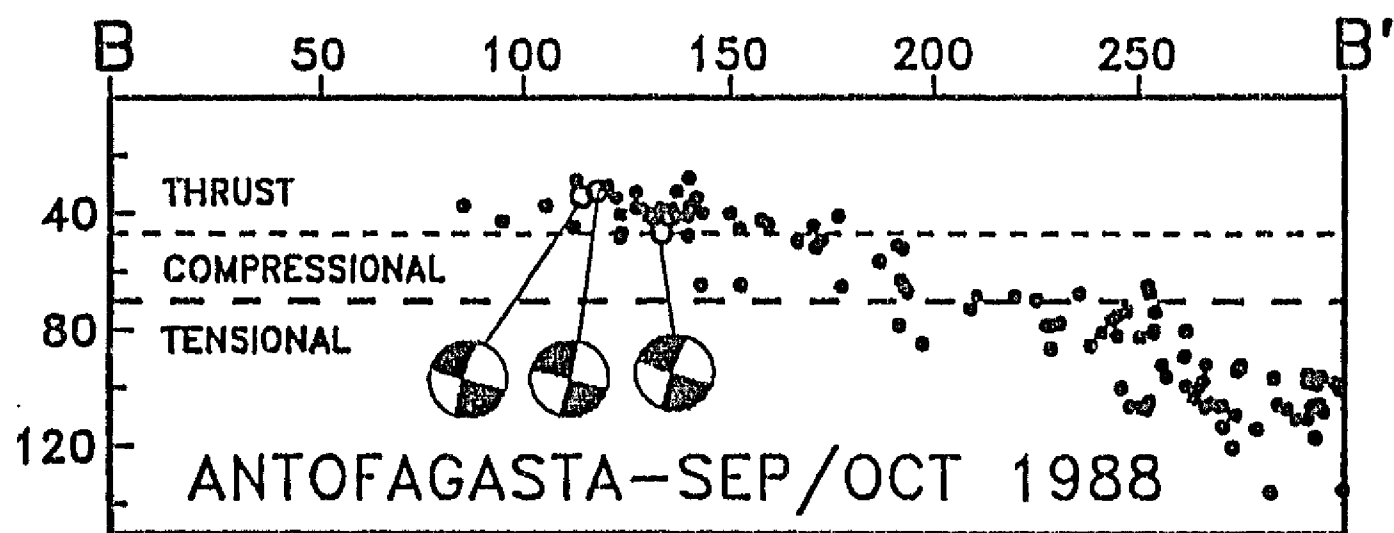
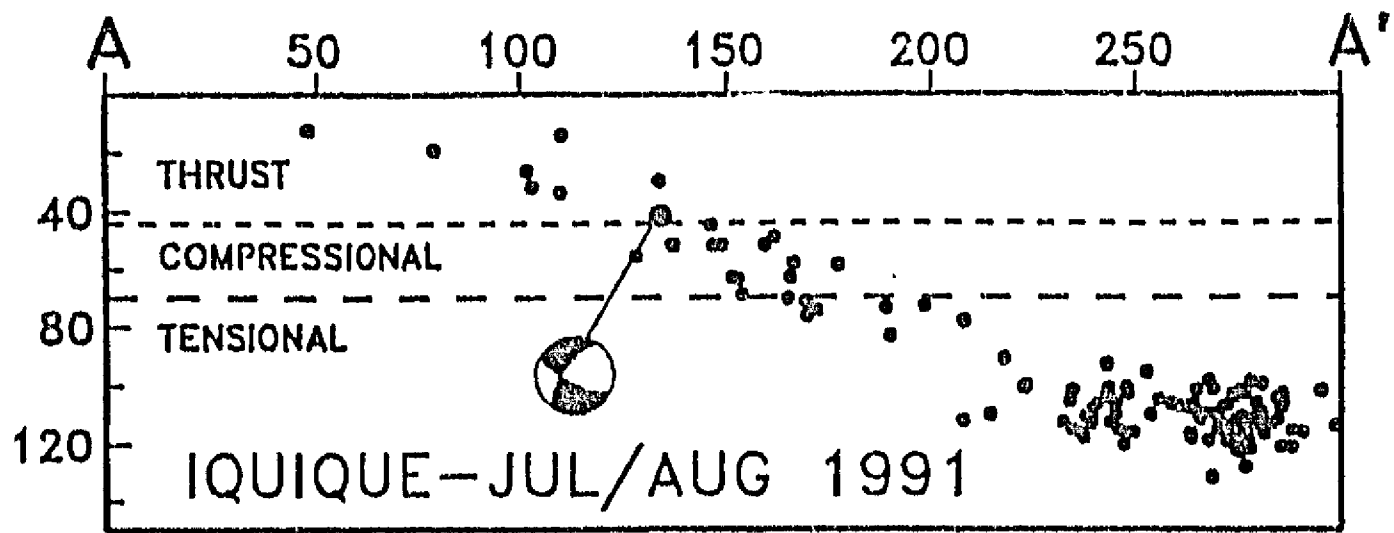


#### FIGURE CAPTIONS

Figure 1. Map of the western coast of South America showing the Chilean subduction zone. The dashed line is the trench and the hatched areas are the rupture zones of the earthquakes referenced by the date to the right of them. The vertical lines on the left reflect the inferred rupture zones of the great 1877 and 1922 earthquakes. The focal mechanisms of the interplate thrust microearthquakes are shown in a lower-hemispheric projection where solid and open circles are compressions and dilations respectively. The cross-sections presented on Figure 2 are shown as AA', BB', and CC'. The dashed semicircles around the cities of Iquique, Antofagasta, and Valparaiso show the extent of the temporary seismic networks.

Figure 2. Cross-sections AA', BB', and CC' shown on Figure 1. Solid circles are the microearthquakes and open circles are events that show thrusting focal mechanisms. The focal mechanisms are projected on a side-looking, lower-hemispheric projection where dark quadrants indicate compression and white ones dilations. The short-dash line shows the maximum depth of thrust faulting in each of the cross-sections. The long-dash line marks the depth where a change from high-angle, reverse faulting to down-dip tensional events is observed.





# Velocity Structure in Northern Chile: Evidence of Subducted Oceanic Crust in the Nazca Plate

Diana Comte <sup>1,2</sup>, Steven W. Roecker <sup>3</sup>, and Gerardo Suárez <sup>1</sup>

<sup>1</sup>Instituto de Geofísica, Universidad Nacional Autónoma de México, México D.F.

<sup>2</sup>Depto. de Geofísica, Universidad de Chile, Casilla 2777, Santiago, Chile

<sup>3</sup>Department of Earth and Environmental Sciences, Rensselaer Polytechnic Institute, Troy, NY 12180, USA

*Geophysical Journal International, en prensa*

## SUMMARY

Two-dimensional  $P$  wave velocity models were determined for the subduction zones near Iquique and Antofagasta in northern Chile, simultaneously inverting  $P$  and  $S$  wave arrival times from locally recorded earthquakes for velocity structure and hypocentral locations. A two-dimensional parametrization was used because of the paucity of data, but is justified by the lack of significant variations along the strike of the subduction zone observed from both refraction profiles and simple three-dimensional inversions. The crust and upper mantle are parameterized by constant velocity regions of irregular shape, with the size and boundaries of these regions governed by prior information about the structure and by the ability of the data to resolve  $P$  wave velocities. Beneath the Antofagasta region there is evidence of an approximately 10 km-thick layer of oceanic crust attached to the top of the subducting Nazca plate. This crust has a  $P$  wave velocity of  $7.3 \pm 0.1$  km/s and is observed down to a depth of  $60 \pm 10$  km. This depth corresponds as well to the maximum depth of seismogenic coupling in the Chilean subduction zone. The subducted oceanic crust overlies an oceanic upper mantle with a  $P$ -wave velocity of  $8.0 \pm 0.1$  km/s. Apparently, oceanic crust is being subducted beneath Iquique as well. However, this feature is less constrained by the data available from this region.

**Key words:** P-wave velocity structure, northern Chile, subducted oceanic crust, Nazca Plate

## 1 INTRODUCTION

Northern Chile is located in one of the most active seismic zones of the circum-Pacific belt. Here, the Nazca plate subducts beneath the South American plate with a relative convergence rate of about 8.4 cm/yr (DeMets *et al.* 1990). The associated high rate of background seismicity is well documented, but the historical seismicity in northern Chile is not clearly established due to the lack of reliable documents before the nineteenth century. Nevertheless, we know that a great earthquake, for which a complete description of damage exists, occurred here on May 10, 1877. The magnitude estimated for this event is  $M_w \approx 8.7$  (Abe 1979; Comte & Pardo 1991; Kausel 1986; Lomnitz 1971). The estimated rupture length is about 450 km, and ranges from the south of Arica to the north of Antofagasta (Fig. 1). The absence of earthquakes of comparable size since 1877 suggests that northern Chile is an important seismic gap.

To better understand the tectonic framework of this gap, two microearthquake investigations were carried out in northern Chile using portable analog and digital seismological instruments. One of these investigations was conducted in 1988 near Antofagasta at the southern end of the estimated rupture zone of the 1877 earthquake. The second took place in 1991 near Iquique in the central part of the 1877 rupture. The principal objective of those investigations was to constrain better the shape and structure of the Wadati-Benioff zone in northern Chile (Comte *et al.* 1993a; 1993b). The earthquakes recorded during these investigations are used in this study to determine the two-dimensional  $P$  wave velocity structure along the down-going Nazca plate and the western margin of the continental South American plate.

## 2 DATA ACQUISITION AND PROCESSING

The set of arrival times used in this analysis were recorded by two microearthquake investigations performed in northern Chile: Iquique (near 20°S) during July and August of 1991, and Antofagasta (near 24°S) during September and October of 1988. These datasets sample non-overlapping volumes of the subsurface and, therefore, each was analyzed separately.

### 2.1 The Iquique investigation

The temporary seismological network in the Iquique region consisted of 11 portable

analog and 9 digital stations installed within a 150 km radius of the city of Iquique (Fig. 1, Table 1). Reported arrival times are of variable quality and were weighted accordingly. For the analog records, the accuracies of the *P* and *S* readings are about 0.1 s and 0.5 s respectively, whereas for the digital stations they are about 0.01 s and 0.2 s respectively. The highest precision *S* wave arrival times were obtained using the horizontal components of the digital instruments.

From the approximately 350 local earthquakes recorded by this array, a subset of the best constrained locations was selected to be used in the velocity inversions. We used only those events recorded with more than a total of eight arrival times and with a minimum of three *S* waves for the first cut. The hypocenters of this preliminary dataset were initially located in a one-dimensional structure inferred from the seismic refraction studies conducted by Wigger et al. (1993) near Iquique (Table 2). *S* wave velocities for this model were derived from Wadati diagrams that show an average  $V_p/V_s$  ratio of  $1.76 \pm 0.01$  for events between 0-200 km in depth (Fig. 2a). Also, we selected only those events that had an RMS residual of less than 0.3 s in their location. An additional filter designed to reduce the possibility of grossly incorrect raypaths was to vary the initial depth from 0 to 250 km in variable intervals (10-25 km) and to keep only those events that converged consistently to the same location. After the application of these filters, 220 earthquakes were considered to be of sufficient quality for use in the inversion analysis (Fig. 1).

## 2.2 The Antofagasta investigation

The Antofagasta network consisted of 13 analog and 16 digital portable stations installed within a 150 km radius of the city of Antofagasta (Fig. 1, Table 4). The precision of the *P* and *S* -wave readings is similar to that determined for Iquique for both the analog and digital stations.

From an initial dataset of 380 earthquakes recorded by the network, 217 were considered reliable to be used in the inversion using the same criteria described above. In this case, however, the one-dimensional model used to compute the initial locations was inferred from seismic refraction studies near Antofagasta (Wigger 1988; Table 4). A  $V_p/V_s$  ratio of  $1.73 \pm 0.01$ , determined by constructing Wadati diagrams for events between 0-200 km in depth (Fig. 2b), was used to specify the *S* wave velocities.

### 3 THE INVERSION METHOD

Arrival times of  $P$  and  $S$  waves recorded by local seismic networks are used to determine simultaneously the hypocentral locations and the local  $P$  and  $S$  wave velocity structures. The technique, based on the method originally proposed by Aki & Lee (1976), is similar to that used by other authors (*e.g.*, Abers & Roecker 1991; Roecker 1982; Roecker *et al.* 1987). A detailed explanation of the method can be found in those papers and is discussed here briefly. The area of study is parameterized as a set of constant velocity blocks of arbitrary dimension.  $P$  and  $S$  wave velocities are specified and determined as independent parameters within each block. While  $S$  wave velocities are generally poorly resolved, the inclusion of  $S$  phases helps to stabilize the hypocentral locations. Rays are traced through the three-dimensional structures using an approximate method proposed by Thurber & Ellsworth (1980) to determine travel times and derivatives. All calculations were done using a spherical Earth geometry combined with an Earth-flattening transformation.

We made use of the reparameterization technique (Abers & Roecker 1991) to group elementary blocks into larger structures or "metablocks". These metablocks allow us to introduce, in a simple way, geometries that incorporate information about boundaries between major structures, and also permit us to combine parameters that are poorly resolved individually.

The inversion applies an iterative, nonlinear formulation similar to that described by Tarantola & Valette (1982). The techniques of progressive inversion and parameter separation were also incorporated (Pavlis & Booker 1980; Roecker 1982). This means that earthquakes are relocated prior to perturbing the structure and that the hypocentral parameters are formally decoupled from the velocity parameters when solving for structural perturbations.

Because of the intrinsic smoothing resulting from the use of metablocks, no additional smoothing constraints are applied. Thus, the *a priori* covariance matrix of the model is diagonal. Generally, the size of this diagonal element had to be rather large, typically an order of magnitude greater than what might be presumed from simple considerations of *a priori* uncertainties, in order to stabilize the iterative procedure.

Station corrections were not included because all the stations were installed on hard rock. Therefore, the near-surface structure is not expected to produce a significant delay. Mean sea level is taken as the origin, and compensation for elevation differences

of the various stations are explicitly computed for each ray. The inversion was iterated until changes in velocities became small ( $< 0.05$  km/s) and the variance reduction became insignificant ( $< 2\%$ ). In general, two or three iterations were sufficient to fit these criteria.

#### 4 PREVIOUS SEISMIC REFRACTION STUDIES

The initial velocity models were derived from seismic refraction profiles carried out in northern Chile from 1982 to 1989 by the Mobility of Active Continental Margins research group established by the University of Berlin in cooperation with local institutions from Argentina, Bolivia and Chile. The recording lines and shot points of these crustal seismic studies cover an area from the Coastal Cordillera to the Western Andean Cordillera, and range in latitude from  $20^{\circ}\text{S}$  to  $26^{\circ}\text{S}$ . We used a profile near  $24^{\circ}\text{S}$  of the Global Geoscience Transect 6 (Wigger *et al.* 1991) as the initial model for the analysis of the Antofagasta data, and a profile near  $21^{\circ}\text{S}$  (Wigger *et al.* 1993) for the analysis of the Iquique data.

Both profiles show strong east-west variations in crustal structure. There is a rapid increase in crustal thickness: it varies from about 40 km under the Coastal Cordillera to a maximum of 65-70 km about 200 km inland from the coast. The structure of the upper crust changes dramatically in velocity and thickness in the area of the Pre-Cordillera; the western part has average velocities of 6.4-6.6 km/s, whereas the eastern part has a velocity of only 6.0 km/s. Strata with velocities less than 6.4 km/s are thin in the west and thicken progressively towards the east, reaching 30-40 km under the active volcanic arc. The upper crust has a velocity of 6.7 km/s under the Coastal Cordillera and Central Valley, 6.3 km/s in Pre-Cordillera, and an average of about 5.9 km/s under the Andean Cordillera. These variations in the average velocities of the crust from east to west led Wigger *et al.* (1991) to infer that the forearc is colder and more rigid than the lower crust beneath the magmatic arc.

In both profiles ( $21^{\circ}\text{S}$  and  $24^{\circ}\text{S}$ ), a low velocity zone is present in the uppermost mantle beneath the continent. Wigger *et al.* (1991) proposed several alternative explanations for the presence of this low velocity zone, including the presence of magmatic restite, underthrust continental crust, subducted oceanic crust of the Nazca plate, serpentinized mantle material, or a combination of these.

In contrast to the significant variations in structure seen along the east-west profiles, a



north-south profile along the Coastal Cordillera from Iquique to the south of Antofagasta (Wigger *et al.* 1993) revealed no significant north-south variations in the velocity structure of the continental crust and upper mantle. Combining this inference with observations of a similar north-south uniformity in surficial geology and offshore bathymetry in this region, we surmise that the crust and upper mantle in this region is approximately two-dimensional.

## 5 RESULTS OF THE VELOCITY INVERSIONS

### 5.1 Selection of the initial model

The distribution of raypaths for both the Iquique and Antofagasta investigations is insufficient to constrain a detailed three-dimensional velocity structure. However, as discussed above, prior information from refraction studies and surficial features suggest that a two-dimensional representation is locally sufficient. Initial trials with simple three-dimensional structures also failed to reveal significant north-south variations in structure along the strike of the subduction zone. Nevertheless, the dip angle of the Wadati-Benioff zones is slightly steeper beneath Iquique than it is beneath Antofagasta, and there is a lack of overlap between both investigations. Therefore, we determined two independent models, one for each investigation. The block boundaries are oriented in a direction parallel to the convergence of the Nazca plate relative to South America (N77°E; DeMets *et al.* 1990). The size and position of the metablocks was governed both what are likely to be major structural elements in this area (*e.g.* thick continental crust, subducting oceanic lithosphere) and by the ability of the data to resolve the structures.

The initial velocities and boundaries of the metablocks making up the continental crust were inferred from the results of the refraction profiles. Thin alternating high and low-velocity layers were represented by an equivalent layer averaging the velocities of the included strata. Due to the absence of crustal seismic activity in the forearc, the shallow structure of the continental crust cannot be constrained by these datasets. For this reason, we used the velocity structures determined by the refraction investigations for the upper crust and held them fixed during the inversions.

The boundaries of the metablocks corresponding to the oceanic lithosphere were inferred from the patterns of seismicity in the Wadati-Benioff zones. The lower boundary of the upper oceanic lithosphere is unconstrained. However, because the

raypaths do not travel deeply into the slab, this is not an important consideration.

A series of inversions with different vertical and horizontal boundaries of the metablocks were run to test the sensitivity of the results relative to the choice of boundaries. In general, the velocities in the major units change by less than  $\pm 0.05$  km/s if these boundaries are shifted by about  $\pm 5$  km. Larger shifts in the location of the boundaries result in averaging of the velocity between blocks (e.g., higher velocities in the crust or lower velocities in the mantle). The fit to the data does not change significantly as most of these boundaries are moved, and thus our estimates of where these boundaries are likely to be can provide significant constraints.

A series of inversions with initial velocities in individual units varying by as much as  $\pm 1$  km/s were performed to investigate the sensitivity of the inversion results to the initial velocity model used. In each case, after about 4 iterations the results from the different models converged to similar velocity distributions, well within the expected uncertainties, demonstrating an acceptable insensitivity of the inversion results to the starting values.

*S* wave velocities were also determined and they tend to mimic the *P* wave structures, but in general their values are poorly constrained by this dataset.

## 5.2 The Iquique Inversion

The initial velocity model near Iquique and the distribution of earthquakes located with a one-dimensional model (Table 2) using HYPO71PC (Lee & Valdes 1985) near Iquique are shown in Fig. 3a (model I0, Table 3). For purposes of discussion, the metablocks corresponding to the continental lithosphere are labeled with the prefix CI, those to the upper mantle beneath the continental lithosphere with CM, and those to the upper and lower lithosphere with OI and OMI, respectively. Velocities in the three shallowest blocks (CI1, CI2, and CI3) were fixed. Of the other six metablocks, only four (CI4, CI6, OI, and CMI) had associated resolution diagonals ( $R_d$ ) exceeding 0.5 (Table 3), meaning that more information was derived from the data than from the *a priori* constraints for these perturbations. The best resolved metablock is the one associated with the subducted slab (OI), which has a velocity of  $8.1 \pm 0.2$  km/s and an  $R_d$  of 0.8. This velocity is typical of that observed in the upper mantle of the slab (e.g., Spudich & Orcutt 1980). The other four metablocks (CI4, CI6, OI, and CMI) had a lower  $R_d$  value of 0.6 and estimated uncertainties of  $\pm 0.2$ - $0.3$  km/s.

Considering that the best resolved metablock was the one associated with the

subducted oceanic lithosphere (OI), we subdivided it to see if finer structure could be determined (Table 3, model I1). The subducted slab was thus separated into two metablocks, one representing the upper part of the oceanic crust (OI1) from a depth of 10 to 150 km, and another (OI2) associated with the lower part of the oceanic crust. Although we allowed the velocity to vary in this new crustal layer, the velocity obtained in model I0, of  $8.1 \pm 0.1$  km/s with an  $R_d$  of 0.7 was again obtained.

Another inversion (Fig. 3b, Table 3, model I2), where the upper part of the oceanic crust was divided into two metablocks (OI1 and OI2), resulted in a lower velocity of  $7.7 \pm 0.2$  km/s and an  $R_d$  of 0.7 for the OI1 block. The associated oceanic upper mantle velocity of  $8.3 \pm 0.3$  km/s ( $R_d$  of 0.7) also appears to be less well constrained. Nevertheless, this model provided a significantly better fit to the arrival times (a 7% improvement in data variance compared to the model without an oceanic crust). We conclude that the Iquique dataset is capable of resolving a low velocity region at the top of the subducted slab. The depth to which this feature extends is not well constrained, but it appears that subduction of low velocity crust could reach a depth of about 60 km.

### 5.3 The Antofagasta Inversion

The starting model used in the analysis of the Antofagasta data (Fig. 4a, model A0 Table 6) is similar to that used in Iquique. Velocities in five shallow metablocks (CA1 to CA5) are fixed. The results of the inversion of the Antofagasta data with this starting model showed a low velocity zone (CMA) in the continental upper mantle (Fig. 4b). In an attempt to determine the extent of this low-velocity zone, the metablock corresponding to the upper-mantle was separated in model A1 using two smaller metablocks (CMA1 and CMA2, Fig. 5a, Model A1 Table 6)).

The only poorly resolved metablock in the inversion using model A1 is the one corresponding to the deeper part of the slab (OMA, Fig. 4a). The average  $P$  wave velocity obtained for the slab (OA) is  $7.6 \pm 0.1$  km/s with an  $R_d$  of 0.9. The three metablocks corresponding to the continental crust (CA6 to CA8) were better resolved than in the case of Iquique. The shallower continental block (CA6) converged to a velocity of  $6.7 \pm 0.2$  km/s with an  $R_d$  of 0.7. The other two metablocks beneath it (CA7 and CA8) have velocities of  $7.0 \pm 0.1$  km/s and  $7.8 \pm 0.2$  km/s with  $R_d$  values of 0.9 and 0.8, respectively. The vertical boundary between the two metablocks in the continental upper-mantle (CMA1 and CMA2) was displaced ( $\pm 5$  km) on a trial and error basis as a test of sensitivity to this boundary. In general the position of this

boundary is inconsequential, the only difference being small changes in the associated resolutions and uncertainties. A low-velocity ( $7.3 \pm 0.2$  km/s,  $R_d$  of 0.8) region is observed in the western subblock of the upper mantle (CMA1), whereas the eastern sub-block (CMA2) has a significantly higher velocity of 8.2 km/s. However, the block CMA2 is poorly resolved ( $R_d$  of 0.5) and has large uncertainties ( $\pm 0.4$  km/s).

As in the case of Iquique, the metablock representing the upper part of the slab (OA) was the best resolved and therefore, we subdivided this metablock into two independent blocks (OA1 and OA2, model A2 on Table 6) in order to determine additional details of structure in the upper part of the subducted slab. In the first test, the resulting velocities (7.6 and 7.7 km/s for OA1 and OA2 blocks, respectively) are almost the same as those obtained in model A1 for the single metablock OA of the oceanic slab.

A series of inversions was attempted where the uppermost metablock of the subducted slab was divided into two parts, and the boundary between them was varied. The model with the largest reduction in data variance (31% improvement from .083 s<sup>2</sup> to .057 s<sup>2</sup>), the lowest associated uncertainties, and the best resolution (Model A3, Table 6, Fig. 5b) suggests that the shallower part of the slab (OA1) has a lower velocity ( $7.3 \pm 0.1$  km/s) than the deeper part of the plate (OA2). The lower sub-block of the slab (OA3) has a *P* wave velocity of  $8.0 \pm 0.1$  km/s. Both are well resolved with an  $R_d$  of 0.9, which is almost the same as that obtained for the deeper crustal metablock (OA2).

Thus it is possible to identify a smaller scale structure within the subducted slab in the form of a low velocity layer attached to the top of the Nazca plate to a depth of about 60 km. We interpret this low velocity layer to be evidence of subducted oceanic crust, corresponding in *P* wave velocity to layer 3 of typical oceanic crust (e.g. Spudich & Orcutt 1980). We note also that the low velocity structure of the crust beneath the Coastal Cordillera that Wigger *et al.* (1991) observed, may be explained as well by the presence of subducted low-velocity oceanic crust.

We note that the initial low-velocity block (CMA1) for models A1 and A2 converged in model A3 (Figure 5b) to the same value of *P*-wave velocity of the deeper continental crustal layer (CA8), suggesting that both (CA8 and CMA1) may be one single block of a thick continental crust.

As a test of the robustness of the two dimensional models obtained for Iquique and Antofagasta, a set of synthetic *P* and *S* wave arrival times were generated using the final models and the same source-receiver pairs as in the original data sets. Random noise with a zero mean and a standard deviation of 0.2 s was added to these synthetic

arrival times. The resulting velocity models for Iquique and Antofagasta are very similar ( $\pm 0.1$  km/s) to the models obtained using real data (Figs. 6a and 6b), suggesting that the trends observed are not simply artifacts of the inversion procedure.

#### 5.4 Earthquake Locations

As discussed above, the initial microearthquake locations obtained using a flat one-dimensional velocity structure were reasonably well constrained. Nevertheless, the hypocenters are displaced slightly when they are relocated in the two dimensional models (Figs. 7 and 8). The changes between the two-dimensional and the one-dimensional epicentral locations are less than 1 km inside each network, and they are generally less than 3 km for events located outside the network. In the case of Iquique, the 2D-1D epicentral difference vectors show slight overall shift toward the center of the network, which is observed mainly for events located far away from it. The Antofagasta 2D-1D epicentral difference vectors show less variation than in the case of Iquique. The direction of motion, however, is toward the center of the network, mainly for events located outside of it. The hypocentral depths show more variation and are generally shifted either downwards (for Antofagasta) or upwards (for Iquique) by 2-3 km in the two-dimensional model. The different trends in 2D relocations between the Iquique and Antofagasta data sets primarily is due to the Iquique 2D model being faster, and the Antofagasta 2D model being slower, than their respective 1D models.

## 6 DISCUSSION AND CONCLUSIONS

The inversion method utilized in this study has been successfully applied before in a variety of tectonic environments (*e.g.* Abers & Roecker 1991; Ni *et al.* 1991; Prevot *et al.* 1991; Thurber 1983; 1984). In this case, the inversion is performed using a small number of events and stations where a full three-dimensional inversion with many independent blocks was not justified. Therefore, only large regions corresponding to major tectonic units were allowed to vary. Because the majority of the events recorded are located within the downgoing slab, the metablock associated with it was the best resolved in both the Iquique and Antofagasta investigations. Although the number of events utilized are almost the same in both studies, they are better distributed along the slab in the Antofagasta investigation. This, in addition to a larger number of seismic stations, results in better resolution of structure in the oceanic lithosphere beneath

Antofagasta. Therefore, we will focus our discussion in the results of the Antofagasta analysis.

The *P* wave velocities determined for the upper-mantle below the continent are not as well resolved as in the other blocks. However, they consistently converged to values of about 8.4 km/s in both regions (CMI, Iquique-model 2 and CMA2, Antofagasta-model 3). This value is slightly higher than that expected for the upper mantle. It is not, however, an unreasonable average estimate of velocities between 60 and 150 km depth.

The distribution of seismicity recorded during the Antofagasta investigation allowed us to resolve structural details in the downgoing slab. As mentioned above, we interpret the low velocities in the upper part of the slab (OI1, Iquique-model2 and OA1, Antofagasta-model3) as evidence of subducted oceanic crust beneath northern Chile. Test inversions varying the size of this layer suggest an average thickness of about 10 km. A thicker crust results in significantly larger misfits of the arrival times. The available data is incapable of determining whether the subducted oceanic crust is thinner than ~10 km. At the same time, it is unlikely that any discernible residual would have been generated if it is significantly thinner than ~10 km. The maximum depth extent of the subducted oceanic crust appears to be  $\sim 60 \pm 10$  km; a depth corresponding approximately to the maximum depth of seismogenic coupling in the Chilean subduction zone (Suárez & Comte 1993; Tichelaar & Ruff 1991).

Tichelaar and Ruff (1991) proposed several mechanisms that may control the maximum depth of coupling. Among them: i) a reduction of the frictional strength due to thermally activated creep, ii) the rate of plate convergence and the age of the subducting oceanic lithosphere, iii) the dip angle of the slab and its relation to volcanic activity, iv) the thickness of the continental crust, v) strength variations on the interface associated with sediments, vi) phase changes from basalt to eclogite, and vii) the presence of water at depth. They pointed out that it is difficult to identify which mechanisms, if any, dominate over the others in determining the maximum depth of coupling.

The results of the present study, when compared with studies of the Philippine plate (Hori et al., 1985, Hori, 1990) and the Pacific plate (Hirukawa & Imoto, 1992) suggest that the phase change from basalt to eclogite play a prominent, if not the dominant, role in controlling the maximum depth of coupling. Beneath Antofagasta we are able to resolve a low-velocity layer on top of the subducting slab with a *P*-wave velocity typical of basaltic crust to depths of approximately 60 km, corresponding to the depth

of coupling in this region. This result is similar to that obtained by Hori *et al.* (1985) and Hori (1990), who analyzed the depth of the conversion of oceanic gabbro to eclogite in subducted crust along the Philippine plate. Their results suggest that the subducting oceanic crust remains in a gabbroic phase to depths of less than 60 km along the entire northern boundary of the Philippine plate. Moreover, Hori & Imoto (1992) concluded from an analysis of focal mechanisms of earthquakes that gabbro does not transform into eclogite at depths of less than about 50 km in the Philippine plate and 70 to 80 km in the Pacific plate. Therefore, the estimated depth of about 60 km for which a low-velocity upper crust on the subducted Nazca plate is observed in the inversions of the Antofagasta data set may similarly be associated with the depth of the phase transformation in the oceanic crust from gabbro to eclogite. In turn, this phase transformation may play a role in defining the maximum depth extent of unstable sliding on the interplate contact.

The correlation between the depth of phase transition with the depth of the seismogenic coupling between plates with very different ages, rates of convergence, slab dip angles, thickness of overlying continental crust, and sedimentation history, suggest the dominance of this mechanism over several (but not all) of its competitors listed above.

## 7 ACKNOWLEDGMENTS

We thank M. Schmitz and P. Wigger for providing us with the refraction profile models. We also thank D. Byrne, A. Snoke, B. Tichelaar, and C. Valdés for their useful suggestions. The Antofagasta and Iquique investigations were funded by the Institut Français de Recherche Scientifique pour le Développement en Coopération (ORSTOM) and by the International Development Research Center (IDRC) of Canada through a grant to the Pan American Institute of Geography and History (PAIGH). This work was partially funded by the Fundación Andes in Chile (grant C52040).

## REFERENCES

- Abe, K., 1979. Size of the great earthquakes of 1837-1974 inferred from tsunami data, *J. Geophys. Res.*, **84**, 1561-1568.

- Abers, G. A. & Roecker, S. W., 1991. Deep structure of an arc-continent collision: earthquake relocation and inversion for upper mantle *P* and *S* wave velocities beneath Papua New Guinea, *J. Geophys. Res.*, **96**, 6379-6401.
- Aki, K. & Lee, W., 1976. Determination of three-dimensional velocity anomalies under a seismic array using first *P* arrival times from local earthquakes, 1, A homogeneous model, *J. Geophys. Res.*, **81**, 4281-4339.
- Comte, D. & Pardo, M., 1991. Reappraisal of great historical earthquakes in northern Chile and southern Peru seismic gaps, *Natural Hazards*, **4**, 23-44.
- Comte, D., Pardo, M., Dorbath, L., Dorbath, C., Haessler, H., Rivera, L., Cisternas, A. & Ponce, L., 1993a. Seismogenic interplate contact zone and crustal seismicity around Antofagasta, northern Chile using local data, *Geophys. J. Int.* in press
- Comte, D., Suárez, G., Monfret, T., Pardo, M., Ponce, L. & Dominguez, J., 1993b. Preliminary results of a seismic experiment in northern Chile during July and August, 1991, *Geofísica* in press.
- DeMets, C., Argus, R. G. & Stein, S., 1990. Current plate motions, *Geophys. J. Int.*, **101**, 425-478.
- Hori, S., Inoue, H., Fukao, Y. & Ukawa, M., 1985. Seismic detection of the untransformed 'basaltic' oceanic crust subducting into the mantle, *Geophys. J. R. astr. Soc.*, **83**, 169-197.
- Hori, S., 1990. Seismic waves guided by untransformed oceanic crust subducting into the mantle: the case of the Kanto district, central Japan, *Tectonophysics*, **176**, 355-376.
- Hurukama, N. & Imoto, M., 1992. Subducting oceanic crust of the Philippine Sea and Pacific plates and weak-zone-normal compression in the Kanto district, Japan, *Geophys. J. Int.*, **109**, 639-652.
- Kausel, E., 1986. Los terremotos de Agosto de 1868 y Mayo de 1877 que afectaron el sur del Perú y norte de Chile, *Boletín de la Academia Chilena de Ciencias*, **3**, 8-12.
- Lee, W. & Valdes, C., 1985. HYPO71 PC: A personal computer version of the HYPO71 earthquake location program, *U.S. Geol. Surv. Open-File Report 85-749*, 43 pp..
- Lomnitz, C., 1971. Grandes terremotos y tsunamis en Chile durante el período 1535-1955, *Geofis. Panam.*, **2**, 151-178.
- Ni, J., Ibenbrahim, A. & Roecker, S., 1991. Three-dimensional velocity structure and hypocenters of earthquakes beneath the Hazara Arc, Pakistan: Geometry of the



- underthrusting Indian plate, *J. Geophys. Res.*, **96**, 19,865-19,877.
- Prevot, R., Roecker, S., Isacks, B. & Chatelain, J., 1991. Mapping of low *P* wave velocity structure in the subducting plate of the central New Hebrides, southwest Pacific, *J. Geophys. Res.*, **96**, 19,825-19-842.
- Roecker, S., 1982. Velocity structure of the Pamir-Hindu Kush region: Possible evidence of subducted crust, *J. Geophys. Res.*, **87**, 945-959.
- Roecker, S., Yeh, Y. & Tsai, Y., 1987. Three-dimensional *P* and *S* wave velocity structures beneath Taiwan: Deep structure beneath and arc-continent collision, *J. Geophys. Res.*, **92**, 10,547-10,570.
- Suárez, G. & Comte, D., 1993. Comment on "Seismic coupling along the Chilean subduction zone" by B. W. Tichelaar and L. R. Ruff, *J. Geophys. Res.*, **98**, 15,825-15,828.
- Spudich, P. & Orcutt, J., 1980. A new look at the seismic velocity structure of the oceanic crust, *Rev. Geophys. Space Phys.*, **18**, 627-645.
- Tarantola, A. & Valente, B., 1982. Inverse problem = Quest for information, *J. Geophys.*, **50**, 159-170.
- Thurber, C. & Ellsworth, W., 1980. Rapid solution of ray tracing problems in heterogeneous media, *Bull. Seismol. Soc. Am.*, **70**, 1137-1148.
- Thurber, C., 1983. Earthquake locations and three-dimensional crustal structure in the Coyote Lake are, central California, *J. Geophys. Res.*, **88**, 8226-8236.
- Thurber, C., 1984. Seismic detection of the summit magma complex of Kilauea volcano, Hawaii, *Science*, **223**, 165-167.
- Thurber, C., 1985. Nonlinear earthquake locations: theory and examples, *Bull. Seismol. Soc. Am.*, **75**, 779-790.
- Tichelaar, B. & Ruff, L., 1991. Seismic coupling along the Chilean subduction zone, *J. Geophys. Res.*, **96**, 11,997-12,022.
- Wigger, P., 1988. Seismicity and crustal structure of the central Andes, In: *The Southern Central Andes*, H. Bahlburg, Ch. Breitkreuz, P. Giese (Eds.) *Lecture Notes in Earth Sciences*, **17**, 209-229.
- Wigger, P., Araneda, M., Asch, G., Giese, P., Heinsohn, W.-D., Rower, P., Schmitz, M. & Viramonte, J., 1991. The crustal structure along the central Andean transect derived from seismic refraction investigations, *Global Geoscience Transect 6, Central Andean Transect, Nazca Plate to Chaco plains southwestern Pacific Ocean, Northern Chile and Northern Argentina*. Copublished by the Inter-Union

Commission on the Lithosphere and American Geophysical Union, 13-19.  
Wigger, P., Schmitz, M., Araneda, M., Asch, G., Baldzuhn, S., Giese, P., Heinsohn, W.-D., Martinez, E., Ricaldi, E., Rower, P. & Viramonte, J., 1993. Variation of the crustal structure of the southern central Andes deduced from seismic refraction investigations. In: Tectonics of the Southern Central Andes, 23-48; Reutter, Scheuber & Wigger (Eds.), Springer Verlag, Berlin Heidelberg New York.

#### FIGURE CAPTIONS

**Figure 1.** The rectangular white areas show the location of the inverted volumes in Iquique and Antofagasta. The microearthquakes recorded and seismic stations deployed in both areas are indicated by circles and by squares respectively. Black triangles represent the Quaternary volcanoes. Open arrow shows the convergence direction of the Nazca plate relative to the South America plate (DeMets et al., 1990). The area of intensity VIII MM of the 1877 great earthquake is shown as a dashed line. Bathymetry and topography contours are in meters.

**Figure 2.** Wadati diagrams for (a) the Iquique investigation and (b) the Antofagasta investigation

**Figure 3.** Results from the inversion of the Iquique dataset (Table 3), presented in a 2D profile indicated on Fig.1 (I-I'). Each metablock is identified in its left upper corner, the value that is located to the right or below it corresponds to the P-wave velocity (km/s). White squares show the initial hypocenters of the events using one-dimensional velocity structure. The two first layers were fixed and not included in the inversion. The white metablocks are those that were poorly resolved ( $R_d < 0.5$ ). The projection of the seismic stations and the volcanoes are shown as vertical bars and triangles, respectively. The gray scale representing the velocity scale is shown on the lower part of the Figure. (a) Initial P wave velocity model (I0). (b) Final P wave velocity model (I2).

**Figure 4.** Results from the inversion of the Antofagasta dataset (Table 6) Symbols as on Fig. 3. (a) Initial P wave velocity model (A0). (b) Resulting P wave velocity model (A0).

**Figure 5.** Results from the inversion of the Antofagasta dataset (Table 6) Symbols as on Fig. 3. (a) Initial  $P$  wave velocity model (A1). (b) Resulting  $P$  wave velocity model (A3). The low-velocity layer in the upper part of the subducted slab is interpreted as subducted oceanic crust.

**Figure 6.** Results of a test of the inversion results using synthetic arrival times: (a) The Iquique dataset; (b) The Antofagasta dataset. Symbols as on Fig. 3.

**Figure 7.** Locations of selected earthquakes from the Iquique investigation in the final two-dimensional model. (a) Epicenters are indicated as open circles. For each epicenter a line is drawn from the original location in the one-dimensional structure to the final epicenter in a 2D velocity structure. (b) Cross-section of hypocenters (open circles) along the PI-PI' profile

**Figure 8.** Locations of selected earthquakes from the Antofagasta investigation in the final two-dimensional model. (a) Epicenters are indicated as open circles. Symbols as on Fig. 7. (b) Cross-section of hypocenters (open circles) along the PA-PA' profile.

**Table 1.** Locations of Seismic Stations (Iquique, 1991)

Name	Location	Lat °	Long °	Elev. (km)	Station type +
IQQ	Iquique	-20.213	-70.095	865	M+R; E+L
CHU	Chucumata	-20.530	-70.174	85	M+R
PAT	Patache	-20.809	-70.179	55	M+R
GER	Gertrudis	-21.018	-70.024	730	M+R; E+L
CON	Cóndor	-20.390	-70.004	865	M+R; E+L
SOR	Soronal	-20.588	-69.980	800	M+R; E+L
MAP	Mapocho	-20.048	-69.765	1150	M+R
DIA	Diana	-20.409	-69.821	1050	M+R
BEL	Bellavista	-20.837	-69.702	970	M+R
SAG	Sagasca	-20.241	-69.391	1450	M+R; E+L
CHA	Challacollo	-20.965	-69.174	1650	M+R; E+L
BLA	Pta. Blanca	-21.183	-70.091	50	E+L4C
AGU	Aurora	-19.835	-69.866	1250	E+L
AUR	Aurrerá	-20.637	-69.629	1020	E+L4C

+M+R=MEQ800 analog recorder and Ranger vertical seismometer

E+L = EDA portable digital recorder PRS-4 and Lennartz LE-3D three components seismometer

E+L4C = EDA portable digital recorder and Mark L4C vertical seismometer

**Table 2.**  
Iquique - 1991  
1D-HYPO71  
*P* Velocity model

Vp (km/s)	h (km)*
5.5	0.0
6.9	3.7
7.1	14.3
8.1	29.0
8.0	42.0

\* Depth to bottom of layer

**Table 3 Results of the Iquique Inversions**

Model I0			Model I1			Model I2			
MB	V <sub>Ip</sub> km/s	Resulting V <sub>p</sub> km/s	MB	V <sub>Ip</sub> km/s	Resulting V <sub>p</sub> km/s	MB	V <sub>Ip</sub> km/s	Resulting V <sub>p</sub> km/s	Synthetic V <sub>p</sub> km/s
CI1	5.9	fixed	CI1	5.9	fixed	CI1	5.9	fixed	fixed
CI2	5.3	fixed	CI2	5.3	fixed	CI2	5.3	fixed	fixed
CI3	6.6	fixed	CI3	6.6	fixed	CI3	6.6	fixed	fixed
CI4	6.8	7.2±0.2 (0.6)	CI4	6.8	7.1±0.2 (0.5)	CI4	6.8	7.2±0.2 (0.6)	7.2±0.2 (0.8)
CI5	5.9	R <sub>d</sub> <0.5	CI5	5.9	R <sub>d</sub> <0.5	CI5	5.9	R <sub>d</sub> <0.5	R <sub>d</sub> <0.5
CI6	7.4	7.8±0.2 (0.6)	CI6	7.4	7.7±0.2 (0.7)	CI6	7.4	7.5±0.2 (0.6)	7.5±0.2 (0.7)
CMI	8.7	8.4±0.3 (0.6)	CMI	8.7	8.2±0.3 (0.7)	CMI	8.7	8.3±0.3 (0.7)	8.3±0.2 (0.9)
OI	8.0	8.1±0.2 (0.8)	OI1	8.0	8.1±0.2 (0.8)	OI1	8.0	7.7±0.2 (0.8)	7.7±0.2 (0.8)
			OI2	8.0	7.9±0.2 (0.9)	OI2	8.0	8.3±0.2 (0.8)	8.3±0.2 (0.8)
OMI	8.7	R <sub>d</sub> <0.5	OMI	8.7	R <sub>d</sub> <0.5	OI3	8.0	8.3±0.2 (0.7)	8.3±0.2 (0.9)
						OMI	8.7	R <sub>d</sub> <0.5	R <sub>d</sub> <0.5

MB = Identification of the metablocks for each model  
V<sub>Ip</sub> = Initial P-wave velocities for each model  
The R<sub>d</sub> value is indicated in parenthesis, when it is greater than 0.5.

**Table 4.** Location of Seismic Stations (Antofagasta, 1988)

Name	Location	Lat °	Long °	Elev. (km)	Station type +
CAL	Calama	-22.480	-69.025	2030	M+L4C
HOS	Hornitos	-22.958	-70.278	270	M+L4C
DVM	D. Mejilones	-23.251	-70.344	360	M+L4C
CLB	Culebron	-23.340	-69.768	1320	M+L4C
MIR	Miranda	-23.357	-70.177	1225	M+L4C
CHO	Chacabuco	-23.056	-69.593	1570	M+L4C
FAR	Farol	-23.498	-70.299	950	M+L4C
CUE	Cuevitas	-23.628	-69.939	960	M+L4C
COL	Coloso	-23.777	-70.439	150	M+L4C
TOS	Tosca	-23.914	-70.259	720	M+L4C
YUG	Yugoslavia	-24.021	-69.863	1250	M+L4C
YNG	Yungay	-24.089	-70.086	1070	M+L4C
ROS	Rosario	-24.457	-69.892	1470	M+L4C
SRA	Sierra Gorda	-22.866	-69.347	1800	G+L22
TAM	Tamira	-22.645	-70.243	270	G+L22
ESM	Esmeralda	-22.934	-69.867	1510	G+L22
MBL	Man. Blancos	-23.455	-70.027	840	G+L22
MOR	Moreno	-23.510	-70.550	220	G+L22
MAG	Magnesia	-24.095	-69.597	1400	G+L22
SGR	San Gregorio	-24.218	-69.825	1130	G+L22
LVI	Los Vientos	-24.483	-70.315	1930	DT+L4C
MIC	Michilla	-22.826	-70.233	1527	DT+L4C
ANG	Angamos	-23.101	-70.512	710	DT+L4C
VAL	Valenzuela	-23.166	-69.997	1400	DT+L4C
MAR	Morrito	-23.261	-69.519	1720	DT+L4C
SCR	San Cristobal	-23.446	-69.587	1820	DT+L4C
LMO	Los Morros	-23.566	-70.276	1000	DT+L22
AVI	Aug. Victoria	-24.112	-69.256	2250	DT+L4C
CRI	Cro. Sta. Rita	-24.167	-70.371	1620	DT+L4C

+M+L4C=MEQ800 analog recorder and Mark L4C vertical seismometer  
 G+L22=GEOSTRAS digital recorder and Mark L22 three components seismometer  
 DT+L4C=Digital telemetric recorder and Mark L4C vertical seismometer  
 DT+L22=Digital telemetric recorder and Mark L22 three components seismometer

**Table 5.**  
 Antofagasta - 1988  
 1D-HYPO71  
 P Velocity model

Vp (km/s)	h (km)*
5.5	0.0
6.2	6.0
6.8	10.0
7.2	29.0
8.0	55.0

\* Depth to bottom of layer

**Table 6 Results of the Antofagasta Inversions**

Model A0			Model A1			Model A2			Model A3			
MB	V <sub>Ip</sub> km/s	Resulting V <sub>p</sub> km/s	MB	V <sub>Ip</sub> km/s	Resulting V <sub>p</sub> km/s	MB	V <sub>Ip</sub> km/s	Resulting V <sub>p</sub> km/s	MB	V <sub>Ip</sub> km/s	Resulting V <sub>p</sub> km/s	Synthetic V <sub>p</sub> km/s
CA1	6.0	fixed	CA1	6.0	fixed	CA1	6.0	fixed	CA1	6.0	fixed	fixed
CA2	5.8	fixed	CA2	5.8	fixed	CA2	5.8	fixed	CA2	5.8	fixed	fixed
CA3	5.1	fixed	CA3	5.1	fixed	CA3	5.1	fixed	CA3	5.1	fixed	fixed
CA4	6.3	fixed	CA4	6.3	fixed	CA4	6.3	fixed	CA4	6.3	fixed	fixed
CA5	6.1	fixed	CA5	6.1	fixed	CA5	6.1	fixed	CA5	6.1	fixed	fixed
CA6	6.5	6.7±0.1 (0.6)	CA6	6.5	6.7±0.2 (0.7)	CA6	6.5	6.7±0.2 (0.6)	CA6	6.5	6.6±0.2 (0.7)	6.6±0.2 (0.8)
CA7	7.1	7.1±0.1 (0.8)	CA7	7.1	7.0±0.1 (0.9)	CA7	7.1	7.0±0.1 (0.7)	CA7	7.1	7.1±0.1 (0.9)	7.1±0.1 (0.9)
CA8	7.6	7.8±0.2 (0.7)	CA8	7.6	7.8±0.2 (0.8)	CA8	7.6	7.9±0.2 (0.7)	CA8	7.6	7.5±0.2 (0.8)	7.5±0.2 (0.9)
CMA	8.7	7.2±0.2 (0.6)	CMA1	8.7	7.3±0.2 (0.8)	CMA1	8.7	7.3±0.2 (0.6)	CMA1	8.7	7.5±0.2 (0.8)	7.5±0.1 (0.9)
			CMA2	8.7	8.2±0.4 (0.5)	CMA2	8.7	R <sub>d</sub> <0.5	CMA2	8.7	8.5±0.3 (0.6)	8.6±0.3 (0.7)
OA	8.0	7.6±0.1 (0.9)	OA	8.0	7.6±0.1 (0.9)	OA1	8.0	7.6±0.1 (0.8)	OA1	8.0	7.3±0.1 (0.9)	7.3±0.1 (0.9)
						OA2	8.0	7.7±0.1 (0.9)	OA2	8.0	8.0±0.2 (0.9)	8.1±0.2 (0.9)
									OA3	8.0	8.0±0.1 (0.9)	8.0±0.1 (0.9)
OMA	8.7	R <sub>d</sub> <0.5	OMA	8.7	R <sub>d</sub> <0.5	OMA	8.7	R <sub>d</sub> <0.5	OMA	8.7	R <sub>d</sub> <0.5	R <sub>d</sub> <0.5

Symbols as on Table 3

Figure 1

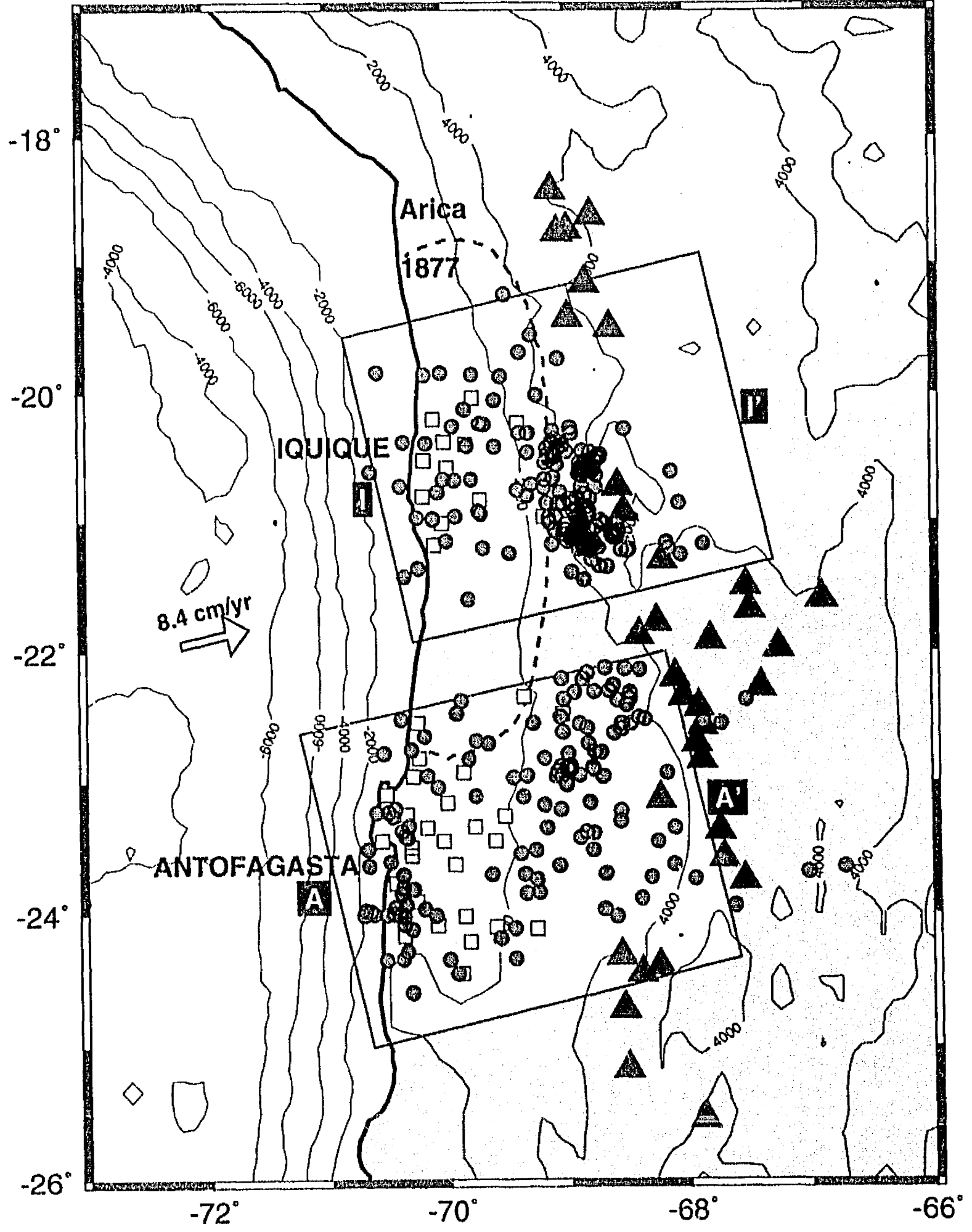




Figure 2

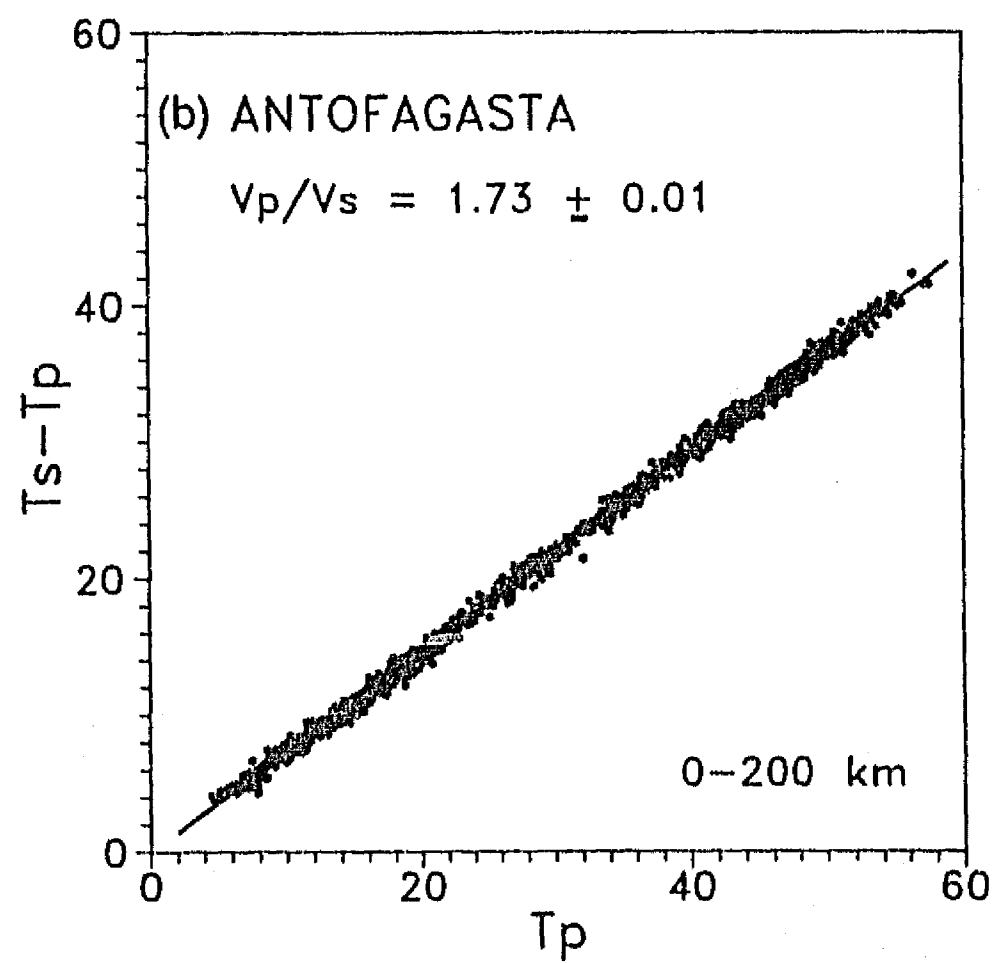
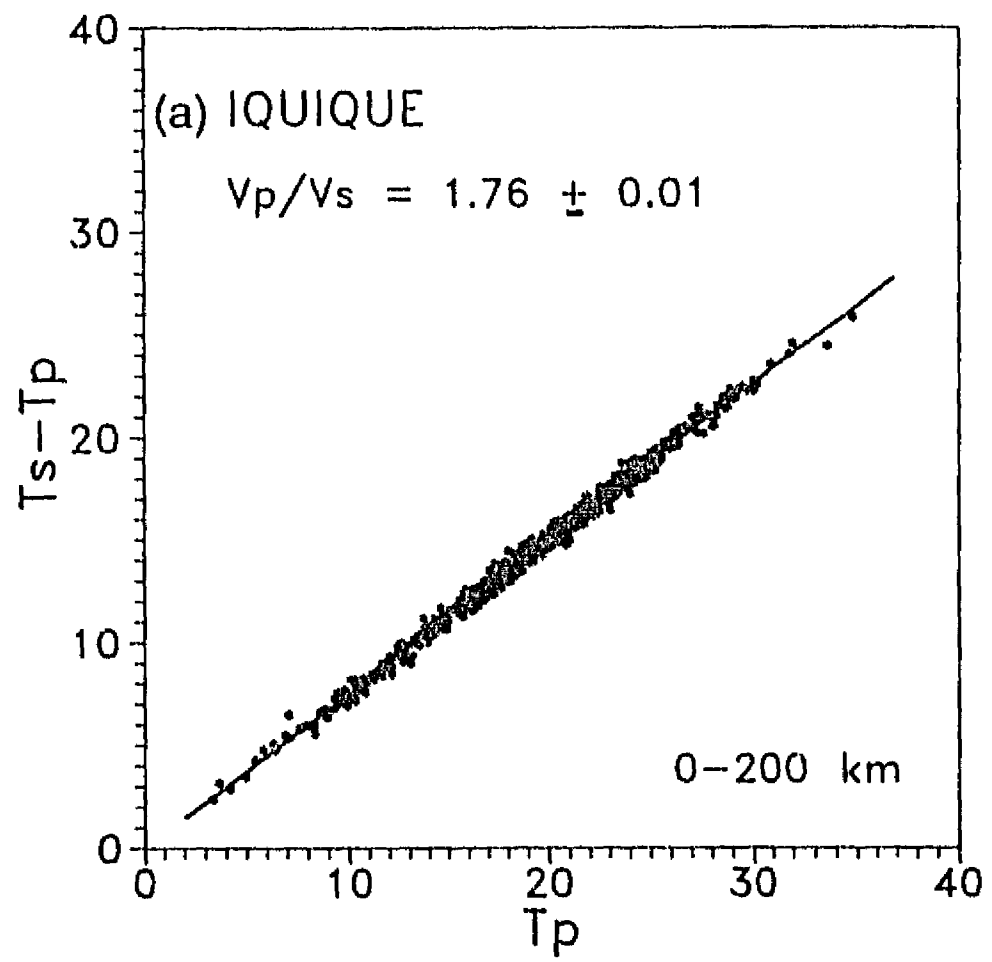
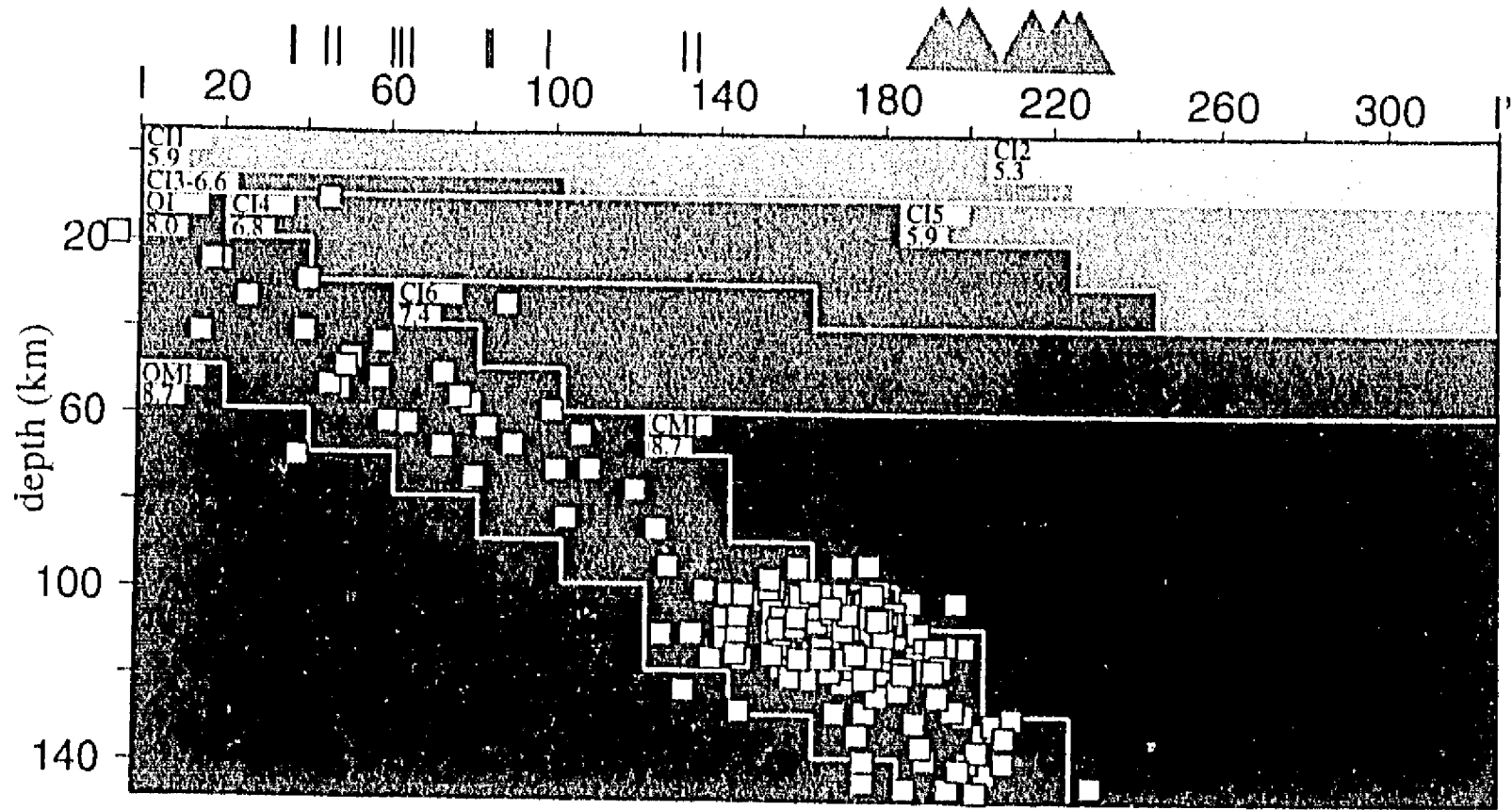


Figure 3

(a) IQUIQUE INITIAL P-WAVE VELOCITY MODEL I0



(b) IQUIQUE FINAL P-WAVE 2D VELOCITY MODEL I2

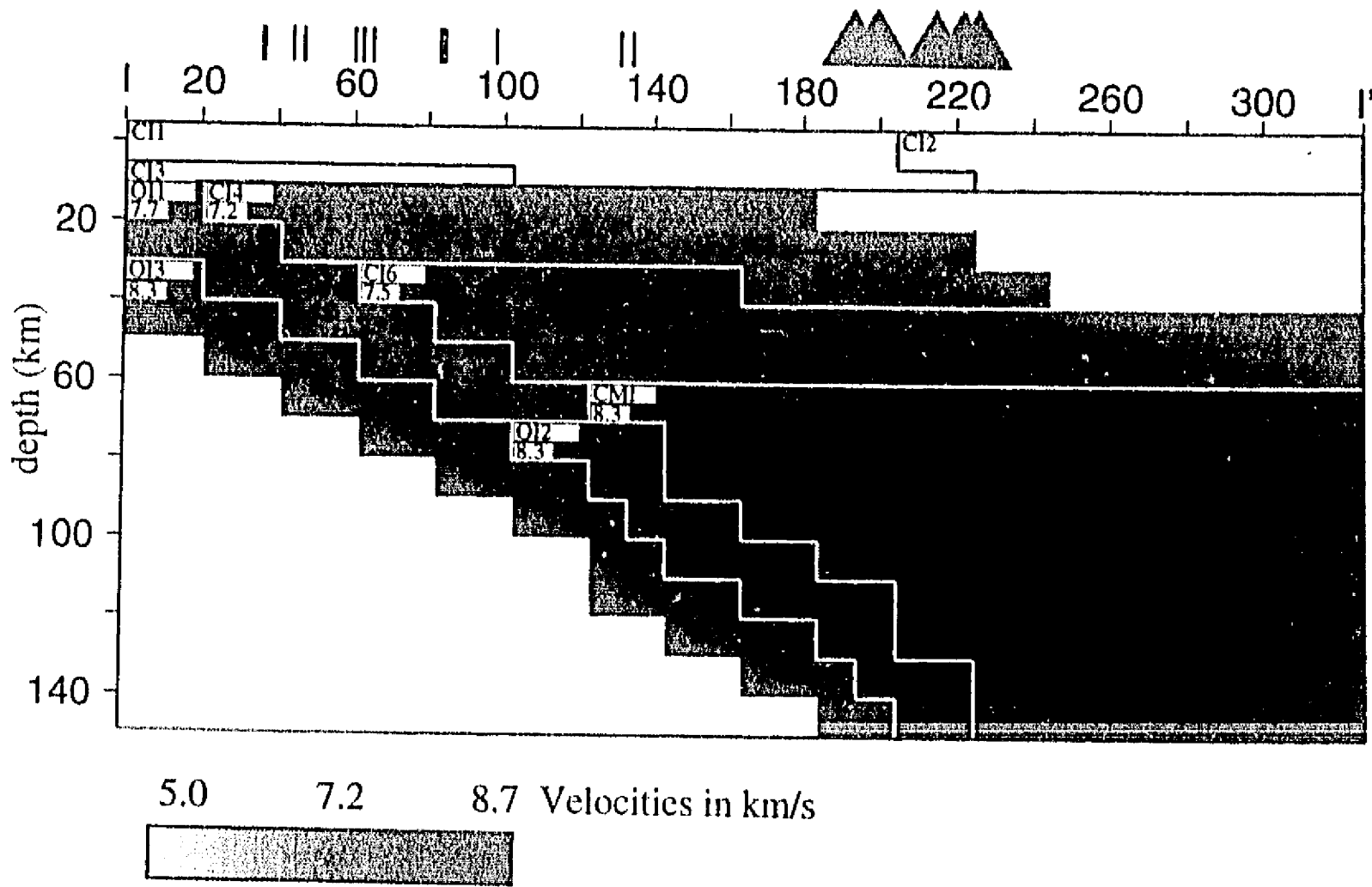
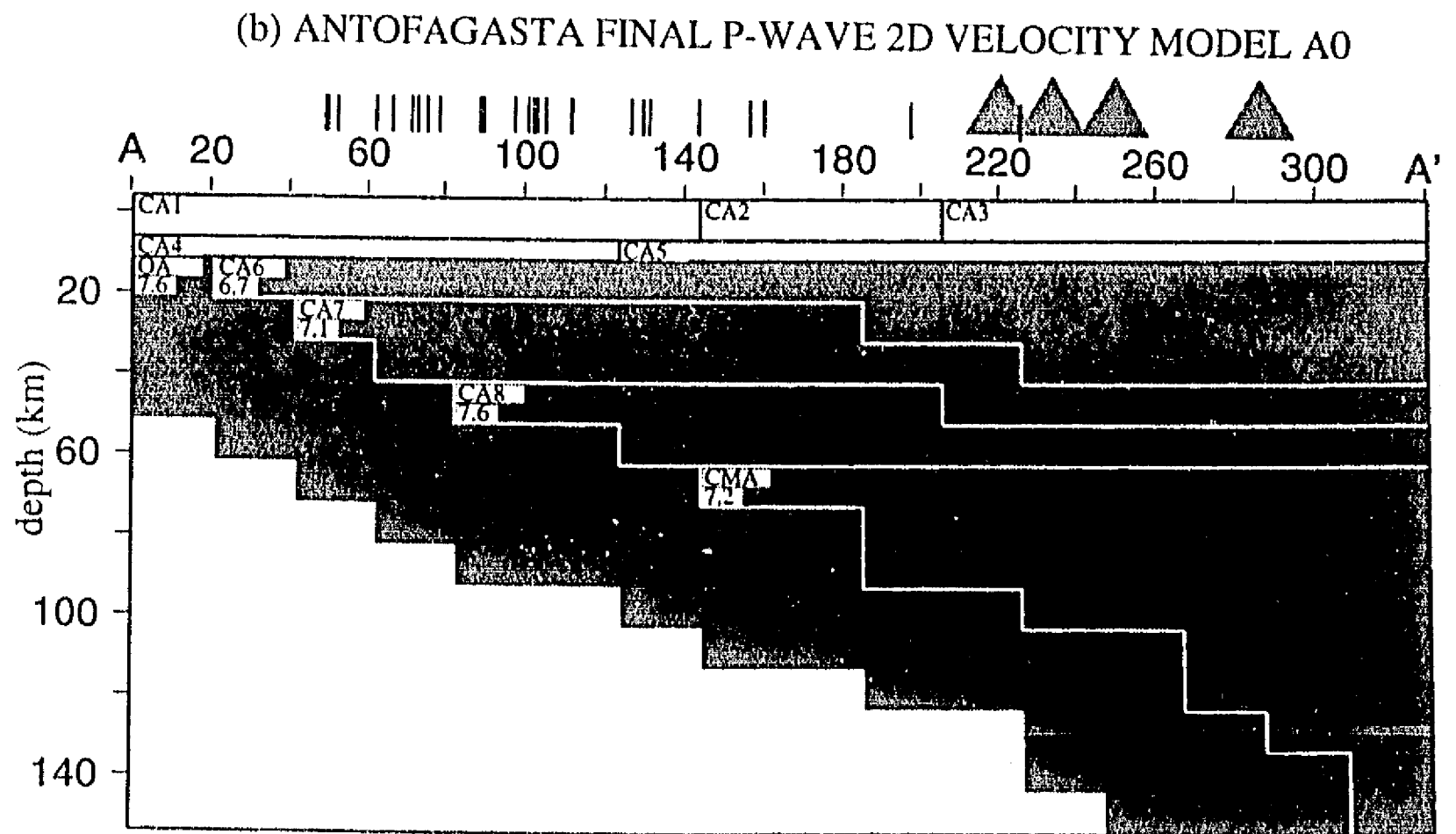
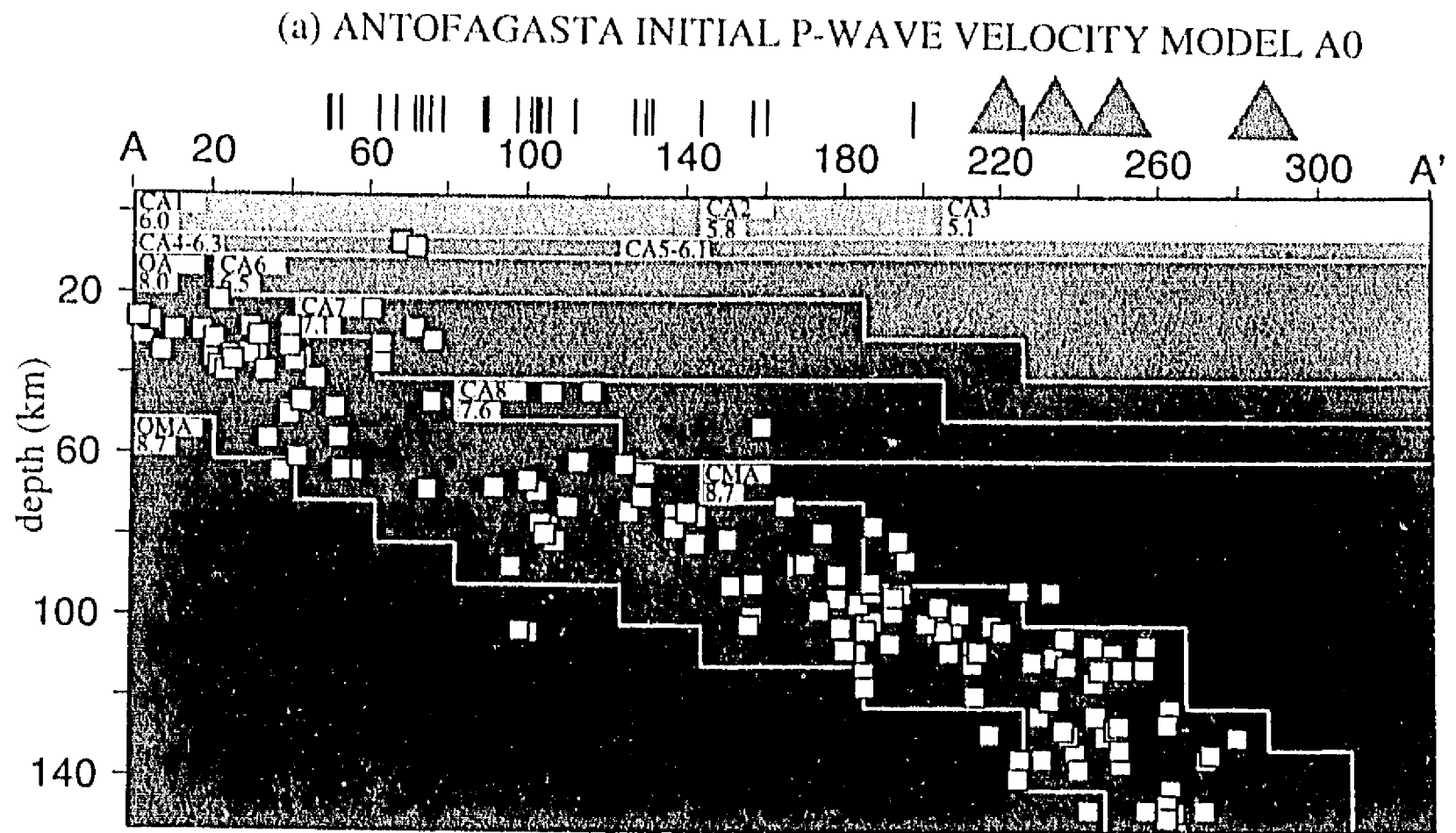


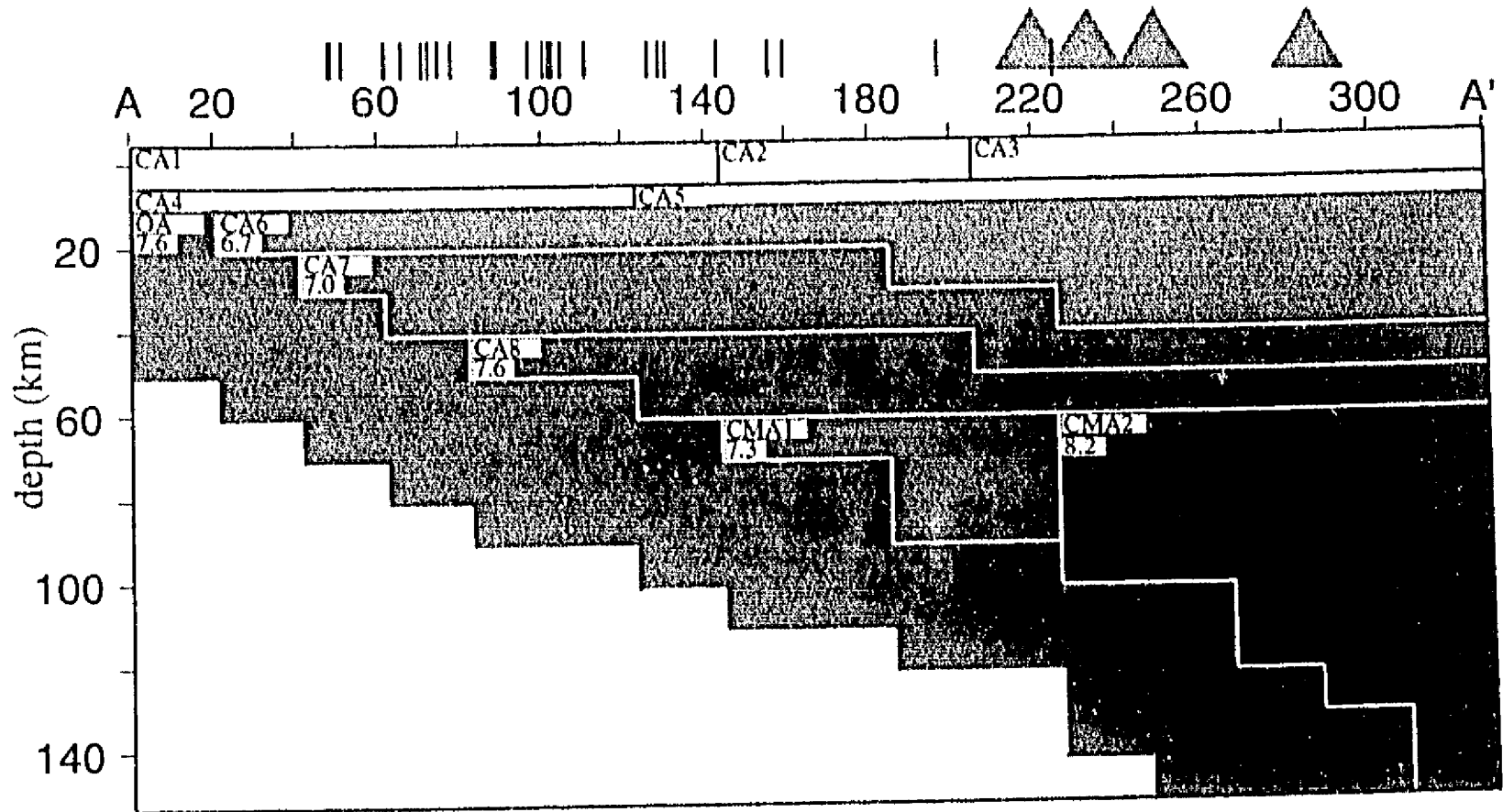
Figure 4



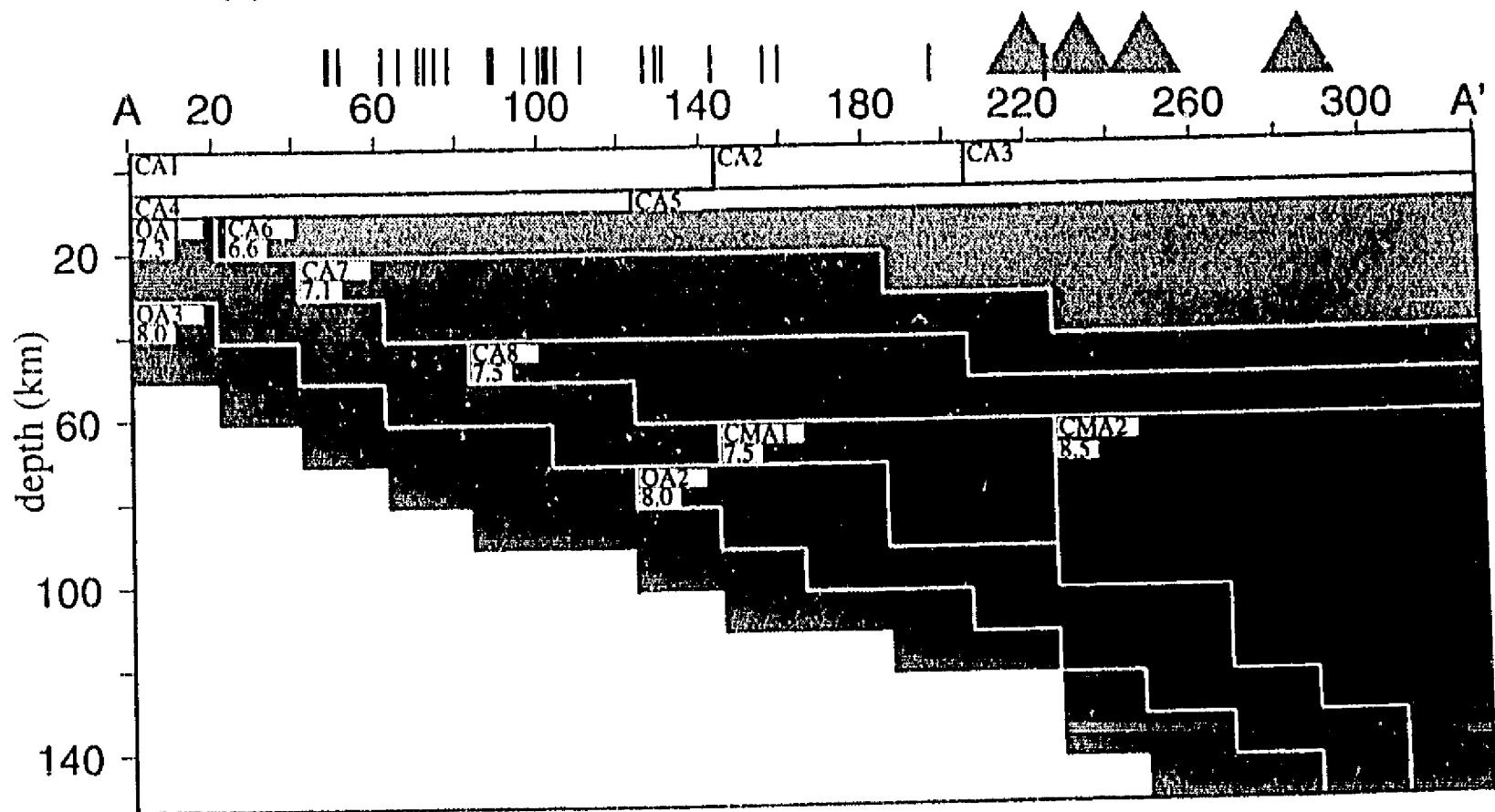
5.0 7.0 8.7 Velocities in km/s

Figure 5

(a) ANTOFAGASTA FINAL P-WAVE 2D VELOCITY MODEL A1



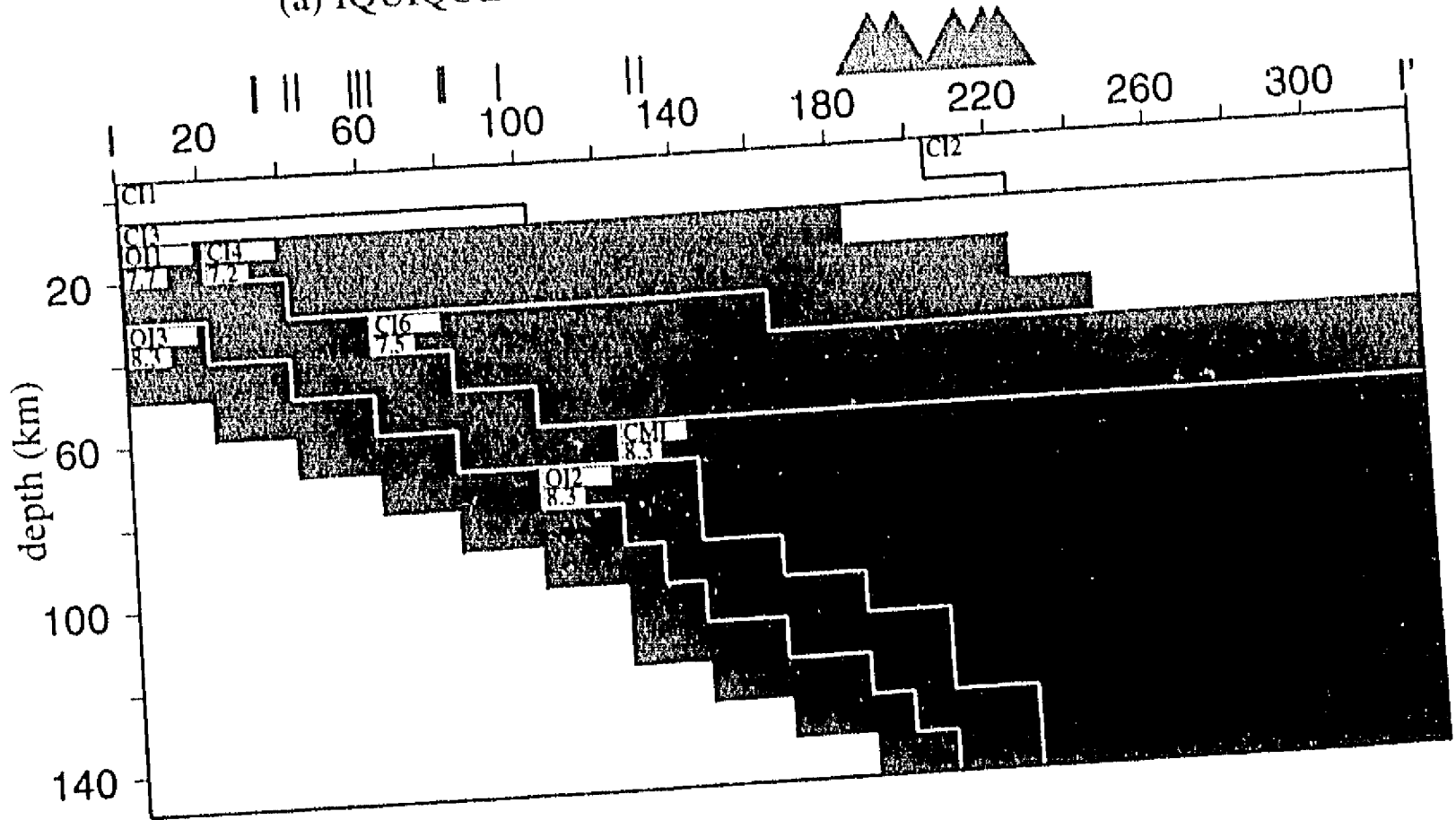
(b) ANTOFAGASTA FINAL P-WAVE 2D VELOCITY MODEL A3



5.0 7.0 8.7 Velocities in km/s

Figure 6

(a) IQUIQUE SYNTHETIC P-WAVE 2D VELOCITY MODEL



(b) ANTOFAGASTA SYNTHETIC P-WAVE 2D VELOCITY MODEL

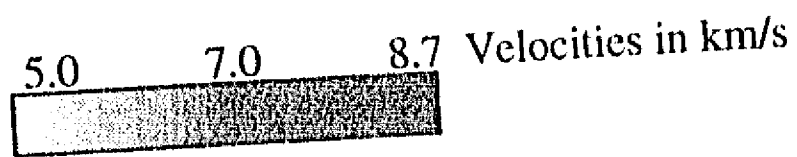
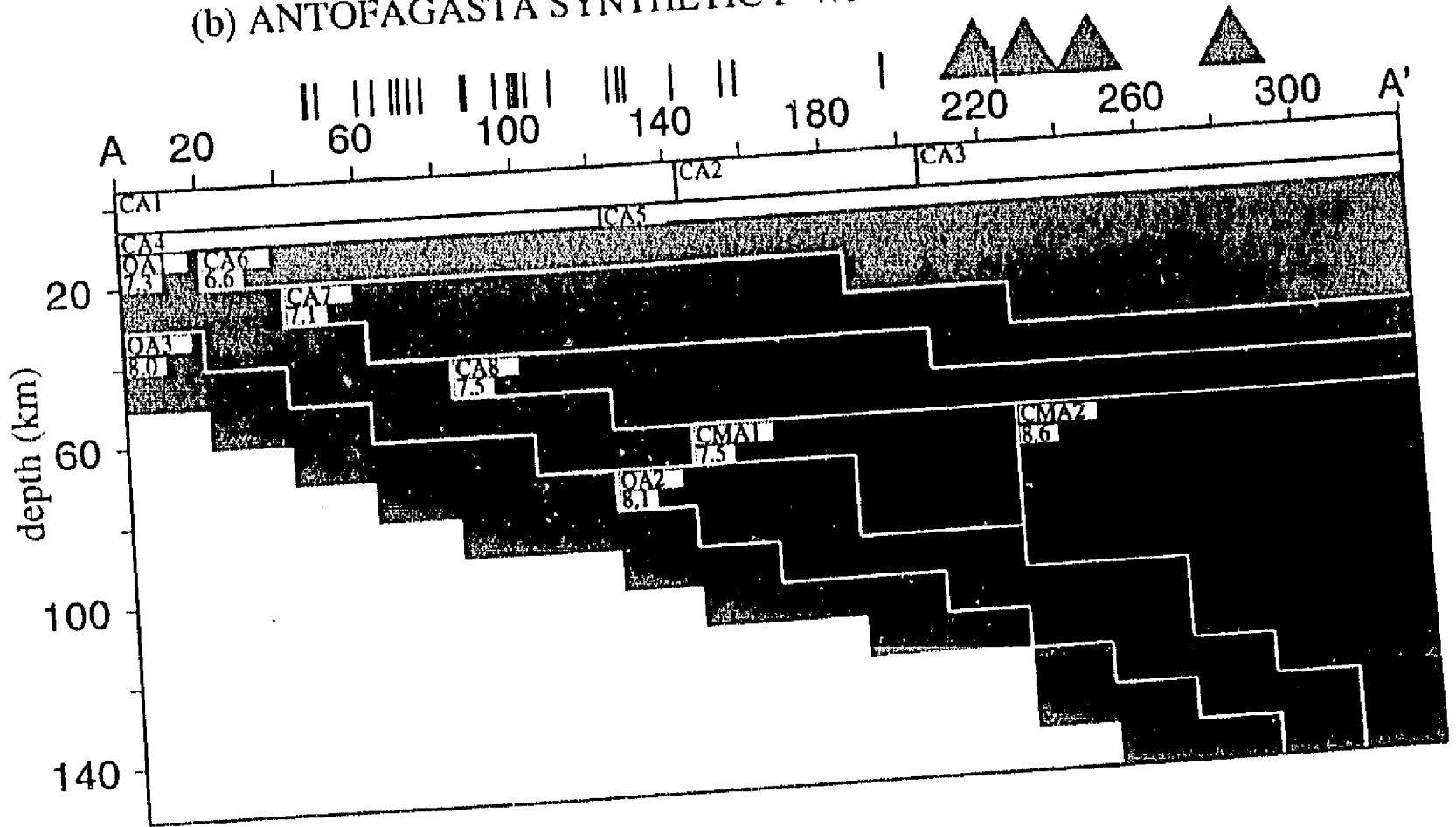


Figure 7

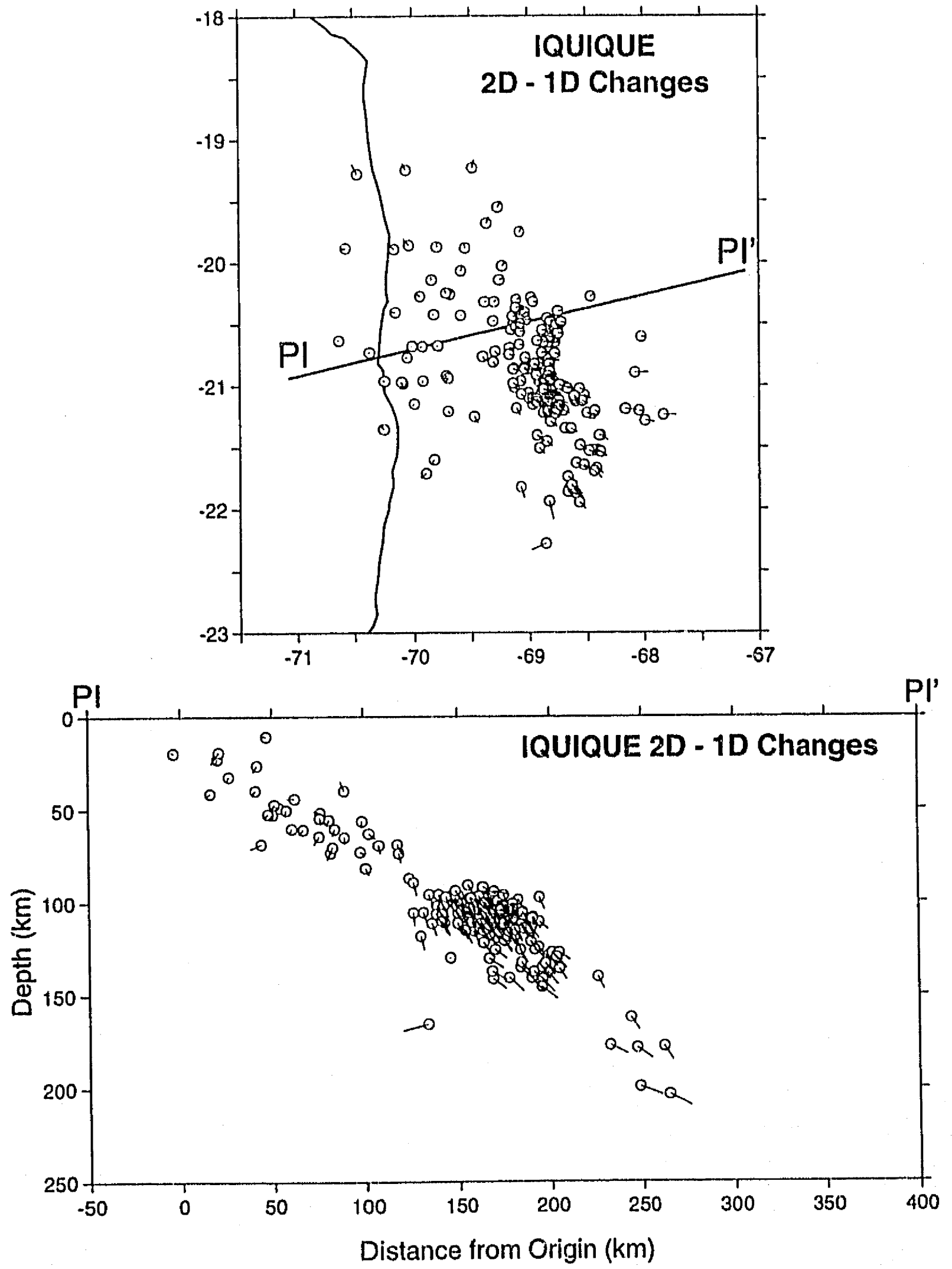
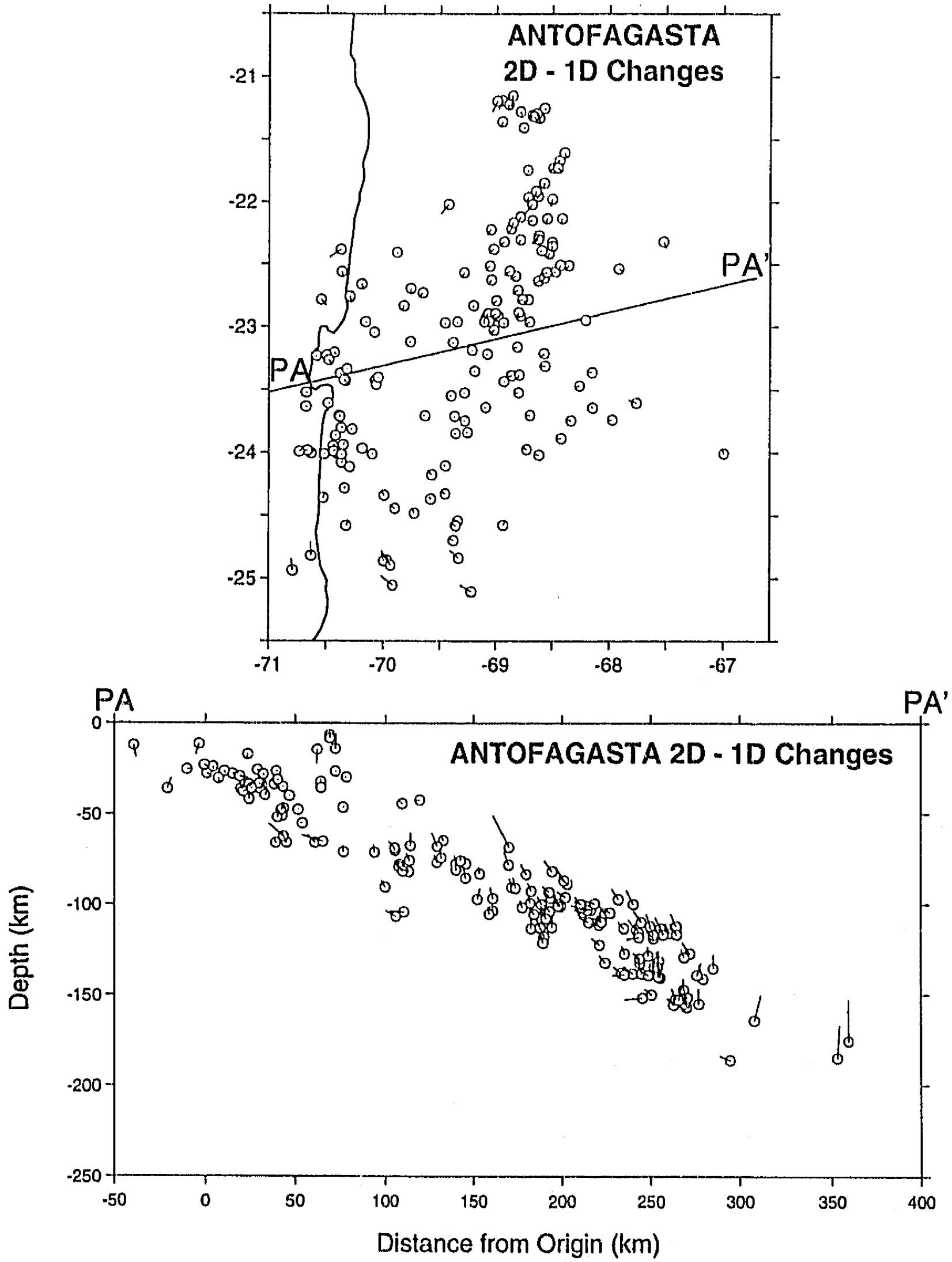


Figure 8



**AN INVERTED DOUBLE SEISMIC ZONE IN CHILE: EVIDENCE OF PHASE  
TRANSFORMATION IN THE SUBDUCTED SLAB**

**Diana Comte**, Instituto de Geofísica, Universidad Nacional Autónoma de México, Apartado Postal 70-172, México D.F., 04510 México and Departamento de Geofísica, Universidad de Chile, Casilla 2777, Santiago, Chile.

**Gerardo Suárez**, Instituto de Geofísica, Universidad Nacional Autónoma de México, Apartado Postal 70-172, México D. F., 04510 México

*Science, en prensa*

Data from two microseismic field experiments in northern Chile revealed an elongated cluster of earthquakes in the subducted Nazca plate at a depth of about 100 km in which downdip tensional events were consistently shallower than a family of compressional earthquakes. This double seismic zone shows a distribution of stresses of opposite polarity relative to that observed in other double seismic zones in the world. The distribution of stresses in northern Chile supports the notion that at depths of between 90 to 150 km, the basalt to eclogite transformation of the subducting oceanic crust induces tensional deformation in the upper part of the subducted slab and compressional deformation in the underlying mantle.

Since the advent of plate tectonics, intermediate and deep earthquakes have been interpreted as evidence of cold lithosphere penetrating into the mantle. At intermediate depths, most subducted lithospheres exhibit downdip tensional faulting, which has been generally interpreted as resulting from the gravitational pull of the slab (1-6). The presence of a more complex state of stress in the subducted slab was observed first in Tohoku, Japan (7). There, a sheet of compressional earthquakes lies above one of downdip tensional events. These two seismic planes are separated by ~40 km at a depth of ~60 km and they merge at a depth of 200 km. Similar double-planed seismic zones have subsequently been reported in other subduction zones (7, 8).

In general, double seismic zones have been associated with the unbending of the subducted slab that undergoes a sharp change in radius of curvature beneath the interplate contact and then become straight (9-11). All subduction zones, however, suffer this bending, and not all of them exhibit this type of seismicity. Thus other mechanisms have been proposed to explain them (12). In this report we describe a



double seismic zone in the subducted Nazca plate beneath the active volcanic arc in northern Chile. The observed distribution of seismicity, however, is inverted relative to other double seismic zones reported in the western Pacific. Thus the arguments offered to explain the presence of traditional double-seismic zones would not account for the inverted polarity of the two bands of seismicity in Chile.

Northern Chile is one of the most active seismic zones of the circum Pacific belt. Here, the Nazca plate subducts beneath the South American plate with a relative rate of convergence of about 8.4 cm/yr (13). The last great earthquake occurred there on 10 May, 1877 ( $M_w \sim 8.7$ ) (14). Two local microearthquake investigations were carried out in this seismic gap (15, 16). The first experiment was located in the southern end of the 1877 rupture zone, near Antofagasta. A second investigation took place near Iquique, in the middle of the 1877 fault break (Fig. 1). A subset of approximately 200 microearthquakes were selected from each experiment. We used these earthquakes for the simultaneous 2-D inversion of both, the hypocenters and the velocity structure in the studied area (16).

The observed seismicity is mainly concentrated inland and within the downgoing slab. In both experiments, an elongated cluster of earthquakes was located at a depth of  $\sim 100$  km. In general, fault plane solutions could be determined for the largest and best recorded earthquakes. The focal mechanisms of these events show both normal and reverse faulting in a close spatial relationship, where the downdip tensional events are consistently shallower than the compressional microearthquakes (Figs. 1 and 2), without showing strong differences in their coda-duration magnitudes ( $M_d \sim 3.4 \pm 0.3$ ).

For the Iquique survey, the tensional events ranged from depths of 88 to 109 km and the compressional events had depths varying from 107 to 126 km. In Antofagasta, the tensional events range from 81 to 108 km, predominantly with depths of less than 104 km. The compressional events were located between 104 to 122 km in depth. Thus the change from the tensional earthquakes to the deeper compressional stress field occurs in both regions at a depth of  $\sim 105$  km. The average separation between the two stress sheets is  $\sim 15$  km (Fig. 2).

Average hypocentral errors are  $\pm 2$  km, as obtained from the *a posteriori* covariance matrix resulting from the joint inversion of hypocenters and the two-dimensional velocity structure (16). Besides these statistical errors, we studied the changes of the epicentral coordinates and of the focal depths when modifications were made in the location scheme (for example, initial trial depth, changes in  $V_p/V_s$  or Poisson's ratio,

modifications of the velocity structure). During these tests, the hypocentral locations did not change by more than 7 km in a few extreme cases and, in general, the changes were of less than 3 to 4 km. Accurate location of the hypocenters was possible because excellent *S* wave readings were available from the three-component digital stations at distances that are smaller than the focal depth of the earthquakes studied.

The change in polarity of the *P*-waves is evident in the traces recorded by two seismic stations of a pair of events located at almost the same epicenter but with different focal depths (Fig. 3): event A7 at a depth of 102 km and A10 at a depth of 110 km (Figs. 1 and 2b). Both events were recorded at the same digital stations (SRA and MAR) and share a similar azimuth and take-off angles.

In general, the spatial orientation of the auxiliary nodal plane of the individual focal mechanisms is not well constrained. Therefore, and to make sure that we are indeed observing two different families of focal mechanisms, we performed a formal inversion of the best-fitting stress tensor based on the first motion polarities of the *P* waves for each of the two seismic bands (17). The focal mechanism solutions (Fig. 1) and the stress tensor (Fig. 4), correspond to those obtained from the inversion. In the case of the deeper tensional earthquakes, the resulting *T* axis of the stress tensor is almost horizontal and oriented in an east-west direction. For the compressional earthquakes beneath, the *P* axis is horizontal and also oriented east-west (Fig. 4). The error estimates determined from the inversion show that the principal axes are within a cone of uncertainty of  $\sim 30^\circ$ .

Intermediate-depth seismicity routinely reported teleseismically in northern Chile is characterized by tensional events (18, 19). However, an intermediate-depth earthquake with a compressional mechanism occurred in northern Chile beneath the Andean volcanic arc (Figure 1) at a focal depth of 130 km, as determined from a body waveform inversion (20). This focal depth clearly places it beneath the sheet of tensional events, which lie at an average depth of 110 km. Kono *et al.* (21) also identified this earthquake and suggested the presence of a double seismic zone. However, they incorrectly assumed that the sheet of downdip tensional events was beneath this reverse-faulting earthquake as in other subduction zones of the western Pacific. This event suggested the presence of a double-planed seismic zone with the same polarity of stresses as that observed with our local data (19), and indicates that the presence of down-dip compressional events beneath a family of tensional earthquakes occurs elsewhere in northern Chile and is not a phenomenon restricted to the

Antofagasta and Iquique areas studied here.

Traditional hypotheses offered to explain the presence of double-planed seismic zones (12) do not account for our observations because the polarity of the stress sheets predicted by these models is opposite to what is observed in northern Chile. Therefore, the inverted double seismic zone observed in Antofagasta and Iquique is probably associated to a different phenomenon than those usually used to explain the other double seismic zones identified mainly in the western Pacific.

The double seismic zone in northern Chile may be explained by bending of the slab beneath the volcanic arc. However, the cross sections clearly show no downward curving of the slab (Fig. 2). On the other hand, the double-planed seismicity in northern Chile is observed beneath the volcanic Andean belt suggesting it is associated with the generation of magma and the production of arc volcanoes. Thus it could be explained as a result of a phase change in the slab, as was recently suggested in the Tonga subduction zone (22).

Kirby and Hacker (23, 24) modeled the distribution of stresses induced by changes in pressure and temperature in the subducting lithosphere at depths of between 90 to 150 km. These authors argued that oceanic plates have a laminated structure with a thin crust on the top composed of basaltic minerals, overlying a thicker mantle composed mainly of peridotite. According to their numerical results (25), the subducting basaltic crust densifies to eclogite due to the increased pressure induced during the plate descent and to the dehydration of the oceanic crust at the source of the volcanic arc. However, the peridotite composing the upper mantle does not suffer a phase change because it is stable to greater pressure.

This differential volume change produces tensional deformation in the transformed crustal layer and induces a smaller compressional deformation near the top of the underlying mantle (23, 24). The distribution of stresses induced by this phase change would explain the inverted double seismic zone observed in northern Chile, and the fact that it is observed mainly with events of smaller magnitude. Furthermore, the separation between the stress sheets suggested by the numerical results is similar to that observed in both Iquique and Antofagasta (~15 km).

REFERENCES

1. B. Isacks and P. Molnar, *Nature*, **223**, 1121 (1969)
2. B. Isacks and P. Molnar, *Rev. Geophys.*, **9**, 103 (1971)
3. D. Forsyth and S. Uyeda, *Geophys. J. R. Astron. Soc.*, **43**, 163 (1975)
4. N. Vlaar and M. Wortel, *Tectonophysics*, **32**, 331 (1976)
5. M. Vassiliou, B. Hager, A. Raefsky, *J. Geodynam.*, **1**, 11 (1984)
6. W. Spence, *Rev. Geophys.*, **25**, 55 (1987)
7. Double seismic zones have been reported beneath Tohoku, Japan by N. Umino and A. Hasegawa [*J. Seismol. Soc. Jpn.*, **28**, 125 (1975)], A. Hasegawa *et al.* [*Tectonophysics*, **47**, 43 (1978)], and by T. Yoshii [*Tectonophysics*, **55**, 349 (1979)]; in the Tohoku-Hokkaido region, Japan by N. Umino *et al.*, [*Zisin*, **37**, 523 (1984)]; in Hokkaido, Japan by S. Suzuki *et al.* [*Tectonophysics*, **96**, 59 (1983)]; in Kurile-Kamchatka by Stauder and Mualchin [*J. Geophys. Res.*, **81**, 297 (1976)]; in the eastern Aleutians by M. Reyners and K. Coles [*J. Geophys. Res.*, **87**, 356 (1982)] and by L. House and K. Jacob [*J. Geophys. Res.*, **88**, 9347 (1983)]. H. Kawakatsu (11) gives a thorough review of these and other regions where double seismic zones have been identified.
8. K. Fujita and H. Kanamori, *Geophys. J. R. Astron. Soc.*, **66**, 131 (1981)
9. E. R. Engdahl and C. H. Scholtz. *Geophys. Res. Lett.*, **4**, 473 (1977)
10. B. Isacks and M. Barazangi, in *Island Arcs, deep Sea Trenches, and Back-Arc Basins*, M. Talwani and W. Pitman III Eds, (Maurice Ewing Ser. **1**, American Geophysical Union, Washington, 99 1977) pp. 99-114
11. H. Kawakatsu, *J. Geophys. Res.*, **91**, 4811 (1986)
12. Proposed mechanisms to explain double seismic zones are: stresses associated with phase changes [K. Veith, *Thesis*, South. Methodist Univ. (1974)]; elastic unbending of the slabs [E. R. Engdahl and C. H. Scholz, *Geophys. Res. Lett.*, **4**, 473 (1977); H. Kawakatsu, *J. Geophys. Res.*, **91**, 4811 (1986)]; sagging of the subducted slab under its own weight [T. Yoshii, *Kagaku*, **47**, 170 (1977); N. H. Sleep, *J. Geophys. Res.*, **84**, 4565 (1979)]; thermo-elastic stresses [K. Goto *et al.*, *Tectonophysics*, **112**, 111 (1985); L. S. House and K. H. Jacob, *Nature*, **295**, 587 (1982)]; and W. Spence (6) suggested that the tensional earthquakes reflect slab pull forces, whereas the shallower compressional earthquakes reflect local resistance to rapid downdip plate motion.
13. C. DeMets, R. G. Argus, S. Stein, *Geophys. J. Int.*, **101**, 425 (1990)

14. D. Comte and M. Pardo, *Natural Hazards*, **4**, 23 (1991)
15. D. Comte, M. Pardo, L. Dorbath, C. Dorbath, H. Haessler, L. Rivera, A. Cisternas, L. Ponce, in press *Geophys. J. Int.* (1993)
16. D. Comte, S. Roecker, G. Suárez, accepted in *Geophys. J. Int.* (1993)
17. L. Rivera and A. Cisternas, *Bull. Seismol. Soc. Am.*, **80**, 600 (1990)
18. L. Astiz, T. Lay, and H. Kanamori, *Phys. Earth Planet. Int.*, **53**, 80 (1988)
19. M. Araujo and G. Suárez, in press, *Geophys. J. Int.* (1993)
20. D. Comte and G. Suárez, in preparation (1993)
21. M. Kono, Y. Takahashi and Y. Fukao. *Tectonophysics*, **112**, 211 (1985)
22. D. Wiens, J. McGuire, P. Shore. *Nature*, **364**, 790 (1993)
23. S. Kirby and B. Hacker. *Eos*, **76**, 70 (1993)
24. S. Kirby and B. Hacker, *Eos*, **72**, 481 (1991)
25. R. Delinger and S. Kirby, *Eos*, **72**, 481 (1991)
26. We thank C. Mendoza, W. Spence, and two anonymous reviewers for comments which greatly improved this paper. ORSTOM, France and the IDRC, Canada offered financial support to conduct the microearthquake investigations. This work was partially funded by Fundación Andes, Chile grant C-52040. This work was completed when one of us (GS) was visiting the U.S. Geological Survey in Golden, Co.

#### FIGURE CAPTIONS

Fig. 1 Epicentral distribution of seismicity recorded by the local seismic networks near Iquique and Antofagasta, northern Chile (solid circles). Lower-hemispheric projection of the focal mechanisms show dilations as open circles and compressions as black circles. Triangles represent quaternary volcanoes in the region. Star is the compressional earthquake of 17 January, 1977 ( $m_b=6.0$ ) (20).

Fig. 2 Cross-sections in the direction of convergence of selected events determined for (a) the Iquique experiment, and (b) Antofagasta. The projection of the seismic stations is shown as vertical bars, and triangles correspond to the projection of active volcanoes in the region. The events included in the box are enlarged to the right of the Figure, where open circles denote the tensional events and solid circles correspond to compressional events. The side-looking, hemispheric projection of the focal mechanism of these events is shown; the T and P axes are represented by a white and black small dots respectively. The events are numbered as on Fig. 1.

Fig. 3 Seismograms recorded at the digital stations SRA and MAR of events A7 and A10. Note the change of the P-wave first motion polarity: dilation for the shallower tensional event (A7) and compression for the deeper compressional earthquake (A10). The take-off angles of these stations are near the center of the lower hemispheric projection.

Fig. 4 Lower-hemispheric projection of the stress tensors resulting from the inversion for the sheet of tensional events (above) and of compressional earthquakes (below). Curves around the principal axes of stress are the estimated errors.  $\sigma_1$  is the axis of largest compressive stress (*P* axis),  $\sigma_3$  is the least compressive stress (*T* axis), and  $\sigma_2$  is the intermediate (*B* axis).

Figure 1

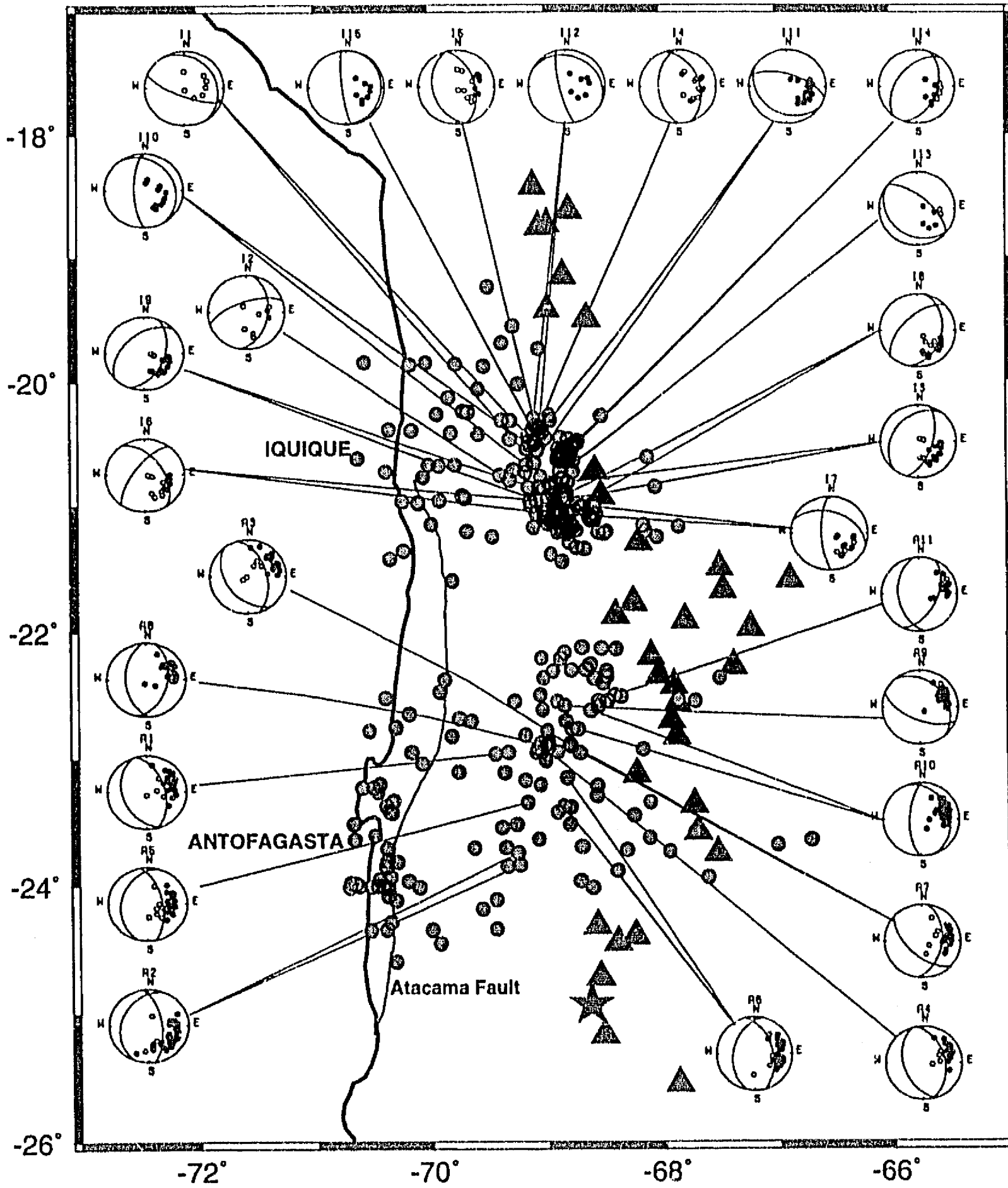
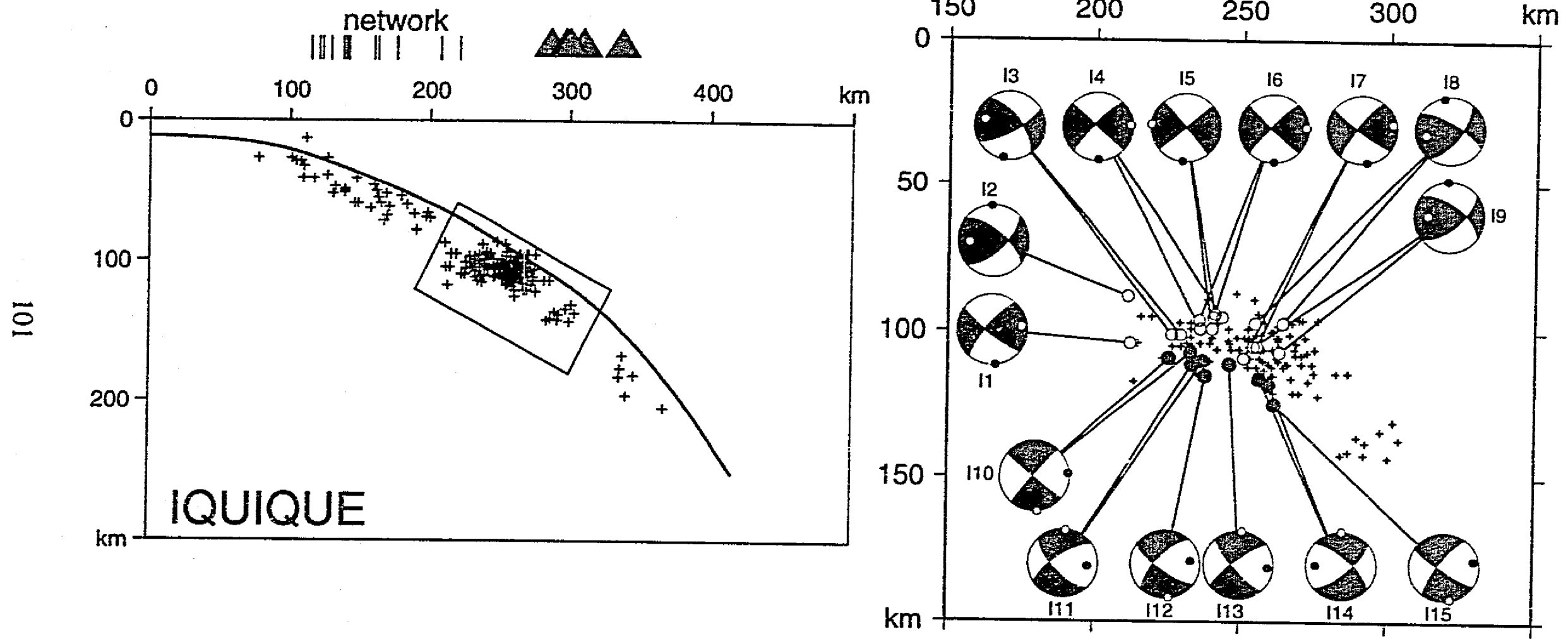


Figure 2a

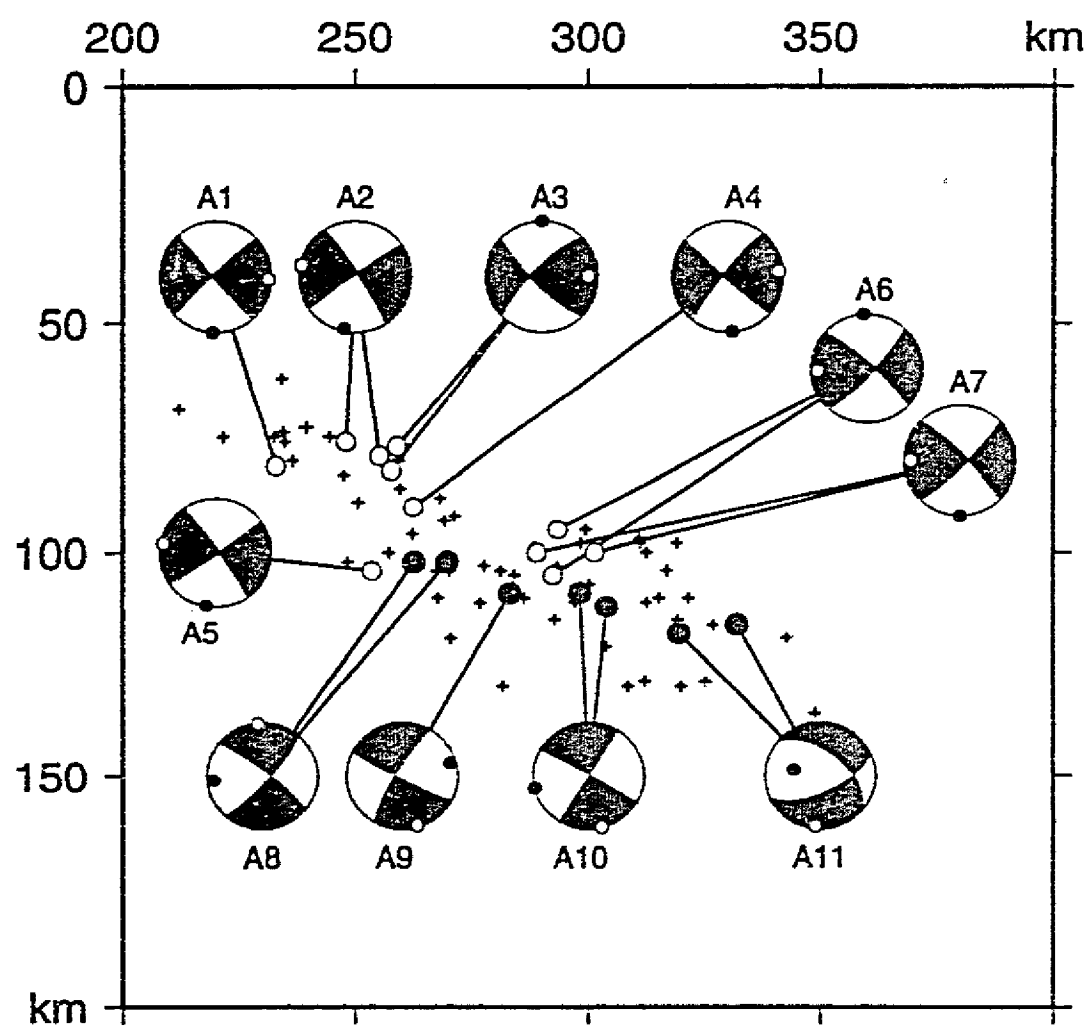
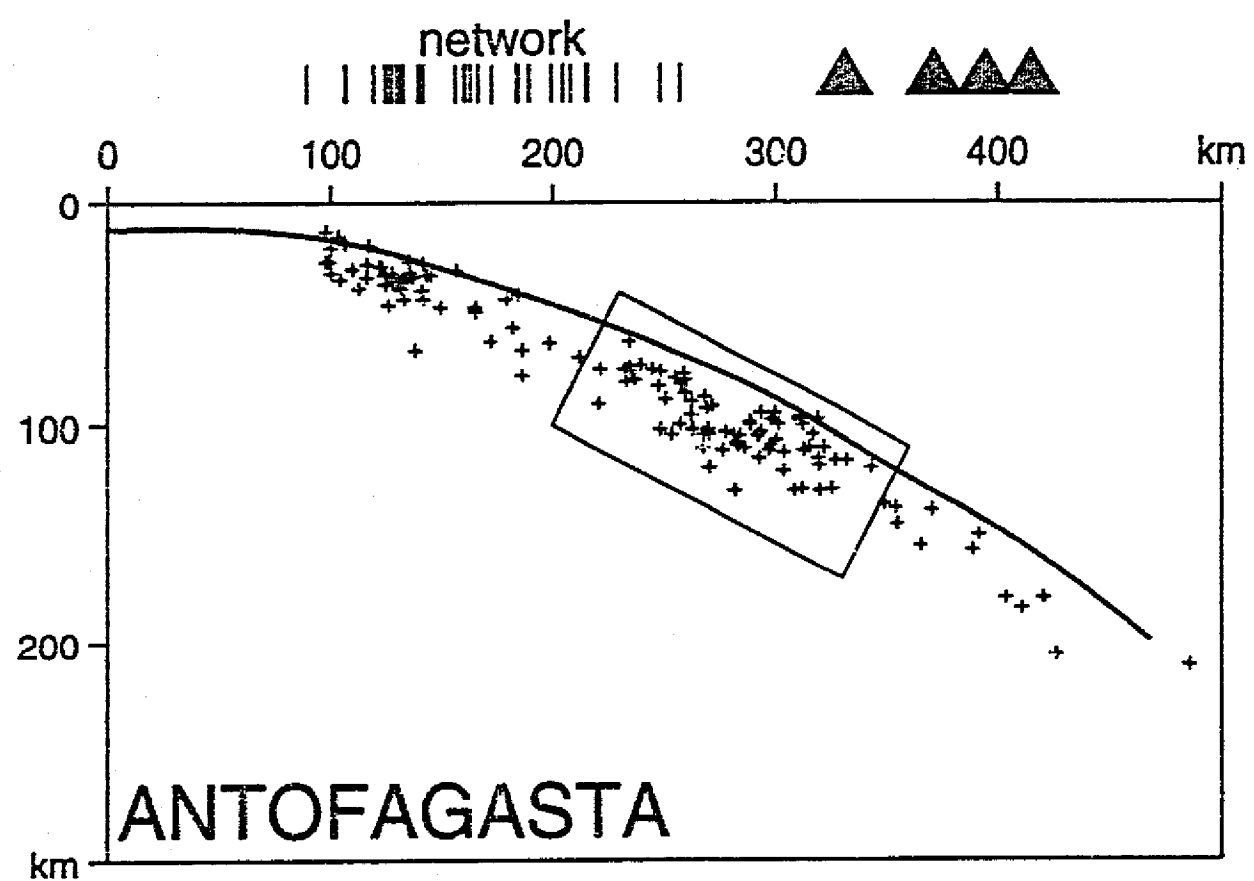


Comte and Suárez: An Inverted Double Seismic Zone



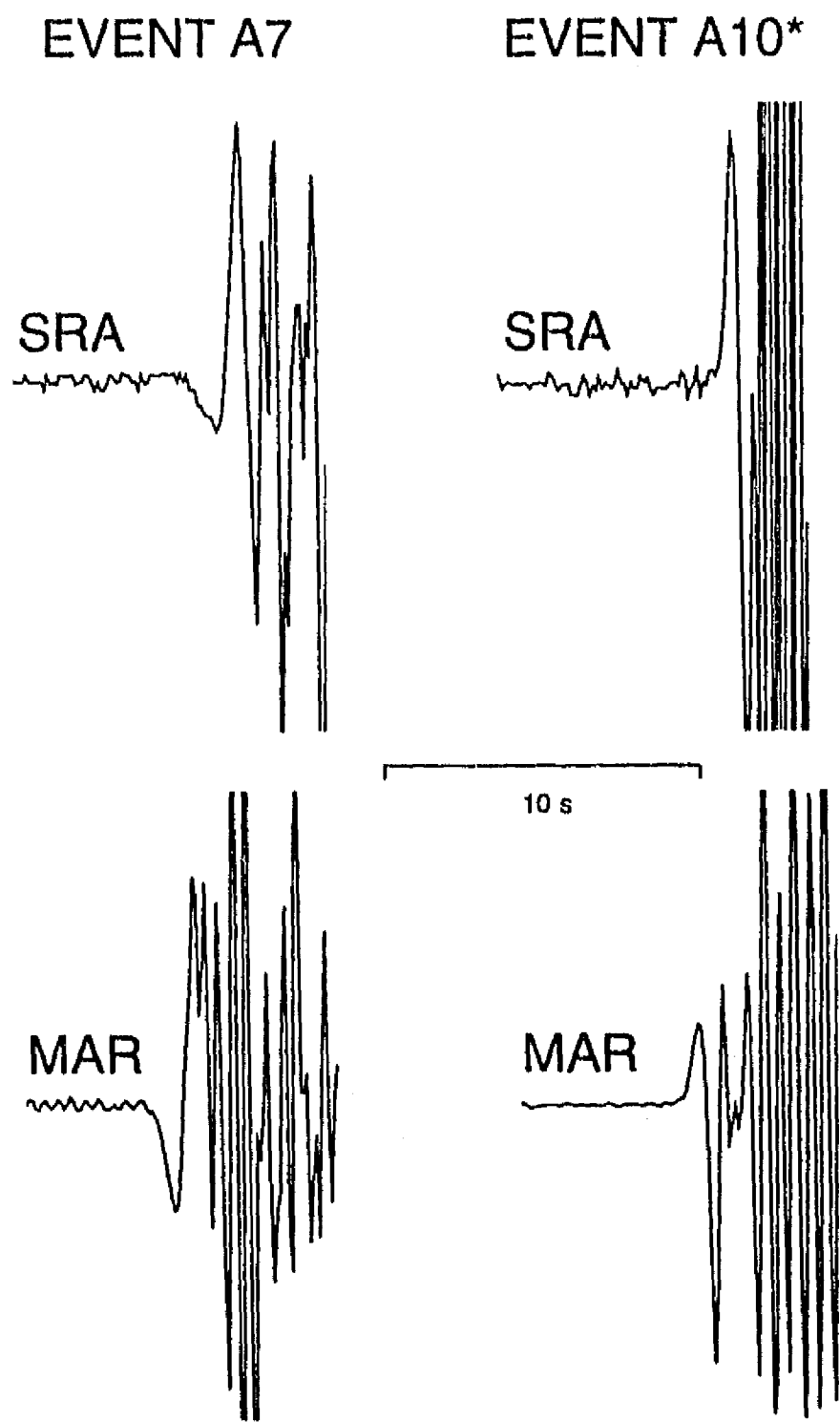
Figure 2b

102

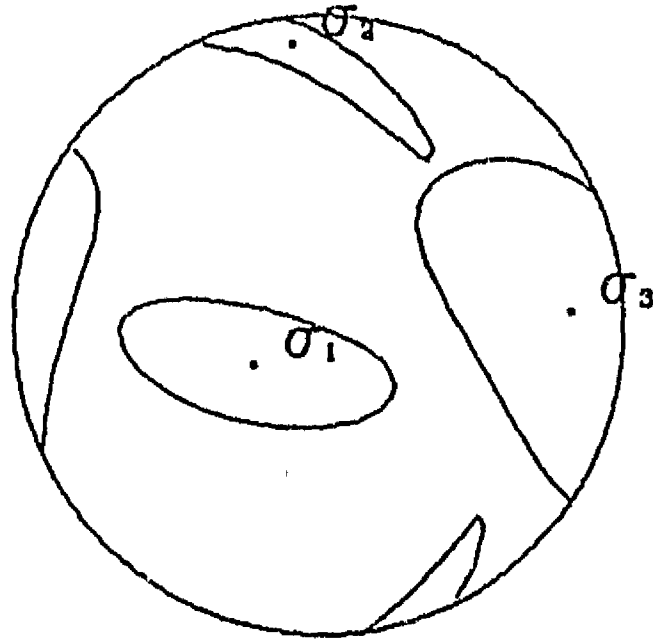


Comte and Suárez: An Inverted Double Seismic Zone

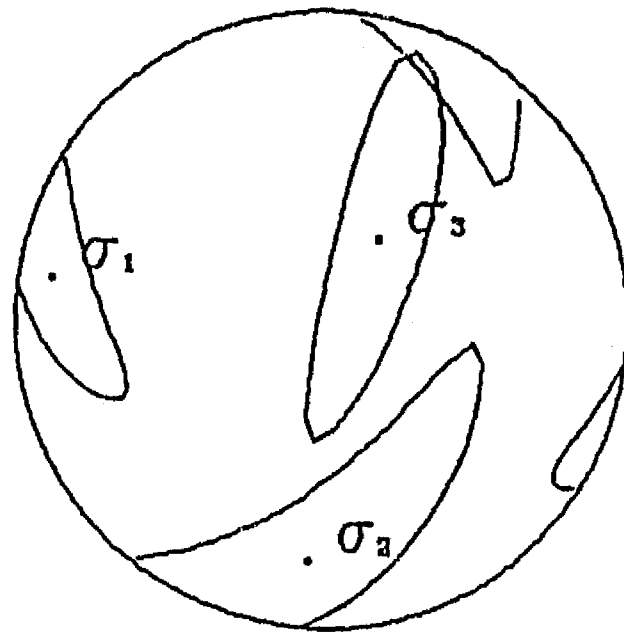
Figure 3



TENSIONAL EVENTS



COMPRESSIONAL EVENTS



**STRESS DISTRIBUTION AND GEOMETRY OF THE SUBDUCTING NAZCA PLATE IN  
NORTHERN CHILE USING TELESEISMICALLY RECORDED EARTHQUAKES.**

Diana Comte\* and Gerardo Suárez

Instituto de Geofísica, Universidad Nacional Autónoma de México,  
Apartado Postal 70-172, México D.F., 04510 México

\* also at Departamento de Geofísica, Universidad de Chile,  
Casilla 2777, Santiago, Chile.

**ABSTRACT**

The stress distribution along the subducted Nazca plate in northern Chile is analyzed using focal mechanism solutions obtained from the inversion of long-period *P*-, *SV*-, and *SH*-waveforms of 15 earthquakes ( $m_b \geq 5.5$ ), and from 107 events with reported focal mechanisms, occurred between 1962 and 1987. A joint hypocentral determination was carried out to control the depth of 261 events ( $m_b \geq 5.0$ ) recorded teleseismically, using locally recorded microearthquakes as calibration events. The shallow dip angle (up to 60 km in depth) of the Wadati-Benioff zone does not show variations along the strike of the trench in northern Chile. However, a gradual southward flattening of the slab is observed at distances greater than 200-250 km from the trench. This change, observed from about 21°S, is correlated with the interaction of the Perdida Ridge with the subduction, and with the variation of age observed in the subducting Nazca plate in this region. However, it also could be interpreted as a regional response of the slab to the sub-horizontal subduction observed to the south (between 27°S and 33°S). The maximum depth of the coupled region is estimated using the compressional to tensional variation of the stress field along the upper-part of the subducting slab. Nevertheless, beneath the seismogenic interplate contact there is a complex distribution of tensional events located in average deeper than the compressional ones. Those normal faulting events are associated with the slab pull that could act in the lower part of interplate coupled region. The downdip intraplate seismicity is characterized by normal faulting events, where the T-axes follow, in general, the shape of the deeper part of the subduction. The presence of a down-dip compressional earthquake located beneath the volcanic belt at a depth of 128 km agrees well with an inverted double seismic zone revealed by locally recorded earthquakes.

## INTRODUCTION

The subduction in northern Chile is controlled by the interaction of the relatively young and fast Nazca plate with the South America plate. This subduction process is capable of generating large thrust events along the interplate contact and downdip intraplate normal faulting events.

Historical seismicity shows that the last great event occurred in this region by the end of the XIX century (May 10, 1877, Figure 1) with a magnitude  $M_w \sim 8.7$ , and an estimated rupture area of about 500 km [Lomnitz, 1971; Abe, 1979; Kausel, 1986; Comte and Pardo, 1991; Díaz, 1992]. There are no reliable historical documents previous to this great earthquake that allow the estimation of recurrence rates. However, the absence of large thrust events ( $M_S > 7$ ) during this century suggests that northern Chile may be a mature seismic gap [Kelleher, 1972; McCann et al., 1979; Nishenko, 1985; Comte and Pardo, 1991].

Previous works based on teleseismically recorded earthquakes analyzed the subduction of the Nazca plate in Chile, where one of the most relevant characteristic is the change of the dip angle along the strike of the trench. A subhorizontal subduction is observed between 28°S and 33°S, bounded by a steep dipping slab, north and south of these latitudes. Alternative models have suggested that these changes occur as tears or smooth contorsions and discuss their relation with regional-scale tectonics of the overriding plate and with the orientation of the stress field in the downgoing plate [*e.g.* Isacks and Molnar, 1971; Sykes and Hayes, 1971; Stauder, 1973; Barazangi and Isacks, 1976; Isacks and Barazangi, 1977; Hasewaga and Sacks, 1981; Jordan et al., 1983; Bevis and Isacks, 1984; Bevis, 1986; Schneider and Sacks, 1987; Isacks, 1988; Cahill and Isacks, 1992, Araujo and Suárez, 1993].

In a recent work Comte et al. [1993a; 1993b] present detailed characteristics of the subduction in northern Chile using microseismic events recorded with local networks installed within the rupture area of the 1877 earthquake [*e.g.*, Comte et al., 1993a, 1993b]. They find variations of the dip angle of the slab from  $\sim 30^\circ$  close to Iquique (21°S) to  $\sim 20^\circ$  near Antofagasta (24°S). The maximum depth extent of the seismogenic interplate contact zone, however, is consistently  $\sim 50$  km deep without variations along the strike of the trench [Suárez and Comte, 1993]. Comte et al., [1993c] interpret a 10-km-thick layer attached to the top of the subducting Nazca plate as an oceanic crust that subducts to depths of  $\sim 60 \pm 10$  km. In addition, an inverted

double seismic zone is observed in northern Chile at ~100 km in depth, beneath the volcanic belt [Comte and Suárez, 1993].

The aim of this study is to make a global and integrated analysis of the stress distribution along the subducted Nazca plate in northern Chile using accurately determined depths and focal mechanism solutions obtained from teleseismically recorded events in combination with locally recorded microearthquakes. Using these data the detailed geometry of the subduction is defined, and we investigate whether there are some differences between the results obtained using events with  $m_b \geq 5.0$  and those obtained using microearthquakes.

## DATA AND METHODS

In order to analyze the stress distribution and the geometry of the subducting Nazca plate in northern Chile ( $18^\circ$ - $26^\circ$ S), 15 teleseismically recorded events ( $m_b \geq 5.5$ ), mainly located along the seismogenic interplate contact zone, were chosen to accurately determine their focal depths and focal mechanism solutions using a body waveform inversion (Table 1, Appendix 1). The resulting focal depths were then used in a joint hypocentral determination to control the depths of other 261 teleseismic events ( $m_b \geq 5.0$ ), where 107 of them have reported focal mechanism solutions (Table 2). Locally recorded events were also used as calibration events in the JHD procedure to improve the epicentral control of the events studied (Table 3).

### *Waveform Inversion*

Following the procedure described by Nabelek [1984, 1985], the parameters of the best fitting double-couple point source, including the focal mechanism, centroid-depth, seismic moment, and source time function, were determined for the events listed on Table 1. A formal inversion of the long-period *P*, *SV*, and *SH* waves recorded at teleseismic distances is performed. In general, the minimum epicentral distance was constrained to  $30^\circ$  for both the *P* and *S* waves, and the maximum distance to  $95^\circ$  and  $70^\circ$  for *P* and *S* waves respectively.

The source time function is parametrized as a series of predetermined number of overlapping triangular elements, and it is convolved with the resulting time series of pulses to determine the final shape of the synthetic seismogram.

The calculated teleseismic body-wave packets are the sum of direct arrivals ( $P$  and  $S$ ) and of reflections from the free surface ( $pP$ ,  $sP$ , and  $sS$ ) whose relative amplitudes, polarities, and arrival times depend on the source mechanism and depth. The relative amplitudes of the elements are determined by the inversion procedure, and the number of elements is chosen so that the end of the source time function smoothly approaches zero. The amplitudes of the seismograms are equalized to a common instrument with a peak magnification of 1500, located at a distance of  $40^\circ$ .

The  $P$  and  $S$  waves were properly weighted in the inversion in order to avoid a bias due to the uneven azimuthal distribution of the data. A compressional wave velocity of 6.0 km/s, Poisson's ratio of 0.25, and density of  $2700 \text{ kg/m}^3$  was found to be adequate for events with depths of less than 70 km; and a  $P$ -wave velocity of 7 km/s was used for events with depths greater than 70 km. These velocities were inferred from tomographic studies of the region [Comte et al., 1993c]. Attenuation coefficients ( $t^* = \text{travel time/space average } Q$ ) of 1 and 4s were assumed in computing the effect of the anelastic attenuation for the  $P$  and  $S$  waves respectively.

The results of the body waveform inversions are summarized in Table 1 and Appendix 1. The  $P$ - and  $S$ -waveforms of the first seven events that occurred between 1962 and 1977 were digitized at 1 sample/s from long period WWSSN teleseismic stations (Table 1). In those events, the presence of short-period peaks that are not modeled in some stations are, in general, attributable to the digitization process.

In the case of two events (December 21, 1967, and January 17, 1977), a single point source proved inadequate to match the observed waveforms. Therefore, two point sources separated in space and time were assumed (Appendix 1); the timing and location of the second subevent relative to the first, as well as the source parameters of each subevent, were included as independent parameters in the inversion.

#### *Relocation of Hypocenters*

The hypocenter relocation of all the studied events was done in a two-stage process [Dewey, 1971]. In the first stage, the joint hypocenter determination (JHD) program was applied to the set of the 15 modeled events (Table 1), fixing their depths to those obtained from the waveform inversions, considering that they have been accurately determined. Epicentral control was obtained using six events recorded by the local network of Antofagasta, that were used as calibration events (Figure 2, Table 3).

Station correction and variances were then estimated for 248 station-phase pairs at regional and teleseismic distances.

In the second stage of the hypocentral relocation, the 261 additional events  $m_b \geq 5.0$  were located using the station corrections and variances computed in the first stage, in a modified single-event procedure [Dewey, 1971].

The final location of the modeled events and their estimated error-ellipses are presented on Figure 2 and Table 2. The maximum horizontal error estimated from the major semi-axis of the error ellipsoid is  $\sim 10$  km (Figure 3a); the largest values of 14 and 18 km correspond to the oldest events (December 29, 1962 and December 3, 1963), and are due apparently to the low number of stations reporting at that time. In the case of the relocated events that were not modeled in this study, the maximum horizontal error is  $\sim 15$  km (Figure 3b and 3c) and the depth error estimated from the minor semi-axis of the error ellipsoid of  $\sim 90\%$  of the events shows errors in depth of less than 12 km (Figure 4a and 4b).

In order to quantify the advantage of the relocation procedure we determine the error ellipsoid for all the events using the ISC location using the same single-event scheme, but without the station-phase corrections determined by this study. In this case, the maximum horizontal errors are always larger than 40 km (Figure 3d, 3e, and 3f), and the average depth errors are about 35 km (Figure 4c and 4d). Thus, it can be observed that the epicentral and depth errors decreased significantly when the data is relocated using locally recorded calibration events.

### **ANALYSIS OF THE RELOCATED SEISMICITY**

Taking into account the space distribution of seismicity, four 200 km-wide profiles oriented in the direction of convergence were chosen (Figure 5). These profiles present the 122 focal mechanism solutions on a side-looking, lower hemispheric projection. The locally recorded microearthquakes were also included in those profiles (Figures 6 and 7) and the isodepth contours were obtained using a continuous curvature surface gridding algorithm [Wessel and Smith, 1992] (Figure 8).

#### *Thrust Faulting Events*



Surprisingly, in the 25 years spanned by this study, only two thrust faulting events ( $M_S \geq 6.5$ ) have occurred in northern Chile. The earthquake of December 29, 1962 ( $M_S = 6.8$ , event M1 on Table 1, Figure 6a) is the oldest event modeled and it is the only thrust faulting earthquake ( $M_S \geq 6.5$ ) located in the northern end of the 1877 rupture area during the last 25 years. The depth of this event is  $35 \pm 2$  km, and it is located at a distance of about 160 km from the trench. The slip direction obtained for this event is  $N62^\circ E$ , which agrees with the estimated convergence direction of the Nazca plate in northern Chile [DeMets et al., 1990]. However, the dip angle ( $34^\circ$ ) of the inferred fault plane is somewhat larger than that estimated for the slab on profile P1 (Figure 6a).

The second thrust faulting event occurred on March 5, 1987 earthquake ( $M_S = 7.3$ , event M12 on Table 1, Figure 7a). This is the largest thrust faulting event modeled in this study and it occurred southward of the 1877 rupture area at a depth of  $38 \pm 3$  km. The east dipping nodal plane shows an angle of  $30^\circ$ , and the slip vector is oriented  $N72^\circ E$ , in agreement with the relative convergence of the Nazca plate [DeMets et al., 1990]. This earthquake was felt at distances  $\sim 800$  km along the coast of Chile and it also generated a local tsunami that was observed between  $18^\circ$  to  $33^\circ S$ . This event had four aftershocks recorded teleseismically, all of which have CMT solutions; three of them (events 93, 95, and 97 on Table 2, Figure 7a) exhibit a focal mechanism very similar to that of the mainshock. One of the aftershocks (event 94 on Table 2), however, shows normal faulting mechanism at approximately the same depth of the reverse faulting aftershocks. The depths of the aftershocks vary from 30 to 51 km.

Also, there is a thrust earthquake on October 28, 1975, ( $m_b = 5.8$ , event 16 on Table 2, Figure 6a) that was analyzed by Kadinsky-Cade [1985]. It occurred seaward of the central part of the 1877 rupture zone at a depth of 34 km. The slip vector ( $N47^\circ W$ ) suggests that its focal mechanism solution could be rotated, considering that the average relative convergence direction is  $N77^\circ E$  [DeMets et al., 1990]. The dip angle ( $7^\circ$ ), however, agrees well with the shape of the subducting slab inferred from the seismicity data.

Interestingly, this relative absence of interplate thrust events ( $M_S \geq 6.5$ ) compared with the intense downdip intraplate seismicity was also observed in northern Chile in the two microseismic field investigations [Suárez and Comte, 1993; Comte et al., 1993a, and Comte et al., 1993b].

*Intraplate Compressional and Tensional Events Near the Seismogenic Interplate Contact*

Up to a distances of about 200 to 250 km from the trench, the stress distribution in northern Chile is characterized by compressional events with focal depths between 30 and 64 km (Figures 6 and 7). Most of these events show an almost pure reverse faulting mechanisms, except for the December 3, 1963 earthquake ( $M_S=6.1$ , event M2 on Table 2, Figure 6b a). This event occurred at a depth of  $29\pm 2$  km and exhibits a reverse focal mechanism with a small strike-slip component. The focal mechanism of this event is well constrained by an adequate azimuthal distribution of stations and shows a good agreement between the recorded and synthetic waveforms (Appendix 1). The depth of this event suggests that it is an intraplate event within the downgoing slab and not a crustal earthquake associated to the Atacama fault system, as was suggested by Chinn and Isacks [1983].

This compressional seismicity at distances of  $\sim 200$  km from the trench occurs together with tensional events mainly located beneath the high angle reverse faulting events. This complex distribution was first reported in northern Chile by Malgrange and Madariaga [1983] using the December 21, 1967, December 25, 1967, June 19, 1970, and November 28, 1970 earthquakes. These three events were reanalyzed here in order to see whether the inclusion of the *SV*- and *SH*-waveforms results in better constrained focal mechanism solutions.

Malgrange and Madariaga [1983] suggested that the normal faulting event on December 25, 1967 ( $M_S=5.8$ ) was the principal aftershock of the intraplate compressional earthquake of December 21 ( $M_S=6.3$ ). The focal mechanism solutions of both events obtained from the inversion (events M3 and M4, respectively on Table 1, Figure 6b), agree with those obtained by Malgrange and Madariaga [1983]. This event is located  $\sim 20$  km deeper from the estimated upper boundary of the slab in the region (Figure 6b) and its focal mechanism does not exhibit a low dip angle typical of thrust faulting events (Appendix 1). Thus, the inversion results give weight to the conclusion that the December 21 earthquake is a complex event located within the subducting Nazca plate and that it is not an interplate thrust event, as was suggested by Chinn and Isacks [1983],

The June 19, and November 28, 1970 earthquakes (events M5 and M6 on Table 1, Figure 6b) present the same pattern of the 1967 sequence. In this case the tensional

event of June 19 is located ~80 km seaward of the compressional earthquake of November 28. The tensional earthquake, however, occurred prior to the compressional one. The focal mechanism solutions obtained here for both events are very similar to those obtained by those authors. The focal depths determined from the inversion, however, are about 10 km shallower than those obtained by Malgrange and Madariaga [1983]. The depths obtained for the June 19 event ( $42 \pm 1$  km) and for the November 28 event ( $41 \pm 2$  km) are adequately constrained by the match of the synthetic and observed depth-phases (Appendix 1).

The December 25, 1967 and the June 19, 1970 earthquakes are not the only tensional events occurring beneath the seismogenic interplate contact. Other tensional events with similar characteristics occur over a wide range of latitudes at the same distances from the trench beneath the interplate contact (Table 4). The average depth of these tensional events ( $47 \pm 3$  km) is about 10 km deeper than the average depth of the compressional earthquakes ( $38 \pm 3$  km). The locally recorded microearthquakes also show tensional events located at the same distance from the trench where the tensional, teleseismic events are observed. Therefore, this complex distribution of tensional events that are deeper than the compressional ones, is not restricted to a particular region of northern Chile and it is observed for a broad range of magnitudes.

Malgrange and Madariaga [1983] suggested that these tensional events could be associated with the occurrence of great thrusting fault earthquakes. However, the presence of microearthquakes tensional events located at almost the same distance from the trench without any evident correlation with thrust events could be interpreted as the effects of the slab pull can be also felt beneath the seismogenic interplate contact, and in the vicinity of a great thrust earthquake (before or after) the slab pull effects is manifested with also great tensional events.

#### *Coupled Zone and Downdip Events*

A sudden change from compressional to tensional stress field can be observed in the subducting slab. This change occurs at distances of ~200-250 km from the trench and at depths of between 50 to 70 km (Figures 6 and 7, Table 5). This change was also observed at the same depth and distance from the trench using the locally recorded microseismicity [Suárez and Comte, 1993]. Thus, it is probably related to the maximum depth extent of the seismogenic interplate contact.

The downdip seismic activity is characterized by tensional events that are observed at distances of ~200-250 km from the trench. The largest intraplate tensional earthquake observed during the studied period of time occurred on August 8, 1987 ( $m_b=6.4$ , event M14 on Table 1, Figure 6a). The intensity reports indicate that it caused serious damages in the Chile-Peru border, and that it was felt at distances of 350 to 400 km from the epicenter. The depth gleaned from the inversion procedure is  $76\pm 4$  km, and it is located within the subducting slab downdip of the coupled-uncoupled transition, in a region where there are no other events with  $m_b\geq 6.0$  reported since 1960.

There is a southward flattening of the slab observed mainly from a distance of ~250 km from the trench (Figures 6 and 7). This flattening can also be noted in the 80 to 160 iso-depth contours (Figure 8), where they suggest that north of ~21°S the subduction has a greater slope than south of this latitude.

In general, all events deeper than  $60\pm 10$  km are characterized by normal faulting where the T-axes are oriented in an almost horizontal direction. The intermediate-depth seismicity tends to cluster beneath the volcanic Andean belt at a depth of ~100 km. Local microseismic experiment revealed in northern Chile a double seismic zone with compressional events deeper than the tensional earthquakes [Araujo and Suárez, 1993; Comte and Suárez, 1993]. In this study, only one teleseismic earthquake of intermediate depth on January 17, 1977 ( $m_b=6.0$ , event m7 on Table 1, Figure 7b) shows reverse faulting at a depth of  $128\pm 3$  km. The average depth of the tensional events located at distances of 250 to 350 km from the trench is  $109\pm 2$  km. Therefore, the compressional 1977 earthquake is clearly located beneath the normal faulting events.

The four deepest intraplate tensional earthquakes modeled in this study are events M9, M10, M13, and M15 (Table 1, Figures 7a and 7b). They occurred at distances of 500 to 570 km from the trench and at depths of ~200 to 230 km

There is a remarkable difference in the deep seismic activity in northern Chile. North of ~21°S there are few events deeper than 120 km in depth, to the south of this latitude, however, there is a notable increase of events with depths greater than 120 km (Figure 8). Moreover, this behaviour is also observed for events with depths from 500 to 650 km. Engebretson and Kirby [1992] suggested that those deeper events could be associated with a detached part of the subducting slab, based on a probable age discontinuity within the Nazca plate. Kostoglodov [1989, 1993], however, shows that

the maximum depths of those events are in agreement with the thermal model of sinking slab with a depressed metastable olivin-spinel phase transition boundary.

## DISCUSSION AND CONCLUSIONS

### *Shape of the Wadati-Benioff Zone*

The upper surface of the subducting Nazca plate in northern Chile was inferred from the distribution of teleseismic and locally recorded earthquakes (Figures 6 and 7). Considering the absence of shallow thrust events ( $m_b \geq 6.0$ ), the shape of the interplate contact was constrained by thrust faulting microearthquakes [Comte et al., 1993; Suárez and Comte, 1993]. In order to quantify the changes in dip along the strike of the trench, we parametrized the geometry of the Wadati-Benioff zone measuring the changes in dip angle as function of depth in each profile (Figure 9, Table 6). This parametrization may be summarized as follow:  $D_S$  is the shallow dip angle measured from the trench to a depth of 20 km. This depth range is associated with the transition from weak and unconsolidated material of the accresionary prism to the stronger and more consolidated material capable of nucleating an earthquake rupture.  $D_C$  is the dip angle between depths of 20 to 60 km, and it is associated to the maximum depth extent of seismogenic coupling.  $D_I$  is the dip angle defined by the shape of the upper part of the slab between 60 to 100 km in depth. This part of the slab is associated with the phase transformation from gabbro to eclogite.  $D_V$  is the dip angle obtained from depths of 100 to 150 km, this segment is associated with the arc volcanism that occurs above this portion of the slab; and  $D_D$  or deeper dip angle obtained in an interval from 150 to 300 km in depth.

The angles  $D_S$  and  $D_C$  are constant along the northern Chile region (Figures 6, 7, and 8), indicating that the seismogenic interplate contact does not show variations in dip along the strike of the trench, from 19°S to 27°S, down to depths of ~60 km. However, the angles  $D_I$ ,  $D_V$  and  $D_D$  show a constant southward decrease from 21°S to 26°S, suggesting a gradual flattening of the slab.

The conditions influencing the changes in the slab dip are not known. However, the possible factors affecting the geometry of subduction zones can be summarized as follow: the relative convergence rate, the absolute motion of the upper plate, subduction of aseismic ridges, the age of descending plate, accretion of sediment in

trenches, and the duration of subduction and age of the arc [*e.g.*, Cross and Pilger, 1982; Jarrad, 1986].

Cahill and Isacks [1992] postulated that the descending plate responds to changes in the polarity of the lateral curvature in the South American margin by reversing the orientation of its vertical curvature. On the other hand, Isacks [1988] proposed that the present shape of the plate margin may be due to the variable shortening rate along the plate margin.

In the northern Chile case, the rate of convergence (8.4 cm/y, [DeMetts et al., 1990]) and the absolute motion of the upper plate (3.5 cm/y [Gripp and Gordon, 1990]) are almost constant. However, the age of the subducting plate changes from ~80 m.y. around 20°S to ~60 m.y. around 25°S (Figure 1). Therefore, the lower dip angle observed to the south (P3 and P4 profiles, Figure 8) may be associated with a younger and probably a more bouyant lithosphere than those observed to the north (P1 and P2 profiles, Figure 7).

The other factor that may influence the changes of the dip angle observed in northern Chile is the subduction of the Perdida Ridge (Figure 1). Cahill and Isacks [1992] also suggested that the interaction of bathymetric features with the subduction are not associated with changes in the dip angle along the strike of the trench. They used as an example the Perdida Ridge, where they did not find an obvious variation in the shape of the slab associated with this bathymetric feature. However, our data suggest a correlation between the subduction of this Ridge at about 21°S and the begining of the southward flattening of the slab in northern Chile.

The global mechanisms of the flattening of the slab proposed by Isacks [1988] and Cahill and Isacks [1992] are not in contradiction with the changes in the dip angles observed in this work, because we are suggesting a more refined look of the northern Chile region with more detailed data. They proposed that the end of the normal subduction of the slab occurs at ~24°S and we are proposing that the change from normal to a more subhorizontal mode of subduction could start at ~21°S. Moreover, the gradual southward flattening of the slab observed in northern Chile could be associated with a regional response of the subhorizontal subduction observed between 28° and 33°S.

#### *Maximum Depth of the Seismogenic Interplate Contact*

The seismically coupled zone has been defined as the depth range of the plate interface that is capable of producing great underthrusting events [*e.g.*, Tichelaar and Ruff, 1991]. The depth of the coupled-uncoupled region, corresponding to the transition from unstable to stable sliding along the plate interface, has been usually determined using the observed maximum depth of shallow-dipping thrust faulting events recorded teleseismically. Pacheco et al. [1992] presented a detailed study of the seismic coupling in 19 subduction zones around the world. They found that the maximum depth of nucleation of thrust events varies between 35 and 70 km. Pacheco et al. [1992] suggested that the observed variations of seismic coupling could be attributed to differences in state variables and frictional properties of materials along the plate interface. Also, the subduction of large bathymetric features, the presence of unstable triple junctions, sediment composition, and drastic changes in the age of the oceanic lithosphere along the strike, may explain the variation of seismic coupling along a given subduction zone. Tichelaar and Ruff [1993] analyzed the maximum depth extent of seismic coupling along the circum-Pacific subduction zones and suggested that for most subduction zones, the depth of the downdip edge of the seismogenic interplate contact is  $40 \pm 5$  km.

Comte et al. [1993] and Suárez and Comte [1993] suggested that the change from compressional to tensional stress field along the upper-surface of the slab, observed with locally recorded microearthquakes, may be an alternative way to estimate the maximum depth of the interplate contact in regions where the seismicity is sparse and no geodetic coseismic measurements exist. The change from intraplate high angle reverse faulting events to downdip tensional earthquakes, can be observed also with teleseismic earthquakes at about 200-250 km distances from the trench at depths of about  $60 \pm 10$  km (Figure 6 and 7).

Sometimes there are not enough teleseismic events to follow this transition along the slab. Nevertheless, the boundary determined using local microearthquakes agrees well with that observed teleseismically. Furthermore, the maximum depth of the change from compressional to tensional stress field observed along the upper part of the slab, agrees with the depth of the gabbro to eclogite phase transition [*e.g.*, Ahrens and Schubert, 1975; Pennington, 1983; Hori et al., 1985] and with the maximum depth of the subducting oceanic crust with a typical gabbroid *P*-wave velocity, determined with tomography studies done in the region using local microseismic events [Comte et al., 1993c]. Therefore, the change from tensional to compressional stress field along

the upper part of the subducted slab is observed with teleseismic and locally recorded earthquakes and it could be associated with the maximum depth extent of the coupled zone.

The depth of the transition from compressional to tensional stress field along the upper-part of the subducting slab ( $60\pm 10$  km) is deeper than the maximum depth observed for the thrusting interplate events ( $40\pm 10$  km), meaning that probably at depth of between 40 to 60 km, large low-dip angle thrust event do not nucleate. Seismic slip, however, probably extends down to 40 km in depth. For instance the coseismic slip distribution of the great 1985 central Chile earthquake extends to about 60 km in depth [Barrientos, 1988], and in this region the transition from tensional to compressional stress field can be observed at about  $60\pm 10$  km in depth [Suárez and Comte, 1993].

Another example is the 1986 ( $M_w\sim 8.0$ ) Andreanof Island earthquake where the events on the main interplate thrust zone extend downdip to a bend in the subducted slab. Beyond here, deeper seismicity is associated with downdip tension, and also seaward to about 30-40 km of the deformation front [Engdahl et al., 1989]. This proposed transition was also observed by Clarke [1992] and Clarke and Carver [1992] in the central Aleutian arc and in the southern Cascadia subduction zone. Here the contact between the Gorda plate and the North American plate is reflected by a locked zone dipping with  $\sim 11^\circ$  has a width of about 70-80 km. Downdip of this point on, the seismicity is mainly tensional. In absence of rupture dimensions from past earthquakes, Clarke [1992] used this transition to postulate probable maximum rupture width and possible rupture lengths, which are critical in the estimation of potential earthquake magnitude. The 1985 central Chile and the 1986 Andreanof event are instructive analogs for both the model proposed here and those proposed by Clarke [1992] in order to estimate the dimensions of the interplate coupling through the observation of the nature and distribution of the variations of the stress field along the upper-part of the subducting slab.

#### **ACKNOWLEDGEMENTS**

We thank V. Kostoglodov and J. Pacheco for their critical review of the manuscript. This work was partially supported by Fundación Andes-Chile grant N° 52040.

#### **REFERENCES**



- Abe, K., Size of the great earthquakes of 1837-1974 inferred from tsunami data, *J. Geophys. Res.*, **84**, 1561-1568, 1979.
- Araújo, M. and G. Suárez, Detailed geometry and state of stress of the subducted Nazca plate beneath central Chile and Argentina: Evidence from teleseismic focal depth determinations, *in press, Geophys. J. Int.*, 1993.
- Ahrens, T. J., and G. Schubert, Gabbro-eclogite reaction rate and its geophysical significance, *Rev. Geophys and Space Phys.*, **13**, 383-400, 1975.
- Barazangi, M., and B. Isacks, Spatial distribution of earthquakes and subduction of the Nazca plate beneath South America, *Geology*, **4**, 686-692, 1976.
- Barrientos, S., Slip distribution of the 1985 central Chile earthquake, *Tectonophysics*, **145**, 225-241, 1988.
- Bevis, M., The curvature of Wadati-Benioff zones and the torsional rigidity of subducting plates, *Nature*, **323**, 52-53, 1986.
- Bevis, M., and B. Isacks, Hypocentral trend surface analysis: Probing the geometry of Benioff Zones, *J. Geophys. Res.*, **89**, 6153-6170, 1984.
- Cahill, T., and B. Isacks, Seismicity and shape of the subducted Nazca plate, *J. Geophys. Res.*, **97**, 17,503-17,529, 1992.
- Chinn, D. S., and B. Isacks, Accurate source depths and focal mechanisms of shallow earthquakes in Western South America and in the New Hebrides island arc, *Tectonics*, **2**, 529-563, 1983.
- Clarke, S. H., Cascadia subduction zone seismic potential: implications from structure and seismicity of the Central Aleutian arc, (abstract), *Eos Trans. AGU* **73**, 497, 1992.
- Clarke, S. H., and G. A. Carver, Late Holocene tectonics and paleoseismicity, southern Cascadia subduction zone, *Science*, **255**, 188-192, 1992.
- Comte, D. and M. Pardo, Reappraisal of great historical earthquakes in the northern Chile and southern Peru seismic gaps, *Natural Hazards*, **4**, 23-44, 1991.
- Comte, D., M. Pardo, L. Dorbath, C. Dorbath, H. Haessler, L. Rivera, A. Cisternas, and L. Ponce, Seismogenic interplate contact zone and crustal seismicity around Antofagasta, northern Chile using local data, *in press, Geophys. J. Int.*, 1993a.
- Comte, D., G. Suárez, T. Monfret, M. Pardo, L. Ponce and J. Domínguez, Preliminary results of a seismic experiment in northern Chile during July and August, 1991, *in press, Geofísica*, 1993 b.

- Comte, D., S. W. Roecker, and G. Suárez, velocity structure in northern Chile: Evidence of subducted oceanic crust in the Nazca plate, *in press, Geophys. J. Int.*, 1993c.
- Comte, D., and G. Suárez, An inverted double seismic zone in Chile: Evidence of phase transformation in the subducted slab, *in press, Science*, 1993.
- Cross, T. A., and R. H. Pilger, Jr., Control of subduction geometry, location of magmatic arcs, and tectonics of arc and back-arc regions, *Geol. Soc. Am. Bull.*, **93**, 545-562, 1982.
- DeMets, C., R. G. Argus, and S. Stein, Current plate motions, *Geophys. J. Int.*, **101**, 425-478, 1990.
- Dewey, J. W., Seismicity studies with the method of joint hypocentral determination, Ph.D. thesis, University of California, Berkeley, 116 pp., 1971.
- Díaz, J., Estudio de fuentes de tsunamis y terremotos: aplicación en el norte de Chile y sur del Perú. Oceanographer thesis, Universidad Católica de Valparaíso, 1992.
- Engebretson, D. and S. Kirby, Deep Nazca slab seismicity: Why it is so anomalous?, (abstract), *Eos Trans. AGU* **73**, 397, 1992.
- Engdahl, E. R., S. Billington, and C. Kisslinger, Teleseismically recorded seismicity before and after the May 7, 1986, Andreanof Islands, Alaska, earthquake, *J. Geophys. Res.*, **94**, 15,481-15,498, 1989
- Estabrook, C. H., J. Nabelek, and A. L. Lerner-Lam, Tectonic model of the Pacific-North American plate boundary in the Gulf of Alaska from broadband analysis of the 1979 St. Elias, Alaska, earthquake and its aftershocks, *J. Geophys. Res.*, **97**, 6587-6612, 1992.
- Gripp, A. E. and R. G. Gordon, Current plate velocities relative to the hotspots incorporating the Nuvel-1 global plate motion model, *Geophys. Res. Lett.*, **17**, 1109-1112, 1990
- Hasewaga, A., and I. S. Sacks, Subduction of the Nazca Plate beneath Peru as determined from seismic observation, *J. Geophys. Res.*, **86**, 4971-4980, 1981.
- Hori, S., H. Inoue, Y. Fukao, and M. Ukawa, Seismic detection of the untransformed 'basaltic' oceanic crust subducting into the mantle, *Geophys. J. R. Astron. Soc.*, **83**, 169-197, 1985.
- Isacks, B., Uplift of the central Andean plateau and bending of the Bolivian orocline, *J. Geophys. Res.*, **93**, 3211-3231, 1988.

- Isacks, B., and M. Barazangi, Geometry of the Benioff zones: Lateral segmentation and downward bending of the subducted lithosphere, in *Island Arcs, deep Sea Trenches, and Back Arc Basins, Ewing Ser. vol. 1*, edited by M. Talwani, and W. Pitman, pp.99-114, AGU, Washington, D.C., 1977.
- Isacks B., and P. Molnar, Distribution of stresses in the descending lithosphere from a global survey of focal mechanism solutions of mantle earthquakes, *Rev. Geophys.*, **9**, 103-174, 1971.
- Jarrad, R., Relations among subduction parameters, *Rev. Geophys.*, **24**, 217-284, 1986.
- Jordan, T. E., B. Isacks, R. W. Allmendinger, J. A. Brewer, V. A. Ramos, and C. J. Ando, Andean tectonics related to geometry of subducted Nazca plate, *Geol. Soc. Am. Bull.*, **94**, 341-361, 1983.
- Kadinsky-Cade, K. A., Seismotectonics of the Chile margin and the 1977 Cauçete earthquake of western Argentina, Ph.D. thesis, 253 pp., Cornell Univ., Ithaca, N. Y., 1985.
- Kausel, E., Los terremotos de Agosto de 1868 y Mayo de 1877 que afectaron el sur del Perú y norte de Chile, *Boletín de la Academia Chilena de Ciencias*, **3**, 8-12, 1986.
- Kelleher, J., Ruprute zones of large South American earthquakes and some predictions, *J. Geophys. Res.*, **77**, 2089-2103, 1972.
- Kono, M., Y. Takahashi, and Y. Fukao, Earthquakes in the subducting slab beneath northern Chile: A double-seismic zone?, *Tectonophysics*, **112**, 112-225, 1985.
- Kostoglodov, V., Maximum depth of earthquakes and phase transitions in the lithosphere descending into the mantle, in *Physics and internal structure of the Earth*, Moscow, 52-57, 1989.
- Kostoglodov, V., Chilean subduction system: structure, tectonics, and related seismicity, (extended abstract) *Second Symposium Geodynamique Andine-ISAG93*, 99-102, 1993.
- Lomnitz, C., Grandes terremotos y tsunamis en Chile durante el período 1535-1955, *Geofis. Panam.*, **2**, 151-178, 1971.
- Malgrange, M. and R. Madariaga, Complex distribution of large thrust and normal-fault earthquakes in the Chilean subduction zone, *Geophys. J. R. Astron. Soc.*, **73**, 489-505, 1983.
- Mayes, C. L., L. A. Lawver, and D. T. Sandwell, Tectonic history and new isochron chart of the South Pacific, *J. Geophys. Res.*, **95**, 8543-8547, 1990.

- McCann, W. R., S. P. Nishenko, L. R. Sykes, and J. Krause, Seismic gaps and plate tectonics: Seismic potential for major boundaries, *Pure Appl. Geophys.*, **117**, 1082-1147, 1979.
- Nàbelek, J., Determination of earthquake source parameters from inversion of body waves, Ph.D. thesis, Mass. Ins. of Technol., Cambridge, 1984.
- Nàbelek, J., Geometry and mechanism of faulting of the 1980 El Asnam, Algeria earthquake from inversion of teleseismic body waves and comparison with field observations, *J. Geophys. Res.*, **90**, 12,713-12,728, 1985.
- Nishenko, S., Seismic potential for large and great interplate earthquakes along the Chilean and southern Peruvian margins of South America: A quantitative reappraisal, *J. Geophys. Res.*, **90**, 3589-3615, 1985.
- Pacheco, J. F., L. R. Sykes, and C. H. Scholz, Nature of seismic coupling along simple plate boundaries of the subduction type, *J. Geophys. Res.*, **98**, 14,133-14,160, 1993.
- Pennington, W. D., Role of shallow phase changes in the subduction of oceanic crust, *Science*, **220**, 1045-1047, 1983.
- Schneider, J. F., and I. S. Sacks, Stress in the contorted Nazca plate beneath southern Peru from local earthquakes, *J. Geophys. Res.*, **92**, 13,887-13,902, 1987.
- Stauder, W., Mechanism and spatial distribution of Chilean earthquakes with relation to subduction of the oceanic plate, *J. Geophys. Res.*, **78**, 5033-5061, 1973.
- Suárez, G., and D. Comte, Comment on "Seismic coupling along the Chilean subduction zone" by B. W. Tichelaar and L. R. Ruff, *J. Geophys. Res.*, **98**, 15,825-15,828, 1993.
- Sykes, L., and D. Hayes, Seismicity and tectonics of South America and adjacent oceanic areas, *Geol. Soc. Am. Programs*, Cordilleran section, **3**, 206, 1971.
- Tichelaar, B. W., and L. R. and Ruff, Seismic coupling along the Chilean subduction zones, *J. Geophys. Res.*, **96**, 11,997-12,022, 1991.
- Tichelaar, B. W., and L. Ruff, Depth of seismic coupling along subduction zones, *J. Geophys. Res.*, **98**, 2017-2038, 1993.
- Wessel, P. and W. H. Smith, Free software helps map and display data, (abstract), *Eos Trans. AGU* **72**, 441, 1991.
- Wessel, P. and W. H. Smith, The GMT-SYSTEM v. 2.1 Technical Reference and Cookbook, 1992.

## FIGURE CAPTIONS

**Figure 1.-** Bathymetric and topographic contours in northern Chile and southern Peru regions. The most important bathymetric features, the Nazca and the Perdida Ridges, are also shown. The isochron chart of the region was inferred from Mayes et al. [1990]. Estimated rupture length of the 1877 great earthquake is indicated between bars [Comte and Pardo, 1991; Díaz, 1992]. The arrow indicates the direction of the relative convergence rate between Nazca and South American plate [DeMets et al., 1990].

**Figure 2.-** Locations and ellipse-errors of the 15 modeled earthquakes obtained from the joint hypocentral determination. Each earthquake is identified by its date. Their focal mechanism solutions, obtained from the waveform inversions, are shown in a lower hemispheric projection. Stars represent the locally recorded microearthquakes used as calibration events. Triangles corresponds to Quaternary volcanoes and dark triangles represent active volcanoes.

**Figure 3.-** Histograms of the maximum horizontal error estimated from the major semi-axis of the error ellipsoid obtained from the joint hypocentral determination using locally recorded calibration events from (a) to (c); and using the ISC location fixed from (d) to (f).

**Figure 4.-** Histograms of the depth error estimated from the minor semi-axis of the error ellipsoid obtained from the joint hypocentral determination using locally recorded calibration events (a) and (b); and using the ISC location fixed (c) and (d).

**Figure 5.-** Distribution of the direction of P-axis (black bars) of compressional events (dark circles) and of T-axis (black arrows) of tensional events (white circles). In the lower-right part the azimuthal diagram represents the histogram of the P (in black) and T axis (in white) of all the relocated events. The P1 to P4 profiles, oriented in the direction of convergence of the Nazca plate are also shown.

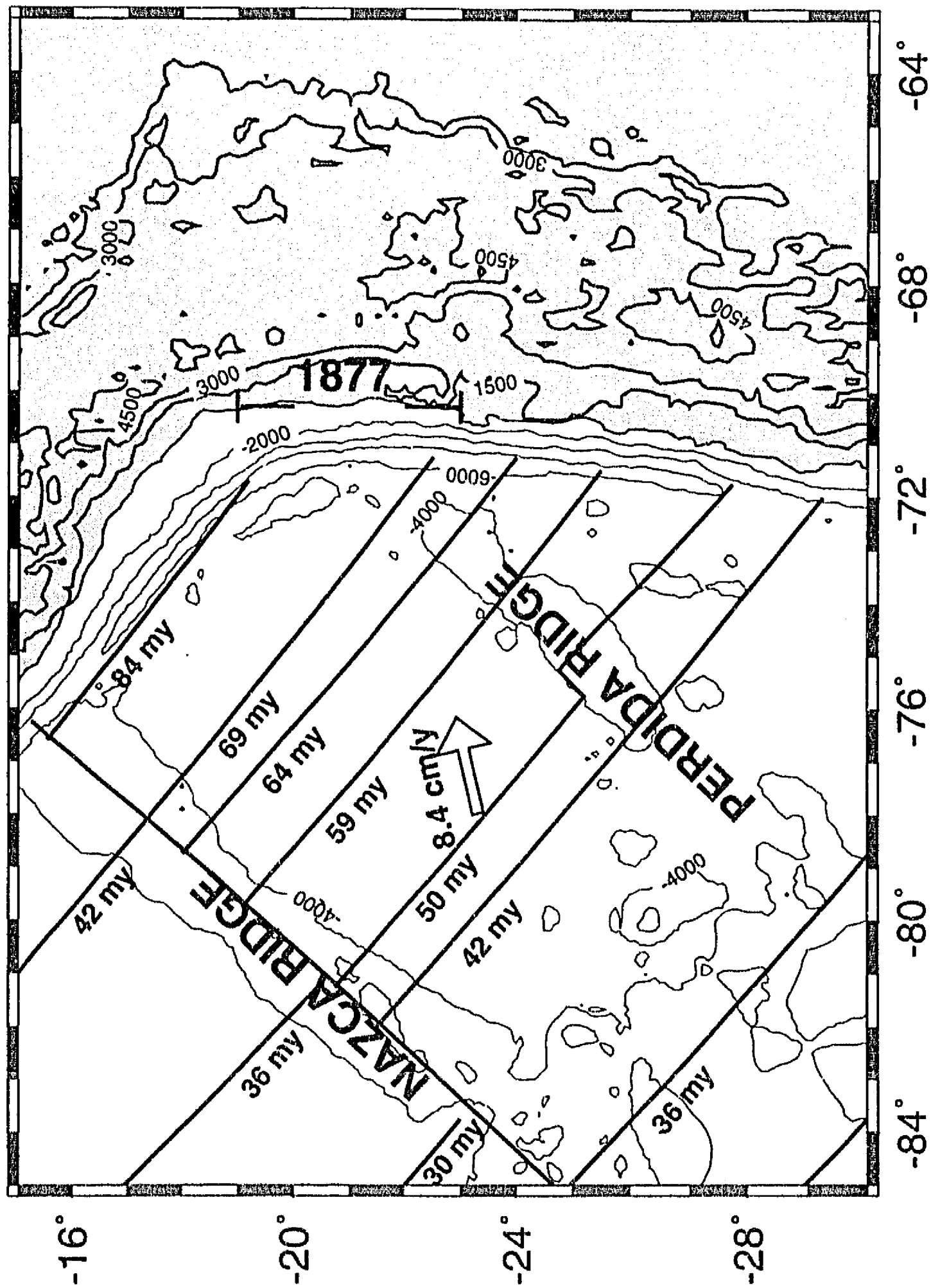
**Figure 6.-** Distribution of seismicity along the P1 and P2 profiles indicated in Figure 5. Each event is identified by its number (Tables 1 and 2). The vertical lower hemispheric projection of the focal mechanism solutions are presented for the events modelled in this study (dark circles) and also for the other reported events (grey circles). Each focal mechanism has P axis (dark dot) and T axis (white dot). Open circles correspond to teleseismically recorded events that have no reported focal mechanism solutions, and open squares are locally recorded microearthquakes. Upper-part of the subducting slab was inferred from the distribution of the locally and teleseismically recorded events. Projection of the active and Quaternary volcanoes are shown with dark and open triangles, respectively.

**Figure 7.-** Distribution of the seismicity along the P3 and P4 profiles indicated in Figure 5. Symbols as Figure 6.

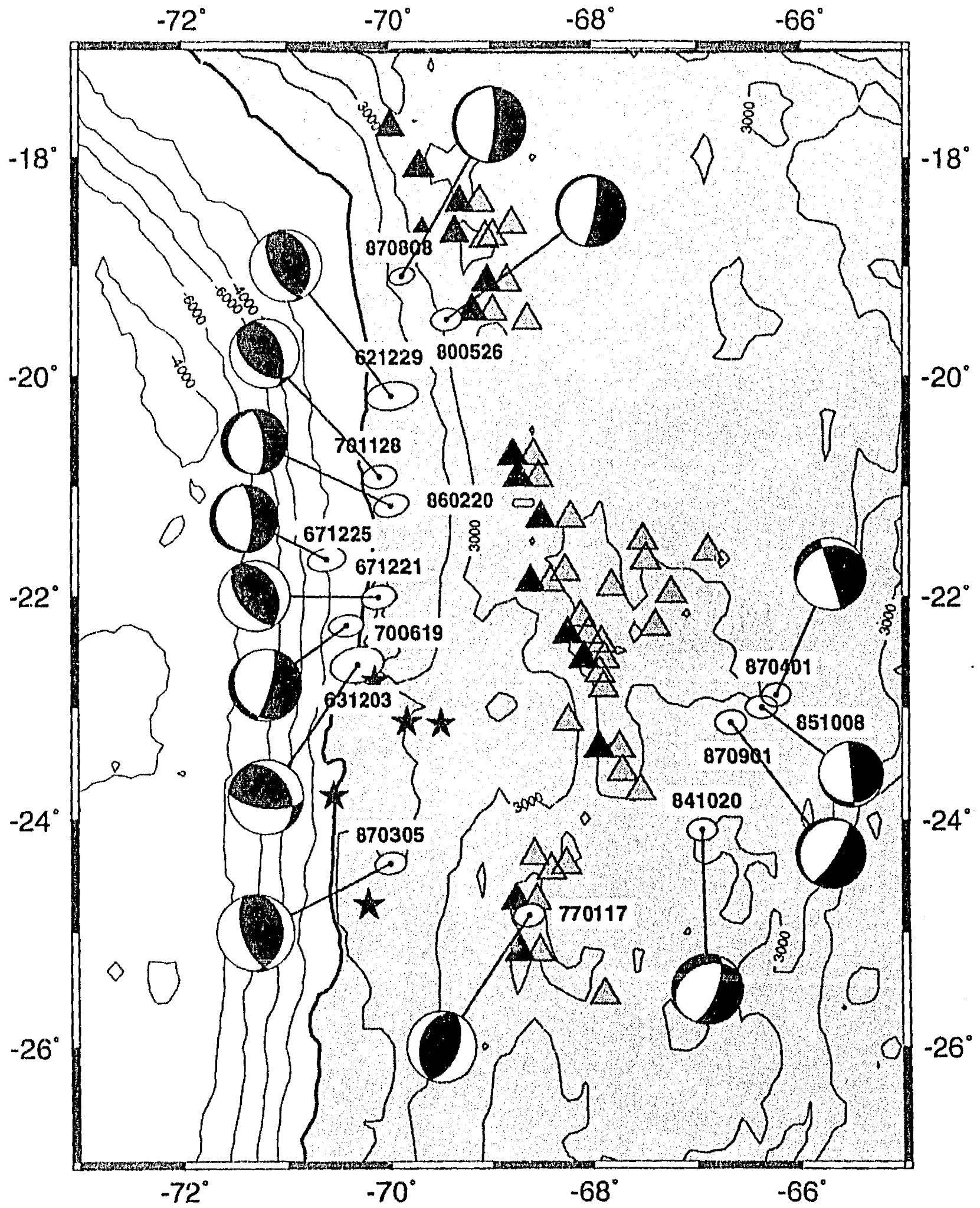
**Figure 8.-** Space distribution of seismic events used in this study. Dark and gray circles represent modeled events (Table 1), and events with reported focal mechanisms (Table 2), respectively. Open squares are microseismic events locally recorded. Dark and gray triangles correspond to active and Quaternary volcanoes, respectively. Continuous and dashed lines correspond to reliable and uncertainly iso-depth contours. The Peru-Chile trench is also shown.

**Figure 9.-** Summary of the shape of the P1 to P4 profiles indicated on Figures 5, 6, and 7. The position of the main changes of the dip angles along each profile is indicated by different grayed slices, and the name of each dip angle is shown to the right.

Figure 1



# Figure 2





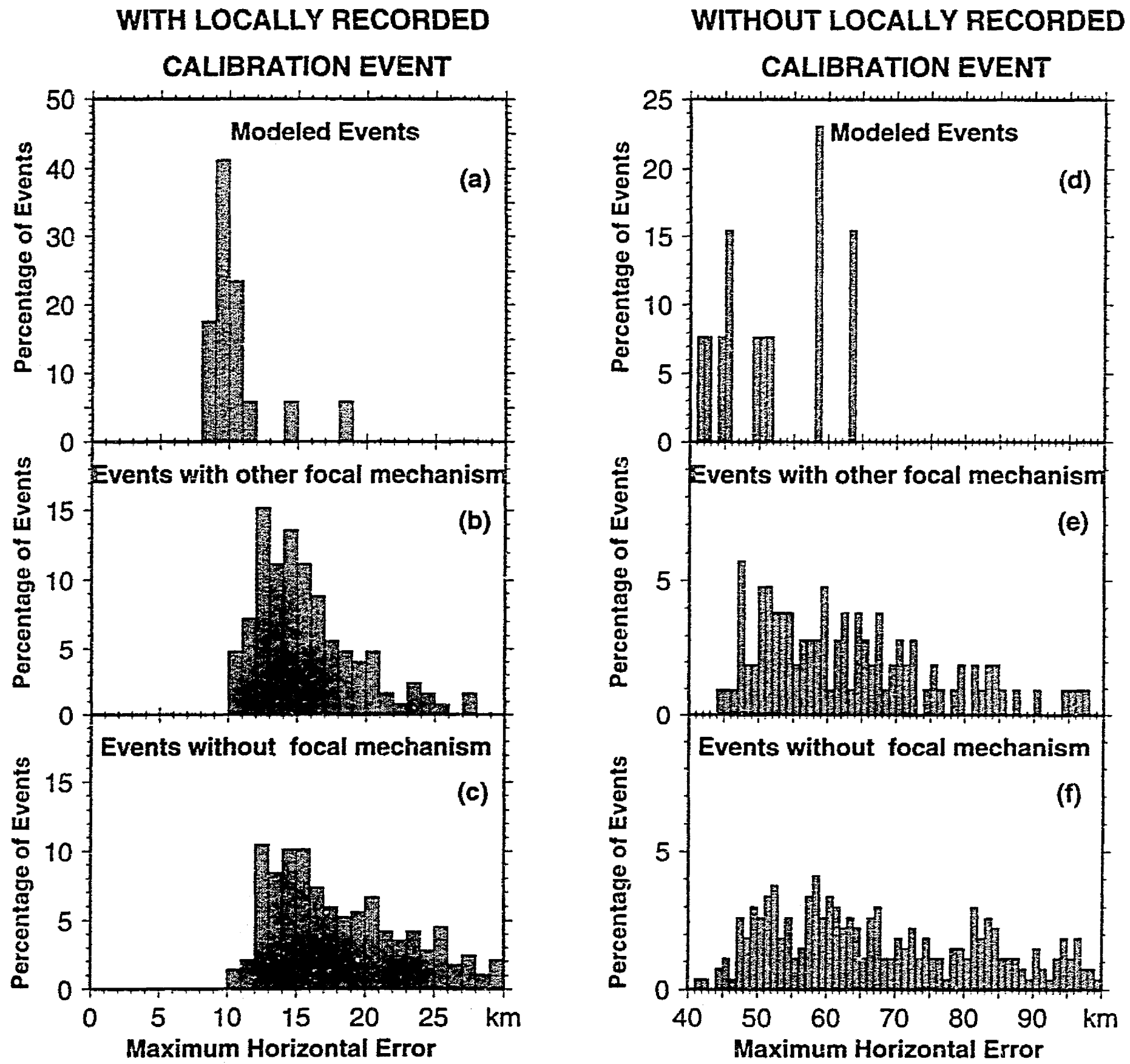
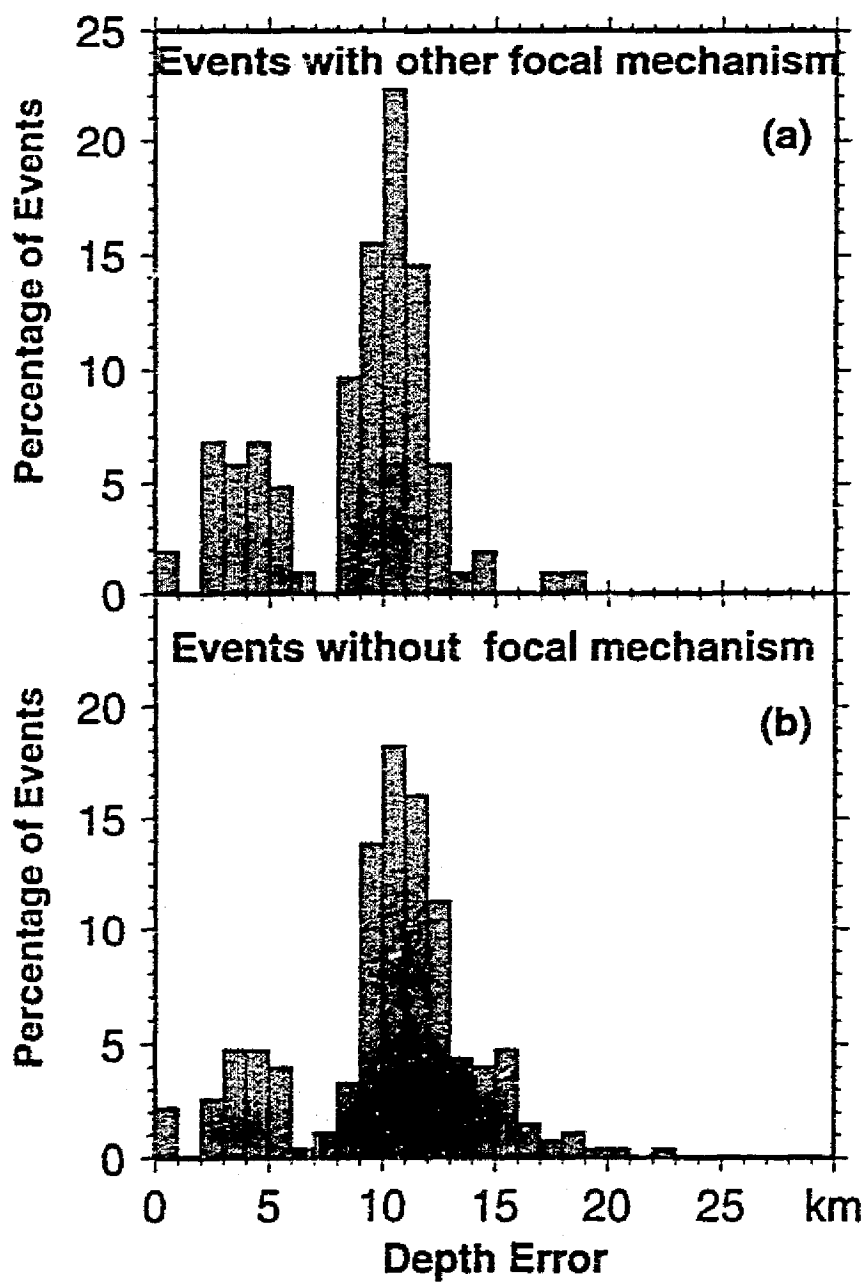


Figure 3

WITH LOCALLY RECORDED CALIBRATION EVENT



WITHOUT LOCALLY RECORDED CALIBRATION EVENT

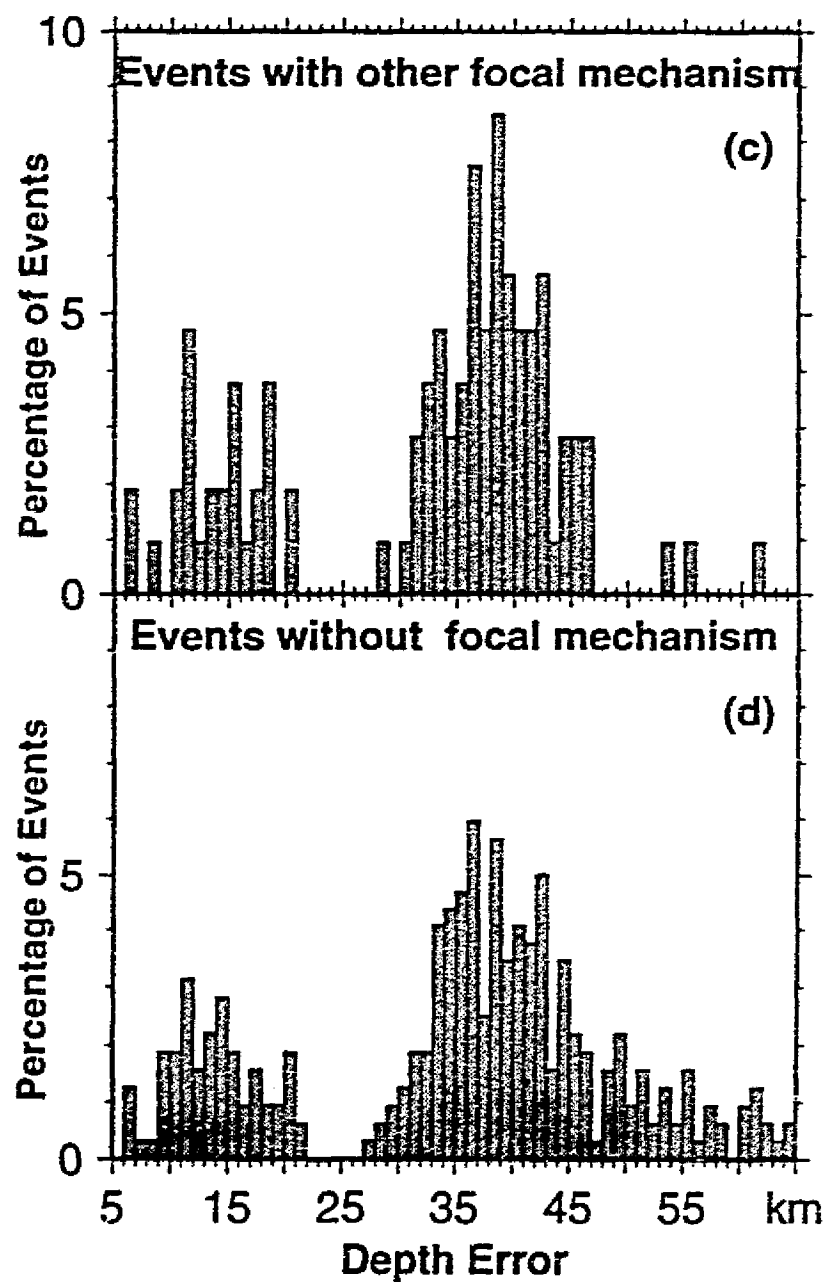


Figure 4

Figure 5

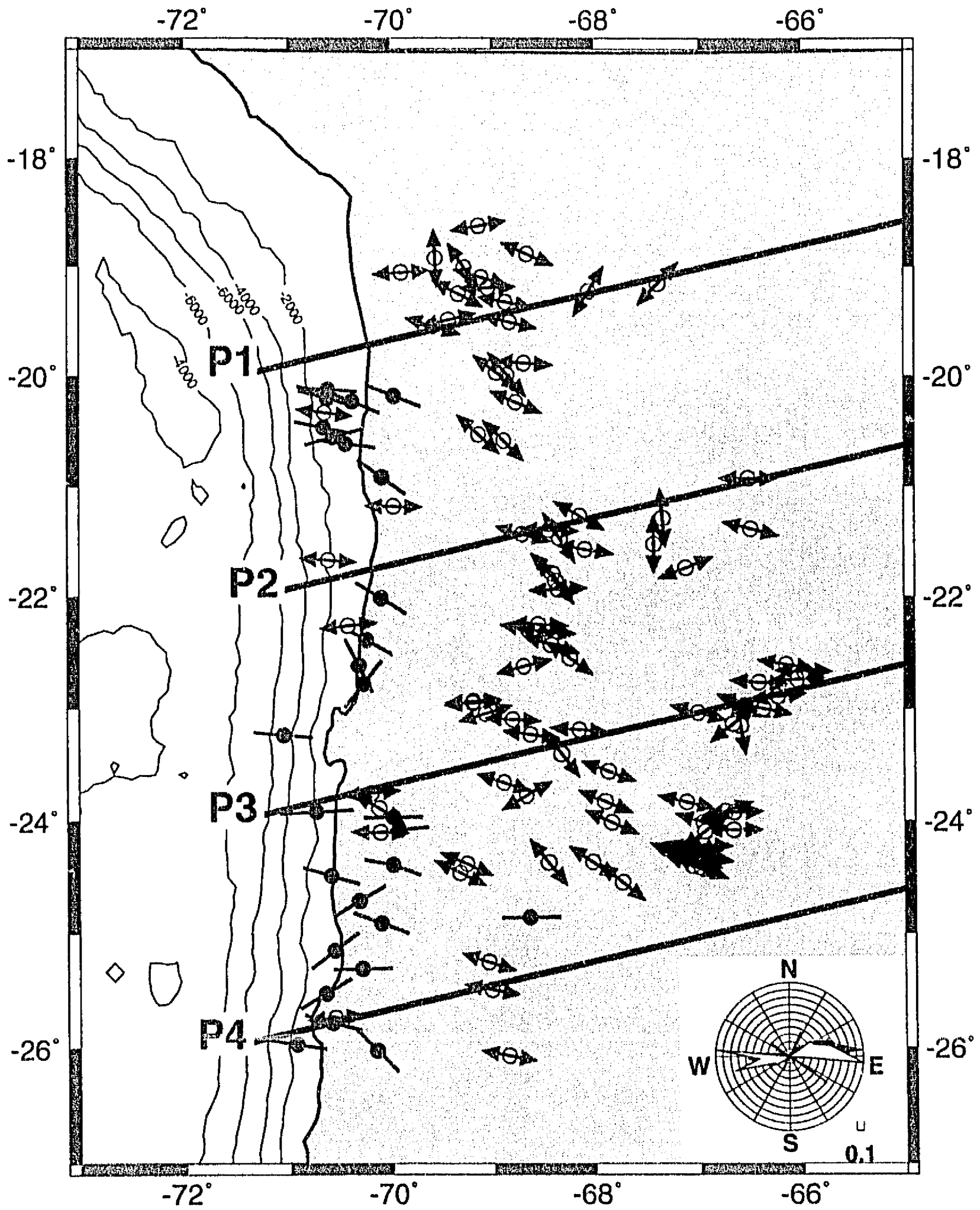


Figure 6

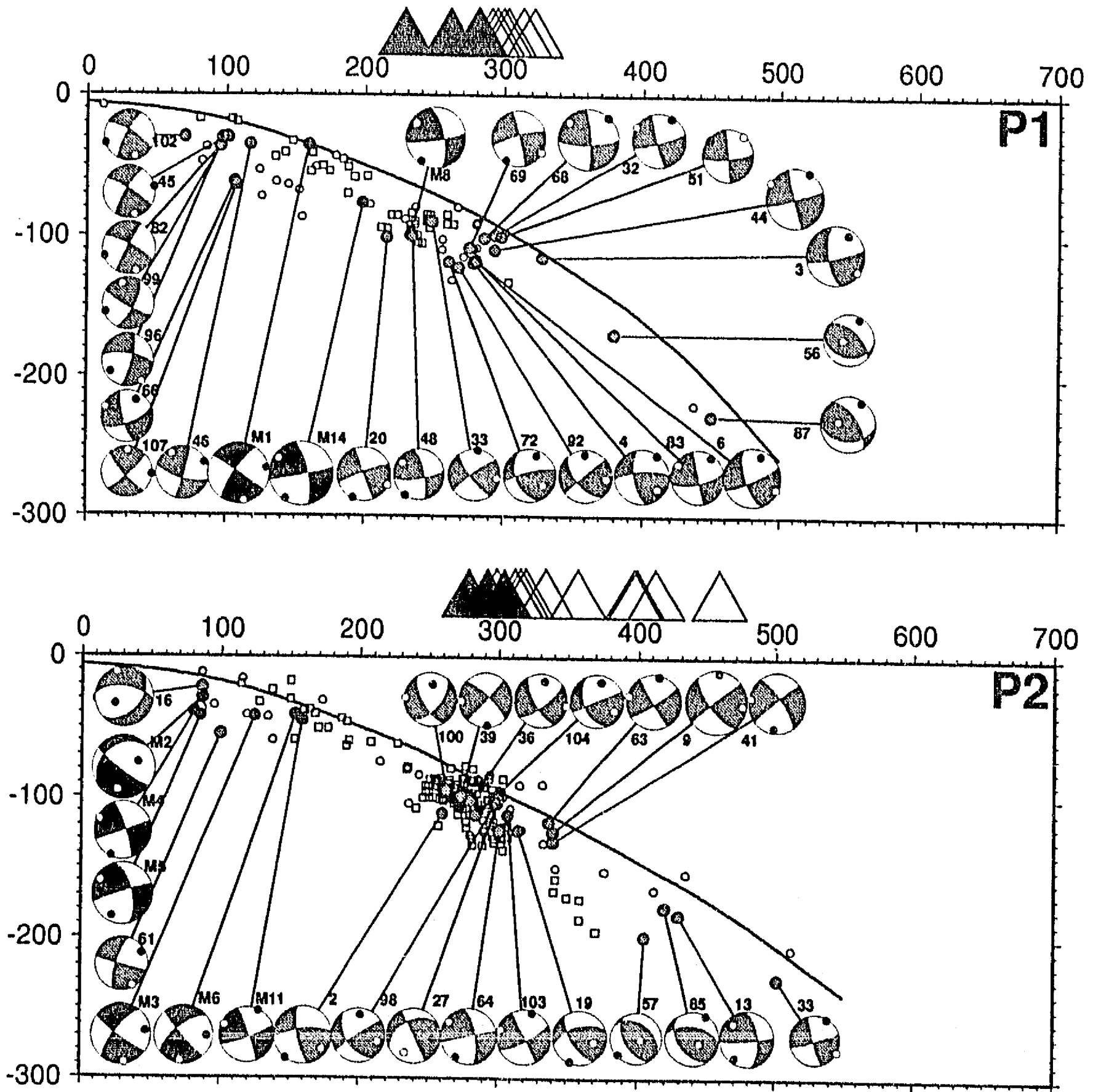


Figure 7

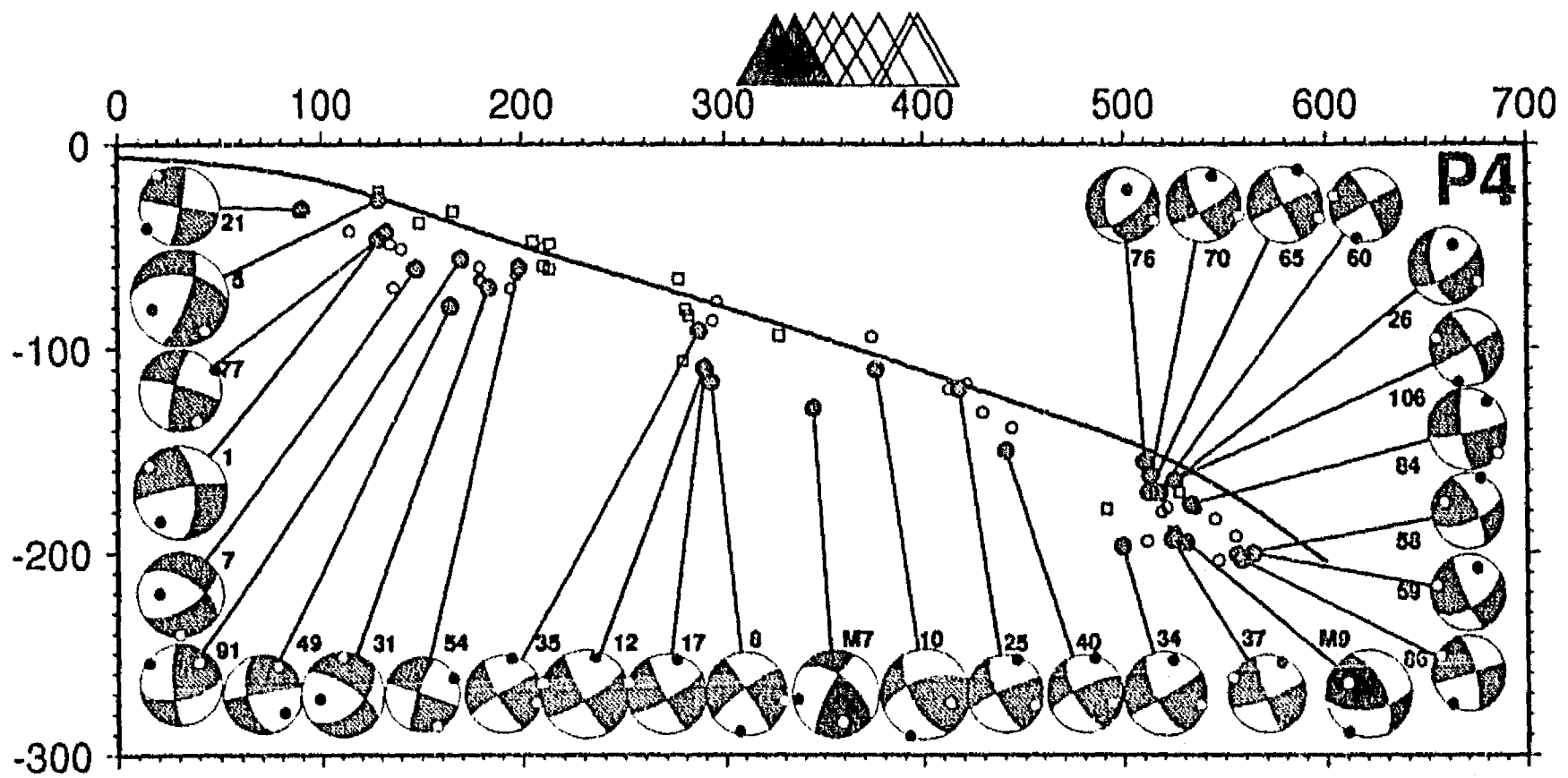
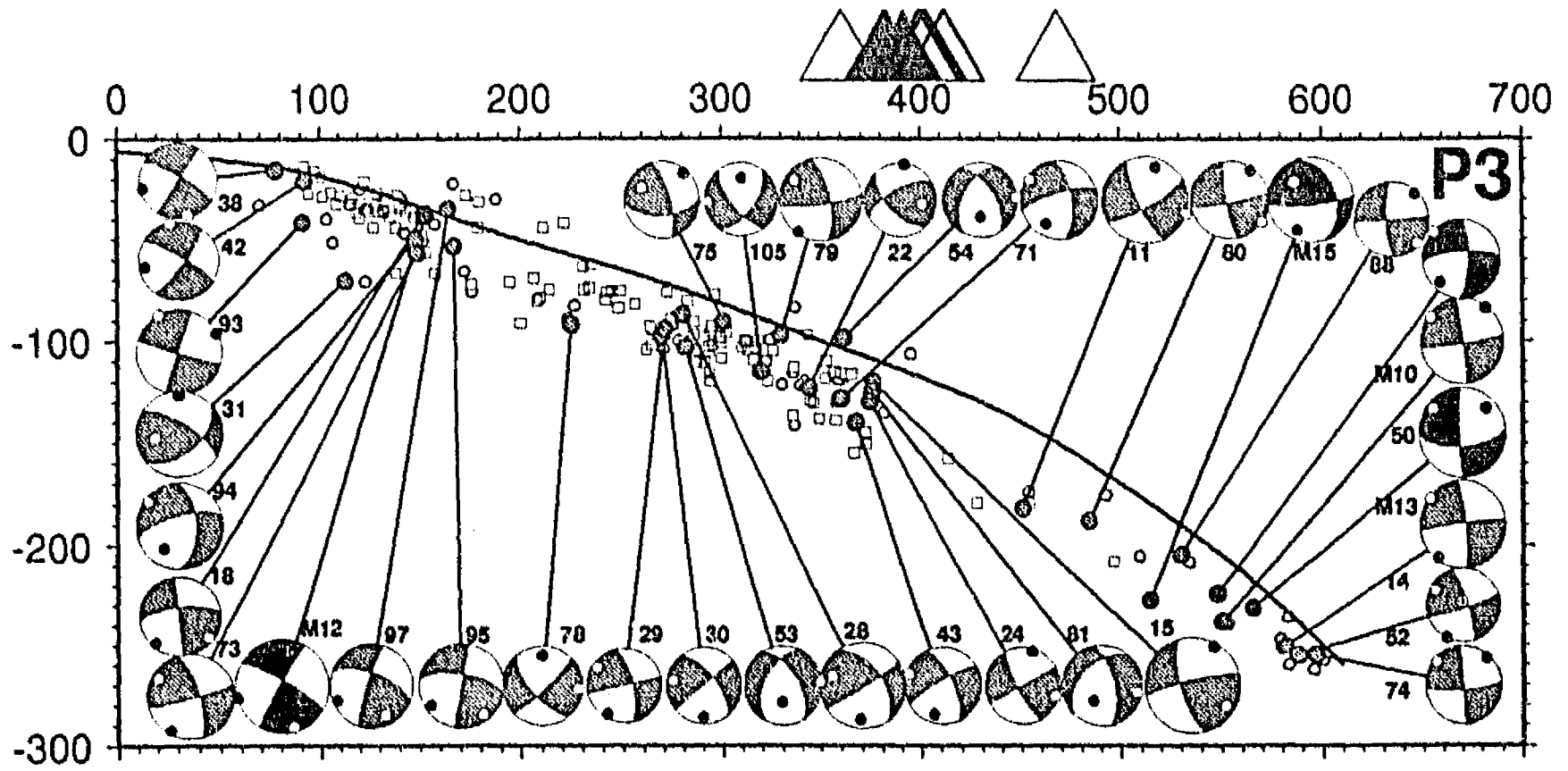


Figure 8

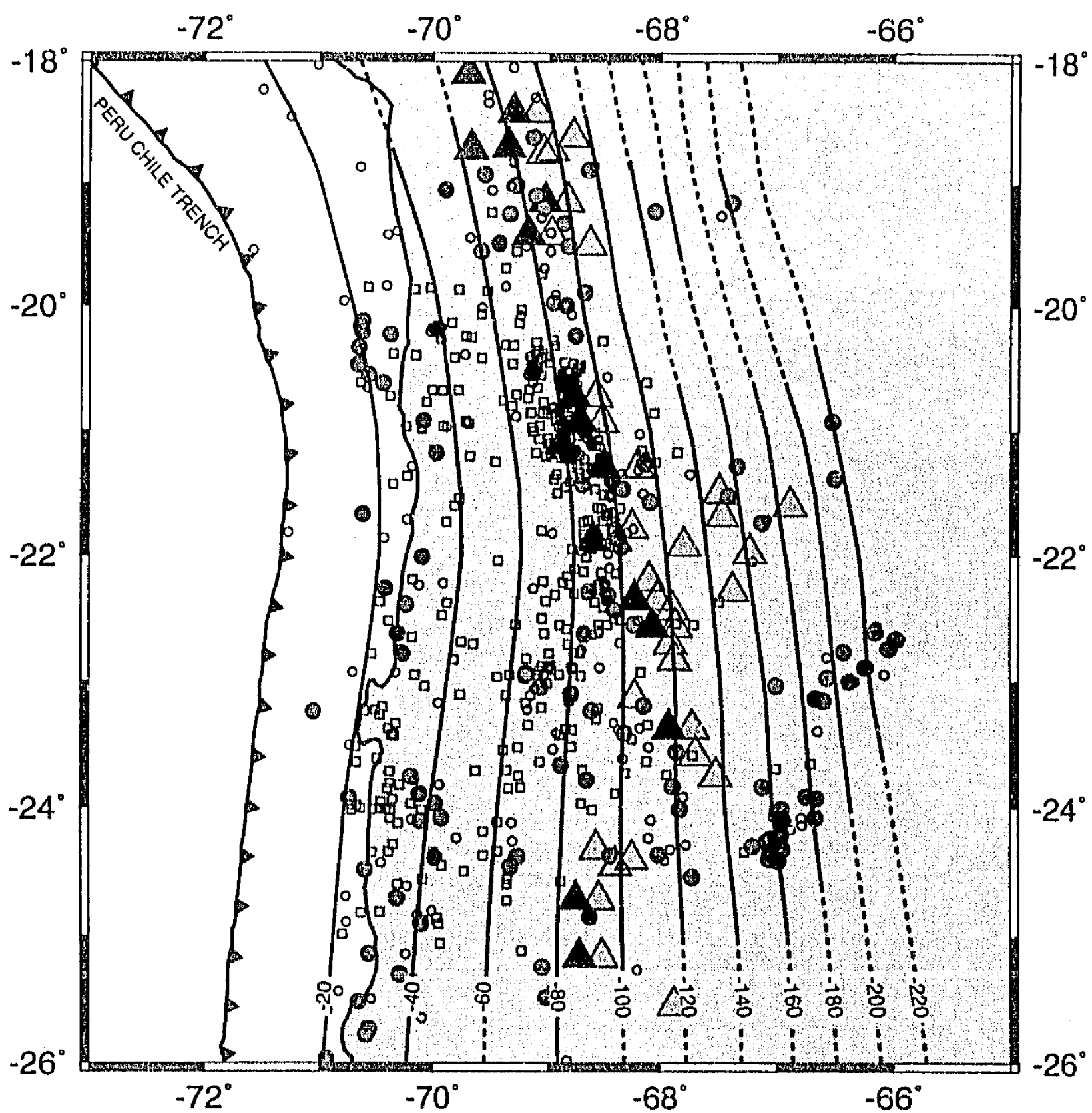


Figure 9

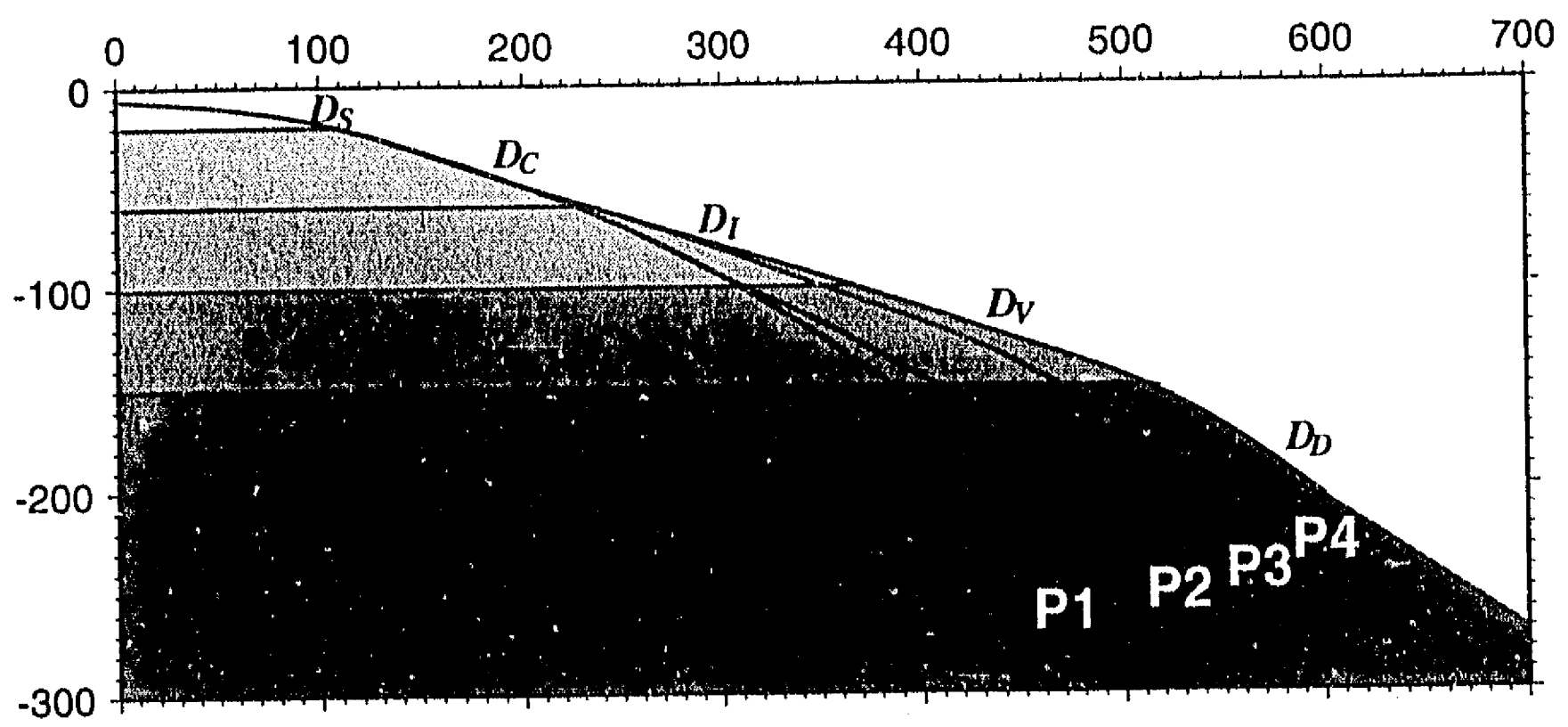


Table 1 Source parameters of the earthquakes modelled using the waveform inversion

Id	Date	TO hr:mn	Lat °	Lon °	Depth km	mb	Ms	M0 10 <sup>25</sup> dyn-cm	Strike °	Dip °	Rake °	rms	Dur s
(M1)	Dic. 29, 1962	10:41	-20.19	-69.97	35±2	-	6.8	2.11	349.6±17	33.7±3	105.1±11	0.49	6
(M2)	Dic. 3, 1963	23:03	-22.62	-70.31	29±2	-	6.1	1.29	330.0±24	37.6±5	137.1±16	0.46	8
(M3)	Dic. 21, 1967	02:25	-22.01	-70.09	41±3	6.0	6.3	37.20	336.8±13	36.3±2	99.1±9	0.52	12
	Dic. 21, 1967	d(10s)			39±4			11.50	334.7±30	32.8±4	90.8±19		6
(M4)	Dic. 25, 1967	10:41	-21.67	-70.61	39±2	5.7	5.8	1.37	357.8±7	70.3±3	-89.3±11	0.56	6
(M5)	Jun. 19, 1970	10:56	-22.27	-70.42	42±1	6.1	6.2	2.91	14.1±6	78.0±3	-77.9±15	0.52	6
(M6)	Nov. 28, 1970	11:08	-20.92	-70.08	41±2	5.8	6.0	0.37	339.2±11	49.5±3	110.1±5	0.47	6
(M7)	Jan. 17, 1977	21:27	-24.85	-68.63	120±7	6.0	6.1	1.99	35.3±26	48.5±19	120.1±27	0.62	3
	Jan. 17, 1977	d(5s)			128±3			12.30	21.7±8	52.8±2	92.9±6		9
(M8)	May 26, 1980	18:41	-19.49	-69.43	99±3	6.0	6.1	11.32	203.7±34	11.0±3	-76.9±33	0.43	12
(M9)	Oct. 20, 1984	17:59	-24.09	-66.94	195±2	5.9	-	2.12	244.6±10	30.8±4	-49.6±8	0.53	6
(M10)	Oct. 8, 1985	09:47	-23.00	-66.37	224±4	5.5	-	0.61	89.5±19	14.5±14	-184.5±20	0.57	8
(M11)	Feb. 20, 1986	09:16	-21.18	-69.97	45±2	5.5	-	0.37	190.6±12	22.4±2	-74.2±10	0.48	6
(M12)	Mar. 5, 1987	09:17	-24.39	-69.99	38±3	6.5	7.3	103.50	5.0±13	30.6±2	110.0±8	0.43	12
(M13)	Apr. 1, 1987	01:48	-22.89	-66.23	231±2	6.1	6.2	28.04	342.6±4	88.0±3	-116.0±6	0.51	16
(M14)	Aug. 8, 1987	15:48	-19.09	-69.86	76±4	6.4	6.9	38.34	3.6±6.8	79.0±5	-90.5±13	0.60	9
(M15)	Sep. 1, 1987	04:26	-23.14	-66.67	227±4	5.9	-	3.15	175.7±49	11.4±8	-126.8±47	0.59	8

Id: Identification of each event; Lat and Lon: relocated epicenter; mb and Ms: magnitudes obtained from the ISS and ISC catalogs; Dur: duration of the source time function; Depth, Strike, Dip, and Rake: focal mechanism solutions, the error were estimated from the  $1\sigma$  (standard deviation) obtained from the inversion were multiplied by 2 (strike, dip, and rake) and 10 (depth) [Nabelek, 1984; Estabrook et al., 1992]; rms: normalized root mean square error. In the cases of (m3) and (m7) events, the d value in parenthesis corresponds to the time delay between the two point sources.



Table 2 Earthquakes relocated using JHD method, that were not modeled in this study

Id	Date	T0 hr:mn	Lat °	Lon °	Depth km	mb	Strike °	Dip °	Rake °	Ref
(1)	650223	22:11	-25.74	-70.55	43	6.3	16	86	-78	MM83
(2)	650612	18:50	-20.54	-69.13	111	5.7	95	18	-145	ST73
(3)	650820	09:42	-18.85	-68.65	115	5.9	206	15	-31	ST73
(4)	660308	20:46	-20.00	-68.84	119	5.5	93	15	-137	ST73
(5)	661228	08:18	-25.52	-70.65	27	6.6	70	41	150	MM83
(6)	670511	15:05	-20.24	-68.76	118	5.9	191	25	-46	ST73
(7)	670621	20:09	-25.15	-70.56	61	5.8	40	46	94	MM83
(8)	670820	15:03	-25.25	-69.05	116	5.7	150	36	-108	MM83
(9)	671227	09:17	-21.27	-68.14	124	6.3	163	37	-73	ST73
(10)	700611	06:02	-24.37	-68.45	110	6.2	109	31	-117	AS93
(11)	710221	10:35	-23.83	-67.12	182	6.0	194	32	-53	AS93
(12)	710617	21:00	-25.49	-69.01	109	6.0	188	33	-65	AS93
(13)	710814	15:00	-21.74	-67.13	183	5.6	222	8	-67	AS93
(14)	730201	05:14	-22.61	-66.15	250	6.0	145	8	-120	AS93
(15)	740102	10:42	-22.55	-68.24	121	6.6	136	15	-102	AS93
(16)	751028	06:54	-22.78	-70.27	22	5.8	66	32	110	KK85
(17)	760418	19:40	-26.07	-68.85	110	5.5	188	31	-66	AS93
(18)	770605	2:46	-23.89	-70.12	37	5.6	94	20	-162	HCMT
(19)	770618	16:49	-21.47	-68.34	123	5.4	101	35	-120	HCMT
(20)	770630	2:46	-19.55	-69.58	101	5.4	149	22	-108	HCMT
(21)	770702	5:9	-25.97	-70.93	32	5.4	342	11	79	HCMT
(22)	770823	3:12	-21.41	-68.32	123	5.2	125	37	-94	HCMT
(23)	780402	9:7	-19.25	-69.34	90	5.3	155	37	-87	HCMT
(24)	780607	14:8	-23.83	-67.90	130	5.3	167	28	-78	HCMT
(25)	790113	8:39	-24.37	-68.02	120	5.3	148	24	-89	HCMT
(26)	790418	17:59	-24.42	-66.98	171	5.4	206	37	-19	HCMT
(27)	790504	17:21	-21.79	-68.41	104	5.6	100	51	-146	HCMT
(28)	790514	23:04	-23.05	-69.07	87	5.9	174	33	-121	AS93
(29)	790515	17:32	-22.94	-69.19	94	5.3	169	13	-107	HCMT
(30)	790522	8:33	-22.95	-69.20	97	5.5	165	40	-117	HCMT
(31)	790528	14:59	-24.71	-70.31	70	5.8	21	37	-104	AS93
(32)	790617	19:33	-19.33	-68.86	99	5.3	199	18	-54	HCMT
(33)	790810	1:28	-21.39	-66.50	229	5.1	183	17	-69	HCMT
(34)	791122	02:41	-24.30	-67.21	197	5.7	324	65	-106	AS93
(35)	791228	13:46	-24.46	-69.33	91	5.3	158	30	-86	HCMT
(36)	800414	23:57	-21.43	-68.69	102	5.4	195	40	-47	HCMT
(37)	800502	19:9	-24.33	-66.95	193	5.4	197	23	-57	HCMT
(38)	800530	16:56	-23.24	-71.05	15	5.3	6	32	105	HCMT
(39)	800616	5:45	-22.25	-68.54	99	5.5	6	44	-77	HCMT
(40)	801108	21:35	-24.54	-67.73	150	5.4	137	28	-95	HCMT
(41)	801211	18:15	-21.48	-68.09	131	6.1	159	38	-111	HCMT
(42)	810107	16:26	-23.92	-70.73	20	5.5	5	33	93	HCMT
(43)	810127	14:25	-23.19	-68.15	140	5.4	147	32	-130	HCMT
(44)	810326	18:4	-19.51	-68.82	110	5.8	179	14	-76	HCMT
(45)	810416	22:5	-20.21	-70.61	30	5.1	2	33	114	HCMT
(46)	810621	10:30	-20.23	-70.37	35	5.2	299	24	40	HCMT
(47)	810920	10:48	-23.15	-66.60	221	5.1	65	23	-136	HCMT
(48)	811102	14:30	-18.93	-69.56	100	5.1	224	17	-51	HCMT
(49)	811117	7:11	-26.02	-70.15	80	5.4	144	11	101	HCMT
(50)	820210	20:38	-22.76	-66.42	238	5.8	205	11	-57	AS93
(51)	820322	21:44	-19.89	-68.67	100	5.1	232	12	-25	HCMT
(52)	820419	11:54	-22.74	-66.05	255	5.3	194	19	-76	HCMT
(53)	820503	7:26	-23.66	-68.89	103	5.5	24	63	-23	HCMT
(54)	820529	3:26	-22.43	-68.42	98	5.2	172	23	-67	HCMT

Table 2 Continued

Id	Date	T0 hr:mn	Lat °	Lon °	Depth km	mb	Strike °	Dip °	Rake °	Ref
(55)	820529	17:22	-24.91	-70.10	60	5.1	348	19	100	HCMT
(56)	820603	6:43	-19.23	-68.05	170	5.2	29	48	-133	HCMT
(57)	820610	11:43	-21.52	-67.42	199	5.0	51	57	-152	HCMT
(58)	820719	23:52	-23.91	-66.74	201	5.2	219	31	-62	HCMT
(59)	820903	20:14	-23.92	-66.66	201	5.4	218	44	-36	HCMT
(60)	820911	14:12	-24.24	-67.05	171	5.1	167	29	-99	HCMT
(61)	821024	10:43	-22.39	-70.24	55	5.4	337	16	97	HCMT
(62)	821231	1:35	-21.57	-68.09	117	5.3	183	33	-74	HCMT
(63)	821231	3:47	-21.05	-68.46	67	5.8	340	11	130	HCMT
(64)	830110	09:17	-21.93	-68.35	123	5.6	200	5	-74	AS93
(65)	830126	1:5	-24.26	-67.08	171	5.2	163	25	-91	HCMT
(66)	830127	07:35	-24.34	-70.65	61	5.2	216	31	-29	HCMT
(67)	830201	4:22	-23.10	-68.80	99	5.2	143	28	-137	HCMT
(68)	830225	22:49	-18.63	-69.13	101	5.9	253	15	-14	HCMT
(69)	830523	0:54	-19.10	-69.11	109	5.5	133	18	-129	HCMT
(70)	830606	16:22	-24.35	-67.05	163	5.3	190	32	-53	HCMT
(71)	830721	7:11	-22.32	-68.46	128	5.5	122	22	-160	HCMT
(72)	830921	10:27	-19.01	-69.28	118	5.3	129	17	-84	HCMT
(73)	831016	9:59	-23.75	-70.20	56	5.7	185	16	-90	HCMT
(74)	840101	22:8	-22.66	-65.98	228	5.4	238	13	-20	HCMT
(75)	840106	15:1	-23.78	-68.66	91	5.4	253	35	-26	HCMT
(76)	840424	18:27	-24.40	-67.06	156	5.2	209	45	-9	HCMT
(77)	840724	4:49	-25.78	-70.58	47	5.6	14	18	126	HCMT
(78)	840812	11:51	-24.38	-69.26	92	5.6	180	45	-56	HCMT
(79)	841211	23:22	-22.62	-68.68	97	5.6	217	13	-62	HCMT
(80)	841231	13:0	-23.03	-67.01	188	5.5	195	12	-54	HCMT
(81)	850214	8:30	-24.01	-67.83	125	5.6	111	61	-167	HCMT
(82)	850221	21:52	-20.62	-70.43	30	5.3	10	30	114	HCMT
(83)	850518	16:59	-19.20	-69.04	117	5.4	226	24	-32	HCMT
(84)	850623	6:55	-24.02	-66.94	177	5.5	205	13	-40	HCMT
(85)	850827	10:44	-21.29	-67.34	178	5.2	63	37	-136	HCMT
(86)	860312	22:4	-24.08	-66.67	204	5.2	176	15	-96	HCMT
(87)	860315	11:29	-19.16	-67.34	228	5.6	259	50	-42	HCMT
(88)	860409	18:10	-22.97	-66.56	205	5.2	197	3	-48	HCMT
(89)	860510	2:0	-23.56	-67.86	138	5.2	109	47	-174	HCMT
(90)	860912	10:39	-22.64	-70.17	82	5.1	207	26	-74	HCMT
(91)	861024	2:42	-25.31	-70.29	57	5.4	239	32	174	HCMT
(92)	870304	10:4	-19.97	-68.95	122	5.3	166	40	-60	HCMT
(93)	870305	10:55	-24.49	-70.59	51	5.7	336	17	80	HCMT
(94)	870306	7:6	-24.10	-70.11	49	5.8	113	24	-177	HCMT
(95)	870306	9:39	-24.08	-69.93	53	5.7	54	24	154	HCMT
(96)	870308	12:51	-20.56	-70.56	30	5.3	52	22	142	HCMT
(97)	870322	3:23	-23.97	-69.98	34	5.9	40	32	145	HCMT
(98)	870512	16:12	-21.86	-68.38	100	5.4	163	33	-56	HCMT
(99)	870523	5:1	-20.13	-70.61	36	5.2	331	30	56	HCMT
(100)	870601	1:50	-22.29	-68.64	94	5.4	207	55	-34	HCMT
(102)	870611	5:8	-20.48	-70.65	30	5.0	15	34	126	HCMT
(103)	870619	19:0	-21.40	-68.43	112	5.4	196	30	-65	HCMT
(104)	870709	4:7	-20.59	-68.88	112	5.2	167	23	-50	HCMT
(105)	870815	9:34	-23.23	-68.61	115	5.1	319	54	-142	HCMT
(106)	870819	7:52	-24.22	-66.96	165	5.3	171	28	-100	HCMT
(107)	870824	6:9	-20.17	-70.63	64	5.1	178	44	109	HCMT

Ref.: ST73 [Stauder, 1973], MM83 [Malgrange and Madariaga, 1983], KK85 [Kadinsky, 1985], AS93 [Araujo and Suárez, 1993], HCMT [Harvard Centroid Moment Tensor].

**Table 3** Locally recorded microearthquakes used as calibration events

Date	T0 hr:mn	Lat °	Lon °	Depth km	mb	Δmin km	rms s
901120	16:28	-22.67	-70.13	75	5.1	22	0.11
910116	22:56	-23.04	-69.83	77	5.0	16	0.12
920228	09:14	-24.66	-70.20	86	5.7	57	0.09
920821	00:03	-23.06	-69.49	78	5.0	26	0.13
921128	17:20	-23.70	-70.55	36	5.0	26	0.17

Date: Year, Month, Day; T0: Origin time; Δmin: Distance between the nearest station and the hypocenter

**Table 4** Events occurring beneath the seismogenic interplate contact between 80 and 160 km distances from the trench

Compressional Events				Tensional Events			
Id	Lat °	D km	Depth km	Id	Lat °	D km	Depth km
m1	-20.19	159	35	m4	-21.67	81	39
m2	-22.62	87	29	m5	-22.27	85	42
m3	-22.01	124	41	m11	-21.18	158	45
m6	-20.92	153	41	1	-25.74	133	43
m12	-24.39	153	38	18	-23.89	153	37
5	-25.52	129	27	3	-24.71	113	70
7	-25.15	148	61	66	-24.34	106	61
16	-22.78	86	22	73	-23.75	149	56
21	-25.97	90	32	94	-24.10	149	49
42	-23.92	92	20				
45	-20.21	93	30				
46	-20.23	117	35				
61	-22.39	99	55				
77	-25.78	129	47				
82	-20.62	101	30				
93	-24.49	91	51				
96	-20.56	90	30				
99	-20.13	96	36				
107	-20.17	93	64				

Symbols as Table 2, with D: distance from the trench

**Table 5** Minimum and Maximum Distances from the Trench of the Compressional and Tensional Events

Profile	Compressional Events				Tensional Events			
	C-Min km	DC-Min km	C-Max km	DC-Max km	T-Min km	DT-Min km	T-Max km	DT-Max km
P1	83	14	159	35	196	49	449	204
P2	86	15	153	33	262	76	501	206
P3	78	14	167	39	225	58	597	247
P4	90	16	199	50	287	76	556	173

C-Min and C-Max means minimum and maximum distance from the trench of compressional events. DC-Min and DC-Max are the depth of the upper part of the slab associated with C-Min and C-Max distances from the trench. Same for T-Min, T-Max, DT-Min, and DT-Max for tensional events.

Table 6 Shape of the subducting Nazca plate

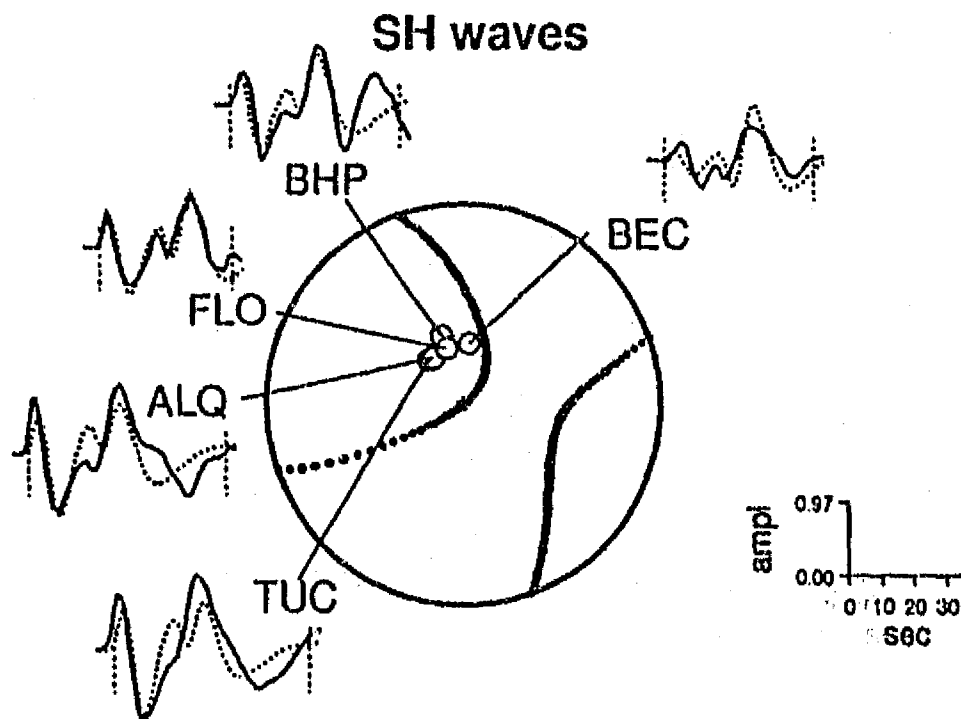
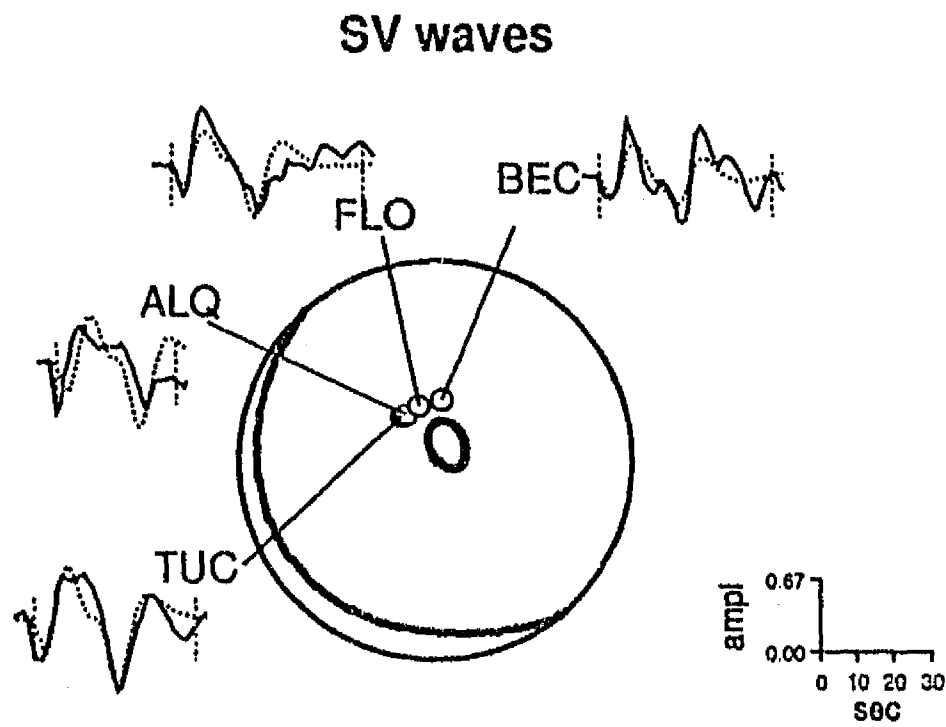
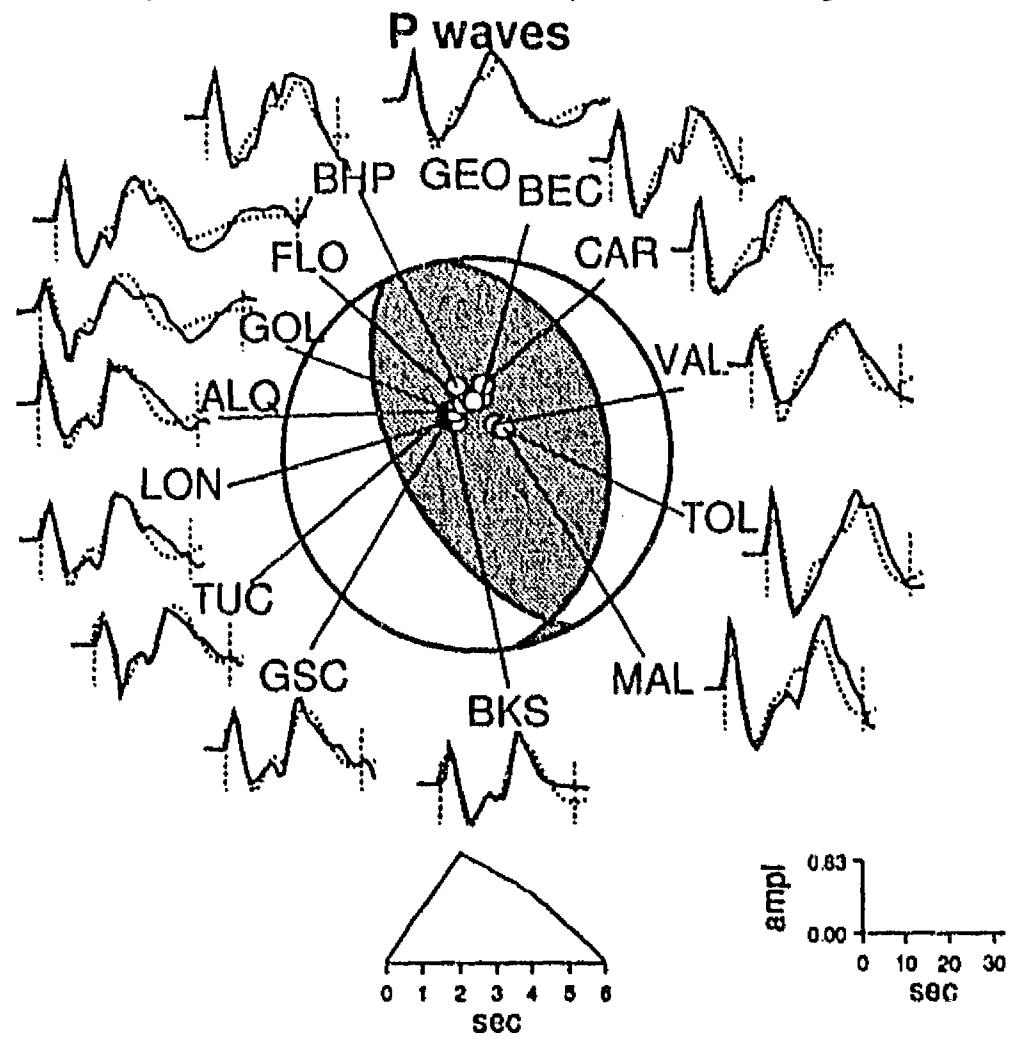
Dip	Depth km	P1 °	P2 °	P3 °	P4 °
D <sub>S</sub>	0-20	6	6	6	6
D <sub>C</sub>	20-60	17	17	17	17
D <sub>I</sub>	60-100	25	24	18	17
D <sub>V</sub>	100-150	32	26	23	17
D <sub>D</sub>	>150	44	36	36	32

Variations of the dip angles (see text for definitions) along the profiles P1 to P4.

**APPENDIX I**

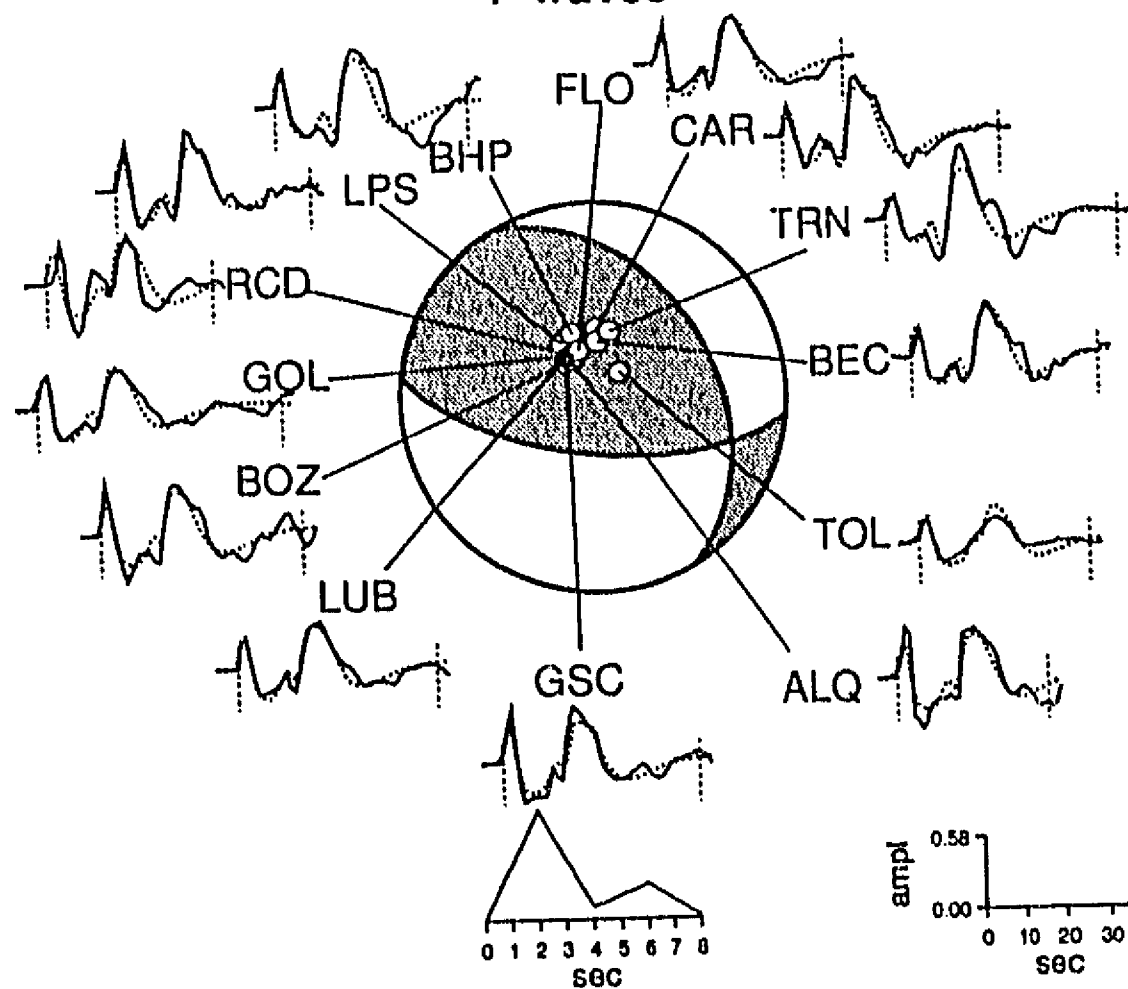
Body waveform inversion of the modeled events. Each event are identified by its label (Table 1), date, magnitude, and determined focal depth. The *P*-*SV*-, and *SH* focal mechanism in a lower hemispheric projection are presented with their observed and synthetic body waves, which are shown with continous and dashed lines, respectively. The source time function, and the amplitude versus time scale are also given.

(M1) 621229, Ms=6.8, 35 km depth

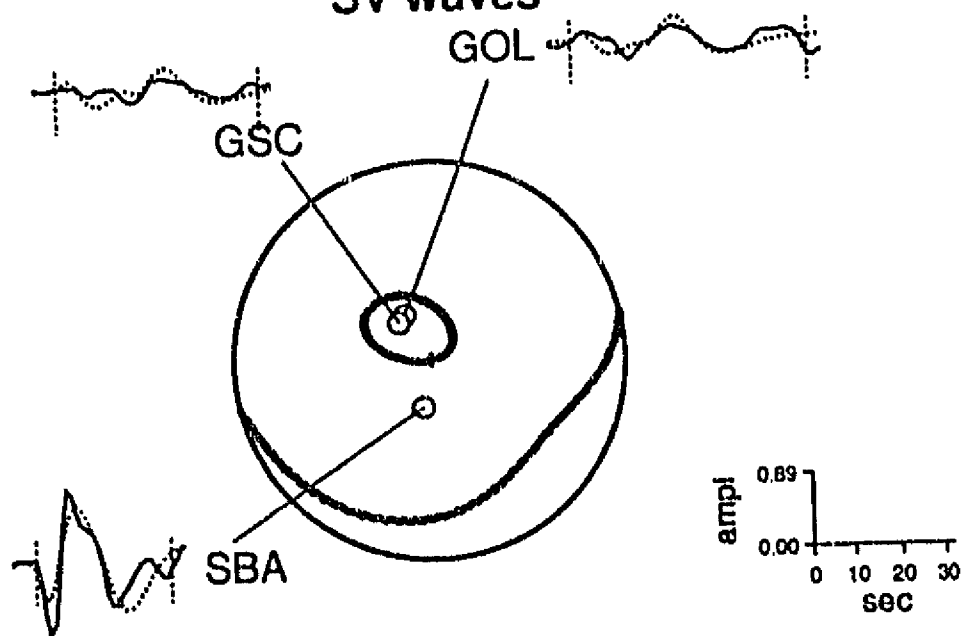


(M2) 631203, Ms=6.1, 29 km depth

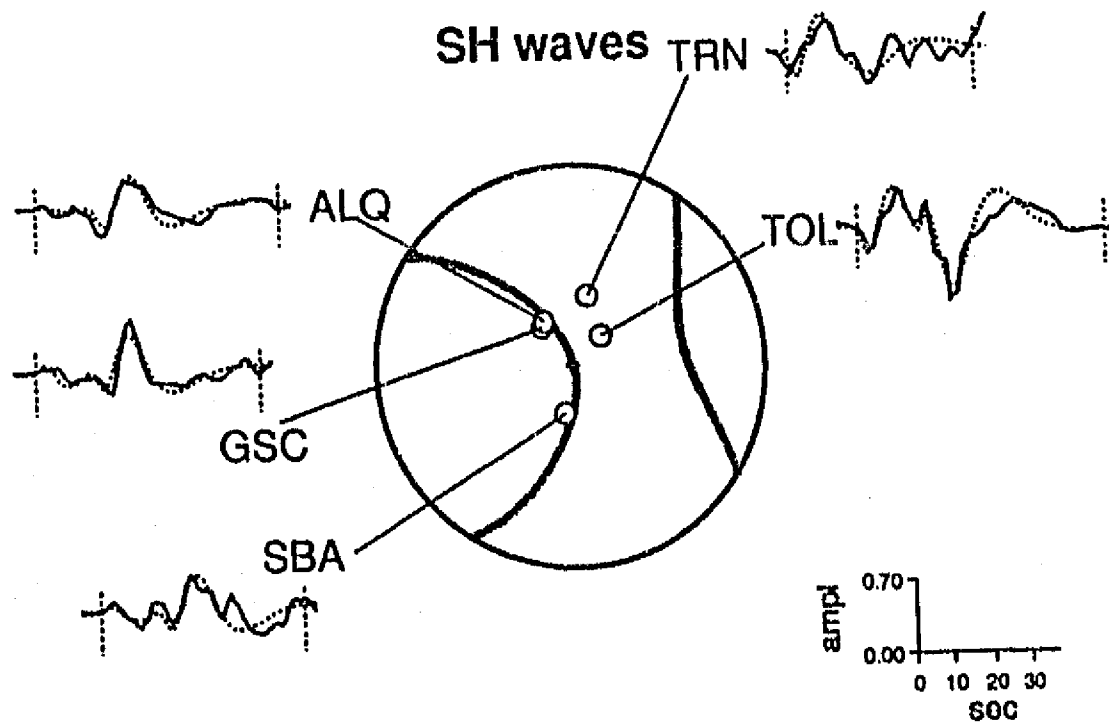
P waves



SV waves

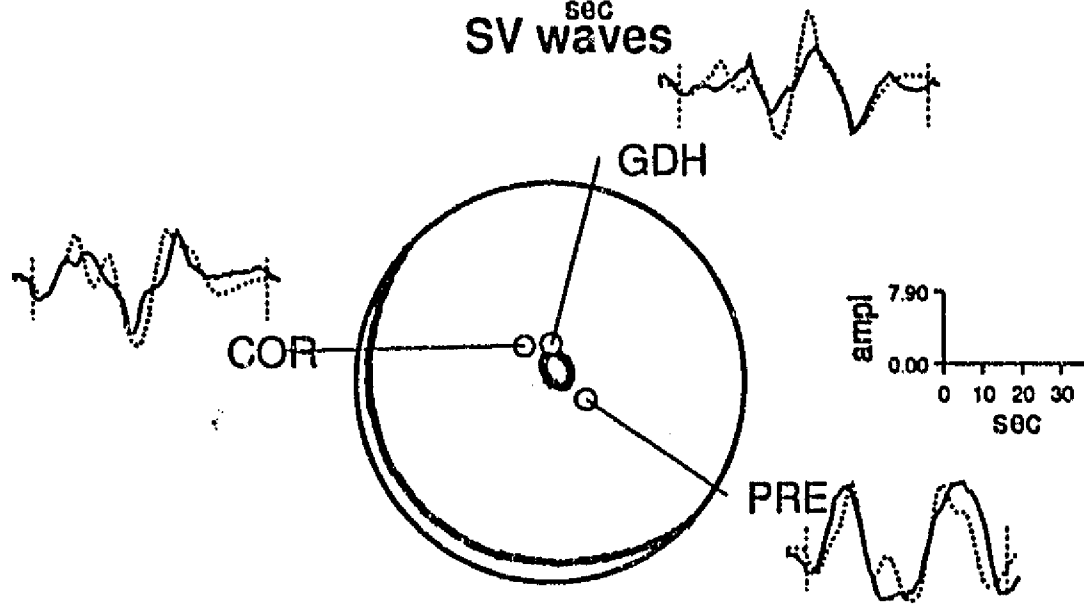
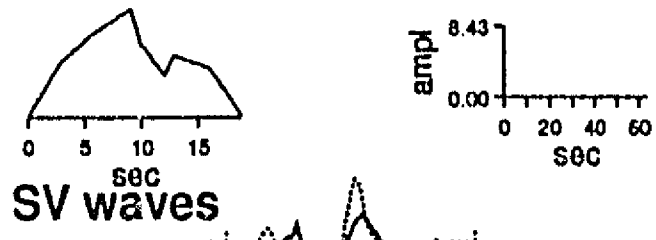
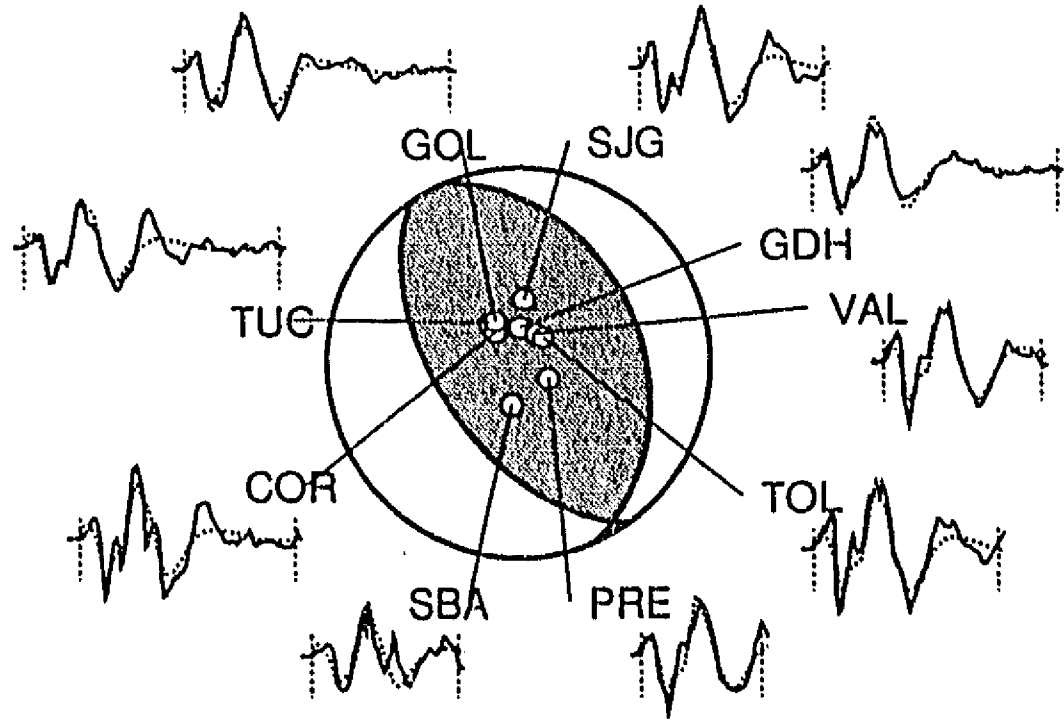


SH waves

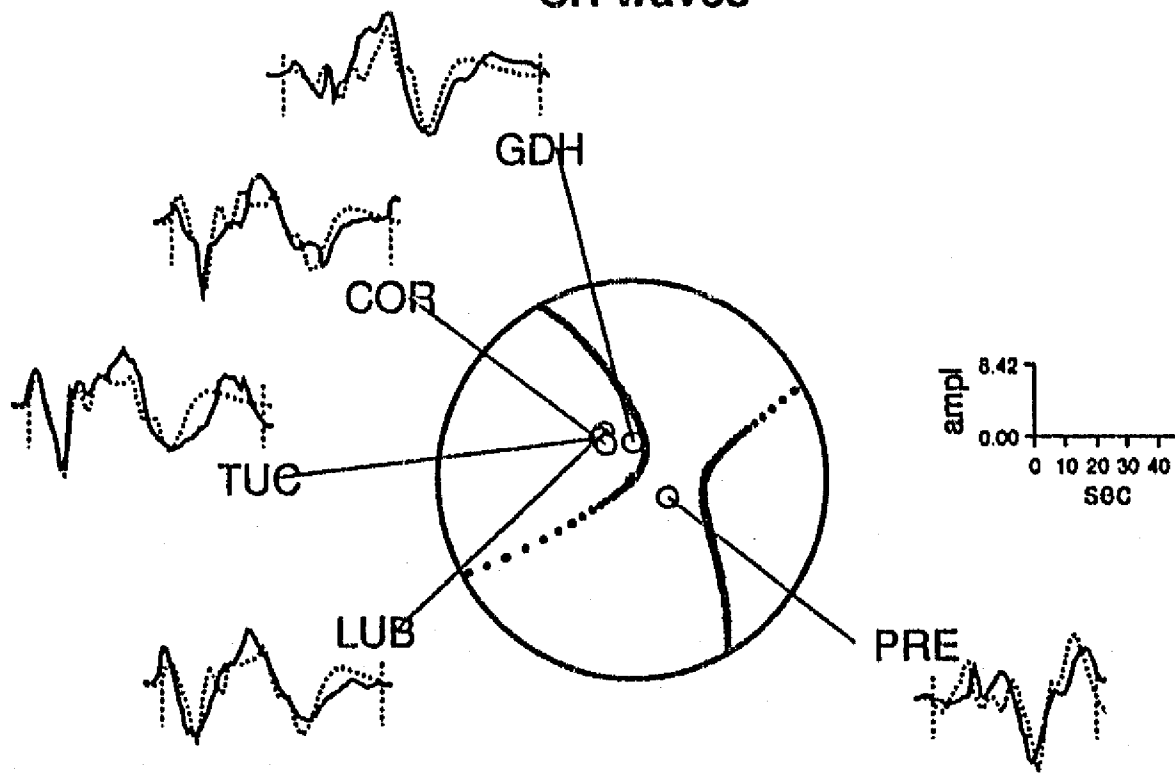


(M3) 671221, Ms=6.3, 41 km depth

P waves



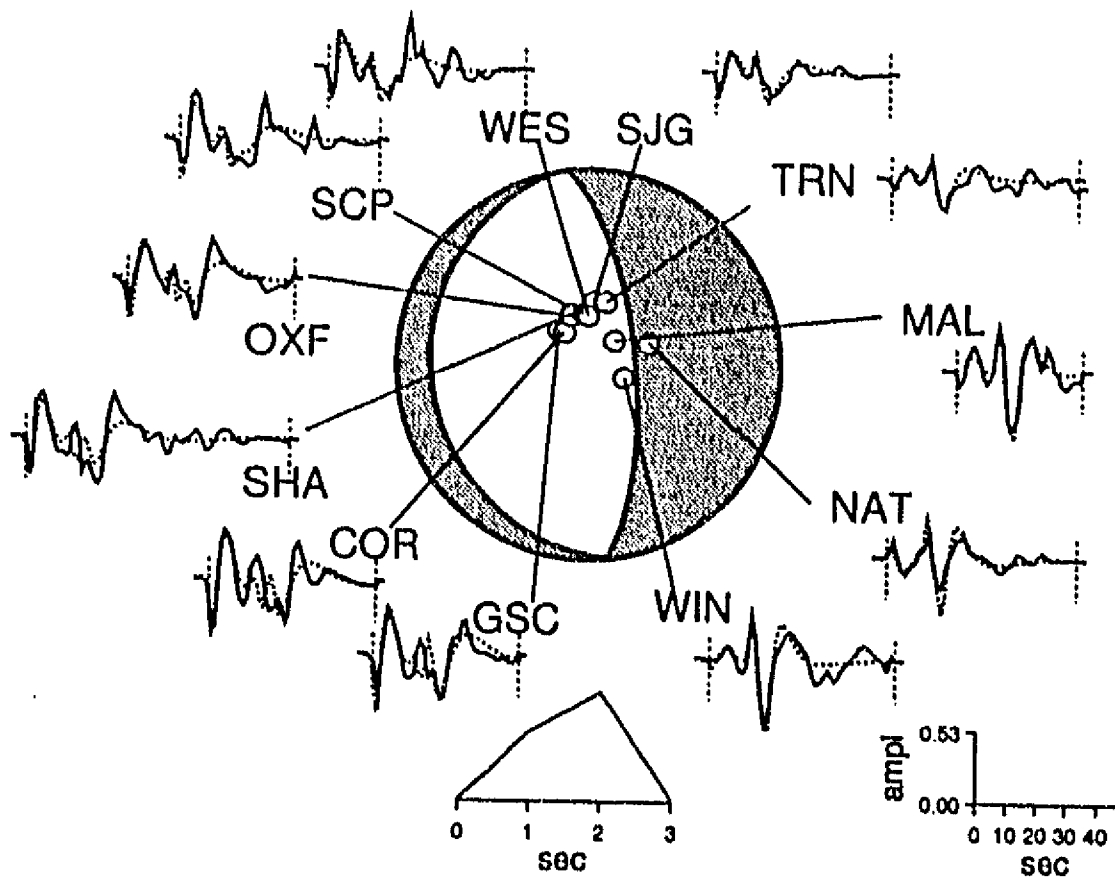
SH waves



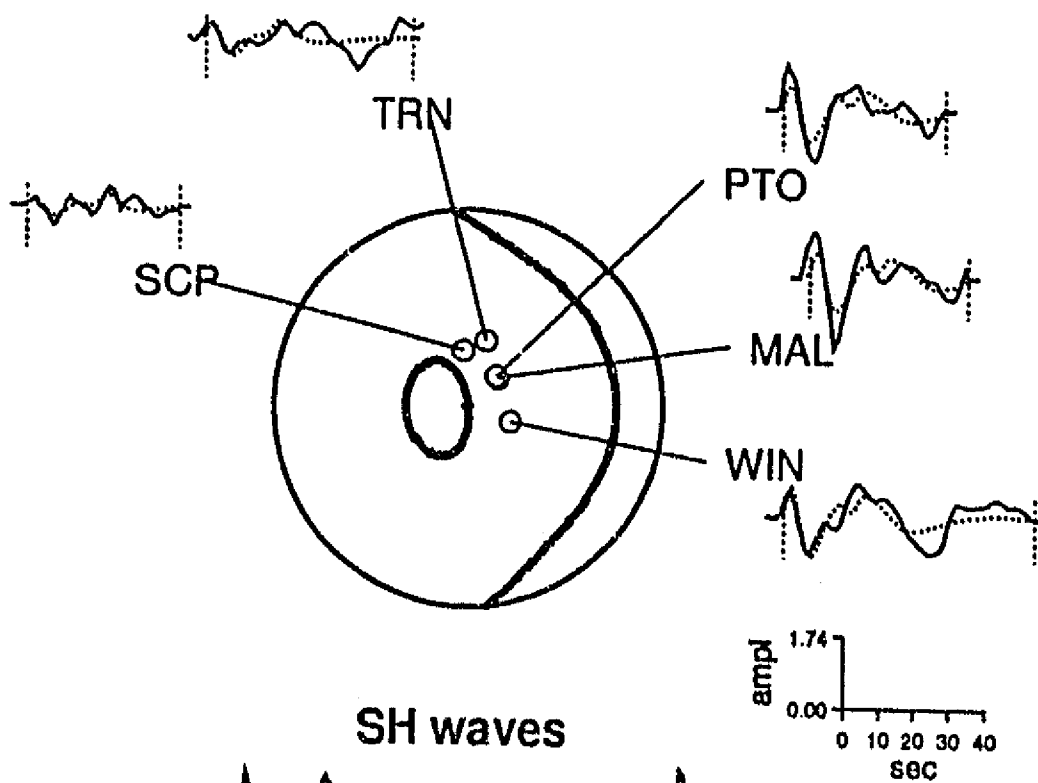


(M4) 671225, Ms=5.8, 39 km depth

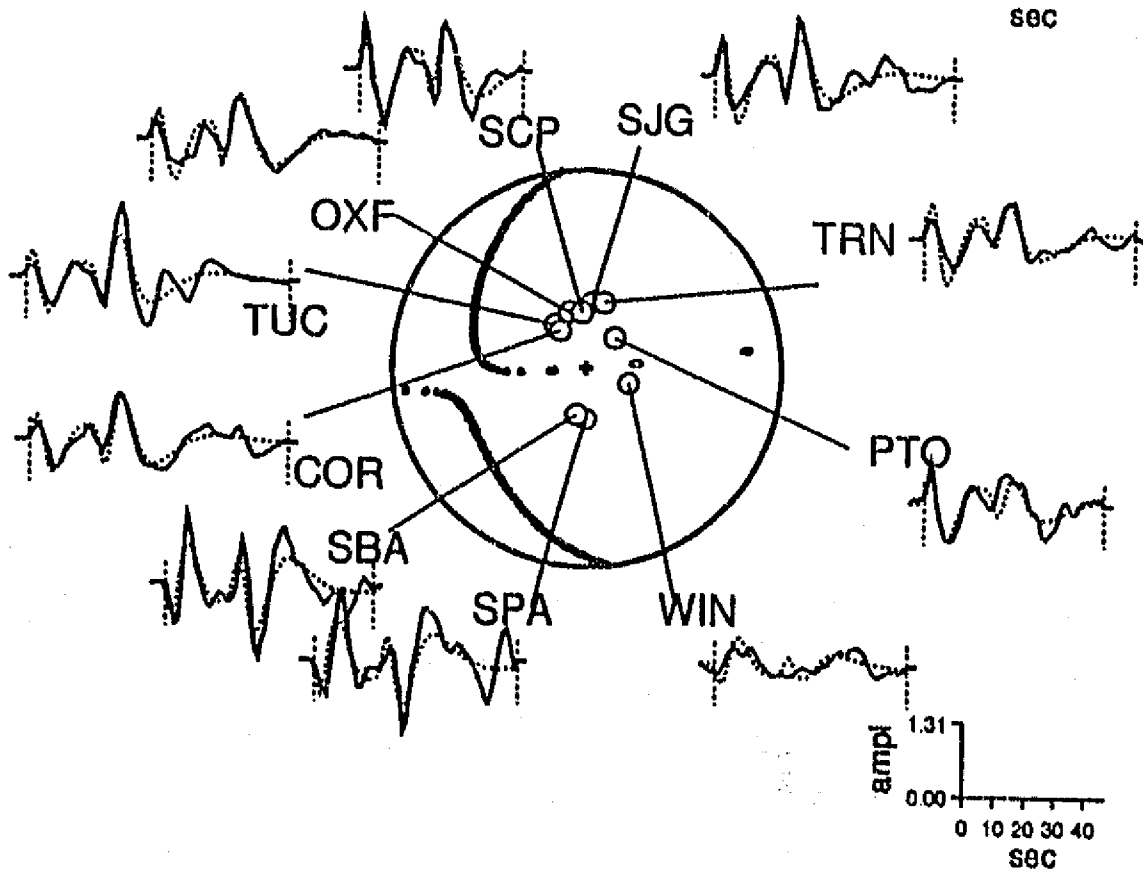
P waves



SV waves

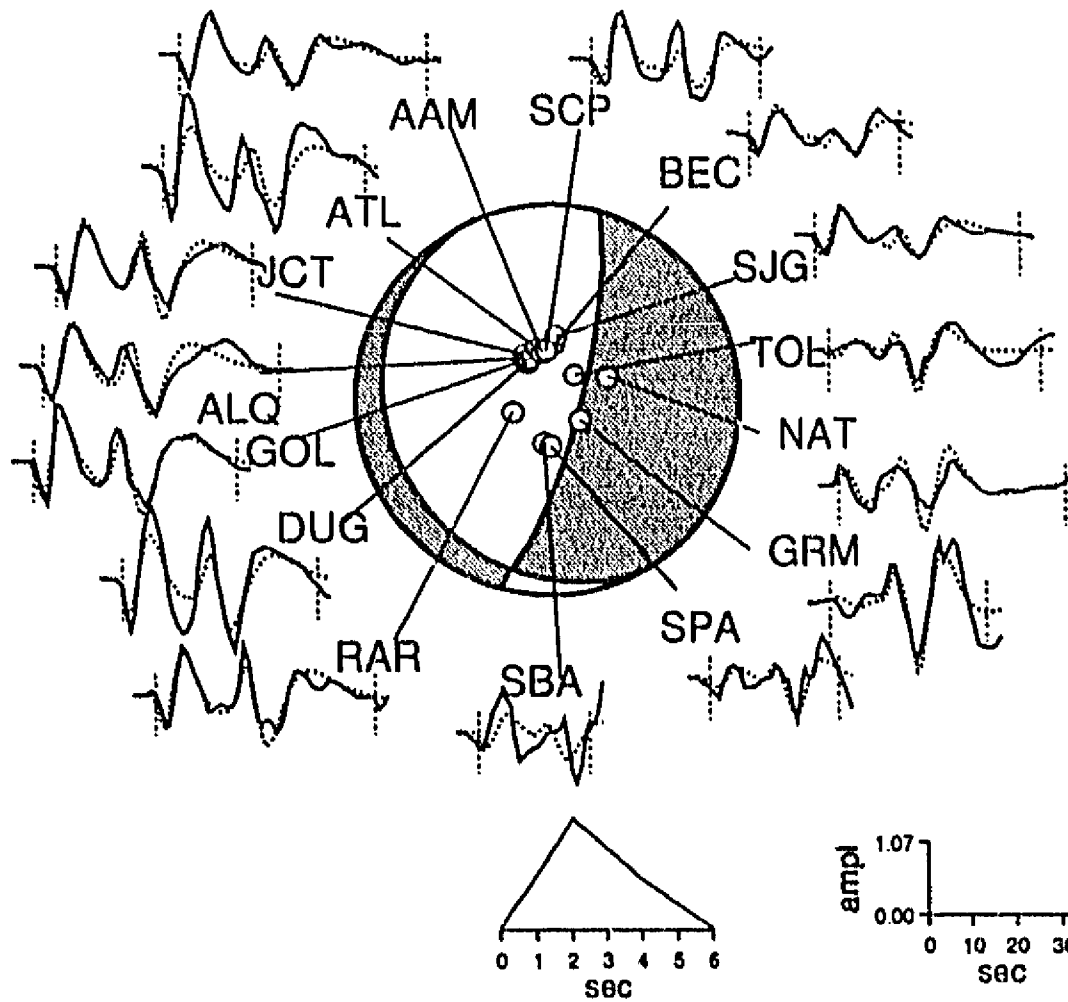


SH waves

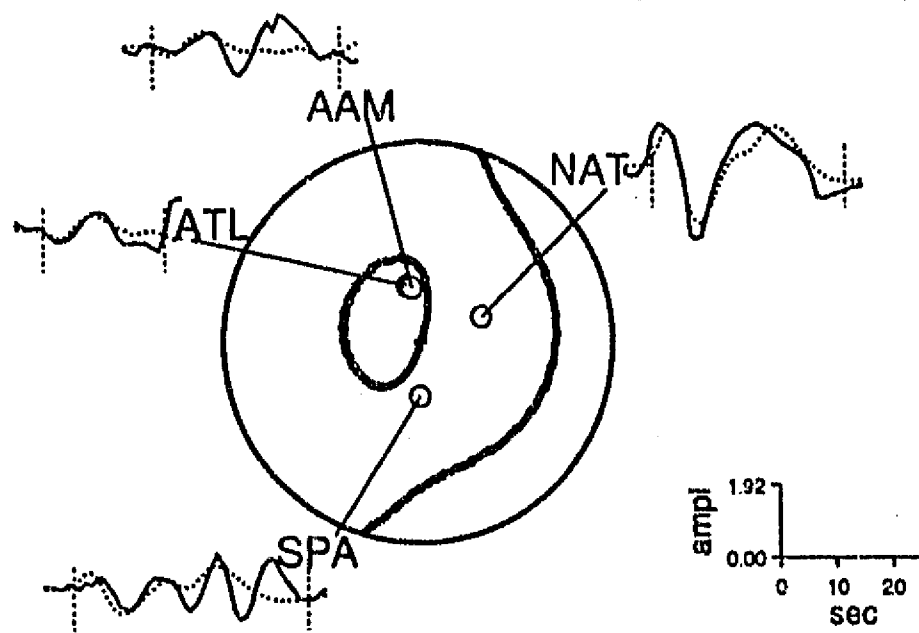


(M5) 700619, Ms=6.2, 42 km depth

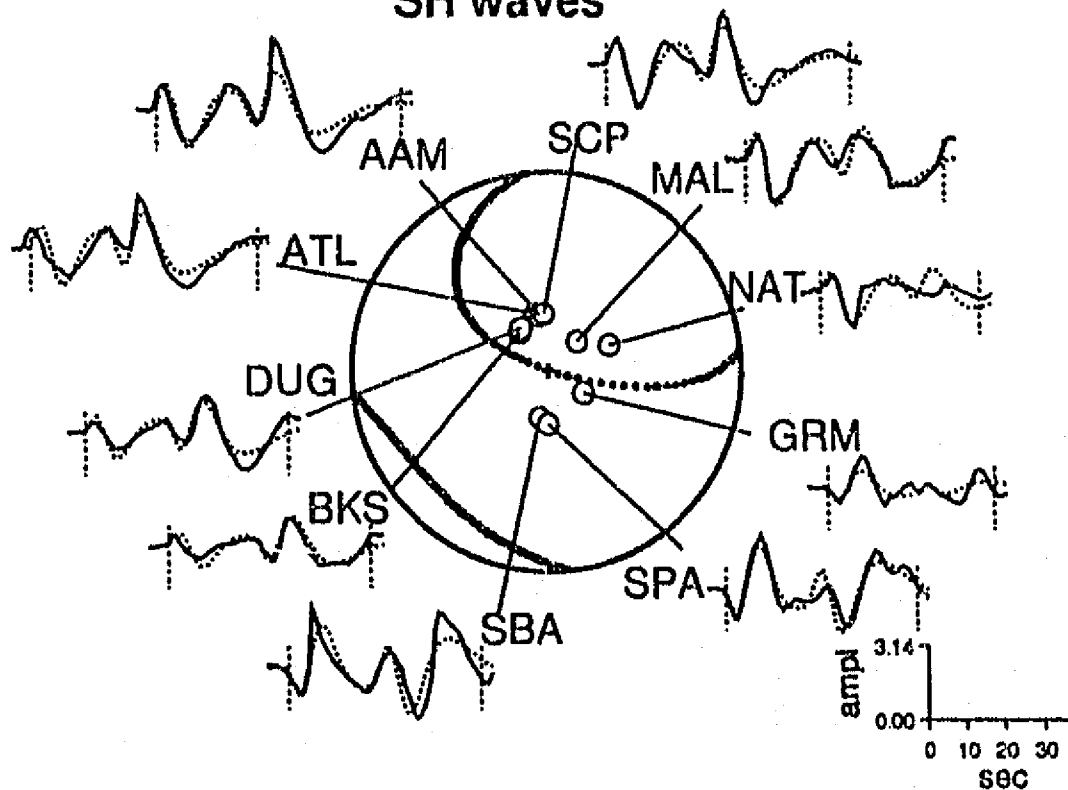
P waves



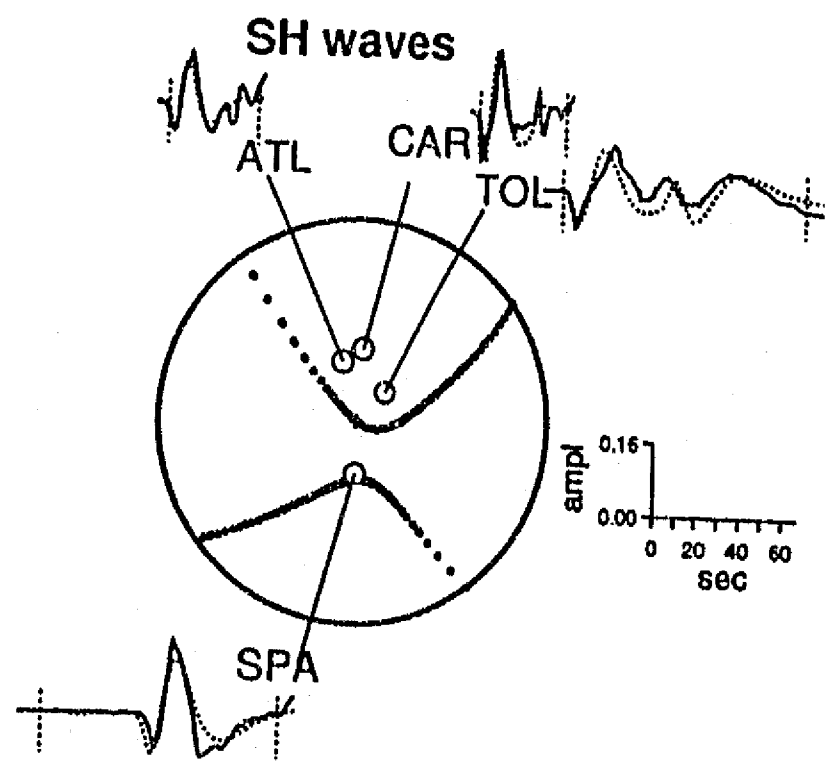
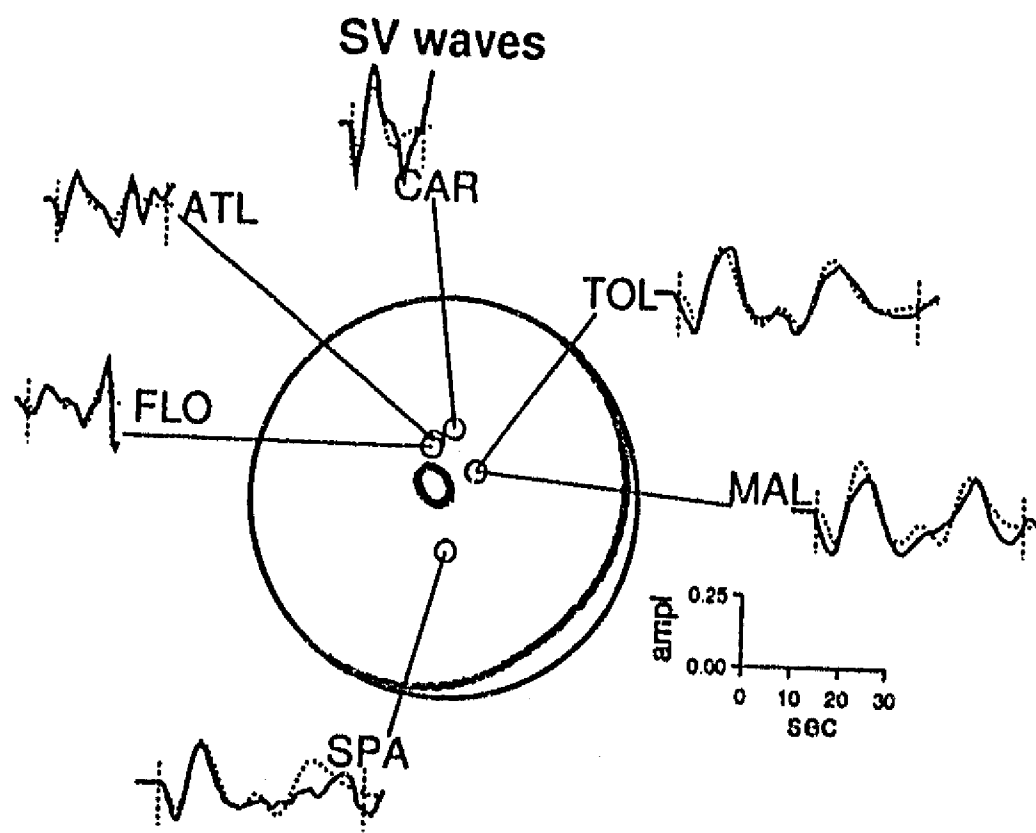
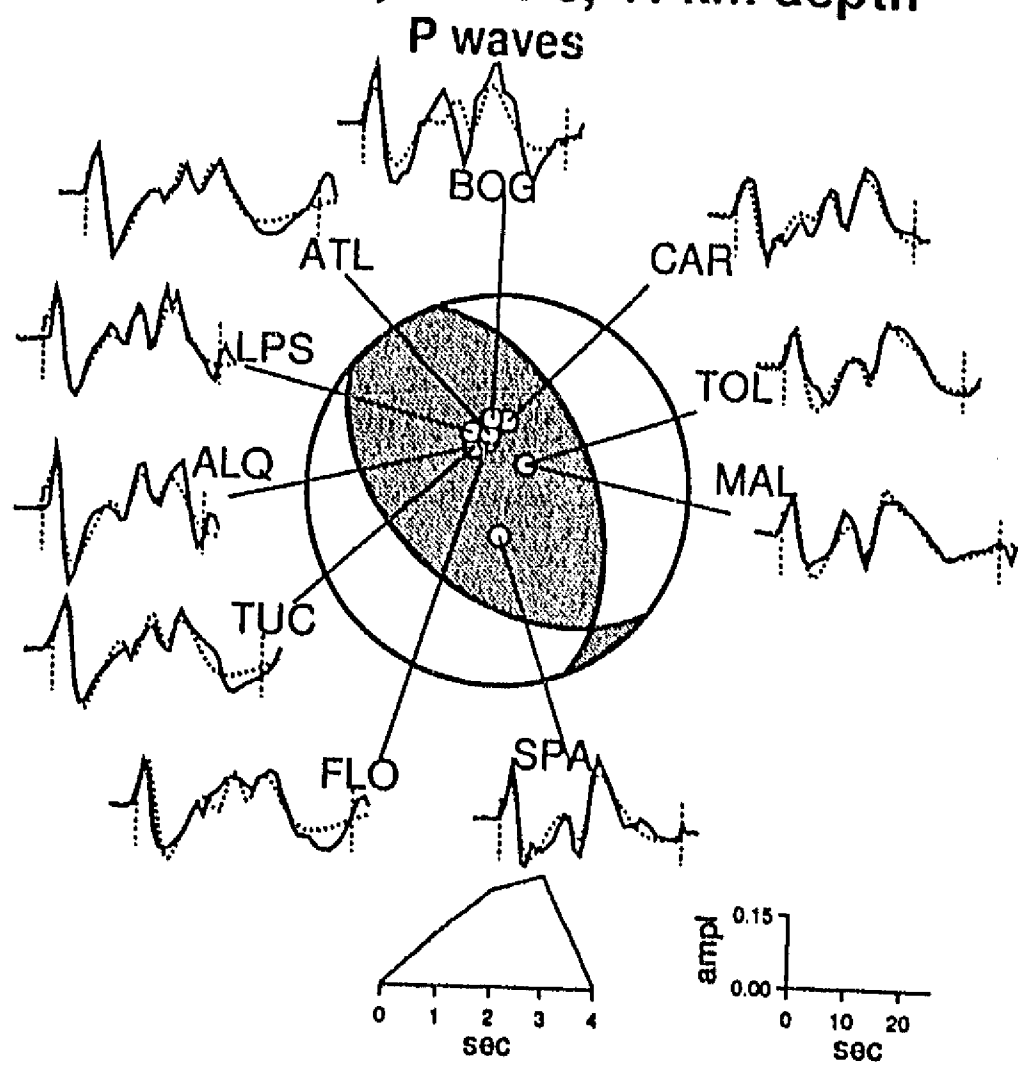
SV waves



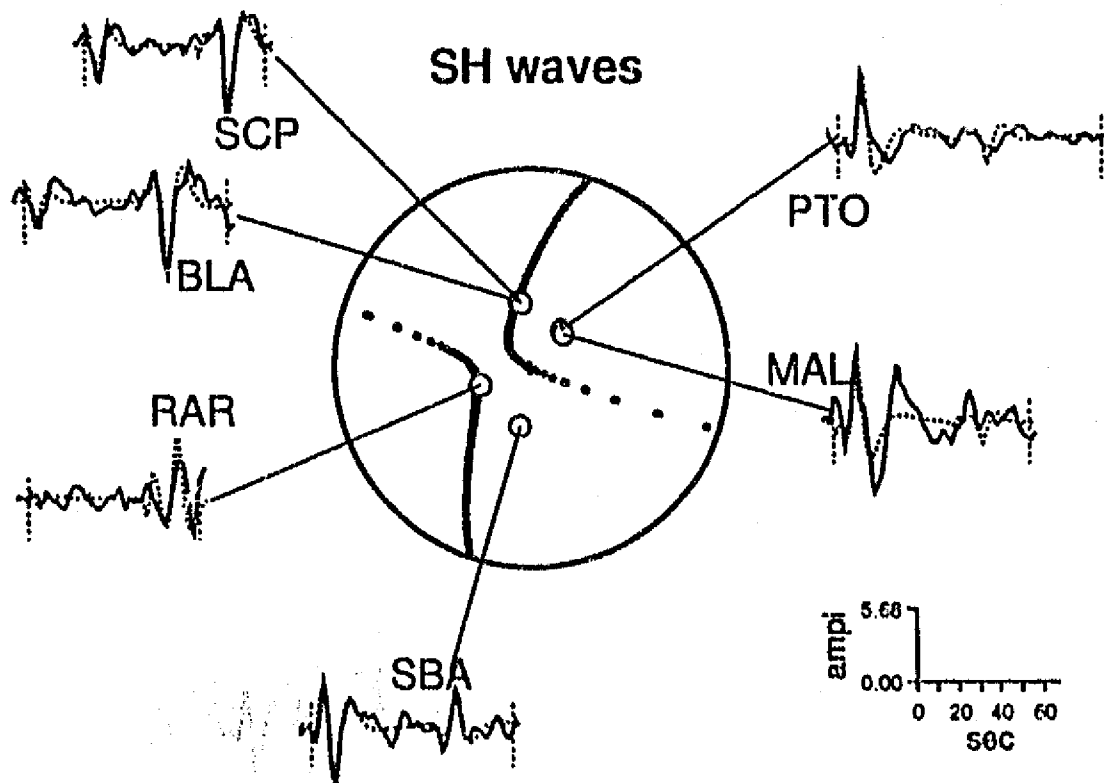
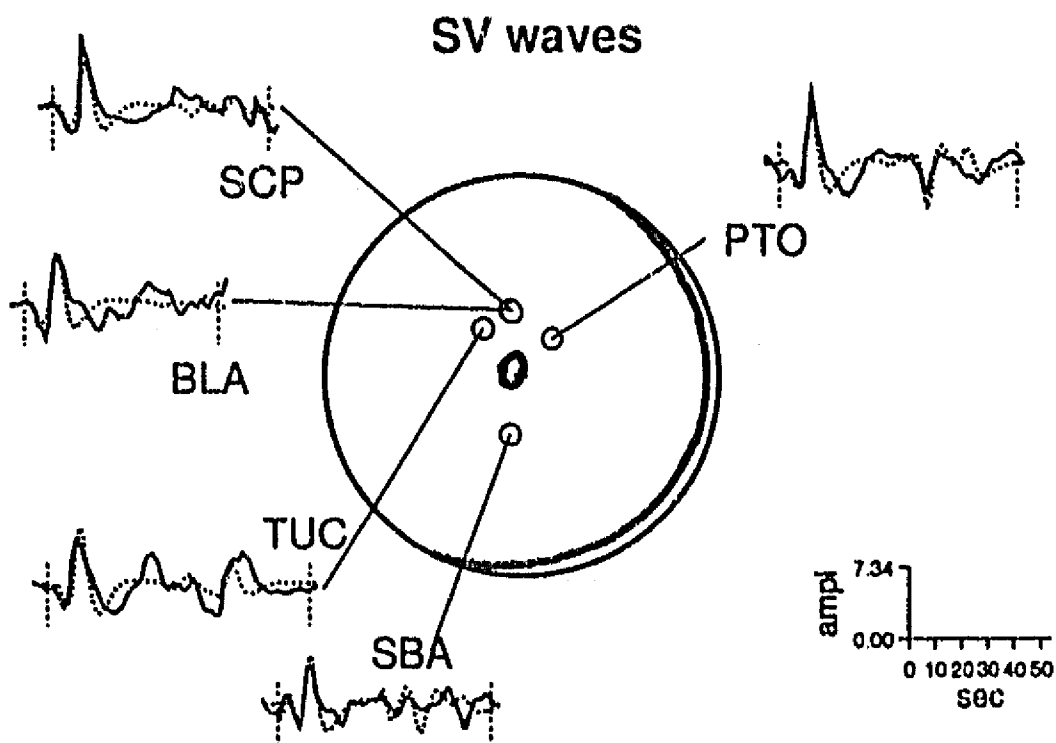
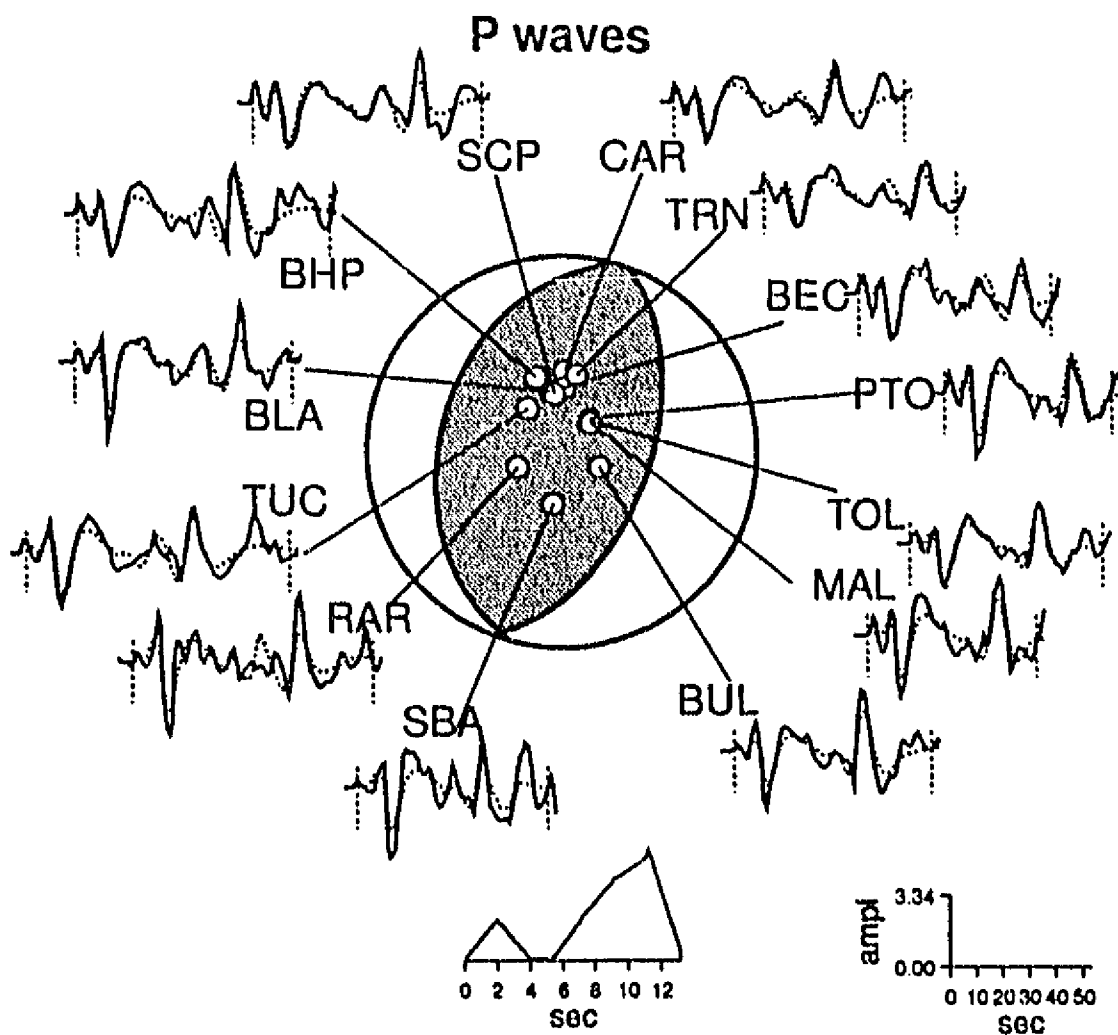
SH waves



(M6) 701128, Ms=6.0, 41 km depth

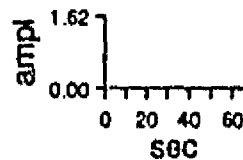
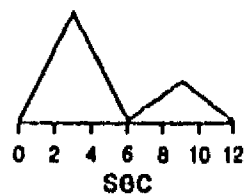
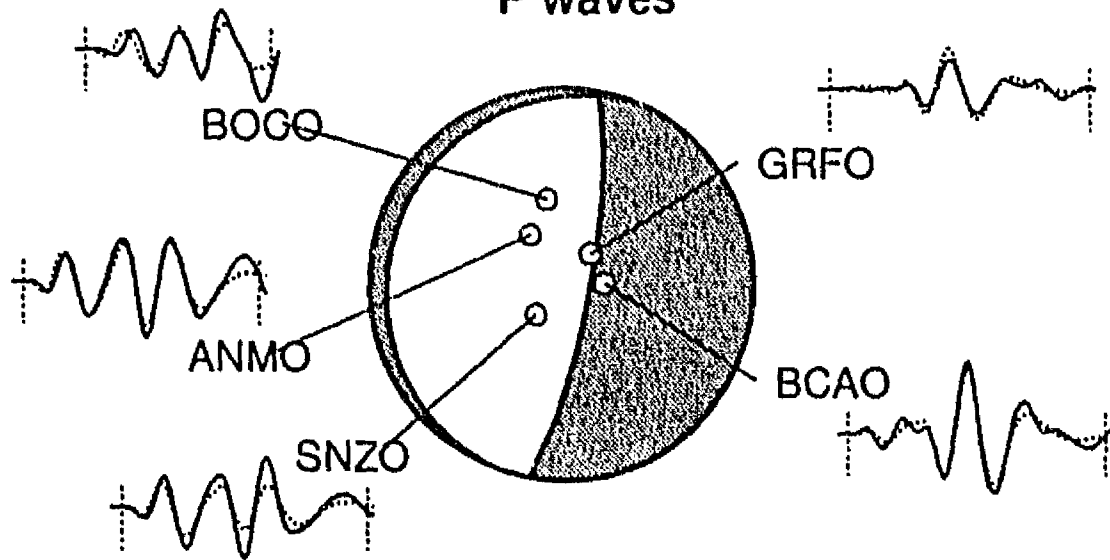


(M7) 770117, Ms=6.1, 128 km depth

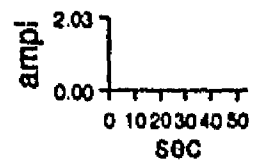
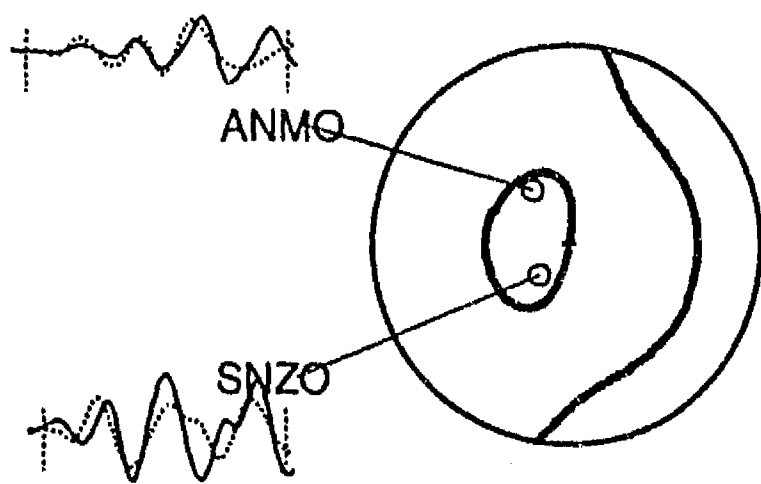


(M8) 800526, Ms=6.1, 99 km depth

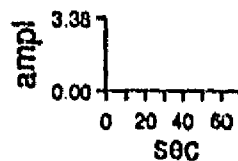
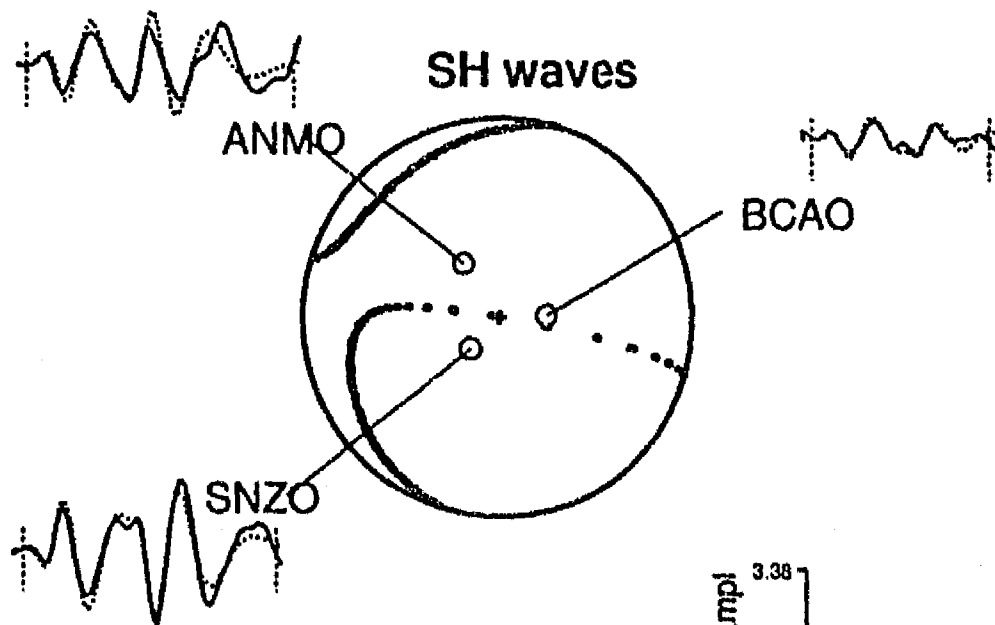
P waves



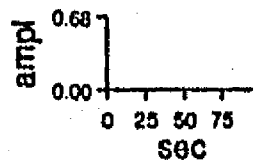
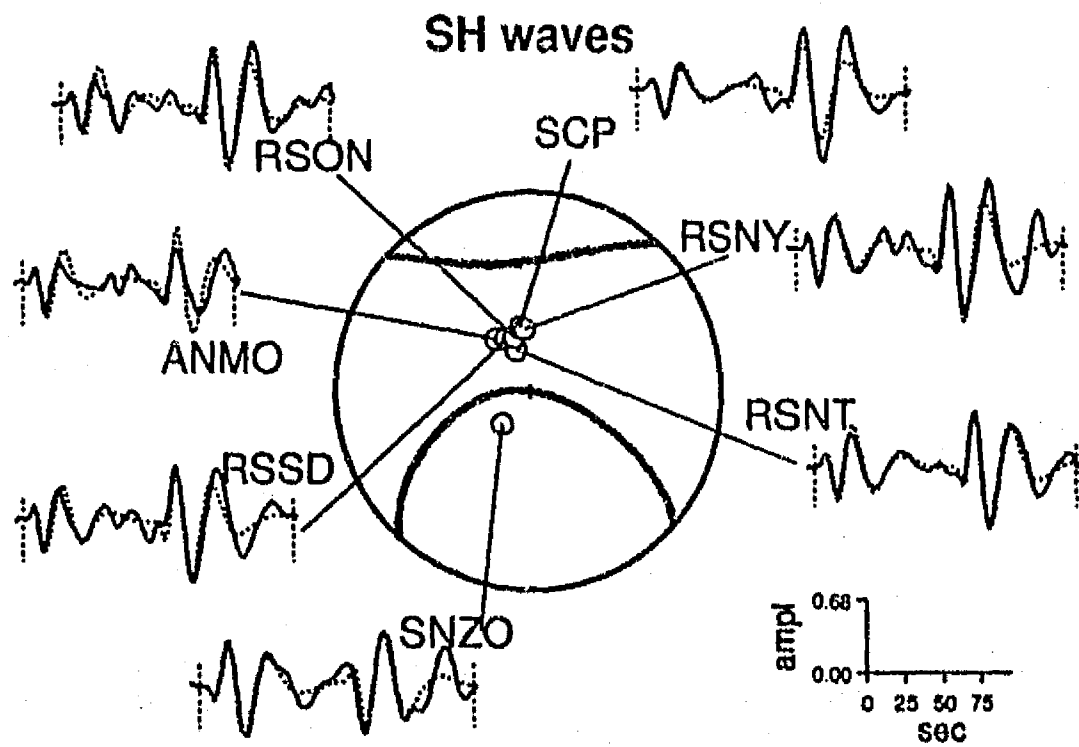
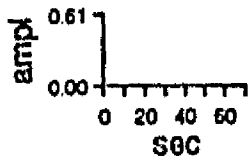
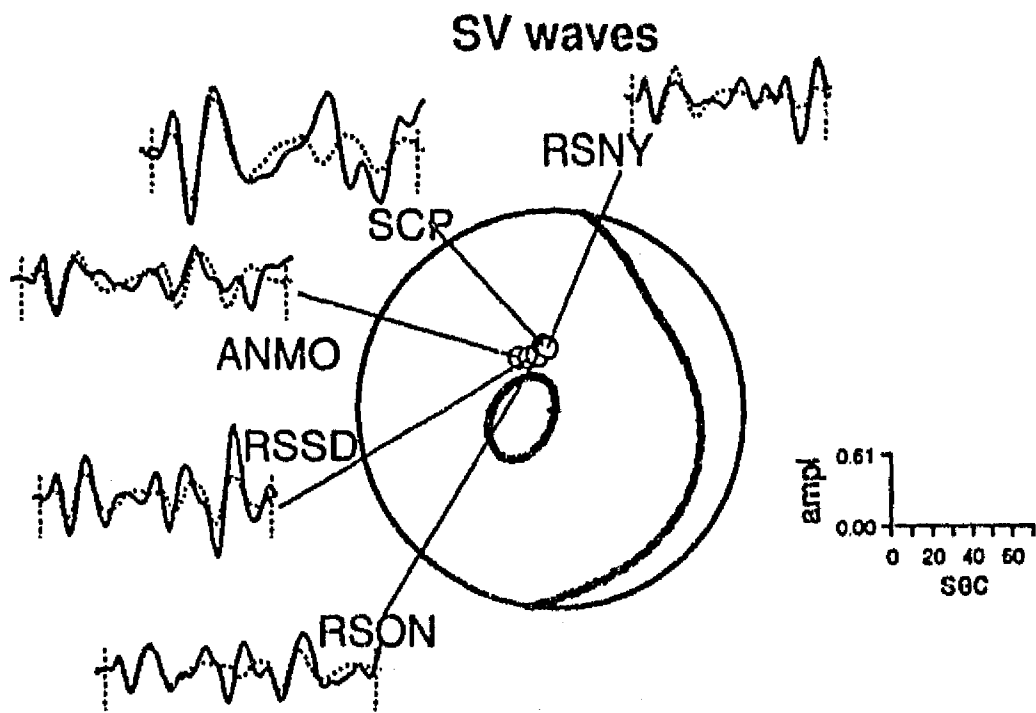
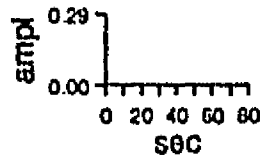
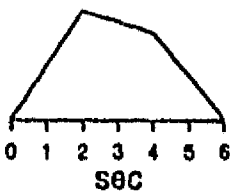
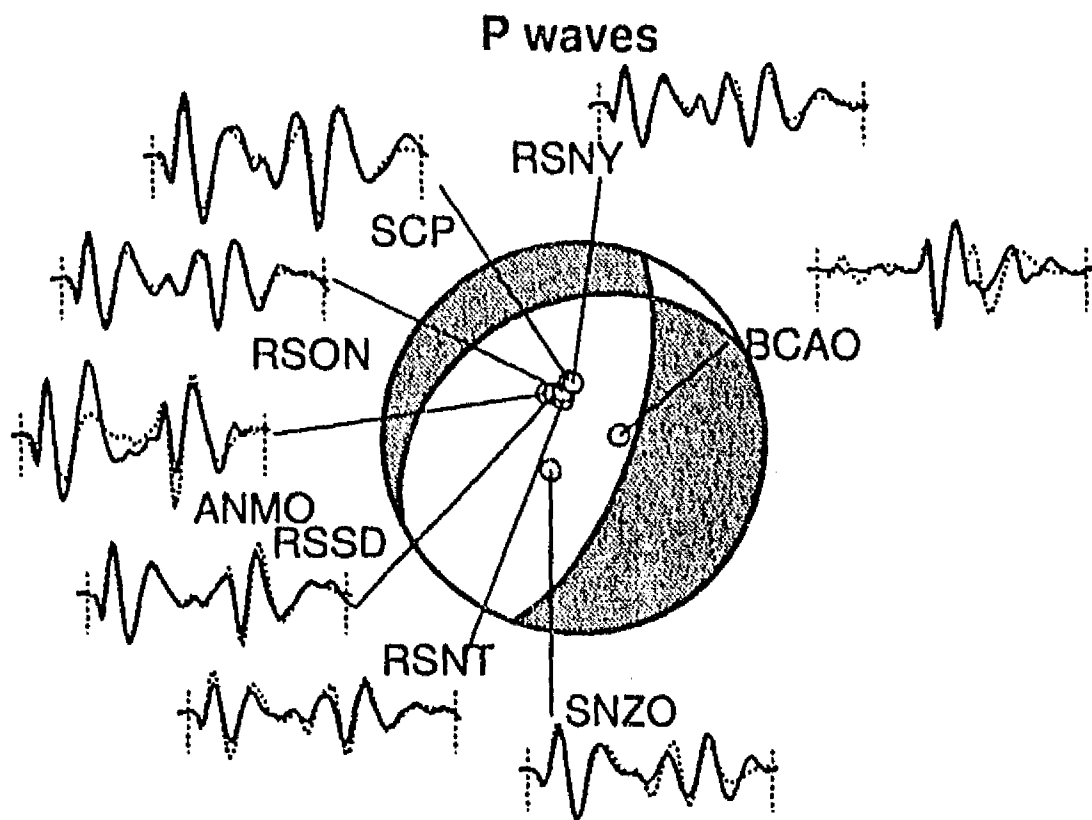
SV waves



SH waves

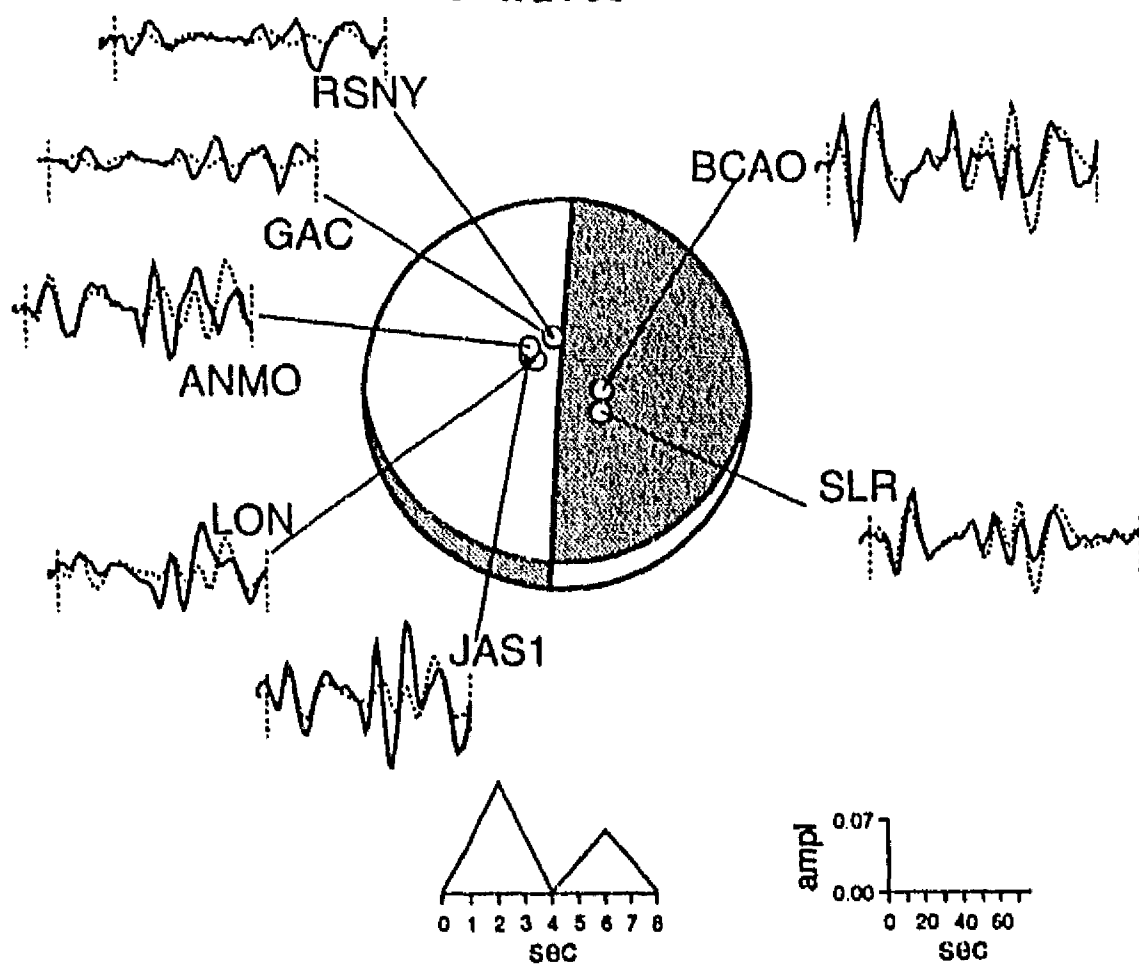


(M9) 841020, Mb=5.9, 195 km depth

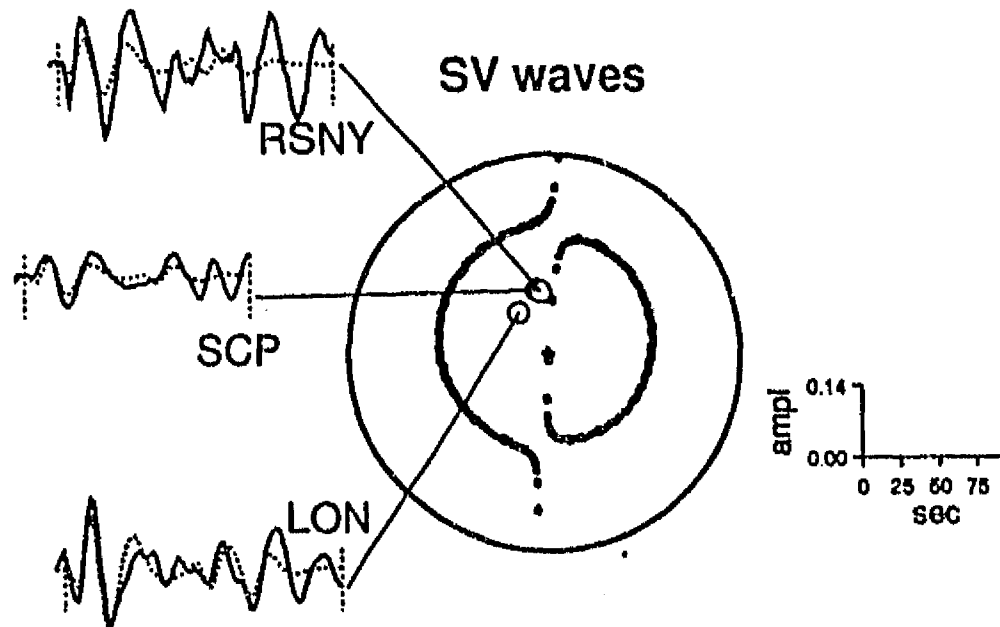


(M10) 851008, Mb=5.5, 224 km depth

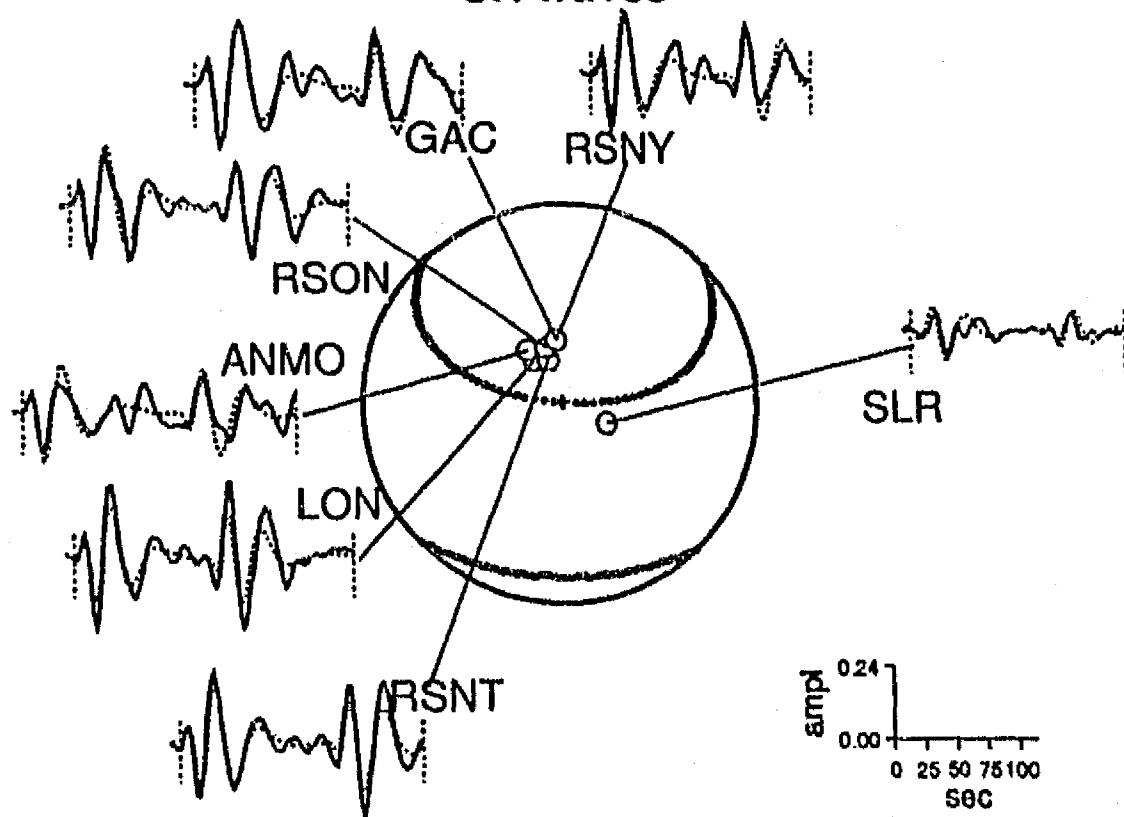
P waves



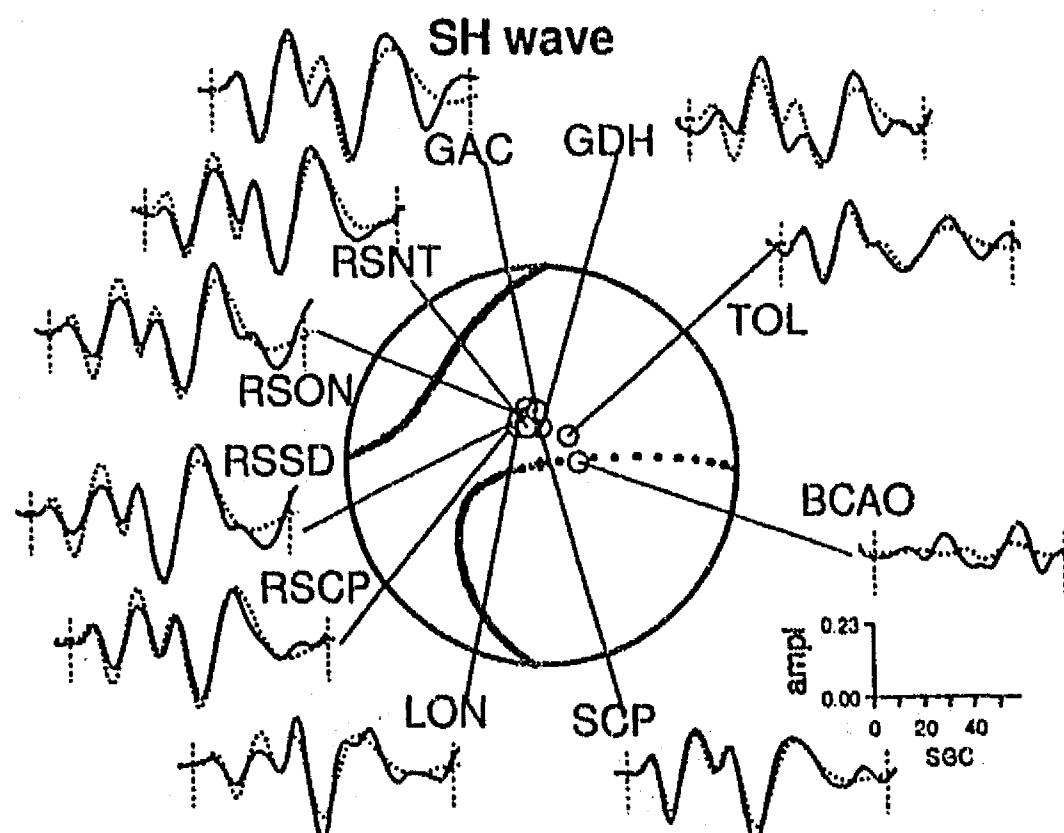
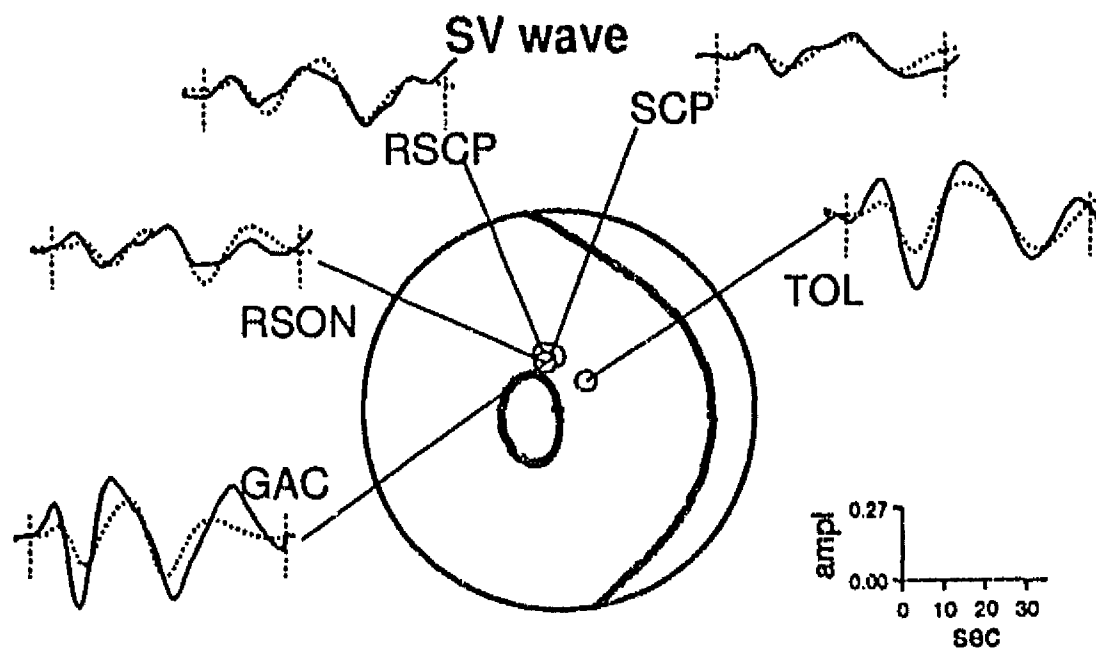
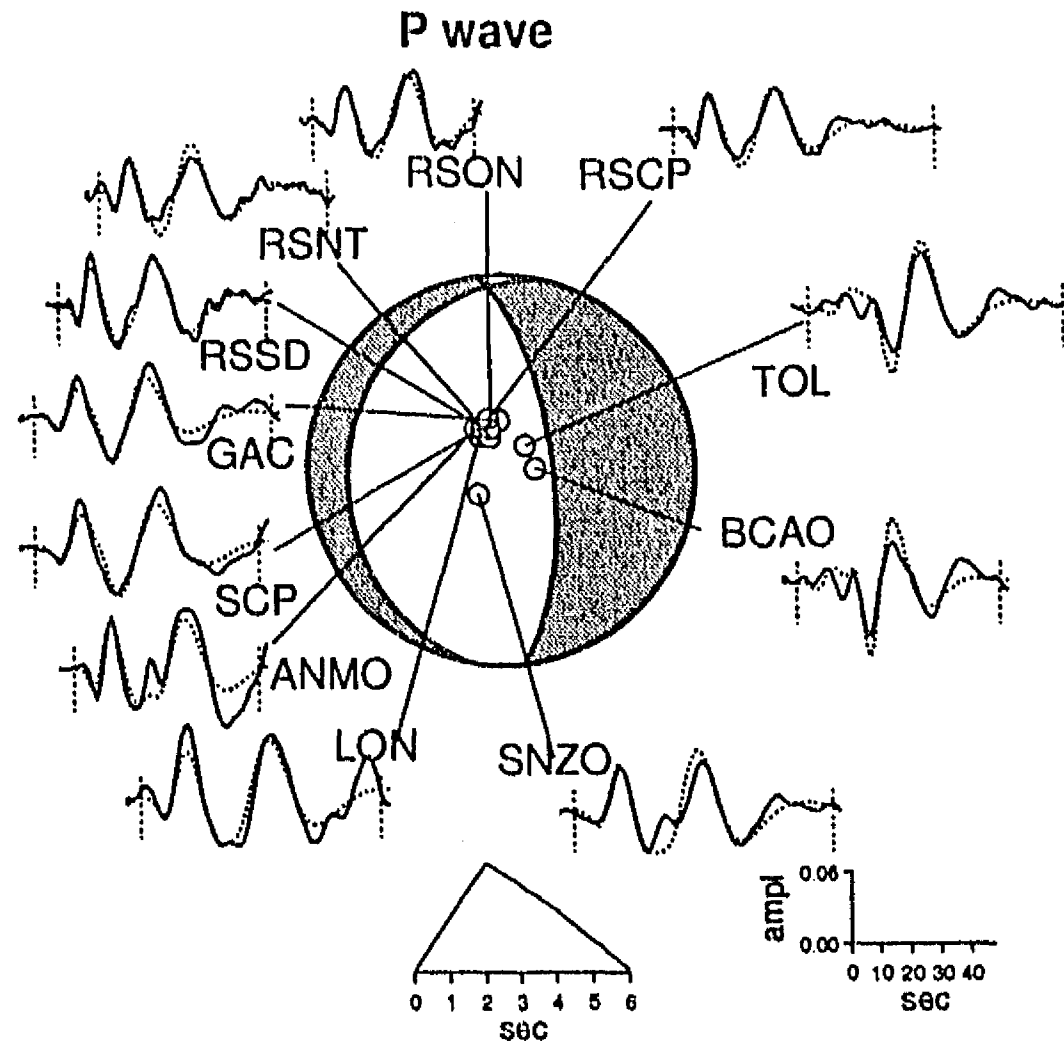
SV waves



SH waves



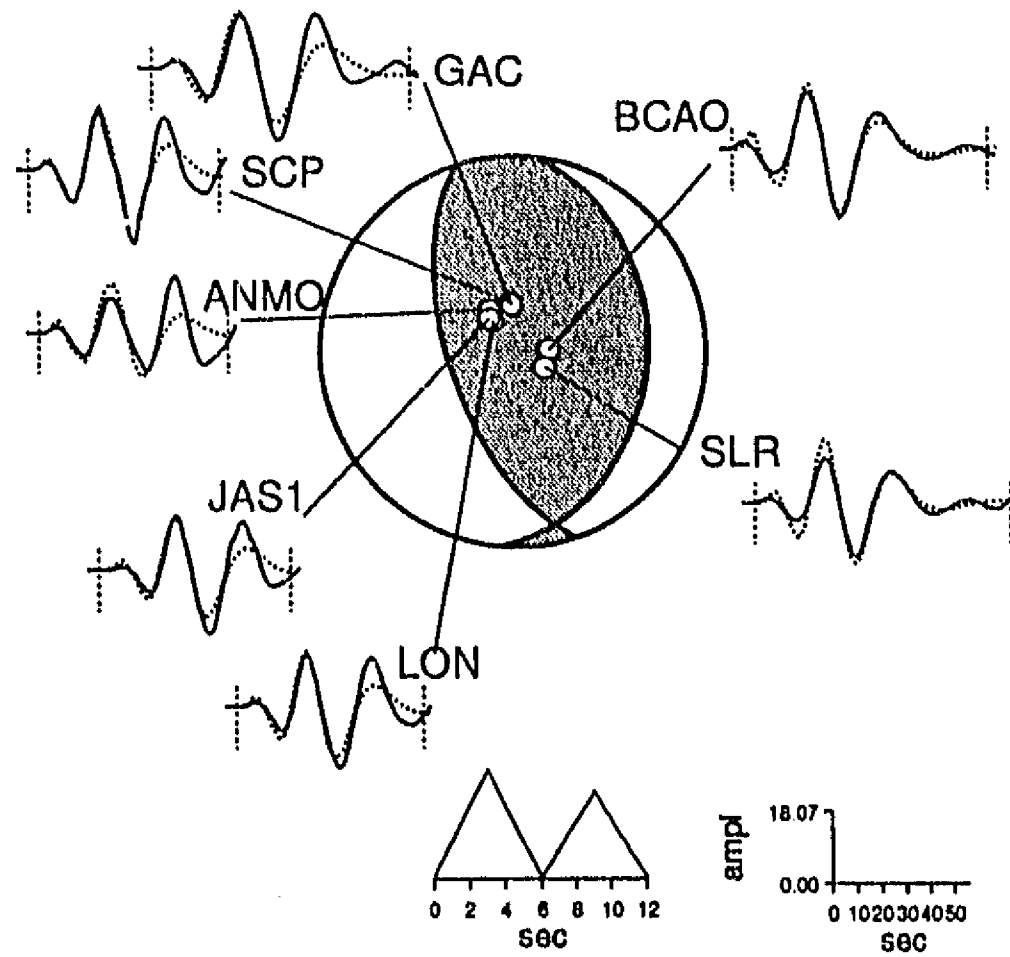
(M11) 860220, mb=5.5 , 45 km depth



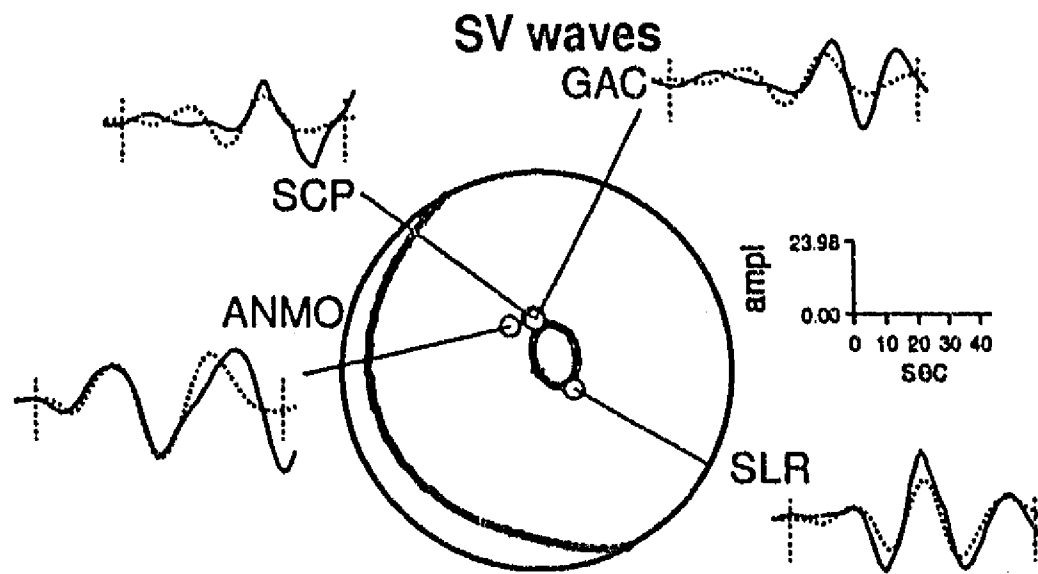


(M12) 870305, Ms=7.3, 38 km depth

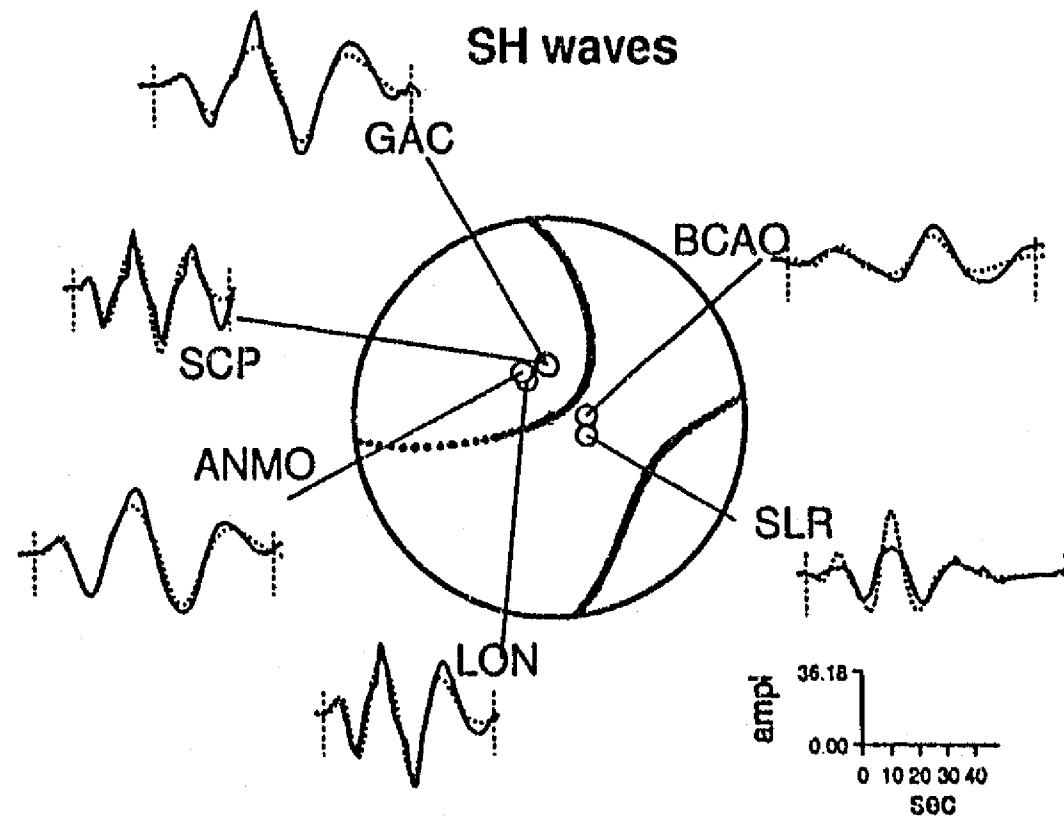
P waves



SV waves

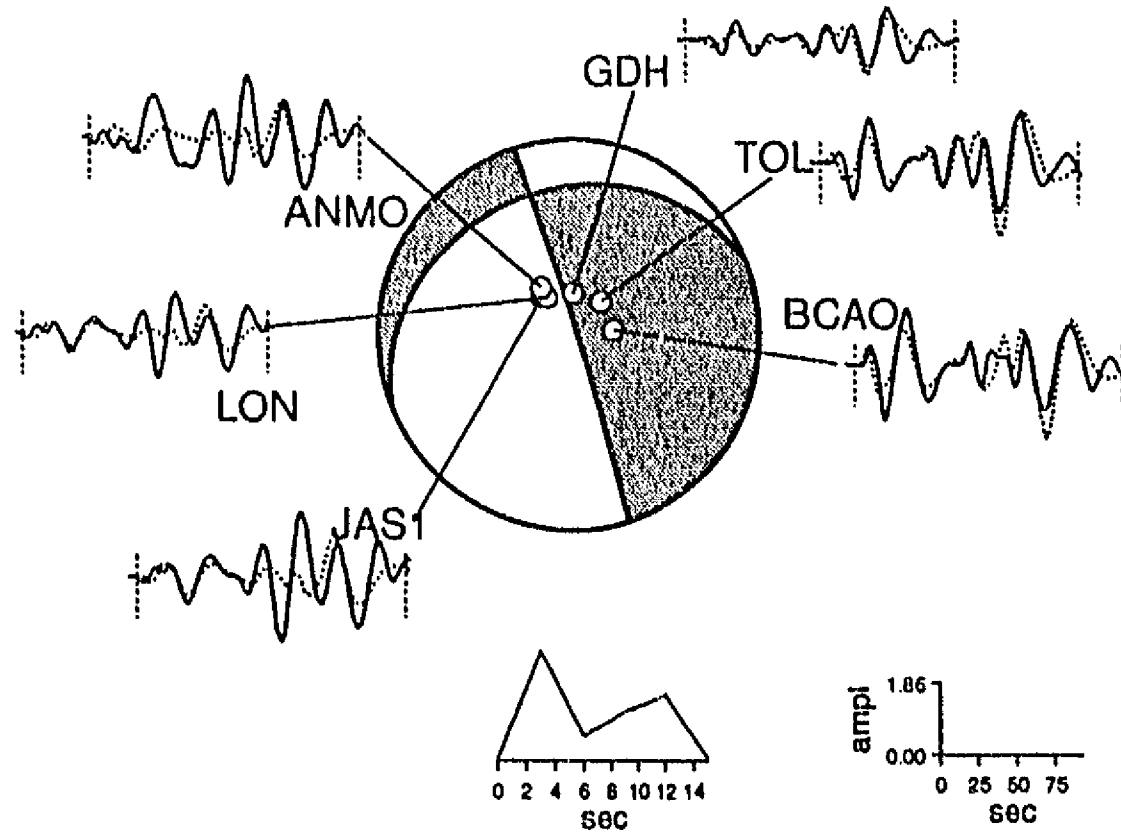


SH waves

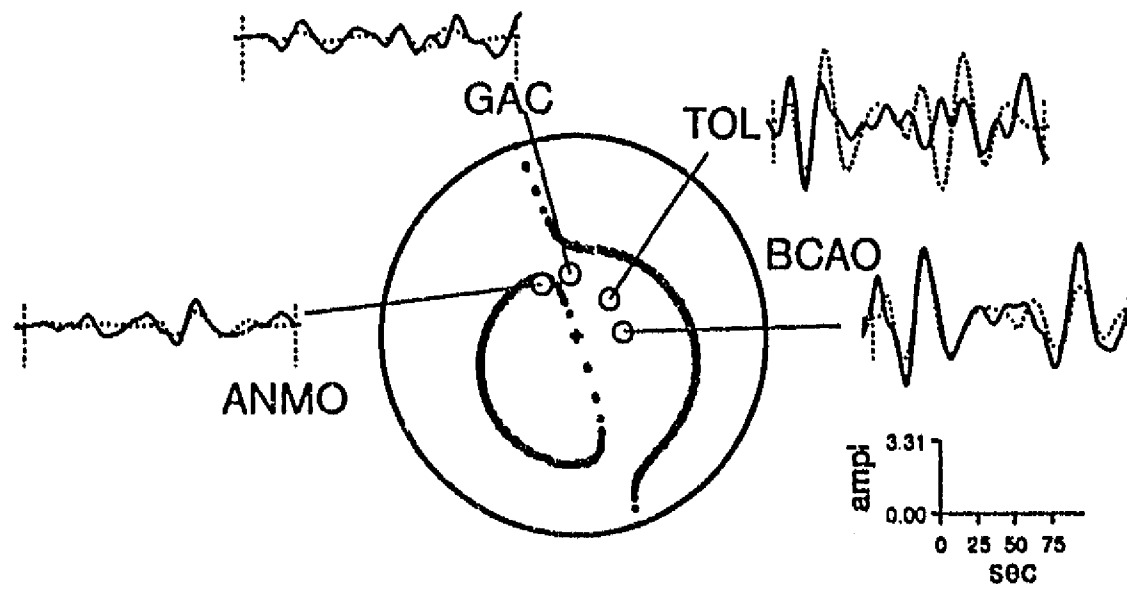


(M13) 870401, Ms=6.1, 231 km depth

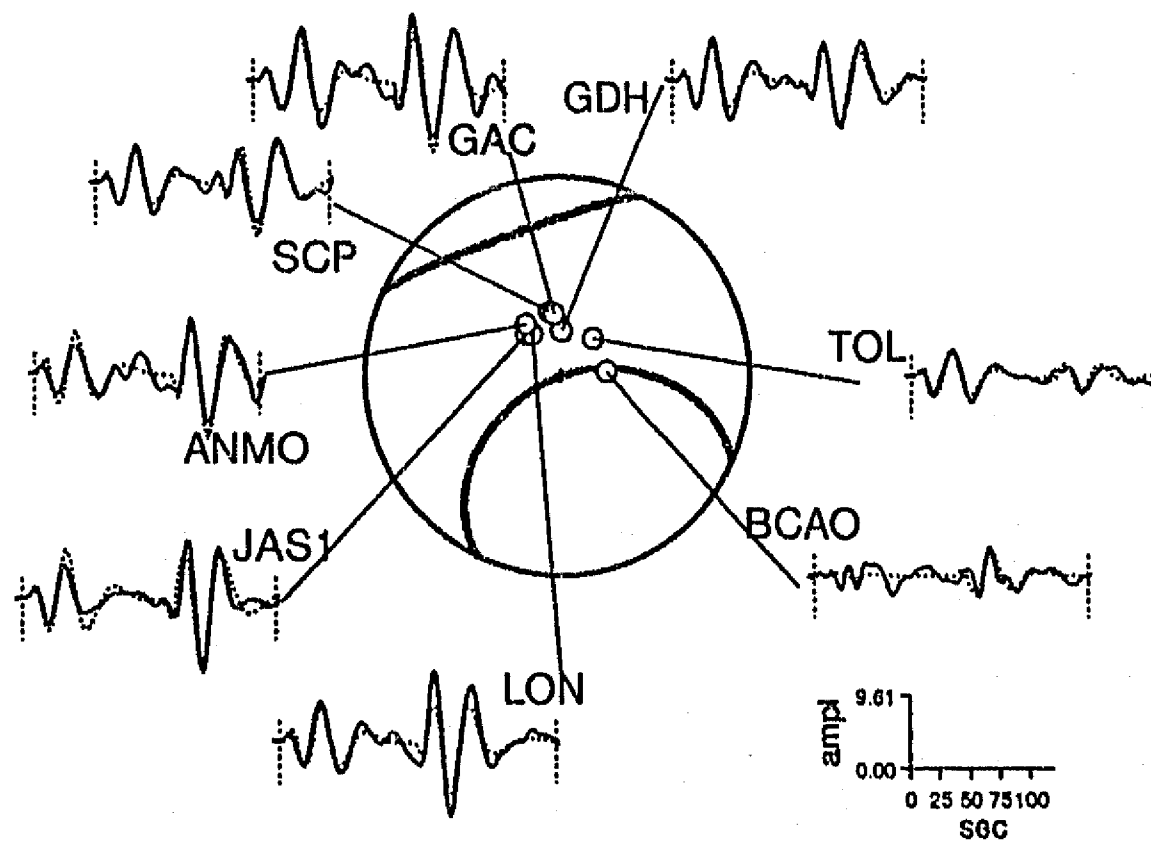
P waves



SV waves

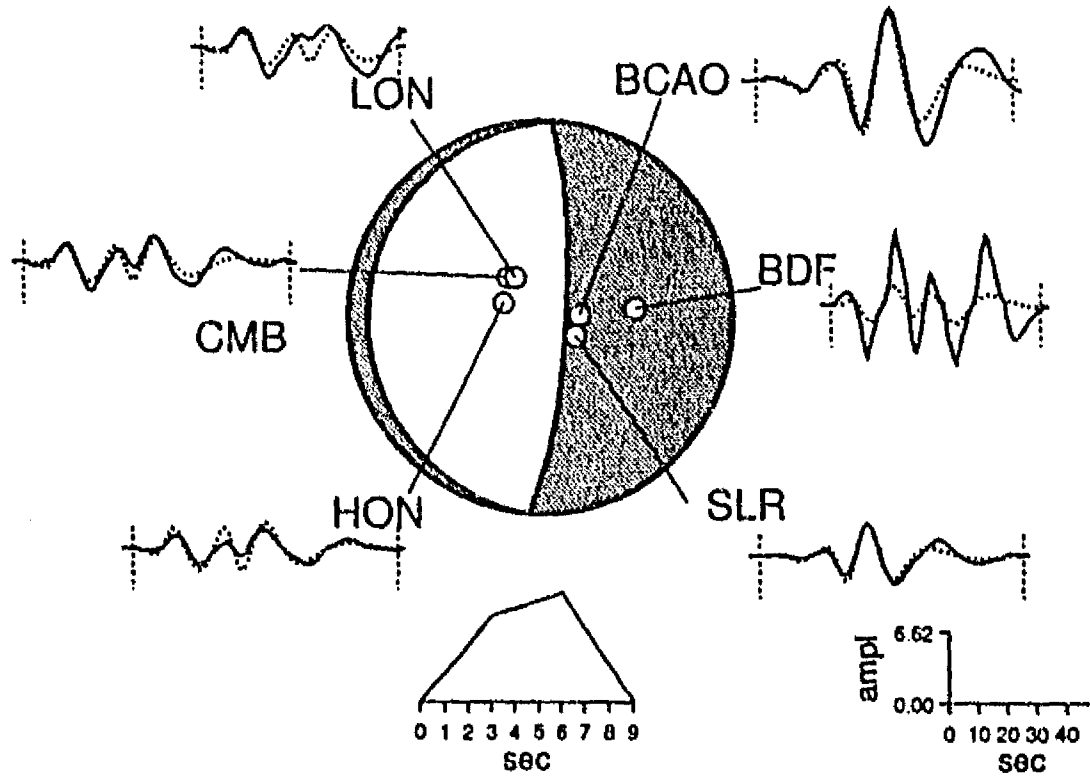


SH waves

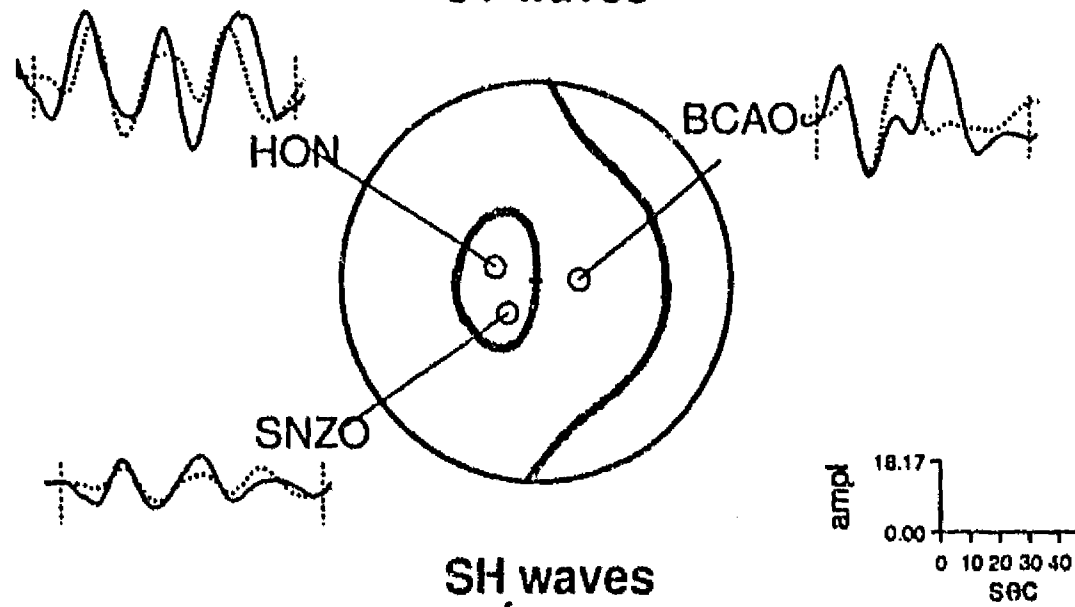


(M14) 870808, Ms=6.9, 76 km depth

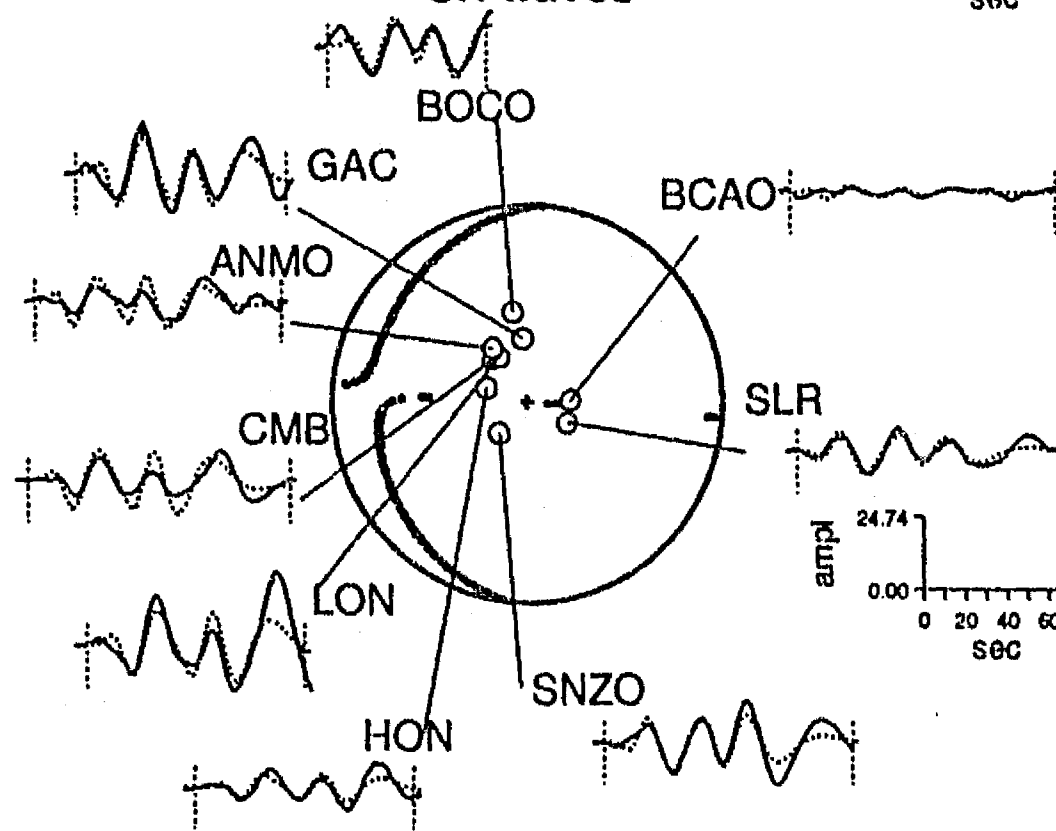
P waves



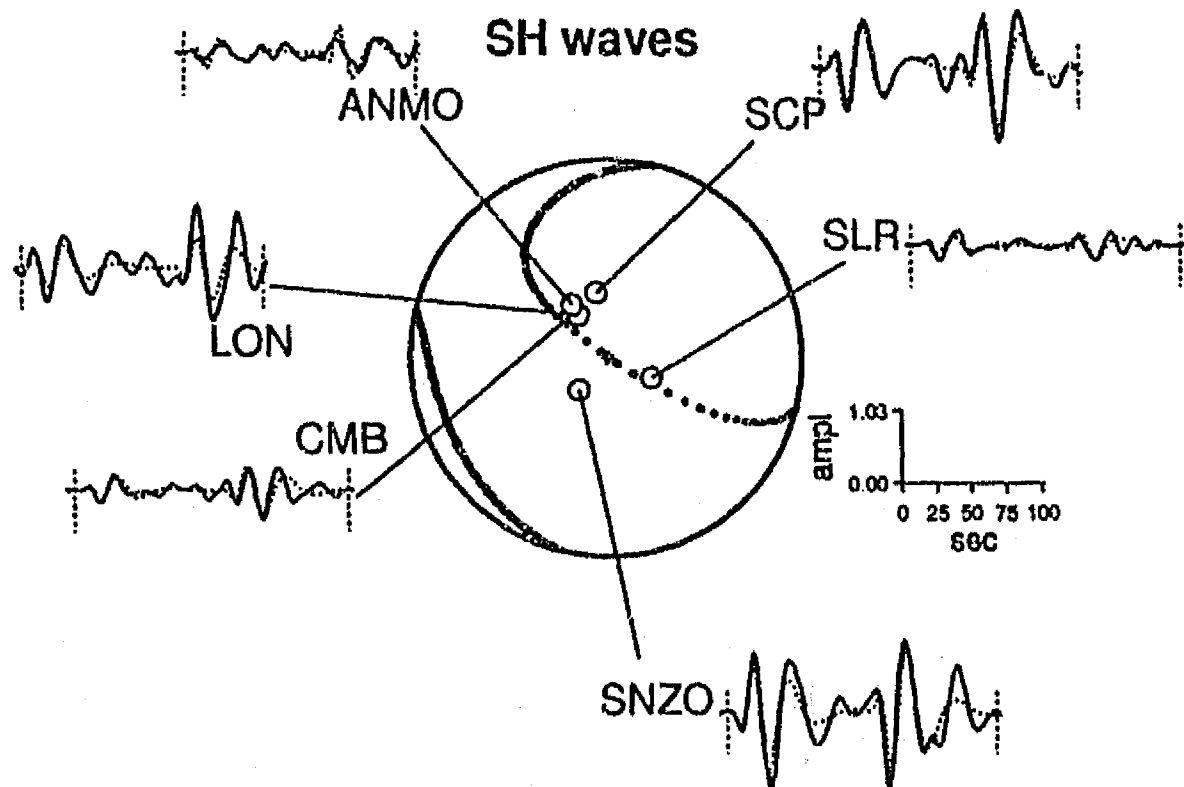
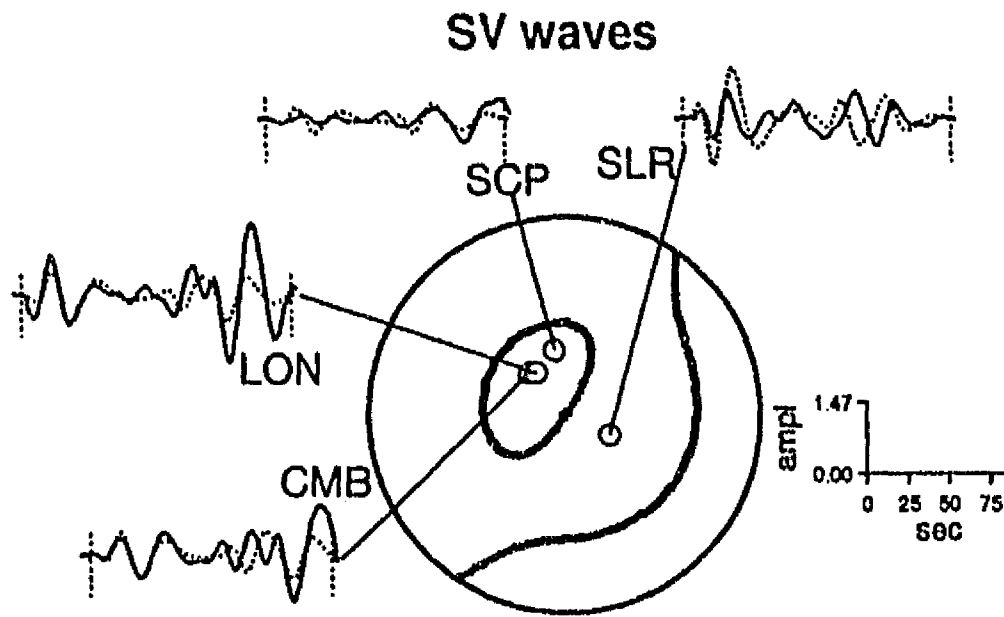
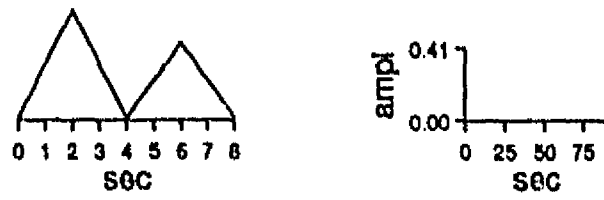
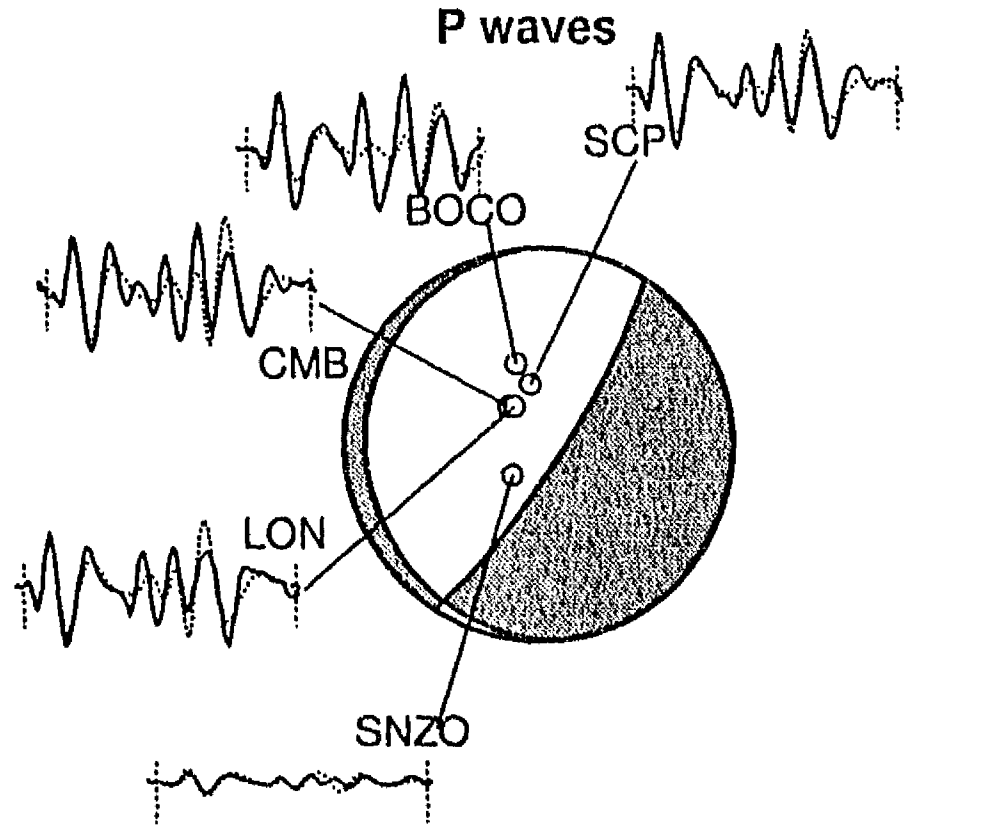
SV waves



SH waves



(M15) 870901, Mb=5.9, 227 km depth



## CONCLUSIONES

La morfología de la subducción de la brecha sísmica del norte de Chile ha sido analizada utilizando eventos registrados telesísmicamente y microsismicidad local obtenida de dos experimentos locales. Los estudios realizados permiten obtener las siguientes conclusiones:

- Las variaciones espacio-temporales de la sismicidad registrada telesísmicamente durante los últimos 26 años no es suficiente para determinar la madurez de la brecha sísmica del norte de Chile, a la luz de modelos simples de acumulación y transferencia de esfuerzos.
- Se observa una zona de bajas velocidades de onda *P* en la parte superior de la placa de Nazca, que es interpretada como corteza oceánica en subducción. Esta corteza tiene un espesor aproximado de 10 km y alcanza una profundidad máxima de  $60 \pm 10$  km, que se asocia al posible cambio de fase de gabro a eclogita a lo largo de la litósfera oceánica en subducción.
- La profundidad máxima de la corteza oceánica en subducción concuerda con la profundidad máxima del contacto sismogénico. Probablemente, el cambio de fase asociado es uno de los mecanismos dominantes que controlan la profundidad máxima del acoplamiento interplaca.
- Se propone un medio alternativo para estimar la profundidad máxima del contacto sismogénico, basado en el cambio de esfuerzos observado en la parte superior de la placa en subducción de compresional a tensional. Este cambio ocurre sistemáticamente en el norte y centro de Chile a una profundidad de  $60 \pm 10$  km.
- Se observa una zona doble invertida ubicada a  $\sim 100$  km de profundidad, bajo el arco volcánico, utilizando tanto eventos registrados telesísmicamente como con microsismicidad local, donde los eventos compresionales se sitúan más profundos que los eventos tensionales. Esta zona doble es coherente con resultados numéricos asociados a cambios de fases productos del aumento de presión y temperatura con la profundidad que también da origen a los arcos volcánicos.

### *Conclusiones*

- No hay variaciones del ángulo de subducción en la zona del contacto sismogénico a lo largo del norte de Chile.
- A partir de la zona desacoplada, se observa una disminución gradual hacia el sur del ángulo de subducción, que comienza aproximadamente en los 22°S. Asumiendo continuidad lateral de la placa de Nazca, la disminución del ángulo de subducción puede ser interpretada como una respuesta regional al modo de subducción subhorizontal observado entre los 27°S y 33°S, sugiriendo que el cambio del modo de subducción normal a subhorizontal es de carácter gradual y podría comenzar a los 22°S.

